SEISMIC VULNERABILITY OF HILL BUILDINGS

Ph.D. THESIS

by

MITESH SURANA

DEPARTMENT OF EARTHQUAKE ENGINEERING
INDIAN INSTITUTE OF TECHNOLOGY ROORKEE
ROORKEE - 247667 (INDIA)
OCTOBER, 2017

SEISMIC VULNERABILITY OF HILL BUILDINGS

A THESIS

*Submitted in partial fulfilment of the
requirements for the award of the degree*

of

DOCTOR OF PHILOSOPHY

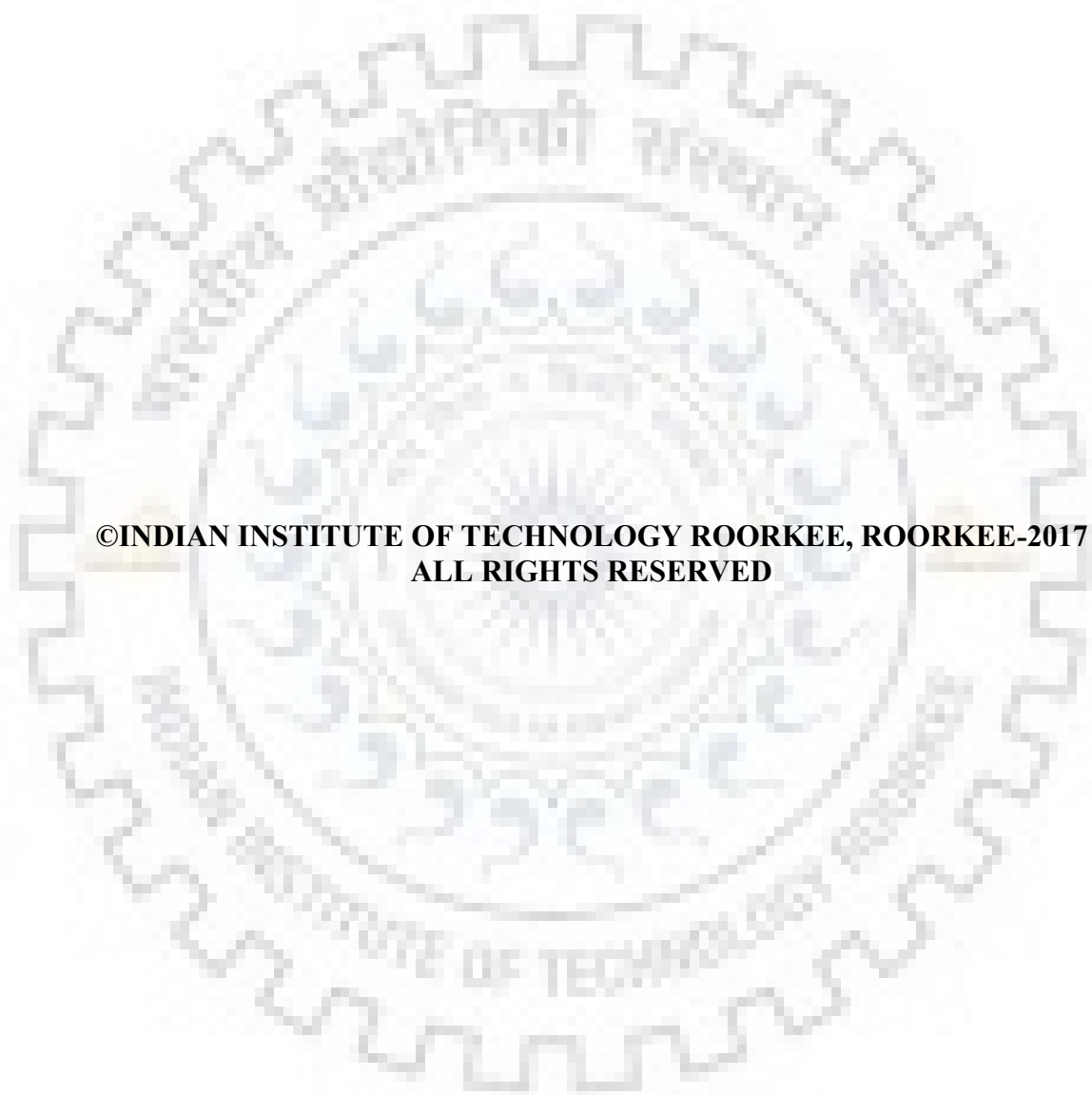*in*

EARTHQUAKE ENGINEERING

by

MITESH SURANA

**DEPARTMENT OF EARTHQUAKE ENGINEERING
INDIAN INSTITUTE OF TECHNOLOGY ROORKEE
ROORKEE - 247667 (INDIA)
OCTOBER, 2017**

INDIAN INSTITUTE OF TECHNOLOGY ROORKEE
ROORKEE

<u>CANDIDATE'S DECLARATION</u>

I hereby certify that the work which is being presented in the thesis entitled "**SEISMIC VULNERABILITY OF HILL BUILDINGS**" in partial fulfilment of the requirements for the award of the Degree of Doctor of Philosophy and submitted in the Department of Earthquake Engineering of the Indian Institute of Technology Roorkee, Roorkee is an authentic record of my own work carried out during a period from July, 2013 to October, 2017 under the supervision of Dr. Yogendra Singh, Professor, Department of Earthquake Engineering, Indian Institute of Technology Roorkee, Roorkee and Dr. Dr. Dominik H. Lang, Head, Department of Earthquake Hazard and Risk, NORSAR, Norway.

The matter presented in this thesis has not been submitted by me for the award of any other degree of this or any other Institution.

(MITESH SURANA)

This is to certify that the above statement made by the candidate is correct to the best of our knowledge.

(Dominik H. Lang)
Supervisor

(Yogendra Singh)
Supervisor

The Ph.D. Viva-Voce Examination of **Mr. Mitesh Surana**, Research Scholar, has been held on _____

Chairman, SRC

Signature of External Examiner

This is to certify that the student has made all the corrections in the thesis.

Signature of Supervisor (s)

Head of the Department

Dated:

ABSTRACT

The structural configurations of buildings in hilly regions are significantly different as compared to flat terrain counterparts, due to topographic constraints. The buildings in hilly regions generally follow the natural slope of the ground, resulting in foundations of a building stretching over different heights. These 'hill buildings' have short-columns on uphill side, and mass and stiffness irregularities in plan as well as along the height. Currently, none of the seismic design codes world-over provides any specific seismic design guidelines for hill buildings. In addition, slope-stability and topographic amplification effects are also crucial, which lead to a further increase in seismic vulnerability of hill buildings. However, the scope of the present thesis is limited to assessing the impact of different structural configurations on seismic vulnerability of hill buildings.

To identify the prevalent structural configurations of buildings in hilly regions, extensive field surveys are conducted in two popular tourist destinations in the Indian Himalayas, viz. Mussoorie and Nainital, both located in seismic zone IV, as per current seismic zoning map of India. Based on the details collected from the field surveys, a building typology classification scheme (considering the various structural configurations of hill buildings) and a building stock inventory database are developed. The typology classification scheme takes into account a building's structural configuration, building height, material of construction, load-bearing system, and roof type. It is identified that, reinforced-concrete (RC) buildings with regular (denoted as 'SC A'), split-foundation (SF; denoted as 'SC B') and step-back (SB; denoted as 'SC C') structural configurations are most common and cover approximately 50% of the building stock in both the test beds. A majority of these RC hill buildings are 'pre-code' buildings whereas only few buildings with 'moderate-code' design level could be observed. These hill buildings are predominantly low- and mid-rise, and high-rise buildings are not observed in the selected test beds. These RC hill buildings have been studied in detail by conducting a numerical study.

A statistical analysis of the plan details of RC buildings surveyed in Mussoorie is carried out to select a representative building plan for numerical study. Three different design levels representative of pre-code (designed for gravity loads alone), moderate-code (designed for gravity loads and earthquake forces, without conforming to strong-column weak-beam design)

and high-code (designed for gravity loads and earthquake forces, and also conforming to strong-column weak-beam design) buildings are considered. Incremental dynamic analysis (IDA) is conducted on the considered buildings using near- and far-field ground-motion record suites, identified in FEMA P695. The effect of the seismic design level and the building height on collapse fragility is studied. The effects of near-field site and seismic zone on collapse fragility are also studied.

It is observed that the period of vibration of SC B and SC C hill buildings is controlled by the number of storeys above the uppermost foundation level. In case of pre-code buildings, SC C buildings (having the highest torsional effects) have the least median collapse capacity whereas regular buildings have the highest collapse capacity. On the other hand, in case of moderate- and high-code buildings, the regular buildings have the highest median collapse capacity whereas SC B buildings have the least median collapse capacity, though, all the buildings (SC A, SC B and SC C) were designed for identical base shear coefficients. The least median collapse capacity in case of SC B buildings designed for moderate- and high-code design level can be attributed to increased torsional effects in the inelastic range.

It is observed that the average spectral acceleration $S_{a,avg}$ (0.2T-3T, 5%), as a collapse intensity measure, captures the effects of higher modes of vibration as well as spectral shape of the ground-motion records. It results in collapse capacities of a building, nearly independent of the ground-motion record suites with a significantly reduced record-to-record variability, in case of moderate- and high-code buildings. This observation is not only valid in case of regular buildings, but also in case of torsionally irregular SC B and SC C hill buildings. On the other hand, in case of pre-code buildings, S_a (T, 5%) results in lower record-to-record variability than $S_{a,avg}$ (0.2T-3T, 5%), due to very limited ductility capacity of such buildings.

The damage patterns obtained from the numerical investigations in the present study suggest that the storey just above the uppermost foundation level is the most vulnerable location in the SC B and SC C hill buildings. This observation is found to be in good agreement with the observed damage in an SC B building after Sikkim earthquake of 2011. It is also observed that even after designing the buildings for a strong-column weak-beam factor of 1.40, the column hinging cannot be avoided, and there is scope for further enhancement of this factor.

Pre-code buildings result in unacceptably high probabilities of collapse (upto 95%) for Maximum Considered Earthquake (MCE) hazard. For all the investigated low- and mid-rise buildings, designed for moderate- and high-code design levels, the collapse probability has been found to be well within 10% for all the considered sites, conditioned on the occurrence of MCE. On the other hand, in case of high-rise SC B and SC C buildings, designed for high-code design level, the collapse probability for MCE hazard has been found to be significantly higher in a near-field site located in seismic zone IV and a far-field site located in seismic zone V.

The floor acceleration demands for regular and irregular hill buildings have also been studied for performance-based design of non-structural components (NSCs). It is observed that peak floor acceleration (PFA) demands reduce with increase in period of vibration as well as inelasticity of the supporting structure. In case of SC B and SC C structural configurations, the PFA demands are controlled by a higher mode of vibration for building portion below the uppermost foundation level, whereas it is controlled by the fundamental mode in the building portion above the uppermost foundation level. The floor response spectrum (FRS) is observed to be better correlated to ground response spectrum (GRS) rather than peak ground acceleration (PGA) as used in current seismic design codes. Further, the spectral amplification factors along the height approximately follow the elastic mode shapes, for both elastic and inelastic supporting structures. In case of SC B and SC C structural configurations responding elastically, the torsional acceleration amplification in floor response is observed to be proportional to the torsional displacement amplification.

Based on the observations and results obtained from numerical study, comprehensive spectral amplification functions are developed and validated for SC A, SC B and SC C structural configurations. The developed spectral amplification functions can be used with a code-based design response spectrum as well as a site-specific response spectrum to construct the floor spectrum. The developed spectral amplification functions are more comprehensive in predicting the floor acceleration demand than currently available models as these take into account the ground-motion characteristics, the dynamic characteristics of the supporting structure (both periods and mode shapes), the level of inelasticity expected in the supporting structure, and the period of vibration of the NSC.

ACKNOWLEDGEMENT

Dated: October 13, 2017   (MITESH SURANA)

CONTENTS

LIST OF FIGURES

LIST OF TABLES

NOTATIONS

Symbol	Explanation
A_0	Spectral amplification factor at zero period
A_1	Spectral amplification factor corresponding to the fundamental mode
A_2	Spectral amplification factor corresponding to the second mode
A_g	Gross cross-sectional area
A_k	Spectral amplification factor corresponding to the kth mode
A_L	Long-period amplification factor
a_p	Component amplification factor
A_v	Area of transverse reinforcement
b	Floor plan dimension perpendicular to the direction of the earthquake excitation
d	Depth of the column
e	Distance between CR and CM at a floor
E_c	Modulus of elasticity of concrete
EI_g	Gross flexural rigidity of a component
EI_{stf40}	Secant value of effective stiffness at 40% of the yield force
EI_y	Secant value of effective stiffness at yield point of the component
f_1	Ratio of the energy dissipated in a degraded loop to non-degraded loop for deformations within pre-capping range
f_2	Ratio of the energy dissipated in a degraded-loop to non-degraded loop for deformations within post-capping range
f_c'	Cylinder compressive strength
f_l	Lowest usable frequency

xxvii

Symbol	Explanation
f_{yv}	Yield strength of transverse reinforcement
g	Acceleration due to gravity
H	Building height measured from the base level
I_g	Gross moment of inertia
$\overline{IM}$	Median value of the intensity measure
IM_{12E}	Intensity measure corresponding to the elastic fundamental and the second mode of vibration
$IM_{1I,2E}$	Intensity measure corresponding to the inelastic first mode period and the elastic second mode period
k	A factor to consider the effect of ductility demand on shear capacity of the columns
M/V	The largest ratio of moment to shear under design loading for a column
M_{nb}	Nominal moment capacity of all beams meeting at a joint in the direction under consideration
M_{nc}	Nominal moment capacity of all columns meeting at a joint in the direction under consideration
M_s	Surface wave magnitude
M_w	Moment magnitude
N	Number of ground-motion records
N_a	Number of storeys above the uppermost foundation level
N_b	Number of storeys below the uppermost foundation level
N_p	A parameter representing proxy to the spectral shape
P	Design gravity load on column
$P[C/S_{a,avg}]$	Probability of collapse for MCE hazard, when $S_{a,avg}$ is chosen as IM
$P[C/S_a]$	Probability of collapse for MCE hazard, when S_a is chosen as IM

Symbol	Explanation
q	Behaviour factor
R	Strength ratio
r	Torsional radius
R_{jb}	Joyner-Boore fault projection distance
R_s	Source-to-site distance
s	Spacing of the transverse reinforcement
S_a	Spectral acceleration
$S_a (C)$	Median collapse capacity in terms of S_a
$S_a (D)$	Seismic demand for MCE hazard in terms of S_a
$(S_a (T), S_a (T^*) / S_a (T))$	Vector-valued intensity measure considering spectral accelerations at periods corresponding to the fundamental and the second mode (in case of structures with significant higher mode effects) or elongated period (in case of structures with significant inelasticity)
$S_a (T, 5\%)$	5%-damped spectral acceleration corresponding to fundamental period of vibration (T)
$S_a (T, 5\%)_{MCE}$	5%-damped elastic spectral acceleration demand corresponding to MCE, computed at the average period (T) of vibration in the two orthogonal directions
$S_a (T, 5\%)_{Median}$	Median collapse capacity
$S_a (T, \varepsilon)$	Spectral acceleration at the fundamental period of vibration (T) of the building, after accounting for the spectral shape through ε
$S_a (T\text{-}T_{eff})$	Average spectral accelerations over the period range from fundamental period of vibration (T) to effective period of vibration (T_{eff})
$S_a (T_{eff})$	Spectral acceleration corresponding to effective period of vibration (T_{eff})
$S_a (T_1, T_2)$	Vector intensity measure considering spectral accelerations corresponding to the fundamental and the second mode of vibration

Symbol	Explanation
$S_{a,AM}(T)$	Arithmetic mean of spectral accelerations of two horizontal components corresponding to the average period (T) of vibration in the two orthogonal directions
$S_{a,avg}$ (0.2T -3T, 5%)	5%-damped spectral acceleration geometrically averaged over a range of periods from 0.2T-3T
$S_{a,avg}$ (C)	Median collapse capacity in terms of $S_{a,avg}$
$S_{a,avg}$ (D)	Seismic demand for MCE hazard in terms of $S_{a,avg}$
$S_{a,avg}$ (T-2T, 5%)	5%-damped average spectral acceleration over a range of periods between T-2T
$S_{a,avg}$ MCE	5%-damped average spectral acceleration over a range of periods between 0.2T-3T, corresponding to MCE hazard
$S_{a,GM}(T)$	Geometric mean of spectral accelerations of two horizontal components corresponding to the average period of vibration (T) in the two orthogonal directions
$S_{AF}(T)$	5%-damped floor spectral acceleration
$S_{AG}(T)$	5%-damped ground spectral acceleration
S_{au}	Spectral acceleration at ultimate point of the structure
S_{ay}	Spectral acceleration at yield point of the structure
S_d	Spectral displacement
S_{di}	Inelastic spectral displacement
S_{du}	Spectral displacement at ultimate point of the structure
S_{dy}	Spectral displacement at yield point of the structure
s_w	Stiffness weighting factor
T	Average of the periods of vibration in the two orthogonal directions
T_1	Period of vibration corresponding to the fundamental mode of vibration, in the direction under consideration
T_2	Period of vibration corresponding to the second mode of vibration, in the direction under consideration

Symbol	Explanation
T_3	Period of vibration corresponding to the third mode of vibration, in the direction under consideration
T_c	Corner period, representing intersection of acceleration- and velocity-controlled ranges of response spectrum
T_{con}	Conditioning period
T_{eff}	Effective period of vibration
T_k	Period corresponding to k^{th} mode of vibration
T_L	Long-period beyond which floor spectral amplification function is considered to be constant
T_p	Period of vibration of the NSC
T_p/T_1	Normalized period
T_{peak}	Period corresponding to peak spectral acceleration for a ground-motion record
T_{pulse}	Period of the velocity-pulse
V/W	Normalized base shear coefficient
V_c	Shear strength contribution from concrete
V_d	Design base shear
V_n	Shear strength of a column
V_s	Shear strength contribution from transverse reinforcement
$V_{s,30}$	Average shear wave velocity in the top 30 m depth
V_y	Yield base shear
W	Seismic weight of the building
Z	Height of the floor level under consideration, measured from the base
α_{m1}	Modal mass participation ratio corresponding to the fundamental mode of vibration, in the direction under consideration

Symbol	Explanation
α_{m2}	Modal mass participation ratio corresponding to the second mode of vibration, in the direction under consideration
α_{m3}	Modal mass participation ratio corresponding to the third mode of vibration, in the direction under consideration
α_{mk}	Modal mass participation ratio corresponding to the kth mode of vibration, in the direction under consideration
β_M	Modelling variability in the seismic response at collapse
β_{RTR}	Record-to-record variability in collapse capacity
$\beta_{RTR}(S_a)$	Record-to-record variability in collapse capacity, when S_a is chosen as IM
$\beta_{RTR}(S_{a,avg})$	Record-to-record variability in collapse capacity, when $S_{a,avg}$ is chosen as IM
β_T	Total variability in collapse capacity
$\beta_T(S_a)$	Total variability in the collapse capacity, when S_a is chosen as IM
$\beta_T(S_{a,avg})$	Total variability in the collapse capacity, when $S_{a,avg}$ is chosen as IM
δ	Torsional displacement amplification factor
$\delta_{cr,i}$	Displacement of CR at i^{th} floor
$\delta_{j,i}$	Displacement of jth element at i^{th} floor
$\varepsilon(T)$	Number of standard deviations by which a given $\ln S_a$ value at a site differs from its mean predicted value derived from an attenuation model
η	Ratio of the torsional acceleration amplification to the torsional displacement amplification
η_s	A parameter proxy to spectral shape
θ_{Max}	Maximum inter-storey drift ratio
θ_p	Pre-capping rotation capacity

Symbol	Explanation
θ_{pc}	Post-capping rotation capacity
θ_T	Torsional acceleration amplification factor
λ	A factor accounting for type of aggregate in shear capacity
μ	Ductility capacity of a building
$\mu_{\ln S_a}(M_w, R_s, T)$	Mean of $\ln S_a(T)$ predicted from an attenuation model
ρ_w	Area of flexural tension reinforcement
$\sigma_{\ln S_a}(T)$	Standard deviation of the predicted $\ln S_a(T)$
Φ	Cumulative normal distribution function
$\phi_{k,i}$	Mode shape coefficient corresponding to k^{th} mode, at i^{th} floor
$\phi_{k,max}$	Maximum mode shape coefficient corresponding to k^{th} mode
$\phi_{1,i}$	Mode shape coefficient corresponding to the fundamental mode, at the ith floor
$\phi_{1,max}$	Maximum mode shape coefficient corresponding to the fundamental mode
$\phi_{1,roof}$	Mode shape coefficient corresponding to the fundamental mode, at the roof level
$\phi_{2,i}$	Mode shape coefficient corresponding to the second mode, at the ith floor
$\phi_{2,roof}$	Mode shape coefficient corresponding to the second mode, at the roof level
Ω	Over-strength factor

ABBREVIATIONS

Abbreviation	Explanation
ACMR	Adjusted collapse margin ratio
AMC	Adaptive modal combination
APA	Adaptive pushover analysis
AS-NSCs	Acceleration sensitive non-structural components
ATC	Applied Technology Council
CBM	Collapse based method
CM	Center of mass
CMR	Collapse margin ratio
CMS	Conditional mean spectrum
COV	Coefficient of variation
CR	Center of rigidity
CS	Conditional spectrum
CSM	Capacity spectrum method
DBM	Displacement based method
DCM	Displacement coefficient method
DL	Damage limitation
DM	Damage measure
DMM	Displacement modification method
DPMs	Damage probability matrices
DS	Damage state
DSHA	Deterministic seismic hazard analysis
DSI	Displacement spectrum intensity
DS-NSCs	Drift sensitive non-structural components

Abbreviation	Explanation
EDP	Engineering demand parameter
ELF	Equivalent lateral force
EMS	European Macroseismic Scale
EPGA	Effective peak ground acceleration
FBD	Force-based design
FEMA	Federal Emergency Management Agency
FF	Far-field
FL	Flexible edge
FRS	Floor response spectrum
GCIM	Generalized conditional intensity measure
GRS	Ground response spectrum
GLD	Gravity load designed
HAZUS	Hazard in United States
HC	High-code
IDA	Incremental dynamic analysis
IDR	Inelastic displacement ratio
IM	Intensity measure
LS	Life safety
LTHA	Linear time-history analysis
MC	Moderate-code
MCE	Maximum considered earthquake
MDOF	Multiple-degree-of-freedom
MMI	Modified Mercalli Intensity
MPA	Modal Pushover Analysis

Abbreviation	Explanation
MSA	Multiple stripe analysis
MSK	Medvedev-Sponheuer-Karnik
NCHE	Normalized cumulative hysteretic energy
NDP	Non-linear dynamic procedure
NEHRP	National Earthquake Hazard Reduction Programme
NF	Near-field
NLTHA	Non-linear time-history analysis
NSCs	Non-structural components
NSP	Non-linear static procedure
OMRF	Ordinary moment resisting frame
PBD	Performance-based design
PBEE	Performance-based earthquake engineering
PC	Pre-code
PEER	Pacific Earthquake Engineering Research
PFA	Peak floor acceleration
PGA	Peak ground acceleration
PGV	Peak ground velocity
PSHA	Probabilistic seismic hazard analysis
PSI	Parameterless scale on Intensity
RC	Reinforced-concrete
RCMRF	Reinforced-concrete moment-resisting frame
RDR	Roof drift ratio
RTD	Risk-targeted design
SAF	Spectral amplification function

Abbreviation	Explanation
SB	Step-back
SC A	Structural configuration A
SC B	Structural configuration B
SC C	Structural configuration C
SCWB	Strong-column weak-beam
SDC	Seismic design category
SDOF	Single-degree-of-freedom
SEAOC	Structural Engineers Association of California
SF	Split-foundation
SMRF	Special moment resisting frame
SR	Storey ratio
SRSS	Square-root-of-sum-of-squares
SSF	Spectral shape factor
SW	Shear wall
TAF	Torsional acceleration amplification factor
TDR	Torsional drift amplification ratio
UHS	Uniform hazard spectrum

CHAPTER 1

INTRODUCTION

1.1 INTRODUCTION

The Indian Himalayas represent one of the world's most seismically active mountain ranges which start from Jammu and Kashmir in the north to Arunachal Pradesh in the north-east covering the states of Himachal Pradesh, Uttarakhand, Meghalaya, Manipur, Nagaland, Mizoram, Tripura, Sikkim, Assam and West Bengal. Each of these states falls under the most severe seismic zones (i.e., seismic zones IV and V) as per the current seismic zonation map of India (IS 1893 Part 1 2016). The mountain ranges representing the Indian Himalayas are, seen from a geological perspective, relatively young geological formations which produced some of the most devastating earthquakes on the Indian subcontinent in the past.

Table 1.1 shows a list of some of the most devastating earthquakes in the past century, which have occurred in the Indian Himalayan region. Each of these disasters resulted in both huge economic losses and great fatality numbers. Figure 1.1 presents the current seismic zoning map of India along with the location of these earthquakes marked by circles.

Table 1.1 Major earthquakes in the Indian Himalayan region, corresponding intensities and reported casualties.

S. No.	Date of the event	Name of the event	Magnitude of the event	Max intensity observed	Number of casualties
1.	April 04,1905	Kangra	7.8 (M_s)	Not known	>20,000
2.	January 15,1934	Nepal-Bihar	8.0 (M_w)	XI	>10,000
3.	August 15,1950	Assam-Tibet	8.6 (M_w)	XI	1,526
4.	January 19,1975	Kinnaur	6.8 (M_s)	IX	47
5.	August 21,1988	Nepal	6.9 (M_w)	NA	~1,000
6.	October 20, 1991	Uttarkashi	6.8 (M_w)	VIII	>2,000
7.	March 28,1999	Chamoli	6.8 (M_w)	VIII	103
8.	October 08, 2005	Kashmir	7.6 (M_w)	VIII	1,30,000
9.	September 18, 2011	Sikkim	6.9 (M_w)	VII	118
10.	April 25, 2015	Nepal	7.8 (M_w)	IX	>8900
11.	May 12, 2015	Nepal	7.3 (M_w)	VIII	218
12.	January 4, 2016	Manipur	6.7 (M_w)	Not known	11

M_s - surface wave magnitude; M_w - moment magnitude; and intensity corresponds to Mercalli intensity scale.

With the advancements in technology, urbanization and rapid population growth, which could be observed in the past few decades, reinforced-concrete (RC) buildings became very popular in the Indian Himalayas. The non-availability of flat land for building construction in hilly regions leads to building construction on slopes. Figure 1.2 presents the most common

structural configurations of RC buildings located on slopes. In general, buildings on slopes can be constructed in two different ways, i.e.:

- the ground can be made flat by cutting or filling;
- the building's configuration follows the natural slope of the ground.

The first option is generally not viable due to the economic constraints and instability of freshly cut steep slopes. That is why the builders generally prefer the second option, in which the building construction ends up with foundations stretching over different levels (Fig. 1.2). These foundations may be at least at two different levels (in case of buildings resting on steep slopes) or at multiple levels (in case of buildings resting on mild and moderate slopes) depending on the slope gradient. Buildings with foundations at different levels are here onwards referred to as "hill buildings".
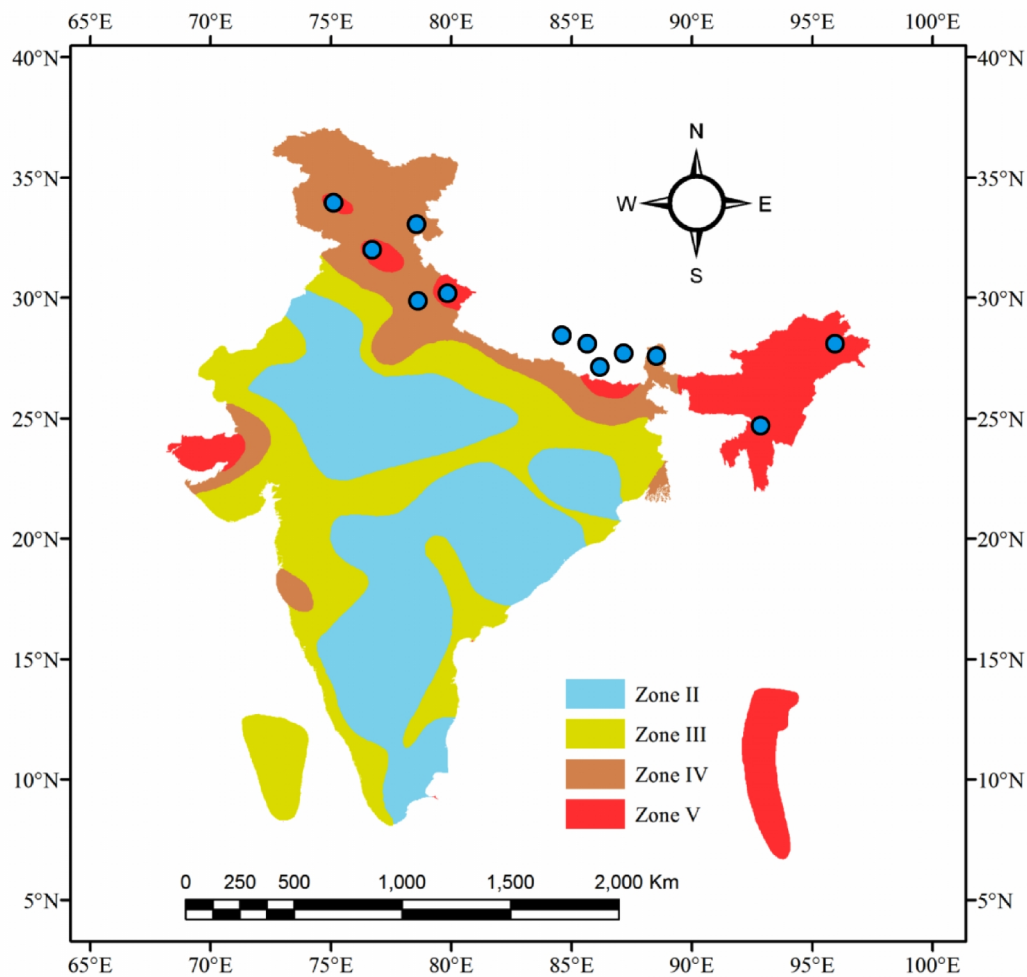
Fig. 1.1 Seismic zoning map of India, along with the major past earthquakes in the Indian Himalayan region shown by circles.

(a) Step-back (SB) building

(b) Split-foundation (SF) building

Fig. 1.2 Typical configurations of hill buildings.

1.2 SEISMIC PERFORMANCE OF HILL BUILDINGS IN PAST EARTHQUAKES

The Sikkim earthquake of 18th September 2011 was one of the major earthquakes in the hilly region of the Indian Himalayas, which for the first time, exposed the seismic vulnerability of multi-storey RC frame buildings on hill slopes. A significantly poor performance of hill buildings has already been reported in various damage reports of the 2011 Sikkim earthquake (Sharma et al. 2011; Murthy et al. 2012b; Vijayanarayanan et al. 2012; Singh et al. 2012; EERI 2012). Figure 1.3 presents damage experienced by a split-foundation (SF) building after the 2011 Sikkim earthquake. The storey nearest to the road level experienced the most severe damage. Although, this earthquake of moment magnitude (M_w) 6.9 exhibited only moderate

ground-motion levels (a Peak Ground Acceleration, PGA = 0.18g was recorded in Gangtok city which was located at 68 km distance south-east of the epicentre), the observed damage extent was fairly high with many buildings suffering severe damage, while few buildings even collapsed (Sharma et al. 2011; Murthy et al. 2012b; EERI 2012).
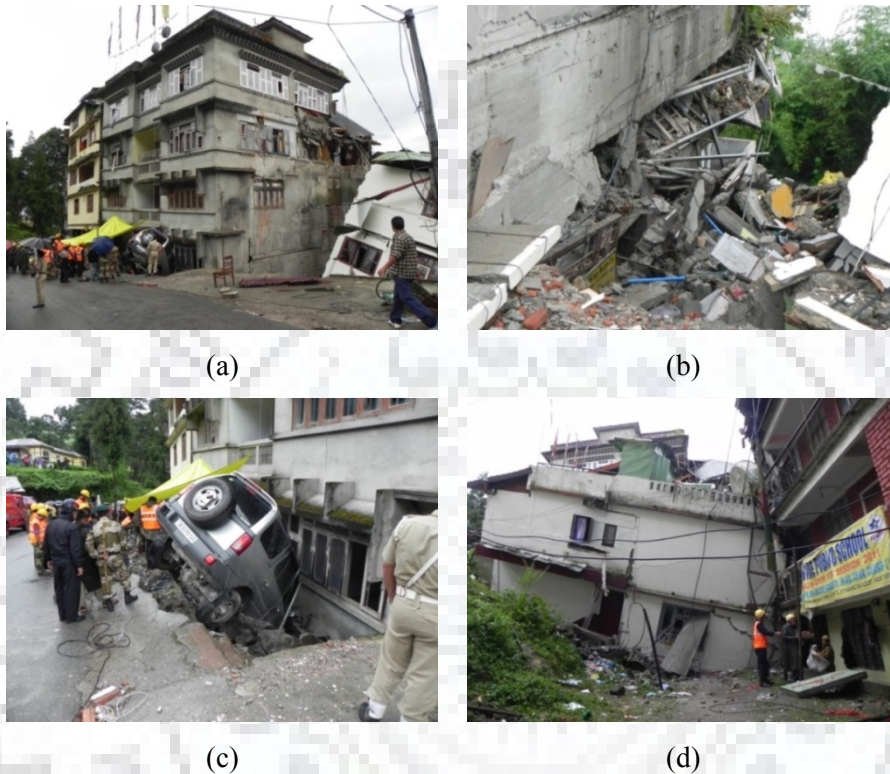
Fig. 1.3 Collapse of a split-foundation (SF) building observed after the 2011 Sikkim earthquake. The collapse of this split-foundation building has also caused collapse of an adjacent building.

The state of Sikkim is situated in zone IV as per the seismic zoning map of India, to which an effective PGA (i.e., EPGA or Zone Factor) of 0.24g is assigned (IS 1893 Part 1 2002; 2016). Since this code design level was much higher than the observed ground-motion level, the excessive damage observed during the post-earthquake field surveys, may be attributed to a number of factors which include the lack of earthquake resistant design features, faulty construction practices, irregular configurations of buildings due to slope topography constraints, slope-instability issues as well as seismic ground-motion amplification caused by local topography (Sharma et al. 2011; Vijayanarayanan et al. 2012; EERI 2012).

High seismicity and poor performance of buildings during the recent major earthquake events in the Indian Himalayas have collectively led both researchers and disaster managers to start focusing on the Indian Himalayas.

1.3 ISSUES IN SEISMIC RESPONSE OF HILL BUILDINGS

In general, there are three important issues in context of seismic behaviour of hill buildings which include: (i) structural configuration effects, (ii) slope-stability effects, and (iii) topographic amplification effects. In this section, the major issues related to the seismic behaviour and vulnerability of hill buildings are identified:

- Hill buildings, as defined in the previous section, exhibit large irregularities both in plan as well as in elevation. Figure 1.4 illustrates the 3D model of a typical step-back (SB) hill building configuration. Hill buildings have a non-uniform distribution of mass and stiffness along the height of the building, which results in a significant elevation irregularity in the lower stories (Fig. 1.5). The extent of mass and stiffness irregularity depends upon the slope angle on which the building is resting. This non-uniform distribution of mass and stiffness along the height of the hill building, alters its dynamic characteristics (periods and mode shapes) and hence its overall dynamic response.

- Hill buildings follow the natural slope of the ground, which results in ground-supported short-columns in each storey on the uphill side (Fig. 1.5). These ground-supported short-columns are highly vulnerable under earthquake excitation, since they attract excessive shear forces due to high stiffness. This excessive shear force results in the shear failure of the short-columns. Further, due to presence of short-columns, the uphill side becomes more rigid as compared to the downhill side. Therefore, under earthquake excitation in across-slope direction, buildings exhibit torsional response. In addition, the tendency of the foundation failure cannot be avoided due to transfer of large shear forces, from the ground supported short-columns to the foundation and finally to the ground.

- Hill buildings have a non-coincident center of mass (CM) and center of rigidity (CR). The location of the CM and CR also varies from storey to storey along the height of the building, resulting in significant torsion.

- Hill buildings are generally constructed on very mild to very steep slopes. The stability of a slope is dependent on many parameters (e.g. inclination of the slope and its material properties, gravity loads from the building, location of the building relative to the slope, effect of adjacent buildings etc.). Therefore, slope-building interaction effects also become crucial in case of hill buildings.

(a) 3D model of a step-back building   (b) Elevation along the slope direction
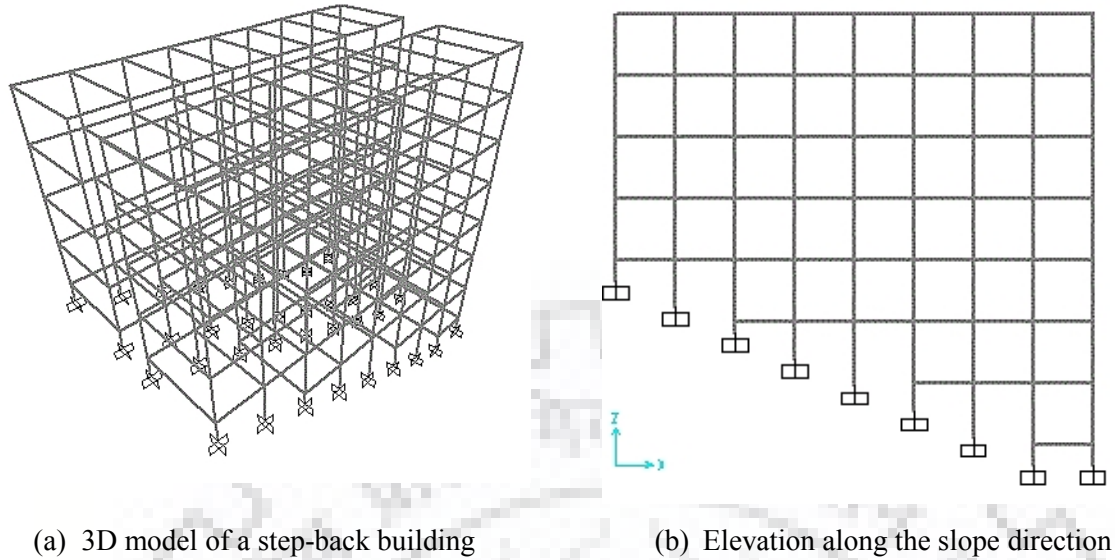
Fig. 1.4 A typical hill building model.
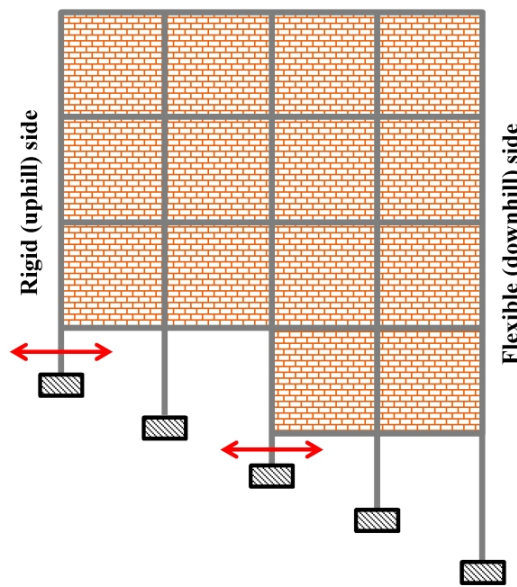
Fig. 1.5 Short-column effect in hill buildings.

- Hill buildings are subjected to topographic amplification effects, which modify the input ground-motion characteristics. Therefore, the building response becomes location dependent (e.g. building resting on a ridge, on a slope, or in a valley).

Out of the above listed research issues; the present study has been focused on structural configuration effects. The slope-stability and topographic amplification effects are beyond the scope of the present research work, and therefore these effects have not been considered both in the field surveys as well as in the numerical study.

6

1.4 RESEARCH OBJECTIVES

The research work conducted in the present thesis has the following objectives:

- To develop a comprehensive building stock inventory for the test bed cities of 'Mussoorie' and 'Nainital' and to develop a generalized building typology classification scheme for hilly regions.

- To evaluate the collapse fragility of pre-code (designed for gravity loads alone) and moderate-code (designed as special moment resisting frame as per IS 1893 Part 1 (2002) and IS 13920 (1993), without strong-column weak-beam provision) multi-storey RC hill buildings, prevalent in the Indian Himalayan region.

- To study the collapse fragility of high-code RC frame hill buildings (designed for recently revised Indian seismic design codes IS 1893 Part 1 (2016) and IS 13920 (2016), incorporating strong-column weak-beam design).

- To develop a comprehensive floor acceleration demand prediction model, for the seismic design of light-weight acceleration-sensitive non-structural components (NSCs) mounted on RC hill buildings.

1.5 SCOPE OF THE RESEARCH WORK AND METHODOLOGY

The Indian Himalayas have sloping terrain in majority of its stretch, with some areas where almost flat or very mild slopes can also be observed. The building configurations relevant to both these areas have been considered in the present study. Extensive field surveys have been conducted in the two most popular tourist destinations in the Indian Himalayas, i.e., Mussoorie and Nainital. Based on these field surveys, during which the structural and socio-economic information of approximately 10% of the total buildings of both Mussoorie and Nainital was collected, a building stock inventory database has been developed. From the developed building inventory database, the typical RC frame hill building structural configurations are identified and studied in detail. Based on details collected during the field survey, a building typology classification scheme for hilly regions is developed. The seismic vulnerability of RC hill buildings with regular, step-back and split-foundation structural configurations has been studied. In addition to these structural configurations, a small percentage of other configurations/typologies has also been observed, but those have not been considered for the

detailed study. In the present study, spectral amplification functions have been developed for the seismic design of light-weight acceleration-sensitive NSCs mounted on RC hill buildings. The scope of the present study is limited to RC bare frame buildings, designed and constructed as per Indian codes and typical construction practices prevalent in the Indian Himalayan region. The RC frame buildings in this region do contain different types of unreinforced masonry infills which are expected to further complicate the behaviour of these buildings. However, the effect of infill on seismic behaviour of these buildings has not been considered in the present study. The study has been conducted on typical configurations existing in Indian Himalayan region, nevertheless, the developed building typology classification scheme, the conclusions drawn about the seismic behaviour of RC frame hill buildings and the developed spectral amplification functions are equally applicable to any other part of the world.

It has been observed that a large variation in the design and construction practices of RC frames exists in the Indian Himalayas. Despite Indian standards for seismic design of buildings already being in existence since the early 1960's, buildings are still being constructed without any consideration of earthquake resistant design practices, even in zones of high seismicity. Therefore, to keep parity between the typical construction practices in the Indian Himalayas and the numerical study, buildings with three different design levels have been studied. The first set of buildings consists of RC Gravity Load Designed (GLD) buildings while the second set of buildings consists of Special Moment Resisting Frame (SMRF) buildings non-conforming to strong-column weak-beam design. In addition, a third set of buildings consists of Special Moment Resisting Frame (SMRF) buildings conforming to strong-column weak-beam design. All the three sets have been designed following the provisions of the relevant Indian standards and have been studied in detail.

In the present study, representative building configurations (plan dimensions, typical bay widths, storey heights, and storey ratio) have been identified from the field survey database. The study has been conducted with its primary focus on residential buildings. The Indian seismic code (IS 1893 Part 1 2002) does not provide any guidelines for modelling of RC beams, columns and beam-column joints. Therefore, the equivalent stiffness properties have been modelled using the guidelines of ASCE 41 (2013). The lumped-plasticity models for beams and columns with hinge properties obtained from ASCE 41 (2013) guidelines have been used. These modelling parameters in ASCE 41 are obtained from cyclic test envelopes and

therefore inherently include strength deterioration effects. In order to consider stiffness deterioration effects, an energy-based degrading hysteretic model has been calibrated iteratively with experimental hysteretic behaviour of RC frame members (both non-conforming for GLD buildings, and conforming for SMRF buildings) tested by Dadi and Agarwal (2015). The parameters obtained from calibration have been used to model the stiffness degradation and hysteretic energy dissipation in RC members. In case of GLD buildings, both the shear and flexural failure modes have been considered whereas in case of SMRF buildings only flexural failure mode of beams and columns has been considered; as shear failure is not expected to occur in SMRF buildings (FEMA P695 2009). However, the shear failure of short-columns has been modelled even in the case of SMRF buildings. The effects of slope topography (topographic amplification), soil and foundation flexibility, as well as slope-stability on the seismic response of buildings have been ignored.

To study the seismic behaviour of RC hill buildings, Incremental Dynamic Analysis (IDA) (Vamvatsikos and Cornell, 2002) has been applied on each building model considering bi-directional excitation. The suite of far-field seismic ground-motion records compiled in the FEMA P695 project has been used to conduct IDA for both pre-code (GLD) and moderate-code buildings (SMRF buildings non-conforming to strong-column weak-beam design). In case of high-code buildings (SMRF buildings conforming to strong-column weak-beam design), to study the effect of the design seismic zone and near-field effects, the three different record suites identified and compiled in FEMA P695 project, including a far-field record suite, a near-field record suite without velocity pulses, and a near-field record suite with velocity pulses, have been used to conduct IDA. From IDA, the typical collapse mechanism, median collapse capacity and record-to-record variability in collapse capacity of the RC hill buildings have been obtained. The median collapse capacity and record-to-record variability obtained from IDA are utilized to develop the collapse fragility curves. The developed collapse fragility curves are utilized to compute collapse probability for the Maximum Considered Earthquake (MCE) hazard.

To evaluate the floor acceleration demands on light-weight acceleration sensitive non-structural components (NSCs), mounted on RC hill buildings, the 'Floor Response Spectrum' (FRS) method has been used. The correlation of floor accelerations has been studied with peak floor acceleration (PFA), peak ground acceleration (PGA) and ground response spectrum (GRS).

The influence of dynamic characteristics and the ductility demand of the supporting structure (a building's load-bearing system is termed as 'supporting structure' throughout this thesis) on floor acceleration demand has been studied. In case of irregular building configurations, the effect of torsion on floor acceleration demand has also been investigated. Both peak floor acceleration (PFA) and floor response spectra of the RC hill buildings along the height, at two different locations on the floor plan, i.e. the center of rigidity (CR) and the flexible edge (FL) have been studied. The obtained PFA and FRS have been compared with the current seismic design code prediction models. The results obtained from the numerical study have been used to identify the parameters governing the floor response of RC hill buildings. Based on the identified parameters governing the floor response of RC hill buildings, comprehensive spectral amplification functions have been developed and validated.

1.6 ORGANIZATION OF THESIS

This thesis has been organized in eight chapters as follows:

Chapter 1 presents an introduction to the research topic, seismic performance of hill buildings during past earthquakes, issues related to hill buildings, objectives, scope and methodology, and organization of the thesis.

Chapter 2 presents the details of the existing building stock in the two test beds 'Mussoorie' and 'Nainital'. The model building typologies existing in 'Mussoorie' and 'Nainital' have been identified and classified based on structural configuration with respect to foundation arrangement and slope-retaining system, building height, construction material, and floor and roof types. In the later part of this Chapter, a building typology classification scheme for hilly regions is developed based on alphanumeric strings; and the corresponding percentage in number of buildings for test beds 'Mussoorie' and 'Nainital' is reported. The typical plan layout, building height, storey ratio, and storey heights have also been identified for further use in the numerical study.

Chapter 3 presents the state-of-the-art review on modelling and analysis of RC buildings for evaluation of seismic response. In this chapter, modelling of the stiffness of the RC members, modelling of non-linear flexural and shear behaviour of the RC members, modelling of hysteretic energy dissipation (hysteretic model), modelling of damping and the methods of

selection and scaling of ground-motion records are presented. In the later part of this chapter, a comparative study of the non-linear static and non-linear dynamic procedures is presented for mid-rise RC frame buildings designed for Indian codes. In order to compare the static capacity curve with the median dynamic capacity curve, a transformation (convolution) methodology based on the displacement modification method (DMM) is also presented.

Chapter 4 presents the state-of-the-art on the seismic fragility evaluation of RC frame buildings. In this chapter, the dynamic capacity curves for different design levels and structural configurations are developed. The median collapse capacity and record-to-record variability is obtained from IDA, and are utilized to develop the collapse fragility curves for the considered structural configurations. The collapse probabilities of 'pre-code' 'moderate-code' and 'high-code' RC hill buildings for MCE hazard level are estimated and compared.

Chapter 5 presents the effect of site conditions and ground-motion characteristics on seismic fragility of RC hill buildings. In this Chapter, the effect of spectral shape of the ground-motion records on collapse fragility is studied. Three ground-motion record suites identified in the FEMA P695 project (far-field ground-motions, near-field ground-motions without pulse, and near-field ground-motions with pulse) are used to perform the IDA of high-code RC structural configurations. In addition, the influence of near-field site conditions on collapse fragility of the considered high-code buildings is also studied by comparing the collapse fragility for near- and far-field sites.

Chapter 6 presents the state-of-the-art on evaluation of floor acceleration demand on light-weight acceleration-sensitive NSCs. In this Chapter, the correlation of floor accelerations with PFA, PGA and GRS is studied. The effect of inelasticity (ductility demand) on the floor acceleration demand is studied and the critical parameters affecting the floor response of regular buildings are identified. In the later part of this Chapter, floor spectral amplification functions have been developed for regular RC frame hill buildings, which can be used to predict the floor acceleration demand directly from the GRS, if a building's dynamic characteristics (periods and mode shapes) and level of inelasticity (ductility demand) are known.

Chapter 7 presents the effect of irregular structural (split-foundation and step-back) configuration of hill buildings on the floor acceleration demand. In this Chapter, the effect of dynamic characteristics (periods and mode shapes) and torsion on the floor acceleration demand is studied. The critical parameters affecting the floor response are identified. In the later part of this Chapter, floor spectral amplification functions have been developed for irregular RC frame hill buildings, which can be used to predict the floor acceleration demands directly from the ground response spectrum, if the building's dynamic characteristics (periods and mode shapes) and torsional drift ratio are known.

Chapter 8 presents the conclusions of the presented research work. As the present study has been conducted with certain assumptions and simplifications regarding support conditions and excitation in hill buildings, the scope for further studies on understanding of the seismic behaviour of hill buildings is outlined.

CHAPTER 2

SEISMIC CHARACTERIZATION OF BUILDING STOCK IN HILLY REGIONS

2.1 INTRODUCTION

As shown in the previous chapter, the typical construction practices in hilly regions are very different as compared to the plane regions, mainly due to the non-availability of flat land for building construction. In the hilly regions, buildings generally follow the natural slope of the ground leading to severe irregularities in elevation, plan and foundation arrangement. These buildings have been termed as "hill buildings" in this thesis.

In the past, a number of building typology classification schemes (e.g., IDNDR 1997; FEMA 2002; Sinha et al. 2008; Brzev et al. 2012; Haldar et al. 2013 and Rossetto et al. 2014) and earthquake loss assessment studies (e.g., Algermissen et al. 1972; Kircher et al. 1997; Craig et al. 2007; Anagnostopoulos et al. 2008; Bal et al. 2008; Jaiswal and Wald 2008; Campos Costa et al. 2010; Lang et al. 2012; Seo et al. 2012; Unnikrishnan et al. 2013; Rautela et al. 2015; Chaulagain et al. 2015; Silva et al. 2015) have already been conducted for almost all parts of the world. However, none of these studies takes into account the topographic conditions, neither in terms of topographic amplification effects on the seismic ground-motion, nor the significant effects caused by the topographic conditions on the building configuration itself. The irregular structural configuration of hill buildings has a significant impact on the building's susceptibility to experience damage and loss while subjected to earthquake shaking. Therefore, consideration of irregular structural configuration is necessary in both the building typology classification as well as in earthquake loss estimation for hilly regions.

In this Chapter, the details of the existing building stock in the two test beds 'Mussoorie' and 'Nainital' have been collected through field surveys and presented. The model building typologies existing in 'Mussoorie' and 'Nainital' have been identified and classified based on structural configuration with respect to foundation arrangement and slope-retaining system, building height, construction material, and floor and roof types. In the later part of this Chapter, a building typology classification scheme for hilly regions has been developed. The developed building typology is based on identification of a building typology using alphanumeric strings.

For each of the identified building typology, the corresponding percentage in number of buildings for test beds 'Mussoorie' and 'Nainital' has been reported. The typical plan layout, building height, storey ratio, storey heights and hill slope angle have also been identified for further use in the numerical study.

2.2 TEST BED CITIES: MUSSOORIE AND NAINITAL

For the present study, extensive field surveys were conducted in the cities of 'Mussoorie' situated in the foothills of 'Garhwal Himalaya' ranges, and 'Nainital' situated in the 'Kumaon foothills' of the outer Himalayas, both situated in the state of Uttarakhand in the Indian Himalayas. The cities are shown on the seismic zoning map of India (Fig. 2.1). Both the cities are located in seismic zone IV as per the seismic zoning map of India. Indian seismic design code (IS 1893 Part 1 2016) assigns an EPGA of 0.24g to this zone.
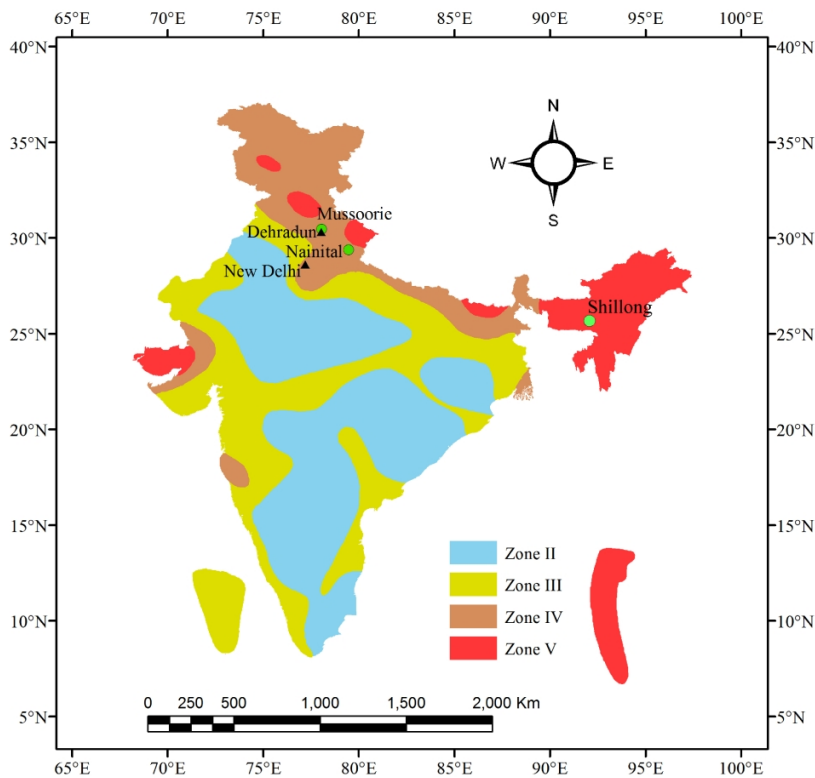
Fig. 2.1 Seismic zoning map of India along with the location of the test beds (Mussoorie and Nainital) shown relative to the state capital (Dehradun) and the national capital (New Delhi). In addition, Shillong site has also been shown in figure which has been used in numerical study.

Figure 2.2 presents the satellite imagery of the test bed cities. It can be observed that both the test beds are highly characterized by hilly topography (Fig. 2.2). The details of the test bed

cities including their distances from the national and the state capitals, average and highest altitude, population and topographical situation are presented in Table 2.1.

(a)

(b)

Fig. 2.2 Study area: (a) Satellite imagery of Mussoorie city; and (b) Satellite imagery of Nainital city. (Source: Google earth, for Fig. 2.2(a) and 2.2(b)).

Figure 2.3 presents a close view of the building stock in 'Mussoorie' and 'Nainital' cities. It can be observed that in 'Mussoorie' city, the buildings are mainly constructed on ridges, whereas in 'Nainital' city, the buildings are mainly constructed on slopes or at the base of a hill feature. Reasons for choosing these two cities for the described study are manifold: both cities exhibit a significant seismic risk potential which is the result of their seismic hazard situation, an increased vulnerability of their building stocks, and their socio-economic characteristics.

Most importantly, the majority of buildings in both the cities are located on sloped terrain, representing the intrinsic seismic vulnerability of typical hill buildings.

Table 2.1 Details of test bed cities.

| Test bed city | Distance (km) | | Average Elevation (m) | Highest Elevation (m) | Highest Point | Population (Census 2011) | Topographical Situation |
	From The National Capital	From The State Capital					
Mussoorie	290	35	1876	2275	Lal Tibba	30, 118	Spread over a number of inter-connected ridges with availability of hard competent rock
Nainital	300	283	2084	2616	Naina Peak	41, 377	Located on slope and base of a hill feature, on deep soil deposits around a pear-shaped lake

(a)

(b)

Fig. 2.3 Study area: (a) A close view of building stock in 'Mussoorie' – buildings located mostly on ridges; and (b) A close view of building stock in 'Nainital' – buildings located mostly on slopes and at the base of a hill feature.

In addition, it may be stated that both cities are quite important for state revenues, since both are among the most popular tourist destinations in the state of Uttarakhand, if not entire India. This circumstance leads to large seasonal variations in the cities' populations between peak season (from April to October) and off-peak season (November to March).
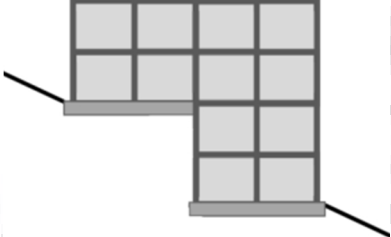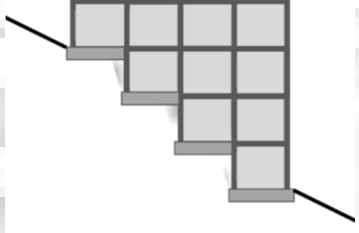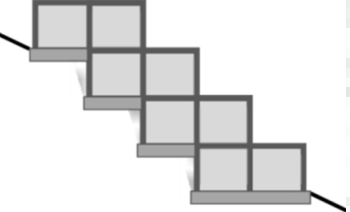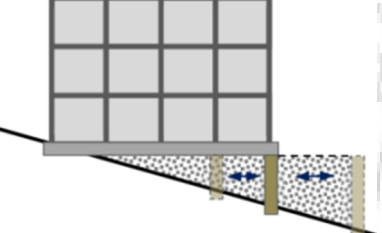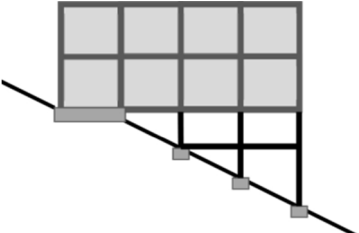
2.3 IDENTIFICATION OF MODEL BUILDING TYPOLOGIES IN INDIAN HIMALAYAS

2.3.1 Structural Configurations Based on Level of Foundations

During the field surveys in the two test beds, the various prevalent structural configurations of buildings on slopes were identified. In principle, a total of six different structural configurations are identified which are presented in Table 2.2. This classification is primarily based on the relative levels of foundations, and the slope-retaining system, if present.

Structural configuration A is similar to a building resting on the flat land. These types of buildings were observed on very mild slopes, where the ground is almost flat or can be made flat very easily. Contrary to this, structural configuration B has been observed where very steep slopes exist, and in such cases the foundations are provided at two largely different levels. This structural configuration is observed where hard rock is available since such steep slopes are not stable in soil deposits. Structural configuration C is the most common structural configuration in which the building follows the natural slope of the ground. This structural configuration is used for building construction in areas where mild to moderate slopes exist. Structural configuration D is an enhancement of configuration C, in which set-backs are provided, which improves the structural stability of the buildings. Structural configurations E and F are special configurations, in which either an artificial platform is created on the downhill side or stilts are provided to support the building. Except for SC A and SC E, all configurations are characterized by a highly irregular distribution of mass, stiffness, and strength in the horizontal direction and along the height of the building, which leads to horizontal as well as vertical irregularities increasing their susceptibility to suffer damage or even collapse under earthquake excitation. Figure 2.4 presents the details of the surveyed buildings based on the strucutral configurations, as identified in Table 2.2. It can be observed that structural configurations A and C are in abundance, and combinely cover approximately 95% of buildings in both the test beds 'Mussoorie' and 'Nainital'.

Table 2.2 Structural configurations with respect to foundation levels and slope-retaining systems.

Structural configuration	Description	Combination with structural typologies
SC A	Similar to buildings resting on flat land Observed on slopes of low inclinations, where the ground is almost flat or can be made flat very easily with little cutting and/or filling of soil/rock	All
SC B	Observed where very steep slopes exist and in such cases the foundations are provided at two different levels Foundation system is invariably associated with competent rock ground conditions as such steep slopes are not stable in soil and highly weathered rock	RC only
SC C	Most common structural configuration where the building follows the natural slope of the ground Structural configuration is used for building construction in the areas where low- to moderately-inclined slopes exist	All
SC D	Enhancement of SC C where set-backs are additionally provided in the building superstructure, thereby improving the building's structural stability	RC only
SC E	A platform is artificially created, by filling and retaining soil on the downhill side	Masonry and RC
SC F	Multiple storey height stilts are provided on downhill side to support the building superstructure	RC only
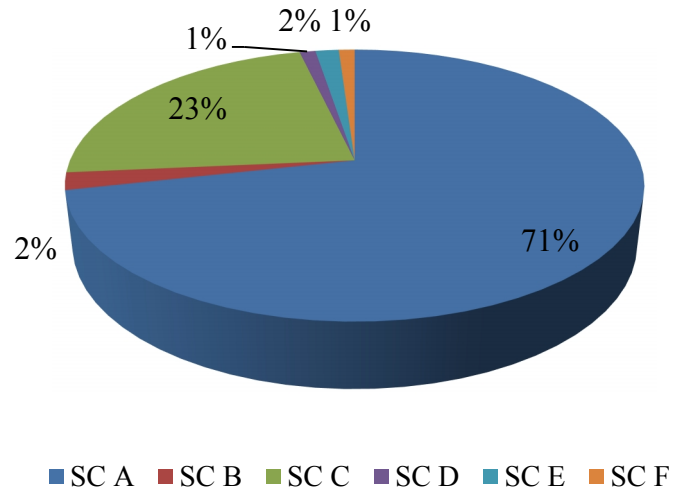
(a) Mussoorie
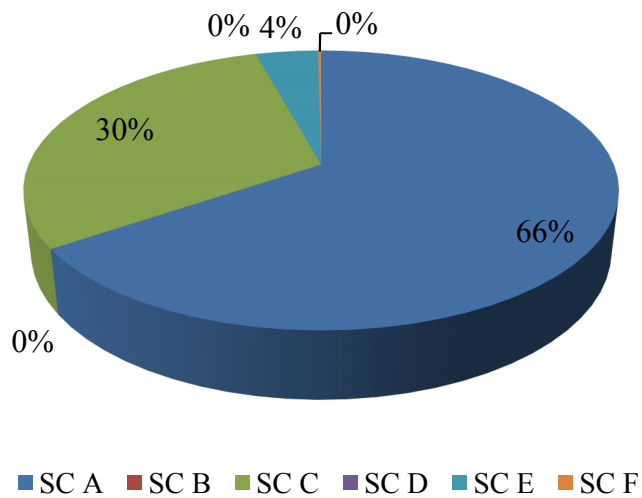
(b) Nainital

Fig. 2.4 Surveyed building details based on structural configurations, including all typologies.

2.3.2 Development of Building Stock Inventory Database for Test Beds

In order to develop the building stock inventory for the cities of 'Mussoorie' and 'Nainital', extensive field surveys were conducted by several teams each consisting of two or more surveyors. The *Stratified Random Sample Survey* technique (Burt and Barber 1996, Prasad et al. 2009) was adopted. In this technique, the whole area of a city/town is subdivided into different clusters based on occupancy of the buildings (e.g., residential, commercial, hotel etc.) and socio-economic level (e.g., slum, low-income, middle-income etc.). In each of these identified clusters, about 10% randomly selected buildings were surveyed. Footprints of all the

buildings in the study area were obtained from Google Earth satellite imagery. The sample ground survey data and the building footprints obtained from the satellite imagery were used to generate the building stock inventory.

Based on the preliminary field survey, a questionnaire was developed considering the existing topographic features and prevalent construction practices in the test beds. This questionnaire included location, year of construction, predominant use (occupancy type), structural configuration with respect to relative foundation levels, construction material, building height, structural (load-bearing) system, floor and roof type of the building, slope-retaining system (if any), and also the number of occupants residing during day and night time. A total of 392 and 585 buildings were surveyed in Mussoorie and Nainital, respectively, which correspond to approximately 10% of the total building stocks of the two test beds. Information about each of the surveyed buildings was collected in the developed questionnaire and the buildings were geographically mapped (georeferenced) using the proprietary Geographical Information System ArcGIS (ESRI 2011).

2.3.2.1 Classification of Buildings Based on Design Level

In both cities, 'Mussoorie' and 'Nainital', habitation started in the middle of the 18th century. During the field survey it has been observed that some of the buildings in the test beds are as old as 150 years. India's first seismic design code was published in 1962 and later revised in the years 1967, 1970, 1975, 1984, 2002, and 2016. A significant change in the earthquake resistant design methodology took place in the 2002 revision of the code, in which the concept of 'Response Reduction Factor' based on the expected inelastic energy dissipation capacity of the building was included. Recently, the Indian seismic design and detailing codes (IS 1893 Part 1 2016; IS 13920 2016) went under major revisions. The recent revision of Indian standard also includes the provisions of strong-column weak-beam (SCWB) design.

The implementation of seismic design codes in the Indian Himalayas, as in case of the rest of the country, is still lacking to a large extent. In this region, both building construction and city planning are controlled by the 'Urban Development and Housing Department', which also provides the building bye laws. The building bye laws are updated with progress in knowledge and the latest building bye laws (Uttarakhand Building Bye Laws 2011) restrict the maximum building height up to G+3 or 11.0 m, whichever is less, for 'Mussoorie' city; and up to 7.5 m,

in the case of 'Nainital' city. However, in the field survey some buildings even up to 20 m height were also observed. This also highlights the lack of implementation of building bye laws in the test beds.

The ideal method to classify the design level of buildings under different categories (e.g., pre-code, low-code, medium-code, high-code etc.) should be based on field checks for adequacy of the seismic design and detailing provisions. However, the unavailability of structural drawings with the owners/authorities makes it a very difficult task. Therefore, in the present study, only the year of construction has been used as the basis for classifying the building stock into three different "eras", viz., buildings constructed before 1962 (pre-code), between 1963-2002 (low-code), and between 2002-2016 (moderate-code). Due to the lack of implementation of seismic design codes, the presented classification based on the year of construction alone, is not adequate, but it presents a lower bound on percentage of 'pre-code' buildings and upper bound on percentage of 'moderate-code' buildings. The recent revision of Indian seismic design code (IS 1893 Part 1 2016) also does not cater to the specific aspects of hill buildings, buildings constructed as per this code are expected to show significantly better performance as compared to the buildings designed and constructed as per previous codes. Therefore, the buildings constructed after 2016 following recent Indian standards falls under the category of 'high-code' buildings. These high-code buildings were not observed during field survey and yet to be constructed since the field surveys were conducted prior to publications of IS 1893 Part 1 (2016) and IS 13920 (2016). However, these high-code buildings have also been included in numerical study (Chapters 4-7).

It can be observed that a majority of the surveyed buildings in 'Mussoorie' as well as in 'Nainital' are pre-code buildings (Fig. 2.5). As discussed earlier, the proportion of 'pre-code' buildings shown in Fig. 2.5 is only a lower bound estimate, and the actual percentage of 'pre-code' buildings is much higher, due to the non-implementation of seismic design and detailing codes.

2.3.2.2 Classification of Buildings Based on Material of Construction

Figure 2.6 presents the building distribution based on construction material for the cities of 'Mussoorie' and 'Nainital', respectively. It can be observed that in both the test beds, RC buildings are abundant covering approximately 50-60% of the total building stock. Further,

masonry buildings are also observed to be significant, whereas only very few adobe and wood buildings are observed.
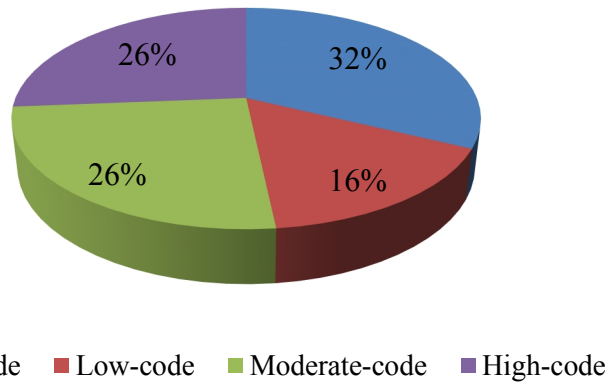
(a) Mussoorie
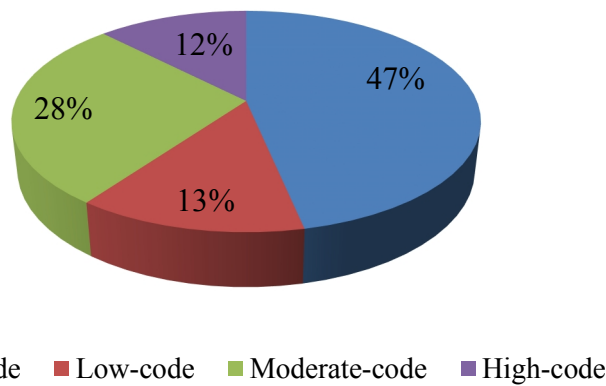
(b) Nainital

Fig. 2.5 Surveyed building details based on year of construction.

2.3.2.3 Classification of Buildings Based on Building Height

Figure 2.7 presents the building stock details in test beds based on the number of storeys above the uppermost foundation level. The building stock is classified considering the number of storeys above the uppermost foundation level, since the dynamic characteristics of these buildings are similar to buildings resting on flat land with number of storeys same as number of storeys above the uppermost foundation level (Singh et al. 2012). It can be observed that low-rise buildings (up to 3 storeys) are abundant and a few mid-rise buildings (4 to 7 storeys) are also observed. High-rise buildings (8 or more storeys above the uppermost foundation level level) are not observed at all.

Figure 2.8 presents the storey ratio (SR, defined as the ratio of the number of storeys below (N_b) to the number of storeys above (N_a) the uppermost foundation level) of the surveyed buildings. It is important to note here that the number of stories below the uppermost foundation level is governed by the slope angle and the building dimension along the slope direction. In the studied regions, the slope angles between 15-30 degrees are quite common and the building width is found to vary typically between 10-25 m. This indicates that 1-4 stories are located below the uppermost foundation level. On the other hand, the number of storeys above the uppermost foundation level varies between 1-6. Accordingly, the ratio N_b/N_a commonly varies between 0.2-2 (Fig. 2.8) for both the test beds.

(a) Mussoorie

(b) Nainital
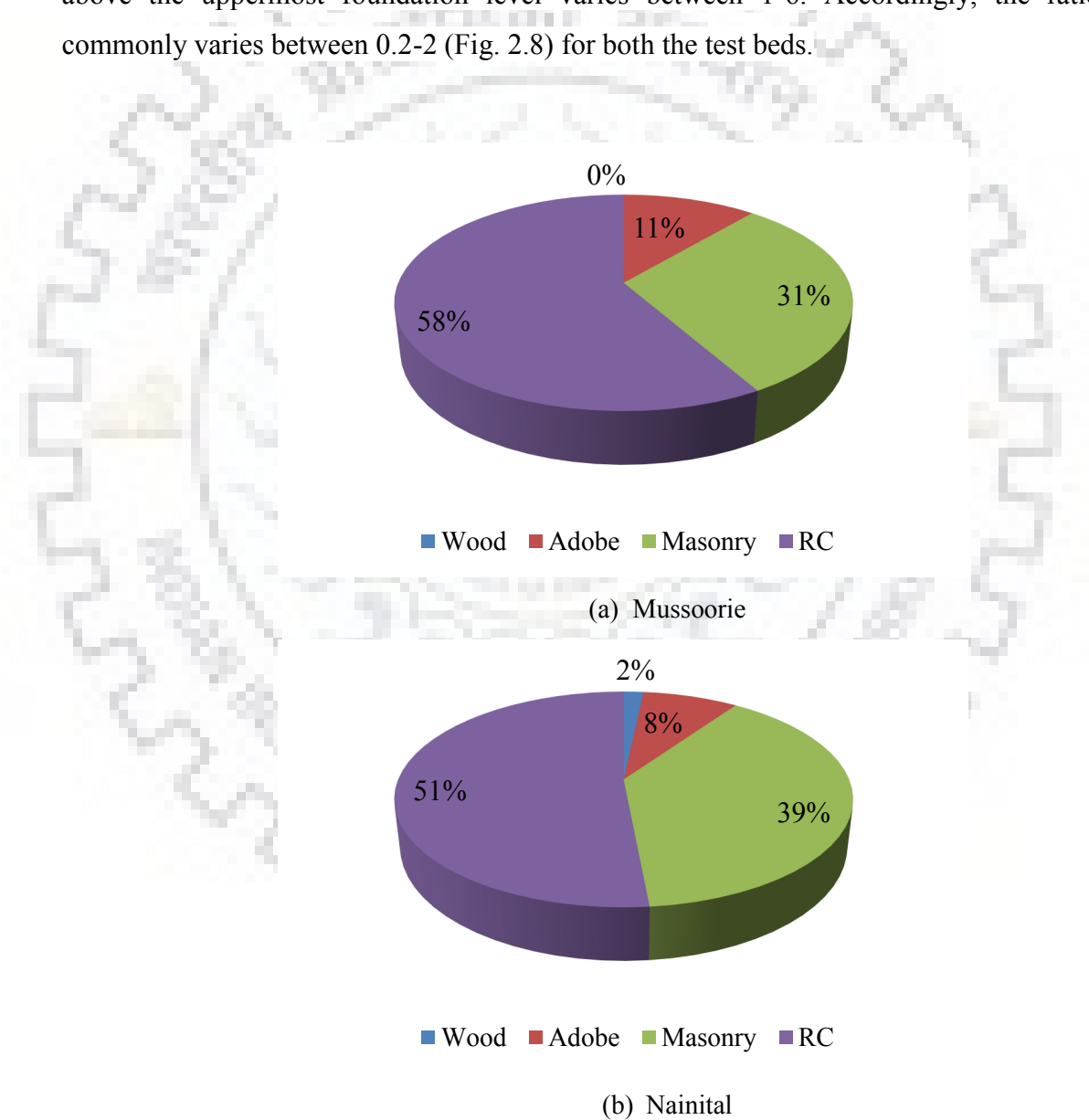
Fig. 2.6 Surveyed building details based on construction material.

2.3.2.4 Classification of Buildings Based on Occupancy Class

Figure 2.9 presents the occupancy class of the surveyed buildings. It can be observed that among the surveyed buildings, residential buildings are the most common occupancy class observed in the test beds. Hotel buildings are the second highest contributor to the occupancy class as both the test beds are popular tourist destinations. The third significant contributor has been found out to be residential and commercial (mixed) buildings, in which the storey just at the level of road is used for commercial purpose (e.g. shops) and remaining portion of the building is used for residential purpose.
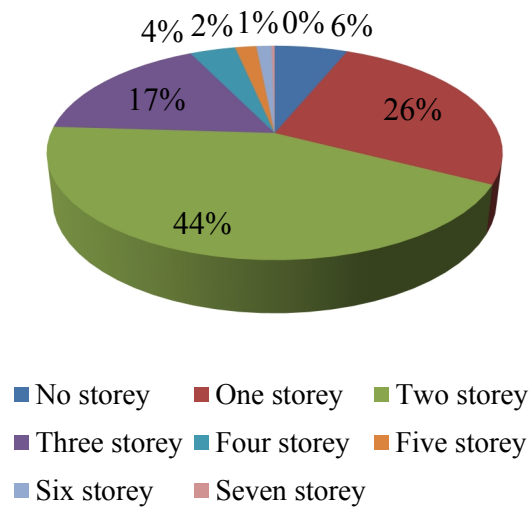
(a) Mussoorie
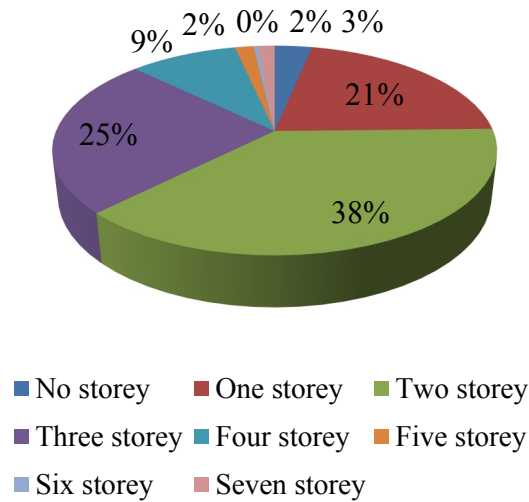
(b) Nainital

Fig. 2.7 Surveyed building details based on number of storeys above the uppermost foundation level.

2% 0% 1% 1% 3%
5%
2%
1%
13%
19%
3%
2%
1%
47%

■ SR_0.20 ■ SR_0.25 ■ SR_0.33 ■ SR_0.50 ■ SR_0.67
■ SR_0.75 ■ SR_0.80 ■ SR_1.00 ■ SR_1.25 ■ SR_1.33
■ SR_1.50 ■ SR_2.00 ■ SR_3.00 ■ SR_4.00

(a) Mussoorie

0% 2% 6%
4%
8%
0%
15%
11%
0%
0%
0%
0%
54%

■ SR_0.20 ■ SR_0.25 ■ SR_0.33 ■ SR_0.50 ■ SR_0.67
■ SR_0.75 ■ SR_0.80 ■ SR_1.00 ■ SR_1.25 ■ SR_1.33
■ SR_1.50 ■ SR_2.00 ■ SR_3.00 ■ SR_4.00
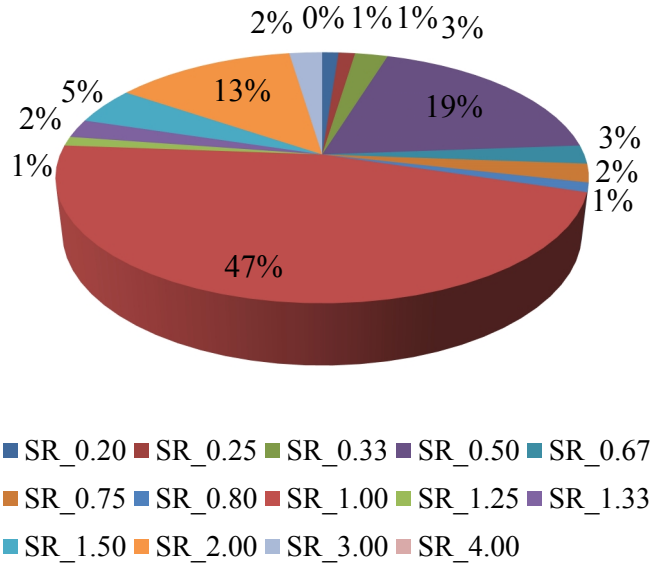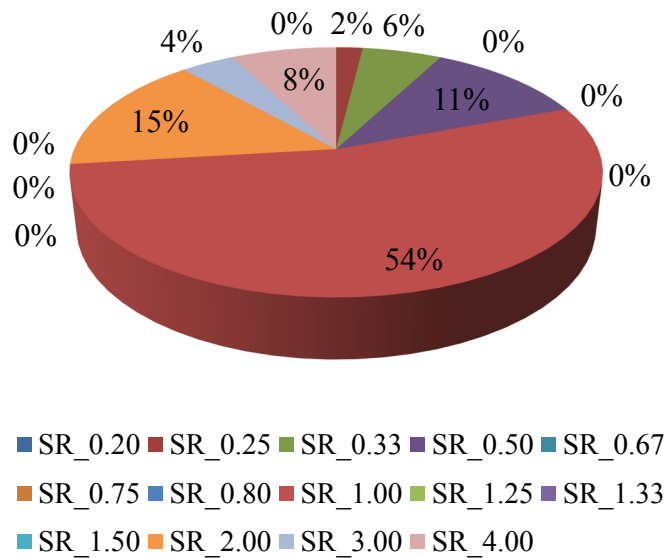
(b) Nainital

Fig. 2.8 Surveyed building details based on storey ratio.

2.3.2.5 Buildings on Slopes

Figure 2.10 presents the distribution of buildings surveyed in Mussoorie with respect to angle of slope on which the respective building is constructed. It can be observed that the majority of buildings are constructed on mild slope angles varying between 15-30 degrees. Further, a significant number of buildings are constructed on steep (45-60 degrees) and very steep slopes (>60 degrees) as well.

25

The trend is comparable with the distribution of slope of the land area in 'Mussoorie' city (Fig. 2.10). The figure indicates that almost 46% of Mussoorie's city area is characterized by slope angles between 15-30 degrees while approximately 31% of buildings are constructed on these mild slopes. It becomes further evident that approximately 1% of Mussoorie's land is characterized by very steep slopes (Fig. 2.10) with 10% of the building stock located on these slopes. The main reason for construction of such a significant fraction of buildings on steep slopes appears to be the availability of competent rock on steep slopes, making them suitable for stable foundations.

(a) Mussoorie

(b) Nainital
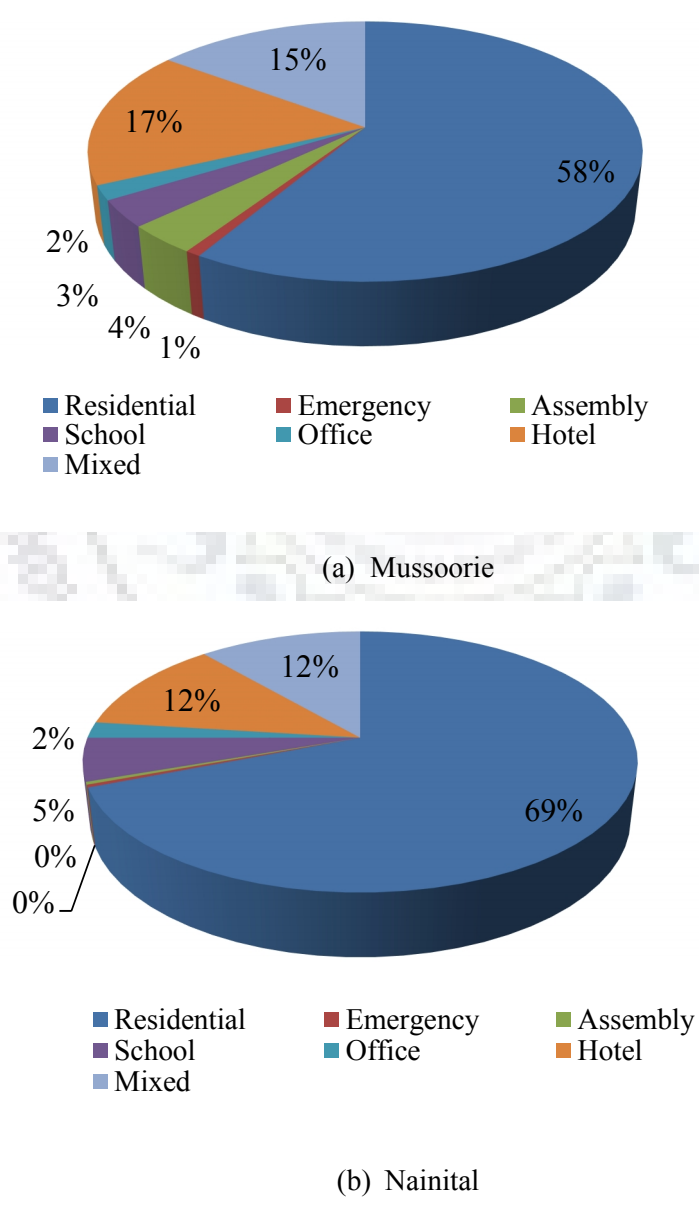
Fig. 2.9 Surveyed building details based on occupancy.
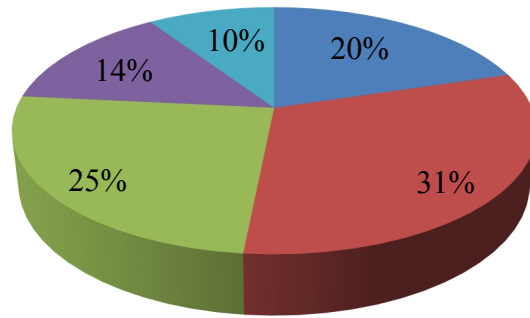
(a) Mussoorie, obtained from field survey
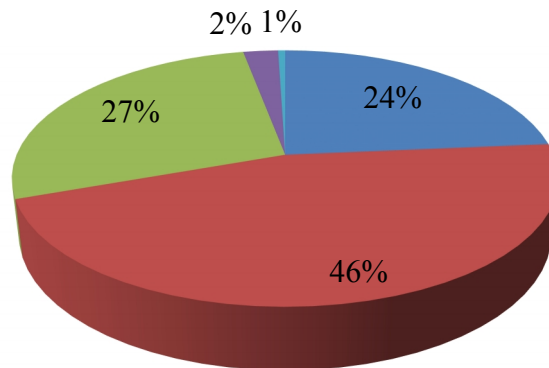
(b) Mussoorie, obtained from digital elevation model

Fig. 2.10 Surveyed building details based on slope angle (in degrees).

2.3.3 Identification using Alphanumeric Strings

In order to classify the buildings with similar characteristics, expected performance, and seismic vulnerability, each of the surveyed building has been assigned an alphanumeric string (typology code). This alphanumeric string takes into account the structural characteristics such as a building's structural configuration with respect to the slope (Table 2.2), number of storeys above the uppermost foundation level, material of construction, load-bearing structural system as well as floor and roof system, which primarily controls the expected performance and seismic vulnerability under earthquakes. The building height has been classified based on number of storeys above the uppermost foundation level. The building height classification has

been considered as per HAZUS (FEMA 2002) guidelines. Table 2.3 presents the definition of the alphanumeric strings used to assign the typology code to each of the surveyed buildings. Some of the surveyed buildings have been assigned a string based on the presented classification and are presented in Figs. 2.11 and 2.12.

Table 2.3 Description of the alphanumeric strings used to classify the building typologies.

Feature category	Sub-category	Label
Structural Configuration	Foundations of the entire building on the same level	A
	Building is founded on two different levels	B
	Step-back configuration	C
	Step-back and set-back configuration	D
	Building is (partly) founded on an artificially created platform that is supported by a retaining wall on the downhill side	E
	Parts of the building are supported by stilts on the downhill side	F
Building Height	Up to 3 storeys – Low-rise	L
	4 to 7 storeys – Mid-rise	M
	8 storeys and above – High-rise	H
Construction Material	Wood	TF
	Adobe/Stone	A
	Masonry	M
	Reinforced Concrete	RC
	Steel	S
Binding Material (Mortar) used in Adobe and Masonry	Mud Mortar	M
	Lime Mortar	L
	Cement Mortar	C
Type of units in Masonry Walls/Infills	Bricks (Clay)	BM
	Concrete Blocks	CB
	Rectangular Stone	RS
Roofing System	Heavy sloping roofs-stones/burnt clay tiles/thatch on sloping rafters	R1
	Heavy flat flexible roof-wooden planks, stone/burnt clay tiles supported on wooden/steel joists with thick mud overlay	R2
	Light sloping roofs-corrugated asbestos cement or GI sheets on sloping rafters without cross bracing	R3
	Trussed roof with light-weight sheeting (without cross bracing)	R4
	Trussed/hipped roof with light-weight sheeting (with cross bracing)	R5
	Rigid reinforced-concrete or reinforced-masonry slab	R6

(a) AL-AM-R3

(b) AL-MC-R3

(c) AL-MC-R3

(d) CL-AL-R3

Fig. 2.11 Typology codes for some of the surveyed adobe and masonry buildings.

(a) CL-RCBM-R6

(b) DL-RCBM-R6

(c) EL-RCBM-R3

(d) FL-RCBM-R6

Fig. 2.12 Typology codes for some of the surveyed RC buildings.

2.3.4 Building Typologies in 'Mussoorie' and 'Nainital' Towns

In total 57 building typologies, as presented in Table 2.4 (the two numbers in parentheses against each typology represent the % of the buildings falling under a particular typology for Mussoorie and Nainital, respectively), could be identified for the study area using the developed classification scheme. Out of the 57 identified typologies, 28 typologies belong to the structural configuration SC A (71.0% and 64.4% of the observed buildings in Mussoorie and Nainital, respectively) and are similar to the buildings located on flat land. The remaining 29 typologies are significantly different than buildings resting on flat land, out of which 18 typologies (25.4% and 29.8% of the observed buildings in 'Mussoorie' and 'Nainital', respectively) have structural configurations SC B or SC C, where buildings follow the natural slope of the ground. In total, structural configurations SC A, SC B and SC C cover 46 typologies and 96.4% and 94.2% of the observed building stock of 'Mussoorie' and 'Nainital', respectively. As highlighted in the previous sections (Section 2.3.2.2), both 'Mussoorie' and 'Nainital' have an abundance of RC buildings, predominantly of structural configurations SC A, SC B and SC C which cover approximately 50% of the total building stock. These RC buildings with structural configurations SC A, SC B and SC C have been further used for numerical study.

Figure 2.13 shows the plan dimensions of the surveyed RC buildings with structural configuration SC A, SC B and SC C, for the city of Mussoorie. The longer and shorter plan dimensions of the buildings have been plotted along their length and width, respectively. The dark blue circle in the figure represents the plan dimension of the building which has been further used for the numerical study presented in Chapters 3-7.
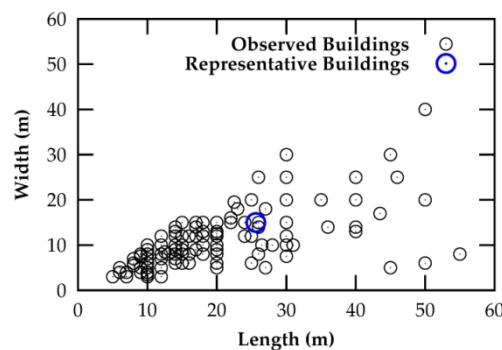
Fig. 2.13 Plan dimensions of the surveyed RC buildings in Mussoorie with structural configurations SC A, SC B and SC C. (The longer dimension is marked as the building's length whereas the shorter dimension is referred as the building's width).

Table 2.4 Observed building typologies.

Structural Configuration	Building typologies and corresponding percentage (Mussoorie, Nainital)[a] in total number of buildings							
	Wood		Adobe		Masonry		Reinforced-concrete	
SC A	AL-TF-R2	(0.00, 0.20)	AL-AM-R2	(1.29, 0.40)	AL-MM-R2	(0.51, 0.00)	AL-RCBM-R6	(30.51, 26.39)
	AL-TF-R3	(0.00, 0.20)	AL-AM-R3	(1.03, 0.00)	AL-MM-R3	(0.51, 0.40)	AM-RCBM-R6	(2.05, 3.96)
	AL-TF-R4	(0.00, 0.20)	AL-AL-R2	(1.80, 0.40)	AL-ML-R2	(2.05, 0.79)	AL-RCCB-R6	(2.30, 0.00)
			AL-AL-R3	(2.31, 0.40)	AL-ML-R3	(1.54, 5.16)	AM-RCCB-R6	(0.26, 0.00)
			AL-AL-R6	(0.77, 0.79)	AL-ML-R6	(2.05, 3.37)	AL-RCRS-R6	(0.77, 0.00)
			AL-AC-R2	(0.51, 0.38)	AL-MC-R2	(0.00, 1.78)	AM-RCRS-R6	(0.26, 0.00)
			AL-AC-R3	(0.26, 0.59)	AL-MC-R3	(3.84, 2.77)		
			AL-AC-R6	(0.77, 1.78)	AL-MC-R4	(0.77, 0.00)		
					AL-MC-R6	(14.35, 12.29)		
					AM-MC-R2	(0.00, 0.59)		
					AM-MC-R6	(0.51, 1.58)		
SC B	Not observed						BL-RCBM-R6	(2.05, 0.00)
SC C	CL-TF-R2	(0.00, 0.59)	CL-AM-R2	(0.26, 0.00)	CL-MM-R6	(0.26, 0.00)	CL-RCBM-R6	(11.28, 17.45)
			CL-AM-R3	(0.51, 0.00)	CL-ML-R2	(0.26, 0.00)	CM-RCBM-R6	(2.56, 2.18)
			CL-AL-R2	(0.00, 0.20)	CL-ML-R3	(1.03, 0.40)	CL-RCCB-R6	(0.51, 0.00)
			CL-AL-R3	(1.29, 0.20)	CL-ML-R6	(0.77, 0.40)	CL-RCRS-R6	(0.26, 0.00)
			CL-AC-R2	(0.51, 0.00)	CL-MC-R3	(1.54, 2.57)		
					CL-MC-R6	(2.30, 5.36)		
					CM-MC-R2	(0.00, 0.40)		
SC D	Not observed						DL-RCBM-R6	(0.77, 0.00)
							DM-RCBM-R6	(0.26, 0.00)
SC E	Not observed				EL-ML-R2	(0.26, 0.00)	EL-RCBM-R6	(0.77, 1.78)
					EL-ML-R3	(0.26, 0.59)	EM-RCBM-R6	(0.00, 0.20)
					EL-ML-R6	(0.26, 0.59)		
					EL-MC-R3	(0.00, 0.20)		
					EL-MC-R6	(0.00, 0.40)		
SC F	Not observed						FL-RCBM-R6	(0.77, 0.00)
							FM-RCBM-R6	(0.26, 0.20)

[a]The two numbers in parentheses represent the % of buildings falling under a particular typology, in Mussoorie and Nainital, respectively.

2.4 SUMMARY

Extensive field surveys were conducted in the two test beds 'Mussoorie' and 'Nainital', both located in seismic zone IV as per the current seismic zonation map of India. The major observations from the data collected through field survey are as follows:

- Structural configurations SC A, SC B and SC C are predominantly used, which approximately cover 95% of the building stock in both the test beds.

- A majority of the buildings are observed to be 'pre-code' buildings, approximately 33% in 'Mussoorie' and 48% in 'Nainital'.

- The reinforced-concrete (RC) buildings are predominantly used in the studied region, covering approximately 55% buildings in both the test beds.

- Low-rise buildings are often observed in hilly regions, with the most common storey ratios (N_b/N_a) of 0.50, 1.00 and 2.00.

- Most of the buildings are located on mild to moderate slopes ranging from 0-45 degrees. However, some buildings are constructed on very steep slopes as well.

From the collected field data, it has been observed that RC buildings with structural configurations A, B and C cover 52.81% and 49.98% of the building stock in 'Mussoorie' and 'Nainital'. Therefore, these structural configurations have been further used for detailed analytical vulnerability assessment study in the Chapters 3-7.

SEISMIC RESPONSE EVALUATION OF BUILDINGS

3.1 INTRODUCTION

Estimation of seismic response of a building in context of seismic design, performance, and vulnerability assessment, is a complex issue. A reliable estimation of the seismic response requires adequate modelling of the building's strength, stiffness and ductility capacity. In this Chapter, the following issues in context of the evaluation of non-linear seismic response are reviewed:

- analytical procedures for evaluating the seismic response of buildings,
- guidelines for modelling stiffness of the RC members,
- prevalent failure modes in RC frame buildings,
- non-linear models to simulate the flexure failure and shear failure for RC members,
- deterioration modes of RC members under reverse cyclic loading effects,
- modelling of damping effects in RC frame buildings for non-linear dynamic analysis,
- selection and scaling of ground-motion records for non-linear dynamic analysis.

Based on the reviewed literature and available guidelines, a detailed numerical study is performed for RC frame buildings designed for Indian codes. Both, the non-linear static and the non-linear dynamic analyses are performed on considered building models. Further, a methodology is presented for comparing the static and dynamic capacity curves.

3.2 PROCEDURES FOR SEISMIC RESPONSE EVALUATION

In earthquake engineering practice, several methods are available in order to compute the design forces and seismic response of structures. Selection of appropriate procedure for design and performance assessment can be considered as an application-specific task. In general, the seismic response of a structure can be estimated using either linear or non-linear modelling in combination with static or/and dynamic procedures, as presented in Fig. 3.1.

The *linear static analysis procedure* is the simplest procedure which is based on a single mode of vibration of the structure; hence, it is applicable to particularly regular (i.e. simple) structures only. This method is also known as Equivalent Lateral Force (ELF) procedure or lateral force

method. The commonly used ***linear dynamic procedure*** is based on response spectrum and relies on the assumption that the dynamic response of a multi-degree-of-freedom (MDOF) system can be identified in each mode of vibration independently and then can be combined using a suitable combination rule (such as *Absolute sum*, *Square Root of Sum of Squares* or *Complete Quadratic Combination*). However, the selection of the combination rule also plays an important role. It has been proven that the absolute sum combination rule is not appropriate since the respective peaks of all modes of vibration will not occur simultaneously. In a similar manner, the SRSS combination rule may not predict the actual response for systems which have closely spaced modes of vibration. In another form, this procedure utilizes actual or synthesized ground-motion records, and is also known as ***linear time-history analysis (LTHA)***.
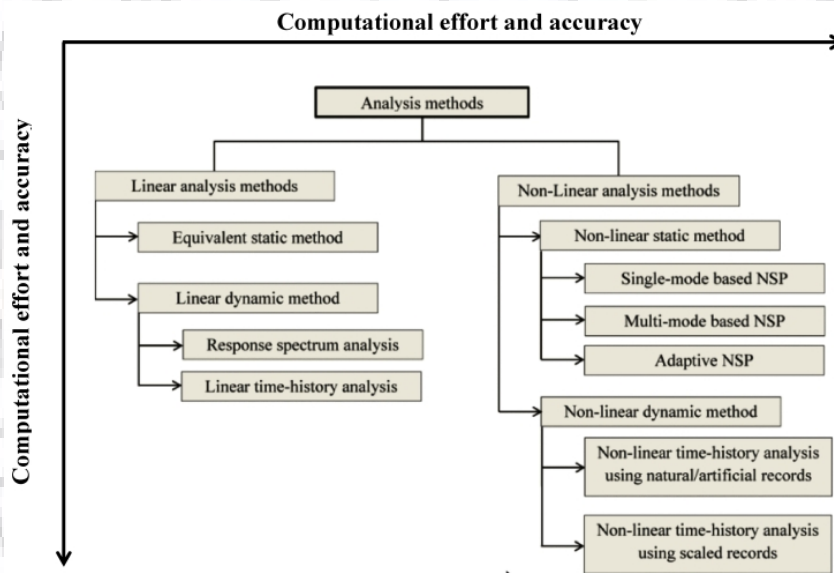
Fig. 3.1 Analysis methods for seismic response evaluation of structures.

The ***non-linear static (pushover) procedure*** is the simplest form of non-linear analysis in which the structure is pushed with a predefined incrementally increasing lateral loading pattern while the structure's horizontal displacement is recorded. This method is able to identify the weak links in the structure as well as provides the insight into non-linear behaviour of the structure.

The ***non-linear time-history analysis (NLTHA)*** is the most rigorous procedure available for computation of seismic forces and displacements of structures. This procedure involves step-wise solution of the equation of motions of the MDOF system. The method requires a suite of ground-motion time histories, which may be real (recorded) or artificially generated (simulated)

accelerograms. Out of this time varying response, the peak response parameters are of primary interest from seismic design point of view. Therefore, these peak response parameters are gathered as an output of the individual NLTHA. The design seismic response of a structure is estimated as its median/mean response if more than seven ground-motion records are used, while its maximum response is considered in case fewer than seven records are used.

In the early 1990's, both non-linear static and non-linear dynamic procedures were mostly used by researchers only (Jangid and Datta 1999). However, with the technological advancements and enhancement in computational power in the past two decades, non-linear methods became quite popular in the structural design consultancy industry as well. As the design practice moves from linear static to non-linear dynamic procedures, the reliability of the computed forces and displacements increases significantly, but the computational efforts increase drastically (Fig. 3.1). Hence, it becomes necessary to find out an amicable balance between the computational effort and accuracy.

3.3 MODELLING OF STIFFNESS OF RC MEMBERS

Prediction of the force-deformation behaviour of structures requires appropriate modelling of stiffness of RC members. Under severe earthquake excitation, RC members are expected to undergo large inelastic deformations in order to dissipate the energy imparted to the structure, which primarily results in the cracking of RC members. The reliable estimation of the effective stiffness of the RC members under reverse cyclic loading is a complex and crucial issue in context of the 'Force-based design' (FBD) as well as 'Performance-based design' (PBD). A widely varying opinion among different building codes, standards and researchers exists regarding effective stiffness of RC members. The common consensus is that the effective stiffness of a RC member depends on axial load (Elwood et al. 2007; Haselton et al. 2007; ASCE 41-13, 2013), reinforcement ratio (Khuntia and Ghosh 2004), eccentricity ratio (Mirza 1990; Khuntia and Ghosh 2004), yield strength of longitudinal reinforcement bars (Elwood and Eberhard 2009), bond slip of reinforcement bars (Elwood and Eberhard 2009), and shear span (Mirza 1990; Elwood and Eberhard 2009) of the member. In order to consider the intrinsic uncertainties in the estimation of effective stiffness of RC members, most of the seismic design codes (i.e. IS 1893 2002; ASCE 7 2010, and NZS-1170.5 2004) recommend a capping on the

design period of buildings, ensuring design for a minimum base shear as a safeguard against unrealistic/assumed stiffness estimates.

The guidelines for modelling stiffness of RC members as provided in different codes are reviewed and presented in Table 3.1. Both, ACI 318M (2014) and Eurocode 8 (CEN 2004) recommend 50% of gross moment of inertia to be considered as effective for beams and columns. ASCE 41-06 (2007) considers the effect of axial loads on the effective stiffness of columns and recommends effective stiffness of RC members considering flexure, shear and axial action. The same stiffness properties recommendations are also adopted by IS 15988 (2013). The recent revision of Indian standard (IS 1893 Part 1 2016) considers the effect of cracking and recommends 35% and 70% of gross moment of inertia to be considered as effective for beams and columns, respectively.

Table 3.1 Stiffness recommendations for beams and columns.

Reference / Standard	Stiffness recommendations	
	Beams	Columns
Eurocode 8 (CEN 2004)	$0.50 \times E_c I_g$	$0.50 E_c I_g$
ASCE 41-06 (2007)	$0.50 \times E_c I_g$	Columns with design gravity loads, $P \geq 0.5 A_g f_c'$, $0.70 E_c I_g$ Columns with design gravity loads, $P \leq 0.3 A_g f_c'$, $0.50 E_c I_g$ For intermediate design gravity loads, linear interpolation is permitted.
IS 15988 (2013)	$0.50 \times E_c I_g$	Columns with design gravity loads, $P \geq 0.5 A_g f_c'$, $0.70 E_c I_g$ Columns with design gravity loads, $P \leq 0.3 A_g f_c'$, $0.50 E_c I_g$ For intermediate design gravity loads, linear interpolation is permitted.
IS 1893 Part 1 (2016)	$0.35 \times E_c I_g$	$0.70 \times E_c I_g$
Haselton et al. (2007)	$EI_y = 0.20 \times E_c I_g$ $EI_{stf40} = 0.35 \times E_c I_g$	$\dfrac{EI_y}{EI_g} = 0.065 + 1.05 \dfrac{P}{A_g f_c'}$, where $0.2 \leq \dfrac{EI_y}{EI_g} \leq 0.60$ $\dfrac{EI_{stf40}}{EI_g} = 0.17 + 1.61 \dfrac{P}{A_g f_c'}$, where $0.35 \leq \dfrac{EI_{stf40}}{EI_g} \leq 0.80$
ASCE 41-13 (2013)	$0.30 \times E_c I_g$	Columns with design gravity loads, $P \geq 0.5 \times A_g f_c'$, $0.70 \times E_c I_g$ Columns with design gravity loads, $P \leq 0.1 \times A_g f_c'$, $0.30 \times E_c I_g$ For intermediate design gravity loads, linear interpolation is permitted.
ACI 318M (2014)	$0.50 \times E_c I_g$	$0.50 \times E_c I_g$

E_c is the modulus of elasticity of concrete, I_g is the moment of inertia of the gross concrete section, A_g is the gross cross-sectional area, f_c' is the compressive strength of concrete, EI_y is the secant value of effective stiffness to the yield point of the component, EI_{stf40} is the secant value of effective stiffness to 40% of the yield force and P is the design gravity load on the column.

Haselton et al. (2007) also provided guidelines to estimate the effective stiffness of the RC members. During experimental investigations, it has been observed that the stiffness of RC members is very sensitive to the applied axial loads. Haselton et al. (2007) defined two different values of effective stiffness of RC members considering the secant value of effective stiffness to the yield point of the component (EI_y), and the secant value of effective stiffness to 40% of the yield force (EI_{stf40}). Furthermore, it was identified that the ratio between these two definitions of effective stiffness are approximately of the order of two. ASCE 41-13 (2013) provided stiffness recommendations which are based on a study by Elwood et al. (2007). ASCE 41-13 guidelines include all significant components of deformations.

It can be observed (Table 3.1) that significant variation exists among the different stiffness recommendations of the different design codes. One of the primary factors to this variation in stiffness prediction is the experimental database which is used to develop these prediction equations. The secondary contributor to this difference is the fact which types of deformations are accounted for. For example, the stiffness recommendations provided in FEMA 356 (2000) and ASCE 41-13 (2013) vary significantly, even though they were developed from the very same database. The main reason may be that the stiffness recommendations of FEMA 356 do not account for bond-slip deformations. In the present study, the stiffness guidelines of ASCE 41-06 (2007) and ASCE 41-13 (2013) have been used for modelling of RC frame members.

3.4 MODELLING OF BEAM-COLUMN JOINTS

Modelling of RC beam-column joints is another complex task in seismic response estimation. Pagni and Lowes (2004) suggested that the strength, stiffness, and deformation capacity are the main parameters which affect the joint damage (Brown and Lowes 2006). In literature, several approaches, including lumped-plasticity models (Otani 1974), multi-spring models (Biddah and Ghobarah 1999), and the finite element approach (Lowes and Altoontash 2003) have been proposed for modelling of joints in RC frames.

The present study concentrates on Gravity Load Designed (GLD) and Special Moment Resisting Frame (SMRF) buildings. In the considered building models, the joint flexibility is modelled implicitly as per the recommendation provided in ASCE 41-13 (2013). Figure 3.2 presents the modelling recommendations provided by ASCE 41 to model the joint flexibility. In

this methodology, if the strength of all columns meeting at a certain joint is greater than 1.2 times of the strength of all beams meeting at the very same joint, the column offsets are modelled as rigid. On the contrary to this, if the strength of all columns meeting at a joint is less than 0.8 times of the strength of all beams meeting at the very same joint, the beam offsets are modelled as rigid. For those cases that may fall in between the above defined conditions, half of the beam and half of the column offsets are modelled as rigid. The same has been used in this study.

$$\Sigma M_{nc} / \Sigma M_{nb} > 1.20 \qquad \Sigma M_{nc} / \Sigma M_{nb} < 0.80 \qquad 0.80 \leq \Sigma M_{nc} / \Sigma M_{nb} \leq 1.20$$
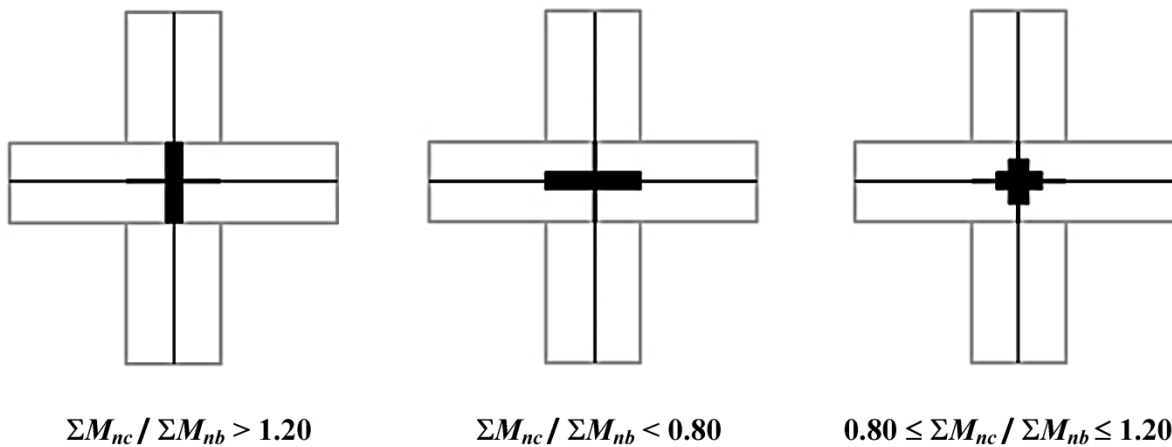
Fig. 3.2 Implicit modelling of beam-column joints as per ASCE 41 provisions.

3.5 IDENTIFICATION OF FAILURE MODES

In the present study, the investigated building models consist of RC frame buildings. In this section, the important contributors to collapse of the RC frame buildings are discussed. Figure 3.3 presents the potential collapse modes of RC frame buildings as suggested in FEMA P695 project. The Indian seismic design code (IS 1893 Part 1 2016) considers two classes of RC frame structural systems, i.e., Ordinary moment resisting frame (OMRF) buildings and Special moment resisting frame (SMRF) buildings. Further, it is mandatory to use SMRF buildings in high seismic zones (viz. zones III, IV and V) as per the requirements of the Indian seismic design code (IS 1893 Part 1 2016). All buildings studied in the present study consist of either 'pre-code' (GLD) or 'moderate-code' and 'high-code' (SMRF) buildings and therefore important contributors to the collapse performance of 'pre-code' and 'moderate-code' and 'high-code' buildings are discussed in this section.

3.5.1 Considered Failure Modes in the Present Study

The governing collapse mode primarily depends on the design and reinforcement detailing of the structural systems (FEMA P695 2009). The design and detailing guidelines for 'moderate-code' and 'high-code' buildings are developed to promote the ductile collapse modes, by using capacity design principles for prevention of brittle collapse modes. It has been already identified that, compared to SMRF buildings, OMRF and gravity load designed (GLD) buildings are highly vulnerable (Kunnath et al. 1995; Filiatrault et al. 1998) to a wide range of collapse modes. Kunnath et al. (1995) and Filiatrault et al. (1998) identified soft storey/column hinging mechanisms as the main failure mechanisms for OMRF and GLD buildings. In addition, these buildings are susceptible to pull-out of the reinforcing bars, joint shear failure and column shear failure.
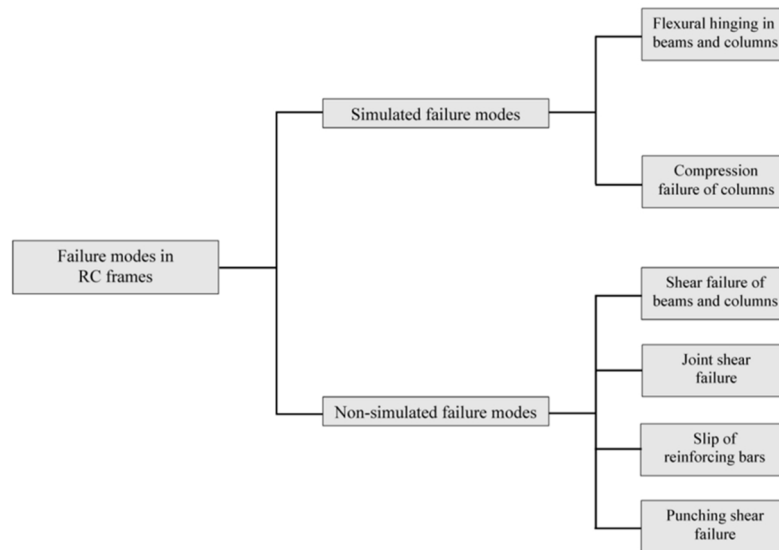
Fig. 3.3 Common failure modes in RC frame buildings.

In this study, in case of 'pre-code' buildings, both the shear and flexural failures have been considered whereas in case of 'moderate-code' and 'high-code' buildings only flexural failure has been considered, as in these buildings, the shear failure of beams and columns is controlled by applying capacity design principles. The bond-slip failure mode is accounted for through the calibration of the hinge model and therefore has not been simulated explicitly for collapse assessment. In addition, in the 'pre-code' and 'moderate-code' and 'high-code' buildings, compression-flexure failure of columns has also been identified as the predominant collapse mode (FEMA P695 2009).

3.6 NON-LINEAR MODELLING AND SIMULATION OF IDENTIFIED FAILURE MODES

The reliable estimation of the non-linear seismic response of the buildings requires careful selection of the component model, acceptance criteria, cyclic deterioration models, modelling of energy dissipation through the use of appropriate damping, and consideration of the P-delta (P-Δ) effects. All these factors are further discussed in detail in this section.

3.6.1 Types of Non-Linear Models

The non-linear models to simulate the behaviour of RC frame members can be categorized into three different categories (PEER ATC-72-1 2010):

(i)   Continuum model,

(ii)   Distributed inelasticity (fiber) model, and

(iii)   Lumped-plasticity model.

A continuum model primarily consists of the non-linear behaviour of the elements that comprise the component. It consists of finite elements which represent concrete, and longitudinal and transverse reinforcement. Each of the elements follows the respective material constitutive laws. These continuum models do not require definition of member strength, stiffness and deformation capacities as these effects are captured inherently through material properties. The distributed plasticity models capture some behaviour explicitly such as the integration of flexural stresses and strains through the cross-section, and other effects implicitly, such as the effective stress-strain behaviour of concrete as a function of confinement (e.g. Rosso et al. 2017). The continuum and distributed inelasticity models can accurately capture the effects such as cracking of concrete and yielding of reinforcement bars but they are unable to capture the strength degradation effects such as reinforcement bar buckling, bond-slip and shear failure causing strain softening, which are more critical for the structure's collapse assessment (PEER ATC-72-1 2010).

The lumped-plasticity models are defined by concentrating inelasticity at a predefined point for simulating a component's force-deformation behaviour. The plastic deformations used as the governing parameter in lumped plasticity models is a more stable parameter in order to define damage or deformation capacity as compared to the material strains used in continuum and

distributed inelasticity models, which vary largely depending upon member dimension, longitudinal reinforcement and material properties (Kazaz et al. 2012). Further, the different performance limit states are also usually specified in terms of the plastic rotation (e.g., ASCE 41 2013) associated with the members; that is why the lumped-plasticity models are preferred over the continuum and distributed inelasticity models and are used in the present study.

3.6.1.1 Lumped-Plasticity Models

In the context of performance-based earthquake engineering, the lumped-plasticity models are used extensively. The component behaviour (back-bone curves) associated with different elements for lumped-plasticity models are presented in various documents (FEMA 356 2000; ASCE 41-06 2007; Elwood et al. 2007; Haselton et al. 2007; and ASCE 41-13 2013). The FEMA 356 project was an important milestone to codify the degrading non-linear models and procedures to evaluate the structural collapse capacity. A key component of this procedure is the assignment of the component force-deformation behaviour (back-bone curve) as a function of the detailing of the structural component.

Figure 3.4 presents the back-bone curve (slightly modified) as defined in FEMA 356 (2000). It consists of the three branches. The first branch represents the elastic behaviour of the component, the second branch represents the post-yield behaviour of the component and the third branch represents the post-peak behaviour of the component (strength drop due to strain softening which is associated with rebar buckling and bond-slip). In the original back-bone curve presented in FEMA 356, the third branch consists of vertical drop, however, it has been observed that the sudden drop in the strength is highly unrealistic and also causes numerical instability in the non-linear analysis using most software tools. However, modelling of this strength dropdown is necessary and important in the structures' collapse assessment (Haselton et al. 2007; Deierlein et al. 2010). In order to avoid this numerical instability, some of the researchers (Elwood et al. 2007; Deierlein et al. 2010; PEER ATC-72-1 2010; FEMA P58 2012) have suggested modifying the back-bone curve for collapse assessment of the structures, as shown in Fig. 3.4.

Even though the back-bone curves in FEMA 356 project were developed for evaluation of existing structures, they were extensively used for performance assessment of new buildings as well. The back-bone curves developed in FEMA 356 project were adopted by ASCE 41-06

(2007). With progress in research and experimental evidences, Elwood et al. (2007) and Haselton et al. (2007) highlighted that the FEMA 356 component back-bone curves are highly idealized and conservative for deterministic evaluations of the response and are noteworthy in terms of their breadth and capability of modelling a full range of behaviour (particularly for near collapse response). Elwood et al. (2007) updated the back-bone curve parameters of FEMA 356 and updated values are also adopted by ASCE 41-13 (2013). The plastic rotation capacities presented in ASCE 41-13 (2013) are approximately two times higher (particularly in the case of columns) than those reported in FEMA 356. In the present study, the back-bone curve parameters have been used following ASCE 41 (2013) guidelines.
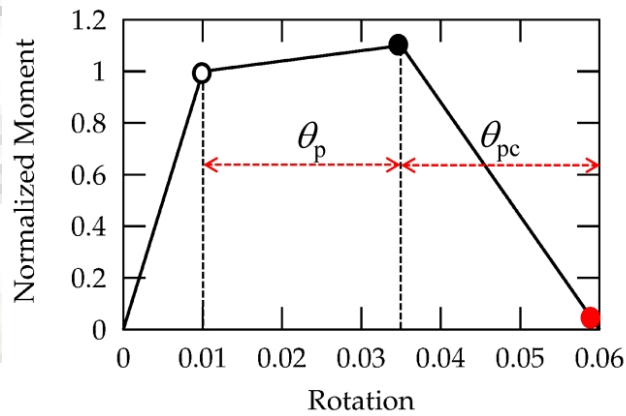
Fig. 3.4 Component force-deformation curve for frame elements in flexure.

3.6.1.2 Modelling of Inelastic and Cyclic Deterioration

In the reinforced-concrete (RC) components, the phenomena such as concrete cracking, concrete crushing and spalling, rebar buckling and fracture, and bond-slip can result in significant deterioration of strength, whereas cyclic loading effects can result in deterioration of stiffness. The modelling of these strength and stiffness deterioration modes is a complex issue and mainly relies on experimental evidences. The accurate modelling of seismic behaviour involves incorporation of all modes which contribute to the strength and stiffness deterioration under the earthquake excitation. On the other hand, negligence of the deterioration modes makes it almost impossible to assess the behaviour near the collapse of the structure (Ibarra et al. 2015). A back-bone curve is a curve which represents the force-deformation boundary in which the hysteresis response of the element is confined. If a component does not undergo any cyclic deterioration effects, than the back-bone curve will be close to a monotonic loading curve (but not identical) and is termed as initial back-bone curve. It is important to note here

that the initial back-bone curve incorporates monotonic strength deterioration for deformations, those exceed the post-capping point. If a component undergoes cyclic deterioration, the branches of the back-bone curve move towards the origin and are updated continuously. This instantaneous curve is known as the cyclic backbone curve. This cyclic curve depends on loading history and keeps on changing after each excursion that causes damage to the component. The use of the initial back-bone curve in analytical models presumes that the cyclic deterioration will be incorporated in the analytical model. In cases where it is not feasible, the initial back-bone curve must be modified in order to account for the effect of cyclic loading. It is usually achieved by reducing the capping and ultimate deformation of the element (PEER ATC-72-1 2010).

It becomes important to note that the initial back-bone curve parameters derived from the cyclic envelop as obtained from cyclic tests, and the initial back-bone curve obtained from a monotonic test, have a basic difference. The cyclic envelope is derived by connecting the peak values of the first loading cycle under an increasing deformation which results in significant differences between cyclic envelope and monotonic back-bone curve. Firstly, except at small deformations, the cyclic envelope curve falls below the monotonic loading curve, and secondly, at relatively small deformations, the cyclic envelope curve exceeds the monotonic loading curve because cyclic hardening effects exceed the deterioration effects. Thirdly, the cyclic envelope curve is dependent upon the loading history.

To account for the cyclic deterioration effects, four different analytical modelling options have been suggested (PEER ATC-72-1 2010). The first option consists of the use of a monotonic back-bone curve along with explicit incorporation of cyclic degradation effects using appropriate hysteresis rules (e.g. Ibarra et al. 2015). The second option consists of the use of a cyclic back-bone curve as initial backbone curve and no cyclic deterioration of the back-bone curve is included in the analytical model. The third option consists of the use of modification factors for modification of initial back-bone curve and no cyclic deterioration is included in the analytical model. The fourth option is that no strength deterioration is included in the analytical model and more stringent deformation limits are imposed (deformations are restricted to 80% of the total deformation).

Out of the four analytical modelling options, the first choice is of course the most realistic, but at the same time the most complex to implement. The second and third choices are compromises, in which cyclic deterioration is accounted for by implicitly modifying the initial backbone curve. The fourth choice, in which no deterioration is considered and deformations are restricted, to 80% of the post-peak deformations. The fourth option results in conservative estimates of the structural capacity.

In this study the second option of analytical modelling has been adopted in combination with ASCE 41-13 (2013) back-bone curve parameters. The strength deterioration effects are inherently considered in ASCE 41 back-bone curves, whereas the degradation of stiffness and energy dissipation capacity has been modelled explicitly using an energy-based degrading hysteresis model in ETABS 2016 (CSI 2016). This hysteresis model requires three parameters to capture the energy and stiffness degradation effects, namely energy factor (f_1) which represents the ratio of the energy dissipated in a degraded loop to non-degraded loop for deformations within pre-capping range, energy factor (f_2) which represents the ratio of the energy dissipated in a degraded-loop to non-degraded loop for deformations in post-capping range and the stiffness weighting factor (s_w) to account for stiffness degradation effects.

In the present study, the parameters f_1, f_2, and s_w have been obtained iteratively, by calibrating the analytical hysteretic model and the dissipated energy with the experimental results by Dadi and Agarwal (2015) for RC elements representative of non-conforming (non-ductile) and conforming (ductile) RC components according to IS 13920 (1993). Figure 3.5 presents a comparison of hysteretic response of the calibrated model, the experimental moment-rotation behaviour and ASCE 41 back-bone curve for a non-conforming (without ductile detailing) and conforming (with ductile detailing) beam. A comparison of the variation of the dissipated energy with displacement ductility demand has also been presented (Fig. 3.6).

It can be observed that the calibrated model is able to simulate the stiffness degradation and cumulative energy dissipation, reasonably close to the experimental results. Further, it can also be observed that ASCE 41 plastic rotation parameters are slightly conservative, in comparison with the experimental results. ASCE 41 defines back-bone curves in which strength drops suddenly post-capping. However, as discussed earlier, such sudden drops are highly unrealistic and cause numerical instability problems in solution algorithm. Therefore, a gradual reduction

in strength as discussed earlier (also recommended in PEER ATC-72-1 (2010) and FEMA P58 (2012)), has been used for the purpose of comparison with experimental results as well as in simulation of collapse of the building models.
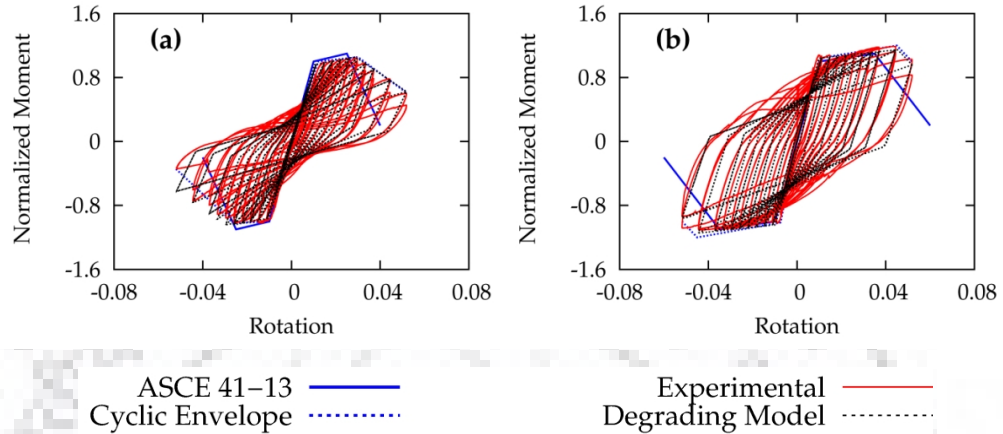
Fig. 3.5 Comparison of simulated hysteretic response with the experimental results: (a) for non-conforming beam ($f_1 = 0.95$, $f_2 = 0.40$ and $s_w = 0.10$); and (b) for conforming beam ($f_1 = 1.00$, $f_2 = 0.55$ and $s_w = 0.10$).
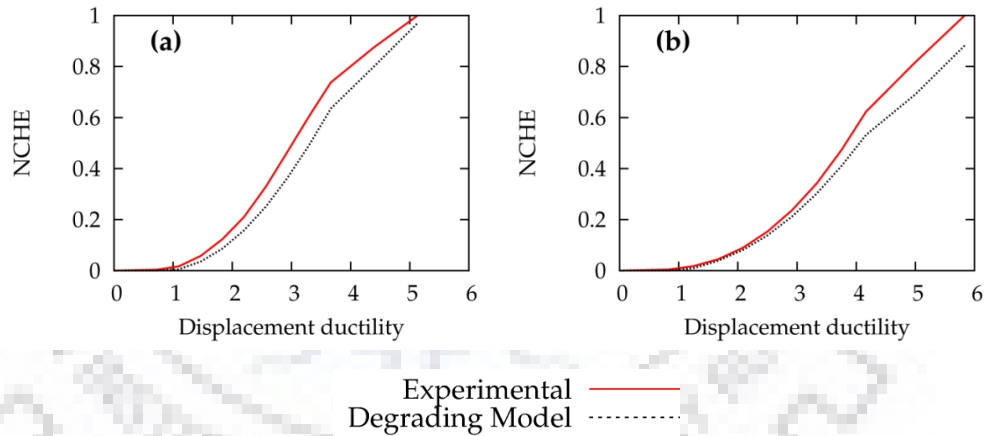
Fig. 3.6 Comparison of simulated normalized hysteretic energy dissipation with the experimental results: (a) in non-conforming beam; and (b) in conforming beam.

3.6.1.3 Effect of Bi-Directional Excitation on Component Behaviour

During earthquake action, RC columns are subjected to axial loads and bi-axial bending moments. However, the experimental evidences on the inelastic response of RC columns under combined axial loads and bi-axial bending are very limited (e.g., Rodrigues et al. 2013a; Rodrigues et al. 2013b). In columns subjected to bi-directional excitations, it has been observed, experimentally, that each damage state has occurred at a drift lower than its corresponding value in case of unidirectional excitation (Rodrigues et al. 2013b). The bi-axial

features of bending moment histories applied to a given RC column section tend to reduce its actual capacity and accelerates the strength and stiffness degradation process during successive load reversals (Bousias et al. 1995; Rodrigues et al. 2012). The maximum strength of columns in a particular direction has been found out to be smaller in case of bi-directional loading as compared to unidirectional loading and this effect was observed to be more pronounced in case of square columns (Rodrigues et al. 2013a). However, it has been observed that the initial stiffness of the column is not affected by bi-axial loading paths (Rodrigues et al. 2013a). Further, the softening phenomenon is more pronounced under bi-axial excitations (Rodrigues et al. 2013a).

In addition, the failure pattern of RC columns is found to be highly dependent on loading path (Rodrigues et al. 2013a). The loading path strongly affects the ductility, strength degradation, and the hysteretic energy dissipation capacity of the columns (Rodrigues et al. 2012; Rodrigues et al. 2013a; Rodrigues et al. 2013b; Rodrigues et al. 2013c; Rodrigues et al. 2013d; Rodrigues et al. 2013e). Further, it has been observed experimentally that the stiffness degradation is not significantly affected by bi-directional excitation when compared with unidirectional excitation (Rodrigues et al. 2013a). Experimental evidence has also shown that plastic hinge zone lengths tend to be stable at around theoretical values and are not strongly affected by bi-axial loading (Rodrigues et al. 2013b). In the past it has been observed that bi-axial loading on RC columns results in higher energy dissipation as compared to the uniaxial loading (Bousias et al. 1995; Qiu et al. 2002; Rodrigues et al. 2012).

3.6.1.4 P-Delta Effects
P-Delta effects are caused by loads acting on the deformed geometry of the structure. P-Delta effects can occur both at the structure level (global) and the member level (local). From a static loading point of view, P-Delta effects lead to an additional load, which increases the member forces and deflections, reduces lateral load resistance of the structure and causes negative stiffness at very large displacements. On the other hand, from a dynamic loading point of view, global P-Delta effects can lead to significant amplification in displacements if the displacement demands during seismic action are large enough to enter in negative tangent stiffness region.

The stability of a structure under P-Delta effects depends on the effective stiffness of the structure at the point of the maximum displacement. If the effective stiffness is positive at the

point of maximum displacement, the structure remains stable, but as soon as this effective stiffness becomes negative, the P-delta effect causes the amplification of the drift demands and structure to become unstable, and the potential for structural collapse increases. The post-capping strength deterioration accelerates this effect, though in some cases, negative stiffness can be attained even if no post-capping strength deterioration occurs (PEER ATC 72-1 2010).

3.6.2 Modelling of Shear Failure

During past earthquakes, it has been observed that shear failure of columns under large lateral deformations can result in loss of axial load carrying capacity, which results in compression failure of columns and hence may cause vertical collapse of the structure (Bertero and Collins 1973; Saatcioglu et al. 2001; Paul et al. 2004). In the earlier developments, shear failure was considered to be a brittle mode of failure leading to loss of axial load carrying capacity in columns at small inter-storey drifts (FEMA 1997). Accordingly, it was considered as a force controlled mode of failure (FEMA 2000, ASCE 41-06 2007). The earlier studies (e.g., Liel et al. 2011) for seismic collapse assessment of RC structures considered the shear-failure as non-simulated collapse mode. In this procedure, the column drifts are utilized to predict the shear failure (Aslani 2005; Liel et al. 2011).

ASCE 41-13 (2013) provides the guidelines to model shear failure, in which the collapse is considered corresponding to the loss of vertical load carrying capacity (Elwood et al. 2007). Although ASCE 41-13 guidelines are based on test results form 274 rectangular reinforced concrete columns (Elwood et al. 2007), these results include only two short-columns (Li and Hwang 2016), which are particularly prone to shear failure. To overcome this limitation, Li and Hwang (2016) have proposed a new model to simulate the shear failure based on experiments on short-columns with height to depth ratio less than 2. This model has two basic differences when compared with ASCE 41 (2013) model. Firstly, this model considers shear-cracking of the concrete prior to reaching strength point; and secondly, after reaching the strength point, the shear strength degrades gradually to zero, at point of axial failure (Fig. 3.7).

A number of shear capacity prediction models have been developed over the past decades based on experimental investigations (e.g., Priestley et al. 1994; Sezen and Moehle 2004; Erduran and Yakut 2007). Table 3.2 presents some of the available models for the prediction of the shear capacity of the columns.
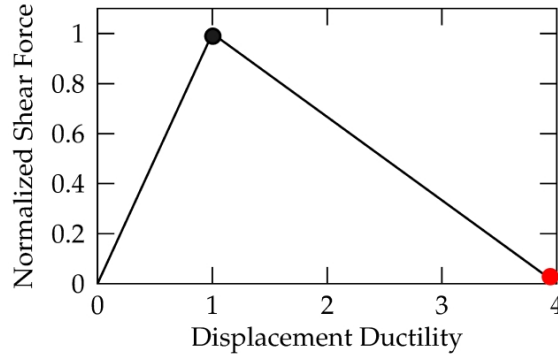
Fig. 3.7 Component force-deformation behaviour of a typical RC member in shear.

Table 3.2 Overview of shear strength models of RC columns.

Standard/ Reference	V_c	V_s
FEMA-356 (2000)	$V_c = k.\lambda \left(\dfrac{0.50\sqrt{f_c'}}{M/V_d} \sqrt{1 + \dfrac{P}{0.50\sqrt{f_c'}A_g}} \right) 0.8A_g \; 2 < M/V_d < 3$ $k = 1.0$ for low ductility region and 0.7 for high ductility region	$V_s = k.\dfrac{A_v f_{yv} d}{s}$
Sezen and Moehle (2004)	$V_c = \left(1 + \dfrac{3P}{A_g f_c'} \right) \left(0.07 + 10\rho_w \right)\sqrt{f_c'}\,A_g$; $0.08\sqrt{f_c'} < \left(0.07 + 10\rho_w \right)\sqrt{f_c'} < 0.2\sqrt{f_c'}$	$V_s = \dfrac{A_v f_{yv} d}{s}$
ASCE 41-13 (2013)	$V_c = k.\lambda \left(\dfrac{0.50\sqrt{f_c'}}{M/V_d} \sqrt{1 + \dfrac{P}{0.50\sqrt{f_c'}A_g}} \right) 0.8A_g$ $2 < M/V_d < 4$ $k = 1.0$ for displacement ductility demand upto 2, and 0.7 for displacement ductility demands greater than or equal to 6. Linear interpolation is permitted for intermediate values	$V_s = k.\dfrac{A_v f_{yv} d}{s}$
ACI 318M (2014)	$V_c = 0.17 \left(1 + \dfrac{P}{14 A_g} \right) \lambda \sqrt{f_c'}\,A_g; \quad if \; P \geq 0$ $V_c = 0.17 \left(1 + \dfrac{P}{3.5 A_g} \right) \lambda \sqrt{f_c'}\,A_g > 0; \; if \; P < 0$	$V_s = \dfrac{A_v f_{yv} d}{s}$

M/V is the largest ratio of moment to shear under design loadings for the column, P is axial load on column, λ is a factor accounting for type of aggregate and taken as 0.75 for light-weight aggregate and 1.00 for normal-weight aggregate, d is the depth of column, ρ_w is the area of flexural tension reinforcement, and A_v, S, and f_{yv} are area, spacing, and yield strength, respectively, of the transverse reinforcement.

The shear strength (V_n) of a column depends on contributions from concrete (V_c) and transverse reinforcement (V_s). The contribution of concrete in shear strength is very complex and is primarily influenced by axial compressive force, column aspect ratio and deformation ductility

demand (Sezen and Moehle 2004; Erduran and Yakut 2007; Li and Hwang 2016). In the present study, guidelines of ASCE 41 (2013) and Li and Hwang (2016) have been used for modelling the shear failure in RC members.

3.7 NON-LINEAR STATIC PROCEDURES (PUSHOVER ANALYSIS)

Performance-based earthquake engineering (PBEE) practice arose from the fact that the seismic design of buildings should ensure the "Life Safety" of the building occupants. The Structural Engineers Association of California (SEAOC) Vision 2000 (1995) and the Unites States National Earthquake Hazard Reduction Programme NEHRP (1997) Guidelines suggested that the performance goal should account for "Life Safety" (LS) of occupants, limitation of damage (DL) and minimizing economic losses.

In order to achieve the targeted performance objective, the performance-based methodology requires estimation of the two most important parameters, i.e., the structure's capacity and the seismic demand. The seismic capacity reflects the structures ability to resist the effects caused by earthquakes, whereas the seismic demand reflects the imposed action on the structure due to earthquakes. In the earthquake engineering practice, the non-linear dynamic procedure (NDP) is the most accurate procedure available for estimating the seismic response of structures, but it requires careful selection and scaling of appropriate ground-motion time histories as well as large computational efforts. On the other hand, the non-linear static procedure (NSP) is a relatively simple analysis method based on response spectrum, and hence is more attractive from a designer's point of view. In addition, it also provides useful insight into the yield pattern and ductility capacity of the structure. Due to these reasons, design engineers are generally more inclined towards NSP.

3.7.1 Conventional Pushover Analysis

The NSP was first introduced by Freeman et al. (1975) in the form of the 'Capacity Spectrum Method' (CSM). The objective to introduce this NSP was to evaluate the peak structural response, peak ductility demand, and equivalent period of vibration and residual capacity of the structure. The NSP is being used from the early 1970's; however, it was first documented in ATC 40 (1996). ATC 40 (1996) suggested use of a loading vector proportional to the fundamental mode of vibration of the building in order to capture the local as well as the global

behaviour of the building. It was documented that the method is applicable to buildings having significant contribution (generally the mass participation higher than 75%) from the fundamental mode of vibration in the direction of application of lateral loading vector (ATC 40 1996). This method is also known as conventional NSP. The various steps involved in this procedure are illustrated in Fig. 3.8.

(a)　　Pushover loading vector　　　　　　(b) Capacity spectrum of the building

(c) Intersection of capacity and demand spectrum (performance point)
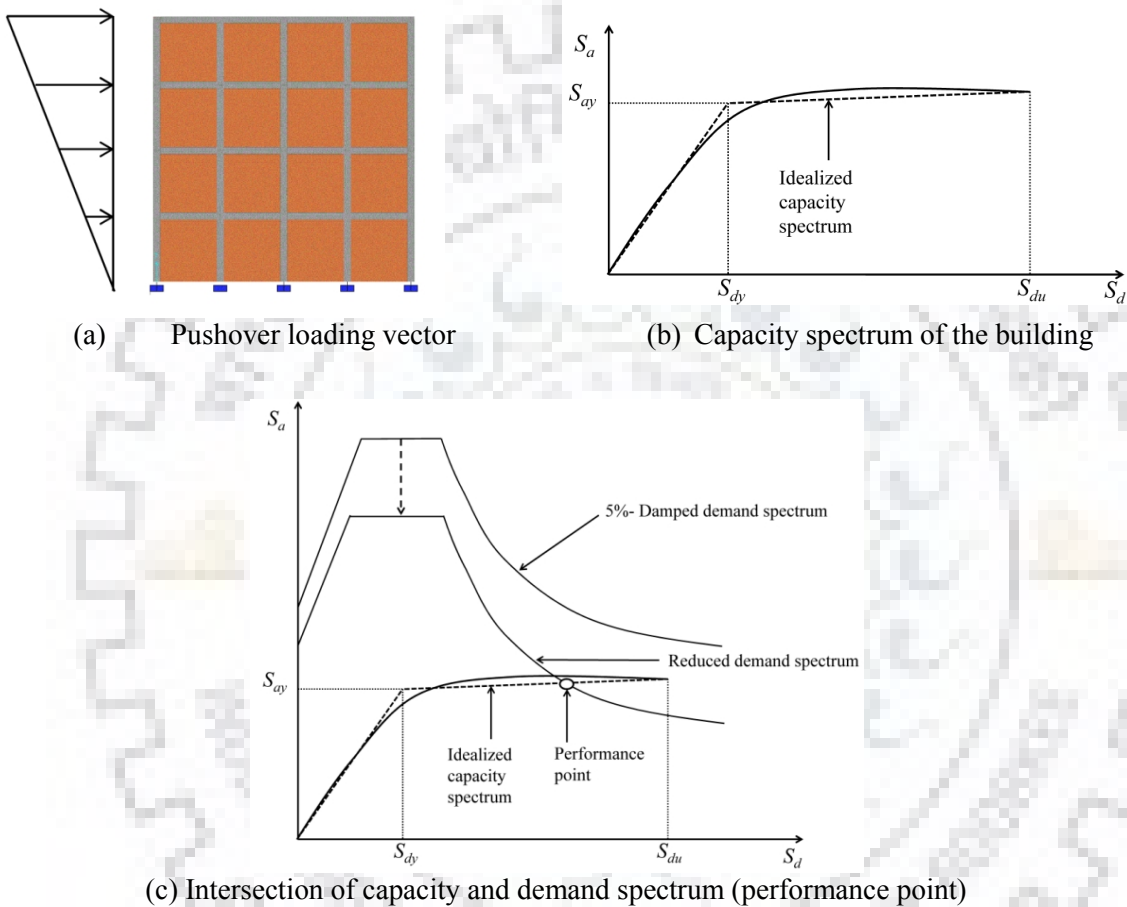
Fig. 3.8 Schematic diagram representing the various steps of the pushover analysis.

This method is able to predict the pattern of yielding, force demands and weak links existing in the building. Later on it was highlighted that since the method does not consider the effect of higher modes of vibration, it is not applicable to structures taller than a certain height and/or buildings with irregularities in elevation (Lawson et al. 1994 and Krawinkler and Seneviratna 1998). Further, the application of lateral loading proportional to the fundamental elastic mode is not adequate throughout the loading duration (i.e. till the structure reaches the target displacement or collapses) since the dynamic characteristics (periods and mode shapes) of the building change as the yielding progress. These limitations have led to the development of the

advanced non-linear static procedures (Paret et al. 1996; Sasaki et al. 1998; Moghadam and Tso 2000; Gupta and Kunnath 2000; Chopra and Goel 2002; Albanesi et al. 2002) for seismic response evaluation of structures.

3.7.2 Advanced Pushover Analysis Methods

In order to overcome the limitations of the conventional NSP, some improvements were suggested by various researchers (Paret et al. 1996; Sasaki et al. 1998; Moghadam and Tso 2000; Chopra and Goel 2002; Sarkar et al. 2016). Chopra and Goel (2002) suggested the concept of the Modal Pushover (MPA) analysis. The MPA consists of the determination of the seismic demands corresponding to the first few modes of vibration and combining these demands using any suitable combination rule in order to get the actual demand. Gupta and Kunnath (2000) and Albanesi et al. (2002) proposed the concept of the Adaptive Pushover analysis (APA) which accounts for the change in the dynamic characteristics of the building at each step of the loading. However, the charm of the conventional pushover analysis lies in its simplicity and ease in visualizing the yield pattern (i.e., the strength hierarchy of different modes) in the structure. As this simplicity and visualization of yield pattern is lost in the processes of MPA and APA, both have not become as popular as the conventional pushover analysis.

3.7.3 Challenges in Implementing NSP

The challenges associated with non-linear static procedures include the selection of an appropriate loading vector, selection of appropriate back-bone curves corresponding to different failure modes, the concentration of inelastic response, inability to capture the variation in the seismic response due to record-to-record variability, inability to capture the bi-directional and torsional response (Sarkar et al. 2005; Sarkar et al. 2010) and non-convergence in solution algorithm due to a sudden drop in the member strength. Further, there is a significant amount of variation in defining collapse using non-linear static procedure. For example, HAZUS (FEMA 2002) defines the collapse state as the damage state when 50% of the components reach the post-capping deformation point in the cyclic backbone curve, whereas FEMA P695 (2009) defines the collapse point as the point where the static lateral force carrying capacity drops down to 80% of the maximum. Based on various shake-table test data on building models, it has been observed that a maximum inter-storey drift ratio of 4% can be considered as a suitable

collapse limit state for buildings (Dymiotis et al. 1999). All these facts raise a serious question on the applicability of NSP's in the seismic performance assessment of structures.

3.8 NON-LINEAR DYNAMIC PROCEDURES

Seismic response of an inelastic structure can be most reliably estimated using the non-linear time-history (dynamic) analysis (NLTHA) procedure. Non-linear dynamic analyses can be performed using recorded accelerograms, synthetic accelerograms or by spectrum-compatible accelerograms. However, the type of accelerogram used for non-linear dynamic analysis depends on the purpose of the analysis, i.e., whether median demands are to be evaluated or if the range of structural response is required. In order to obtain the median demands, one would prefer spectrum-compatible accelerograms, whereas in order to capture the variability in the structural seismic response, recorded accelerograms can be the preferred choice. Several researchers have questioned the applicability of synthetic and spectrum-compatible accelerograms in probabilistic seismic performance assessment of structures. Synthetic accelerograms have the drawback that these are artificially generated, hence they do not include the information regarding magnitude and path characteristics. On the other hand, spectrum-compatible accelerograms have the drawback that in the process of making these accelerograms spectrum-compatible, the phase information is lost. Hence, recorded accelerograms are generally preferred over synthetic and spectrum-compatible accelerograms.

Recent advancements in the framework of performance-based earthquake engineering led to the development of a methodology in which, in order to estimate the seismic capacity of a structure, the NLTHA is performed by gradually increasing the intensity of the input excitation until the structure finally collapses. The procedure is known as Incremental Dynamic Analysis (IDA) (Vamvatsikos and Cornell 2002) and is considered a very powerful tool for fragility analysis as it enables the direct estimation of the record-to-record (inter-event) variability in structural response.

In the past decade, various groups (e.g., Vamvatsikos and Cornell 2002, Haselton et al. 2011a, b, Liel et al. 2011; Wang et al. 2011, Afarani and Nicknam 2012, and Shakib and Pirizadeh 2014; Farsangi and Tasnimi 2016; Moniri 2017) have performed IDA for buildings of both regular and irregular configuration. They have used suites of ground-motion records, each

scaled to a certain level of seismic intensity in order to cover the full range of structural behaviour from the elastic to the inelastic state and finally to global dynamic instability as suggested by Vamvatsikos and Cornell (2002). For each ground-motion record, the output of the IDA can be expressed in the form of a dynamic capacity curve, representing the variation of the chosen Intensity measure (IM) (e.g. spectral acceleration, S_a, average spectral acceleration, $S_{a,avg}$, peak ground acceleration, PGA, base shear, etc.) with the engineering demand parameter (EDP) (e.g. spectral displacement S_d, roof displacement, inter-storey drift ratio, peak floor acceleration, etc.). The selection of IM and EDP is application specific. For example, in order to assess the structural performance, the choice of IM and EDP would be S_a (T, 5%) or $S_{a,avg}$ (0.2T -3T, 5%) and maximum inter-storey drift ratio whereas in order to assess the non-structural performance, the choice of IM and EDP would be S_a (T, 5%) and peak floor acceleration (PFA).

3.8.1 Challenges in Implementing NDP

Implementation of the NDP is a challenging task, since it is very cumbersome and requires huge computational efforts. The major challenge in application of NDP arises in the selection and scaling of ground-motion records. The major international codes (ASCE 7-10 2010; EC-8 2004 and NZS 2004) provide guidelines for both the selection and scaling of ground-motion records. However, these guidelines are very general and not application specific. Another issue is that the orientation of the ground-motion, i.e., whether the ground-motion should be applied along the principal axes or to some other angle that is not specified in most of the codes (Jangid 1996; Jangid 2001; Beyer and Bommer 2006; Beyer and Bommer 2007; Ghazizadeh et al. 2013). Further, the modelling of damping effects, hysteresis behaviour, modelling of interaction effects in members (e.g., moment-shear, bi-axial bending, shear-tension), treatment of cyclic degradation and appropriate statistical parameters in order to represent the results are the issues for which no clear guidelines are available which makes the NDP challenging.

3.8.2 Selection of Ground-Motion Records for NDP

The seismic response of structures is very sensitive to strong-motion record parameters such as peak ground acceleration (PGA), frequency content and duration; hence, structures exhibit large record-to-record variabilities. These strong-motion parameters are affected by the magnitude (M_w), source-to-site distance (R_s), path characteristics and the local soil profile

(generally characterized by $V_{s,30}$, i.e., average shear wave velocity in the uppermost 30 m). Therefore, in order to select appropriate ground-motion records for a particular site, all of these factors need to be accounted for. The major national seismic codes (ASCE 7-10 2010; EC-8 2004 and NZS 1170.5 2004) provide guidelines for the selection of ground-motion records for NDP. These guidelines are based on magnitude (M_w), source-to-site distance (R_s), number of records (N) and site class only. It has been identified that much progress has been made in the selection procedure of the ground-motion records. However, it has not been implemented in the codes yet.

Due to technological and computational advances in the past decade, research in the selection of ground-motion records is boosted significantly. Luco and Bazzurro (2007) showed that the random selection of ground-motion records can introduce a 'bias' in the structural response and this bias increases with increase in the scale factor. Further, this bias is dependent of the fundamental period of vibration, strength of the structure and sensitivity of the non-linear response of the structure to the higher modes of vibration. Beyer and Bommer (2007) suggested the guidelines to select the ground-motion records for bi-directional non-linear dynamic analysis. They compared two different techniques of the selection of the ground-motion records, i.e., ground-motion selection based on scenario earthquake and ground-motion selection based on target spectrum (spectrum matching). They observed that the records selected based on the spectrum matching lead to much reduced coefficients of variation than compared to the scenario earthquakes.

The more recently developed FEMA P695 (2009) methodology provides the most comprehensive criteria for the selection of ground-motion records which takes into account magnitude (M_w), source-to-site distance (R_s), number of records (N), site class, peak ground acceleration (PGA), peak ground velocity (PGV) and the lowest usable frequency (f_l). In the framework of its application, FEMA P695 (2009) uses 28 near-field (NF) and 22 far-field ground-motion records. Wang (2011) proposed a methodology to select the ground-motion records based on a particular earthquake scenario. The methodology takes into account the response spectrum characteristics and ground-motion variability in which the record spectrum is scaled to match a target spectrum generated from the correlated multivariate distribution; hence can capture the statistical distribution of the response spectra of the earthquake scenario. Ay and Akkar (2012) proposed an alternative methodology for selection of ground-motion

records based on the earthquake scenario. They highlighted that the type of faulting and soil conditions also affects the ground-motion amplitude; hence records with specific requirements should be preferred. Bradley (2012) highlighted that the selection of ground-motion records based on spectral shape alone can introduce the biased distribution of both cumulative and duration-based intensity measures. He proposed an algorithm for the selection of ground-motions based on random realizations from the conditional multivariate distribution of ground-motion intensity measures that are obtained from generalized conditional intensity measures (GCIM). The algorithm can be utilized to select recorded, amplitude-scaled, and as well as synthetic/simulated ground-motions.

Some of the recent advancements in the selection of the ground-motion records include selection based on spectral shape and hazard consistency (Baker and Cornell 2006; Sousa et al. 2017), conditional mean spectrum (CMS) (Baker 2011), generalized conditional intensity measure approach (Bradley 2010, 2012), conditional spectrum (CS) (Lin et al. 2013a, b). Both, CMS and CS were primarily developed as ground-motion record selection tools. The CMS provides the mean response spectrum, conditioned on the occurrence of the target spectral acceleration value at the period of interest, also known as conditioning period (T_{con}). This conditioning period may be a single period or a range of periods (Baker 2011). On the other hand, the CS has the advantage over the CMS as it maintains the variability in spectral ordinates at periods other than the conditioning period (T_{con}). The computation of both CMS and CS requires the mean causal moment magnitude (M_w), mean causal distance (R_s), and ε (defined as the number of standard deviations by which a given $\ln S_a$ value differs from the mean predicted $\ln S_a$ value for a given magnitude and distance) value which are all obtained from the deaggregation process of a probabilistic seismic hazard analysis (PSHA). Based on the obtained ε value at the conditioning period, the ε values at the other periods can be computed using cross-correlation coefficients proposed in literature (Baker and Cornell 2006; Baker and Jayaram 2008).

Baker and Cornell (2006) demonstrated that spectral shape of ground-motion is a key characteristic affecting the structural response and the collapse capacity. The spectral shape of a characteristic event (e.g, the MCE) can be significantly different than a uniform hazard spectrum (UHS) specified in the seismic design codes. In earlier studies (e.g., Baker and

Cornell 2006; Haselton and Deierlein 2007; Haselton et al. 2011a, b; Liel et al. 2011), ε is considered as a proxy of the spectral shape of the ground-motion. The expected ε value used for estimating the building response is dependent on the local site conditions, the chosen ground-motion prediction model, as well as the hazard level of interest (Haselton et al. 2011b).

The approach suggested by Haselton et al. (2011b) consists in using a general ground-motion record suite disregarding ε values but later correcting the obtained collapse capacity for the expected ε for the respective site and the hazard level of interest. The simplified procedure based on this approach has also been presented in FEMA P695 (FEMA 2009) in which this adjustment in collapse capacity is based on seismic design category (SDC), building period (T), and ductility (μ). This correction factor affects (results in either increase or decrease depending on expected ε at the considered site for the hazard level of interest) the structure's median collapse capacity by up to 60% (FEMA 2009), hence it is very important to be considered in the collapse assessment of structures. However, the suggested correction factor is applicable for sites in the United States only with the general far-field ground-motion record suite as recommended in FEMA P695 (Haselton et al. 2011a, b). The other disadvantage with ε as a proxy to spectral shape lies in the fact that it is not effective in capturing the spectral shape effects for near-field ground-motion records with velocity-pulses caused by forward directivity effects (Luco and Cornell 2007; Tothong and Luco 2007; Tothong and Cornell 2008; Chioccarelli and Iervolino 2010; Haselton et al. 2011b; Eads et al. 2015; Eads et al. 2016). Further, in many cases, ε fails to predict the spectral shape features, such as peaks or troughs which have been shown to be important indicators of structures' non-linear response and therefore, collapse capacities are poorly predicted (Eads et al. 2016). Mousavi et al. (2011) proposed another proxy to spectral shape called η_s, which is a linear combination of an ε value based on spectral acceleration and an ε value based on peak ground velocity (PGV). Factor η_s has been shown to be a better predictor of ground-motion spectral shape and therefore also of structural collapse, when compared with ε value based on spectral acceleration alone (Mousavi et al. 2011; Eads et al. 2016).

In the recent studies (Raghunandan and Liel 2013; Chandramohan et al. 2016a; Chandramohan et al. 2016b) it has also been identified that the duration of the ground-motion records is also an important parameter which should be considered in the structural collapse assessment. It has

been identified that the structural collapse capacity decreases with the increase in the ground-motion duration, as the longer duration records impose higher energy demands on the structure as compared to spectrally equivalent shorter duration ground-motion records (Raghunandan and Liel 2013). Based on these observations, Chandramohan et al. (2016a) developed procedure to consider the effect of duration in selection of site-specific ground-motion records. However, the effect of duration of the ground-motion records on structural response is considered to be significant for intensities close to MCE or even higher than MCE (Chandramohan et al. 2016a). At lower level of intensities, which do not produce deformations large enough to cause strength and stiffness deterioration, the effect of duration of ground-motion records is much less pronounced (Chandramohan et al. 2016a).

Based on the parameters considered in the ground-motion record selection, a summary of the selection criteria from different seismic design codes and literature for non-linear dynamic analyses has been presented in Table 3.3. As identified from the earlier studies, the ground-motion selection plays crucial role in structural collapse assessment and is also dependent on the building period as well as on the site of the interest. The objective of the present study is to assess the collapse capacity of a class of buildings with different periods of vibration, structural configurations and heights. Therefore, in the present study, three ground-motion record suites as recommended in FEMA P695 (2009) consisting of a far-field record suite, a near-field record suite without velocity pulses and a near-field record suite with velocity pulses have been used in collapse assessment.

3.8.3 Scaling of Ground-Motion Records for NDP

Scaling of earthquake ground-motion records is another key issue in the collapse performance assessment and seismic risk evaluation of structures. The available earthquake ground-motion databases include earthquake records with a variety of source and site characteristics. However, the database is still not adequate to choose sufficient number of records with desired characteristics. In such a situation, scaled records are generally utilized to assess collapse performance. In order to scale an earthquake ground-motion record, a parameter representing its strength (in terms of its "damage potential") is required which is referred to as Intensity Measure (IM). The selection of an IM for scaling of ground-motion records, primarily requires three characteristics (i) sufficiency, (ii) efficiency, and (iii) hazard computability (e.g., Shome

et al. 1998; Baker and Cornell 2005; Luco and Cornell 2007). An IM is considered to be sufficient, if it is able to produce the damage measure (DM) conditionally independent of the earthquake magnitude (M_w), source-to-site distance (R_s) and other earthquake parameters which can affect the structural response whereas efficiency is characterized by reduced dispersion in DM for a given IM (e.g., Baker and Cornell 2005; Luco and Cornell 2007). The hazard computability of an IM corresponds to ease in computing the hazard curve or for the development of an attenuation relationship (e.g., Luco and Cornell 2007). It has been highlighted by several researchers (e.g., Kurama and Farrow 2003; Bommer and Alarcon 2006) that the hazard computability of the parameters such as spectral accelerations is much easier since most of the attenuation relationships are available for spectral accelerations. Therefore, velocity- and displacement-related parameters are not as popular in scaling procedure of the ground-motion records as compared to acceleration-based parameters (e.g., spectral acceleration at the fundamental period of the structure, S_a (T, 5%); average spectral acceleration over a range of periods $S_{a,avg}$ (0.2T-3T, 5%)).

3.8.3.1 Acceleration-Based Intensity Measures

Studies to identify the suitable IMs for scaling of ground-motion records started in the early 1990's. Initially, Peak Ground Acceleration (PGA) was being employed as an IM for scaling the ground-motion records (e.g., Shome et al. 1998). It was observed that the scaling of ground-motion records based on PGA considers only the strong-ground-motion parameter without any structural characteristics, leading to very large dispersion in structural response near the collapse limit state (e.g., Shome et al. 1998). In order to overcome this limitation, Shome et al. (1998) and Shome and Cornell (1999) proposed an IM referred to as spectral acceleration at the fundamental period of the structure, S_a (T, 5%). This IM has been found out to be very efficient and sufficient for structures whose response is dominated by the fundamental mode of vibration. This scalar IM led to a significantly reduced dispersion near collapse, as compared to other IMs such as PGA (Vamvatsikos and Cornell 2002; Kurama and Farrow 2003). Some recent research studies have shown that S_a (T, 5%) is a good predictor of the inter-storey drift (damage) for ordinary ground-motion records (e.g., Ebrahimian et al. 2015; Kostinakis et al. 2015).

With the advancements and progress in research, it was observed that S_a (T, 5%) neither considers the effect of spectral accelerations at higher mode periods nor the spectral accelerations at the elongated period, in case of non-linear MDOF system. Therefore, S_a (T, 5%) alone has been found to be insufficient for collapse assessment of structures (e.g., Corodova et al. 2000; Baker and Cornell 2005; Bianchini et al. 2009; Catlan et al. 2010; Lin et al. 2011; Kazemi et al. 2013; Yakhchalian et al. 2015; Galasso and Rossetto 2015). Further, for plan-irregular buildings, S_a (T, 5%) showed very weak correlation since the torsionally coupled modes are not accounted using this IM (e.g., Lucchini et al. 2011).

Corodova et al. (2000) proposed an IM consisting of two parameters, one accounting for the effect of the fundamental period (T) on the structural response and another accounting for the effect of period elongation (T_{eff}) due to severe non-linear response of the structure. Baker and Cornell (2005) proposed a vector-valued IM, i.e., S_a (T, ε), which takes into account the spectral acceleration at the fundamental mode period as well as the parameter, ε, accounting the spectral shape. The parameter ε is a representative of the deviation of the actual record from the mean expected ground-motion obtained using the attenuation relationship (Baker and Cornell 2006). This IM had been found to be more effective as compared to the S_a (T, 5%) alone for the higher mode dominated structures (e.g., Baker and Cornell 2006).

Baker and Cornell (2008a) investigated the efficiency of a vector-valued IM (S_a (T), S_a (T^*) / S_a (T)) for pulse-like ground-motions. Period T^* has been taken as the elongated period ($2T$) to capture the effect of velocity pulse. They highlighted that the pulse period is an important parameter for pulse-like ground-motions and the parameter S_a (T, 5%) alone is not an efficient IM; hence a vector-valued IM which accounts for the spectral shape and pulse-period has been found to be more efficient. Baker and Cornell (2008b) presented a vector-valued IM considering the spectral acceleration S_a (T) and a factor accounting for the spectral shape, i.e., S_a (T^*) / S_a (T). Period T^* has been taken as the period corresponding to the second mode of vibration if the higher mode effects are significant whereas for highly non-linear systems T^* is taken as the elongated period ($2T$). They found out that this additional factor, which accounts for the spectral shape, reduces the standard deviation of prediction errors by 60% (Baker and Cornell 2008a; Ebrahimian et al. 2015). Bojorquez et al. (2012) investigated the efficacy of different vector-valued IMs for the narrow banded ground-motions in collapse capacity

estimation of steel moment resisting frame buildings. They considered S_a (T) along with a parameter representing peak values, damage potential of earthquake and spectral shape as vector valued IM's. They concluded that a vector-valued IM like (S_a (T), S_a ($T_1...T_N$)/ S_a (T)) is very promising and independent of the type of seismic response parameter considered (Bojorquez et al. 2012; Minas et al. 2014; Minas et al. 2015). Yakhchalian et al. (2015) investigated vector-valued IM's for structural collapse assessment of low- to high-rise buildings. They proposed vector-valued IM (S_a (T), S_a (T)/DSI) (where, DSI is the displacement spectrum intensity, which captures long-period content of ground-motions) which has been found to reduce the dispersion in collapse capacity of an 8-storied building by an order of 50%, as compared to a scalar IM such as S_a (T).

Bianchini et al. (2009) proposed an IM, $S_{a,avg}$, which is the geometric mean of spectral ordinates calculated at the 10 points equally spaced in the logarithmic domain. The period range of T-2T was proposed for fundamental mode-dominated structures whereas 0.2T-2T was proposed for the structures with medium- to long-period structures which are affected by higher modes. Lin et al. (2011) proposed IM's which take into account the effect of inelasticity and higher modes. Bojorquez and Iervolino (2011) proposed a parameter N_p, defined as the ratio of geometric mean of spectral acceleration values between periods T and 2T, i.e., $S_{a,avg}$ (T-2T, 5%), to the spectral acceleration at the fundamental period S_a (T, 5%). This parameter provides a measure on how high or low a spectral ordinate is relative to the spectral acceleration averaged over a period longer than the fundamental period of vibration. N_p has been found out to be a better predictor of the structural collapse capacity than η_s and a much better predictor than ε (Eads et al. 2016).

Eads et al. (2015) proposed a parameter defined as the ratio of the spectral acceleration at the first mode period of the structure, S_a (T, 5%) to the geometric mean of spectral accelerations over a period range of periods, $S_{a,avg}$ (0.2T-3T, 5%). This parameter primarily represents the spectral shape over the range of periods to which the collapse response of structures is sensitive. It has been shown that, when this parameter is used as an IM, it significantly reduces the dispersion in the collapse intensities (Eads et al. 2015; Eads et al. 2016) as it contains sufficient information about the spectral shape by considering spectral ordinates at higher mode periods as well as at elongated period.

3.8.3.2 Velocity-Based Scalar Intensity Measures

FEMA P695 (2009) adopts the methodology in which the record sets are normalized by median PGV. This median PGV is obtained as the geometric mean of PGV of the two horizontal components of the ground-motion record. The median of the normalized record set is collectively scaled upwards or downwards in order to scale the ground-motion for the target parameter, i.e., S_a (T, 5%). Further, it had been highlighted that the scaling parameters based on velocity are more appropriate as compared to acceleration in both the intermediate- and long-period range of vibration (e.g., Kappos and Kyriakakis 2000; Bommer and Alarcon 2006). However, very few ground-motion prediction equations are available which are based on velocity-related parameters (e.g., Kappos and Kyriakakis 2000; Bommer and Alarcon 2006) and hence have not been used in practice yet.

3.8.3.3 Displacement-Based Scalar Intensity Measures

The recent advancements in the field of earthquake engineering led to the development of attenuation models in terms of inelastic spectral displacements (S_{di}) (e.g., Tothong and Cornell, 2006; Tothong and Cornell, 2007). Tothong and Luco (2007) highlighted that the scaling with respect to the inelastic spectral displacement, S_{di}, is an efficient and robust method of scaling for fundamental mode-dominated structures. It leads to results that are comparable with an advanced vector IM such as S_a (T, ε). Later on, Tothong and Cornell (2008) highlighted that for pulse-type ground-motions, the use of elastic IM's like S_a (T) or S_a (T, ε) produces unrealistic results of the collapse capacity of structures. It had been observed that the scaling procedure using an IM like S_{di} is sufficient, efficient and robust even for pulse-type ground-motions, since S_{di} can directly account for the sharp change in pulse spectral shape (Tothong and Cornell 2008).

Based on the parameters considered in the scaling of ground-motion records, a summary of the scaling criterion from different seismic design codes and literature for non-linear dynamic analyses has been presented in Table 3.4. As identified from the earlier studies, a number of IM's have been developed over past decades. In the present study, two different IM's, S_a (T, 5%), and $S_{a,avg}$ (0.2T-3T, 5%) have been used.

Table 3.3 Selection of ground-motion records for non-linear dynamic analysis.

Standard/Group	M_w	R_s	N	PGA	PGV	Site Class	f_l (Hz)	NF	FF	ε	Remarks (if any)
ASCE 7-05 (2005)	✓	✓	✓	•	•	•	•	•	•	•	
EC 8 (2004)	✓	✓	✓	•	•	✓	•	•	•	•	
NZS (2005)	✓	✓	✓	•	•	✓	•	•	•	•	
IS:1893 Part 1 (2002)	•	•	•	•	•	•	•	•	•	•	
FEMA P695 (2009)	✓	✓	✓	✓	✓	✓	✓	•	✓	•	Recommended for far-field record set.
Heo et al. (2011)	•	•	✓	✓	•	•	•	•	•	•	
Huang et al. (2011)	✓	✓	✓	•	•	✓	•	✓	✓	•	
Lucchini et al. (2011)	✓	✓	✓	•	•	✓	•	✓	✓	•	
Ebrahimian et al. (2015)	✓	✓	✓	•	•	✓	•	✓	✓	•	
Yakhchalian et al. (2015)	✓	✓	✓	✓	✓	✓	✓	✓	✓	•	
Kurama and Farrow (2003)	✓	✓	✓	•	•	✓	•	✓	✓	•	
Baker and Cornell (2006)	✓	✓	✓	•	•	✓	•	✓	✓	✓	
Tothong and Luco (2007)	✓	✓	✓	•	•	•	•	•	✓	•	
Hancock et al. (2008)	✓	✓	✓	•	•	✓	•	✓	•	✓	Dark shaded are partly considered.
Tothong and Cornell (2008)	✓	✓	✓	•	•	•	•	✓	•	•	Study considers pulse-like motions only.
Baker and Cornell (2008a)	✓	✓	✓	•	•	•	•	✓	•	•	Study considers pulse-like motions only.
Bojorquez et al. (2012)	✓	✓	✓	•	•	•	•	•	✓	•	Duration was also considered.
Reyes et al. (2015)	✓	✓	✓	•	•	✓	•	•	✓	•	
Beyer and Bommer (2007)	✓	✓	✓	•	•	✓	•	✓	✓	✓	
Kappos and Kyriakakis (2000)	✓	✓	✓	•	•	✓	•	✓	✓	•	
Shome et al. (1998)	✓	✓	✓	•	•	✓	•	✓	✓	•	
Maniyar and Khare (2011)	✓	✓	✓	•	•	✓	•	✓	✓	•	
Vamvatsikos and Cornell (2002)	✓	✓	✓	•	•	✓	•	•	✓	•	
Shakib and Pirizadeh (2014)	✓	✓	✓	•	•	✓	•	•	✓	•	

M_w - magnitude, R_s - source-to-site distance, N - number of ground-motion records, PGA - peak ground acceleration, PGV - peak ground velocity, site class- based on NEHRP site classification, f_l - lowest usable frequency, NF - near-field, FF - far-field, ε - parameter accounting for spectral shape.

Table 3.4 Intensity measures for scaling of ground-motion records for non-linear dynamic analysis.

Standard/Group	PGA	$S_a(T)$	$IM_{I1,2E}$	IM_{12E}	$S_a(T_1,T_2)$	$S_{a,GM}(T)$	$S_{a,AM}(T)$	$S_a(T_{eff})$	$S_a(T\text{-}T_{eff})$	Spectrum Matching	D-Scaling	Remarks (if any)
ASCE 7-05 (2005)	•	•	•	•	•	•	•	•	•	✓	•	
EC 8 (2004)	•	•	•	•	•	•	•	•	•	✓	•	
NZS (2005)	•	•	•	•	•	•	•	•	•	•	•	
IS:1893 Part 1 (2002)	•	•	•	•	•	•	•	•	•	•	•	
FEMA P695 (2009)	•	•	•	•	•	•	✓	•	•	•	•	Median of PGV normalized records is scaled.
Haselton et al. (2011)	•	✓	•	•	•	•	•	•	•	•	•	Effect of epsilon.
Huang et al. (2011)	•	✓	•	•	•	✓	•	•	•	✓	✓	Effect of epsilon.
Heo et al. (2011)	•	✓	•	•	•	•	•	•	•	✓	•	
Lucchini et al. (2011)	•	✓	•	•	✓	✓	•	•	✓	•	•	Effect of epsilon with $S_a(T_1)$, Plan-irregular buildings.
Ebrahimian et al. (2015)	•	✓	•	•	•	•	•	•	✓	•	•	Vector intensity measures were also investigated.
Yakhchalian et al. (2015)	•	✓	•	•	•	•	•	•	•	•	•	Vector intensity measures were also investigated.
Kurama and Farrow (2003)	✓	✓	•	•	•	•	•	•	✓	•	•	
Tothong and Luco (2007)	•	✓	✓	•	•	•	•	•	•	•	•	S_{di} was also used as an intensity measure.
Hancock et al. (2008)	•	✓	•	•	•	•	•	•	✓	✓	•	Spectrum matching for different damping ratios.
Tothong and Cornell (2008)	•	✓	✓	•	•	•	•	•	•	•	•	S_{di} was also used as an intensity measure.
Reyes et al. (2013)	•	•	•	•	•	•	•	•	•	✓	•	ASCE 7-10 scaling was also used.
Reyes et al. (2015)	•	•	•	•	•	•	•	•	•	•	•	MPS and ASCE 7-10 scaling were compared.
Beyer and Bommer (2007)	•	•	•	•	•	✓	✓	•	•	•	•	Intensity measures were used for bi-directional analysis.
Baker and Cornell (2008)	•	•	•	•	•	•	•	•	•	•	•	Vector intensity measures were investigated.
Kappos and Kyriakakis (2000)	✓	•	•	•	•	•	•	•	•	•	•	PGV, SI and other methods were also used.
Vamvatsikos and Cornell (2002)	•	✓	•	•	•	•	•	•	•	•	•	
Shakib and Pirizadeh (2014)	•	•	•	•	•	•	•	•	•	•	•	GM of spectral accelerations over period range of $0.5T_1$-$1.5T_1$.

PGA - peak ground acceleration, $S_a(T)$ - spectral acceleration at fundamental period T, $IM_{I1,2E}$ - spectral acceleration corresponding to inelastic and higher mode period, IM_{12E} - spectral acceleration corresponding to elastic fundamental and second mode of vibration, $S_a(T_1, T^*)$ - vector intensity measure considering spectral accelerations corresponding to fundamental and second mode of vibration, $S_{a,GM}(T)$ - geometric mean of spectral accelerations of the two horizontal components corresponding to fundamental period T, $S_{a,AM}(T)$ - arithmetic mean of spectral accelerations of the two horizontal components corresponding to fundamental period T, $S_a(T_{eff})$ - spectral acceleration corresponding to inelastic period of vibration and $S_a(T\text{-}T_{eff})$ - spectral accelerations over the period range from fundamental period of vibration T to inelastic period of vibration T_{eff}.

63

3.8.4 Modelling of Damping Effects in NLTHA

The damping is generally associated with reduction in the dynamic response of a system due to dissipation of energy in structural as well as non-structural components. In general, damping is often modelled as equivalent viscous damping usually expressed as a percentage of critical damping in one or few modes of vibration. The extent to which a mathematical model can capture energy dissipation associated with hysteretic response in non-linear analysis depends on the characteristics of the adopted non-linear model. For example, lumped-plasticity models cannot capture the energy dissipation associated with steel yielding or concrete cracking prior to the formation of the hinge. On the other hand, the fiber model can capture these effects but may not capture all the sources of damping (e.g., bond-slip). In performance assessment of structures, it is an usual practice that a structural component is modelled with a combination of elastic and inelastic elements and hence, the energy dissipation associated with yielding and cracking in the portion of the element modelled as elastic will not be captured. Apart from these, any structural system has several components such as floor slabs, gravity beams, gravity columns and connections which are not explicitly modelled in the analysis but are expected to undergo large inelastic deformations and hence contribute to damping. Further, non-structural components such as partitions or cladding are expected to contribute to overall damping. Hence, it becomes necessary to account for these effects implicitly in the analysis.

The current force-based design in which a 'Response reduction factor' or 'Behaviour factor' is used for the design of structures is based on the inelastic energy dissipation and it is a well-known fact that a structure can sustain a major earthquake if the energy absorption capacity of the structure is higher than the input seismic energy (Housner and Jennings 1977; Kuwamura and Galambos 1989). The seismic response of a structure is primarily influenced by the mathematical model adopted for the modelling of damping effects in NLTHA. In this section the effect of modelling of the damping, on seismic response of structures is discussed. In the modelling of damping effects, the three most critical issues are: the amount of damping, periods to define the damping effects (for analytical model) and the formulation used for modelling the damping (e.g., mass proportional, stiffness proportional etc.).

3.8.4.1 Amount of Damping

The appropriate amount of damping can be identified by processing the recorded data of the seismic response for instrumented buildings. Goel and Chopra (1997) collected and analyzed data from 8 different strong ground-motions, for 43 instrumented RC buildings, with 2 to 60

storeys in the United States. They observed that for buildings with heights lesser than 35 storeys, the measured damping ranges from 2-12% of critical damping, whereas for buildings with heights above 35 stories, the damping is generally in the range of 2-4% of critical. Satake et al. (2003) collected data for 68 instrumented RC buildings up to 45 stories in Japan. They observed that the damping for these buildings varied from 0.5-8% of the critical damping. The observed difference in damping range obtained by Goel and Chopra (1997) and Satake et al. (2003) was attributed to the difference in displacement amplitudes.

Harder (1989) and Martin and Harder (1989) specified equivalent viscous damping of 5% and 10% of critical damping, for steel and reinforced-concrete buildings, respectively, at the design level ground-motions. The corresponding values for MCE ground-motions are 7.5% and 12% of critical damping, respectively. These values were specified in order to account for hysteresis effects in the linear time-history analysis; hence are inappropriate and not recommended to use in NLTHA (PEER ATC-72-1, 2010). Table 3.5 presents some of the typical values of damping for RC frame buildings as obtained through shake table tests (Oliva 1980; Shahrooz and Moehle 1990; Elwood and Moehle 2003; Moehle et al. 2006; Shin and Moehle 2007). It can be observed that for undamaged state the damping varies from 1.4-3.7%, while for the significant damage state it varies from 3.9-11.11% resulting in significant variation within the same damage states.

Table 3.5 Damping values as obtained from shake table tests.

Group	Building Model	Damage state	Observed damping (%)
Oliva (1980)	RC Frame (2 Storey, 1 Bay) (1/3 Scale)	U	1.9 - 2.2
		D	3.9 - 5.3
Shahrooz and Moehle (1990)	RC frame (3 to 6 storeys, 2 Bays) (1/3 Scale)	U	2.7 - 3.7
		M	4.9 - 6.4
		SD	9.6 - 11.1
Elwood and Moehle (2003)	2 RC Frames (1 Storey, 3 Bays) (1/2 Scale)	U	1.4 - 1.9
		Y	2.1 - 3.7
		SD	3.9 - 5.4
Moehle et al. (2006)	RC Frame (3 Storey, 3 Bays) (1/3 Scale)	U	1.9
Shin and Moehle (2007)	12 RC Frame (1 Storey, 3 Bays) (1/3 Scale)	U	1.4 - 2.9 Avg. = 2.1 COV = 0.31

U – Undamaged; D – Damaged; M – Moderate; SD – Significant damage; Y – Yielded.

However, from these studies and evidences, it is very clear that the damping reduces with increase in building height. Further, it can be observed that as damage progresses, damping increases. At the verge of structural collapse, the damping is expected to be somewhat closer or even higher than as obtained for the significant damage state. From past studies, a damping of the order of 5% of the critical damping seems to be an appropriate choice for low- to mid-rise RC frame buildings. Therefore, in the present study, damping equals to 5% of the critical damping has been used for all NLTHA.

3.8.4.2 Modelling of Damping

Otani (1980) compared the experimentally obtained non-linear seismic response of a three-storied, small-scale RC structure with the response obtained from numerical models. He observed that the choice of the damping model depends on the amplitude of the oscillations. Zahrah and Hall (1984) observed that damping has little effect on the amount of energy imparted to a structure but significantly affects the hysteretic energy dissipation and hence damage. Vidic et al. (1994) studied the ratio of the hysteretic to input energy for inelastic SDOF systems considering mass or tangent stiffness proportional damping. They observed that the ratio of the hysteretic to input energy is significantly influenced by the modelling of damping.

Leger and Dussault (1992) developed a tangent Rayleigh damping model using the proportionality coefficients that are updated at each time step. They considered damping corresponding to first mode and the mode required to obtain 95% effective modal mass. They concluded that for short-period MDOF structures ($T_1 < 0.50$ s), damping proportional to instantaneous stiffness should be used. The Rayleigh damping model using the instantaneous stiffness with proportionality coefficients computed from the elastic properties provides a good agreement with the tangent damping model in medium-period MDOF structures ($0.50 < T_1 < 1.50$ s). For MDOF structures with, $T_1 > 1.50$ s, the seismic response is not affected by the type of the Rayleigh damping model used (Leger and Dussault 1992).

Ibarra and Krawinkler (2005) analyzed the collapse capacity of deteriorating SDOF systems with mass proportional damping only, for two different damping values, viz., 5% and 10%. They observed that the increasing mass proportional damping from 5% to 10% results in an increase in collapse capacity by 15-20%. Hall (2006) highlighted that the Rayleigh damping in the analysis of structures under dynamic loads may result in unrealistically high damping forces under certain conditions. In non-linear dynamic analysis, where the non-linearity is of the

softening type, limits on restoring forces are imposed by yielding, cracking, sliding and buckling. If the damping is formulated considering the initial stiffness proportional damping term, the damping forces in a softening element can reach unrealistically high values as compared to the element's restoring forces as the velocity gradient increases across the softening element. It has been shown that when the system damping matrix is based on the initial stiffness, artificial damping corresponding to lower modes is generated after the yielding of the structure (Charney 2008; Petrini et al. 2008; Hardyniec and Charney 2015; Chopra and McKenna 2015).

Deierlein et al. (2010) provided guidelines to select the damping for non-linear dynamic analysis. It has been recommended to use viscous damping ranging from 1% to 5% of critical damping over the range of elastic periods between $0.2T$ and $1.5T$, for different building heights. It is further recommended that the damping values should be chosen at the lower end of the recommended values for tall buildings as well as for the service level of earthquake analysis. Erduran (2012) investigated the seismic response of code-complaint three- and nine-storied steel moment resisting frame buildings. The mass-proportional damping results in the highest, while the stiffness-proportional damping results in the lowest values of damping force to base shear ratio. The Rayleigh damping leads to a damping force in between the mass- and the stiffness-proportional damping models since it is a combination of the two. The damping model used in inelastic time-history analysis does not significantly influence the story-drift demands of the three-storey building since the response of the low-rise buildings is governed by the fundamental mode of vibration and all the damping models have the same damping ratio corresponding to the fundamental mode of vibration. The storey drift demands are significantly influenced in the upper floors of the nine-storied building due to different damping corresponding to higher modes of vibration. It was recommended to use Rayleigh damping at the elongated first mode period $T = 1.4T_1$ and $T = 0.2$ s as it limits the contribution of the damping forces to the response preventing the suppression of higher modes.

Jehel et al. (2014) developed analytical formulations for Rayleigh damping based on initial and tangent stiffness. They concluded that it is easier to design a Rayleigh damping model with well-controlled damping ratios throughout the inelastic time-history analysis when the tangent stiffness is used. Hardyniec and Charney (2015) highlighted that the damping model has a profound effect on the behaviour of a frame. The variation among different damping modelling techniques (e.g., mass and initial stiffness) is the most apparent near collapse. Chopra and McKenna (2015) highlighted that replacing the stiffness proportional part of Rayleigh damping

by the tangent stiffness matrix is shown to improve the results significantly. They also highlighted that with a distributed plasticity model, the structural response is not sensitive to the damping model and even a Rayleigh damping model can be used. Based on the recommended guidelines, in the present study, 5% Rayleigh damping corresponding to the first mode period and period resulting in a total of 95% mass participation, has been used for all NLTHA.

3.9 COMPARATIVE STUDIES BETWEEN NON-LINEAR STATIC AND DYNAMIC PROCEDURES

In the past two decades, a significant number of research efforts have been made in order to investigate the applicability of the simplified non-linear static procedures for seismic performance assessment of the structures (Lew and Kunnath 2001; Dolsek and Fajfar 2005; Deb and Geddam 2006; Deb 2008; Suresh et al. 2008). Lawson et al. (1994) studied moment resisting frames and highlighted that large differences between drift demands across the storey levels were observed using NSP for high-rise buildings. The obtained drift pattern was found to be sensitive to the loading pattern in the pushover analysis indicating that higher mode effects became important. The NSP was able to identify the weak links in the structures (Lawson et al. 1994; Faella 1996) and drift demands for low-rise buildings (Lawson et al. 1994; Kunnath et al. 1996; Krawinkler and Seneviratna 1998; Peter and Badoux 2000; Gupta and Kunnath 2000; Lew and Kunnath 2001). It was observed that the NSP is unable to capture yielding in columns at the upper storey levels (Lew and Kunnath 2001; Dolsek and Fajfar 2005). The pushover analysis produces conservative estimates of ductility demands (Kim et al. 2001). On the other hand, Albanesi et al. (2002) reported that both the conventional pushover and the energy-based pushover analyses underestimate the maximum displacement demands as compared to non-linear dynamic analysis results.

Gupta and Kunnath (1999) studied the effect of loading pattern on the obtained capacity curve using NSP. They utilized two conventional load patterns (i.e., proportional to fundamental mode as recommended by FEMA and uniform), and a load pattern that changed continuously depending on the instantaneous dynamic properties (adaptive) of the system. They concluded that the adaptive load pattern was able to capture accurately the base shear amplification and progressive yielding while the other two patterns were found to be deficient in predicting the amplification in base shear demand. Skokan and Hart (2000) studied 3-, 9- and 20-storied moment resisting frame buildings using pushover analysis. They evaluated seismic demand

using two different methods, i.e., the 'Displacement Coefficient Method' (DCM) and the 'Capacity Spectrum Method' (CSM) and compared the results with those obtained from non-linear dynamic analyses. Their results depicted that the DCM provided estimates of maximum roof displacement and inter-storey drift within 20% of the results from non-linear dynamic analyses; whereas the CSM tended to underestimate the seismic demands.

Chopra et al. (2003) investigated the applicability of the assumption usually made in pushover analyses that the roof displacement of a building can be estimated from the deformation of an equivalent SDOF system. They considered six one bay frames with 3-, 6-, 9-, 12-, 15- and 18-storeys and multi bay 9- and 20-storied steel moment resisting frame buildings. They observed that the equivalent SDOF system with higher ductility, overestimated the roof displacements and it further increases for longer period systems; whereas the situation was found out to be reversed for low ductility SDOF systems. Papanikolaou and Elnashai (2005a, b) observed that pushover analysis is able to predict the approximate displacement demands for structures that are free of irregularities in plan and elevation. Kalkan and Kunnath (2006) showed that the conventional pushover procedure underestimates the displacement and inter-storey drift demands. Both the MPA method and the adaptive modal combination (AMC) method were found to be satisfactory for estimating seismic demands across the floor levels except for a few cases.

Moshref et al. (2011) studied the applicability of the NSP prescribed in NZSEE (2006) and FEMA 440 (2005) in order to determine peak ground acceleration (PGA) values which cause structural collapse. They found that both NSP overestimate the building collapse capacity. Lagaros and Fragiadakis (2011) studied the DCM, CSM and N2 method (Fajfar 1999) for two regular and two irregular buildings. They observed that both DCM and N2 method predict demand closer to the median demand obtained from the incremental dynamic analysis (IDA). The CSM overestimates the seismic demands slightly for lower intensities, but as the intensity of excitation increases, the CSM largely overestimates the seismic demands.

Ghaffarzadeh et al. (2013) studied seismic response of RC moment resisting frames using NSP and NDP considering three different lateral load patterns in case of NSP, viz. uniform, triangular and mode proportional. They observed that the uniform lateral load pattern overestimates the deformation demands in lower stories. The triangular and mode proportional load patterns predict deformation demands closer to those obtained from NDP.

3.10 NUMERICAL STUDY

In the present study, a set of generic reinforced-concrete (RC) buildings with identical plan layouts (Fig. 3.9) are considered. The plan layout has been selected from the data collected during field surveys in test beds to represent a variety of building characteristics. The height of buildings is considered as 4-, 8- and 12-storeys, representing the mid- and high-rise building stock in India. A constant storey height of 3.3 m is considered which was most commonly observed during field surveys. The buildings have been designed as SMRF according to relevant Indian design codes. It is to be noted that the current Indian code assigns a response reduction factor (behaviour factor) of 5 to SMRF buildings.
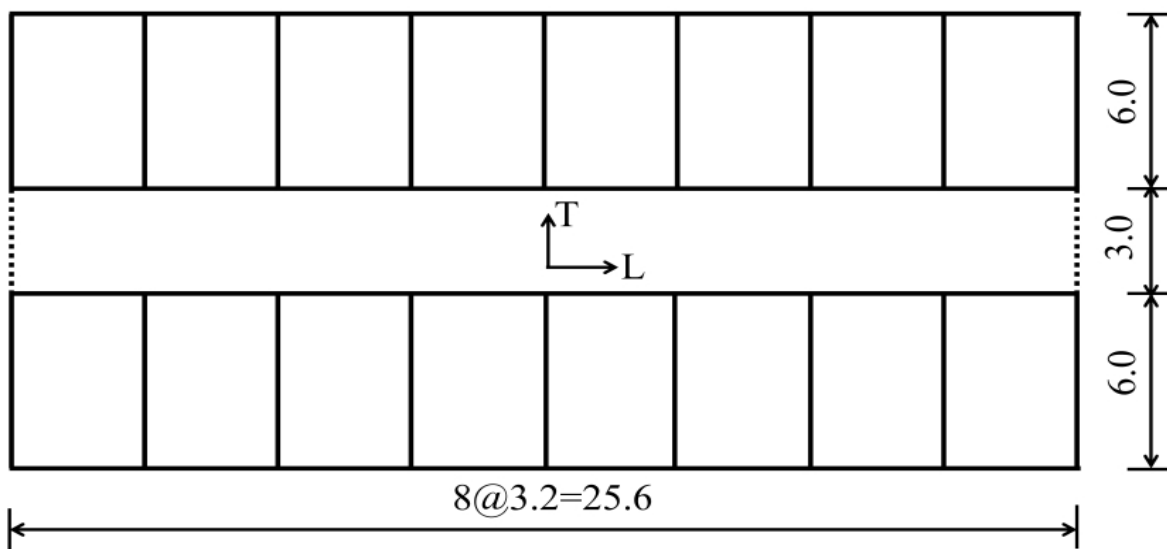
Fig. 3.9 Generic plan of the representative buildings considered in the study. (All dimensions are in meters, L - longitudinal, T - transverse).

The building models are created in the proprietary structural analysis and design code SAP 2000 v 14.2.4 (CSI 2010). Beams and columns are modelled using 3-D frame elements and the slabs have been modelled as rigid diaphragms. The cracked section properties of RC beams and columns are derived following ASCE 41-06 (2007) guidelines. Dead loads and live loads on the buildings have been assigned according to IS 875 Part 1 (1987a) and IS 875 Part 2 (1987b), respectively. The buildings are analyzed and designed as per Indian standards IS 456 (2000) and IS 1893 Part 1 (2002) for the highest seismic zone V on soil type I (rock and hard soil). These building models are representative of design level defined in IS 1893 Part 1 (2002) and do not conform to strong-column weak-beam (SCWB) design criterion. P-delta effect has also been considered in the analysis and design. The beams and columns of the building have been so proportioned that they have about 0.5-1.5% reinforcement at each face of the beams and 1.5-4% longitudinal reinforcement in the columns.

For the estimation of the non-linear response of the considered building models, lumped-plasticity models representing the potential failure modes in the considered buildings are developed. Uniaxial moment plastic hinges and P-M-M interaction hinges have been assigned at both ends of beams and columns, respectively. Since the buildings are designed as SMRF with beams and columns designed for capacity shear, the shear failure mode has been ignored. The idealized force-deformation curve of ASCE 41-06 (2007) shown in Fig. 3.4 has been assigned to each plastic hinge. The member sizes and modelling parameters for typical beams and columns are presented in Table 3.6. For non-linear dynamic analysis, Rayleigh damping of 5% corresponding to first and third mode of vibration has been assigned.

Table 3.6 Member sizes and modelling parameters for typical beams and columns. (For notation, please refer to Figure 3.4).

Building Model	Member	Sizes	θ_p (rad)	θ_{pc} (rad)
4-storey	Beam	0.30m x 0.45m	0.025	0.025
	Column	0.35m x 0.35m	0.019	0.010
8-storey	Beam	0.30m x 0.45m	0.025	0.025
	Column	0.35m x 0.35m	0.016	0.009
12-storey	Beam	0.40m x 0.50m	0.025	0.025
	Column	0.40m x 0.40m	0.013	0.008

In the non-linear static procedure, the incipient collapse state has been considered as the point where instability occurs or strength drops down to 80% of the maximum strength, whichever is occurring first. In the non-linear dynamic procedure, incipient collapse has been considered as the point where a small increment in intensity measure (IM) is able to cause a very large increment in the engineering demand parameter (EDP).

In order to investigate the dynamic response of the considered structural models, Incremental Dynamic Analysis (IDA) (Vamvatsikos and Cornell, 2002) has been performed. The ground-motion records used in the present study have been selected for rock/stiff site conditions (i.e., NEHRP site classes B, C and D) at the recording station, magnitude range ($M_w > 6.5$), and far-field range of source-to-site distance ($R_s > 10$ km). For each of the considered ground-motion records, the period corresponding to peak spectral acceleration (T_{peak}) has also been determined and presented in Table 3.7.

3.10.1 Static and Dynamic Capacity Curves

Figure 3.10 presents the static capacity curves for the considered building models. The static capacity curves are represented in terms of normalized coordinates (base shear V normalized by the seismic weight of the building W) and spectral displacement S_d. Table 3.8 presents the dynamic characteristics, design base shear V_d, yield base shear V_y, over-strength Ω (defined as

the ratio of the yield base shear to the design base shear), and ductility capacity μ of the considered building models.

Table 3.7 The suite of 30 ground-motion records with major component used for the present study. (Records have been selected from the PEER [2011] database).

Event	Station	$V_{s,30}$[1] (m/s)	NEHRP site class	M_w[2]	R_{jb}[3] (km)	PGA (g)	T_{peak}[4] (s)
Imperial Valley-06, 1979	Calipatria Fire Station	205.3	D	6.5	23.2	0.133	0.29
Imperial Valley-06, 1979	Compuertas	274.5	D	6.5	13.5	0.194	0.24
Superstition Hills-02, 1987	Plaster City	345.4	D	6.5	22.2	0.193	0.42
Superstition Hills-02, 1987	Wildlife Liquef. Array	207.5	D	6.5	23.9	0.207	0.11
San Fernando, 1971	Fairmont Dam	684.9	C	6.6	25.6	0.114	0.24
San Fernando, 1971	Lake Hughes #12	602.1	C	6.6	14.0	0.365	0.17
Northridge-01,1994	Burbank Howard Rd.	821.7	B	6.7	15.9	0.143	0.19
Northridge-01,1994	LA - Griffith Park Obs.	1015.9	B	6.7	21.2	0.252	0.50
Spitak-Armenia, 1988	Gukasian	274.5	D	6.8	24.0	0.222	0.16
Irpinia-Italy-01, 1980	Bisaccia	1000	B	6.9	17.5	0.122	0.46
Irpinia-Italy-01, 1980	Calitri	600	C	6.9	13.3	0.186	0.30
Kobe-Japan, 1995	Kakogawa	312	D	6.9	22.5	0.356	0.17
Kobe-Japan, 1995	Shin-Osaka	256	D	6.9	19.1	0.271	0.66
Loma Prieta, 1989	Gilroy Array #6	663.3	C	6.9	17.9	0.180	0.24
Loma Prieta, 1989	UCSC	714	C	6.9	12.2	0.374	0.16
Cape Mendocino, 1992	Fortuna - Fortuna Blvd	457.1	C	7.0	16.0	0.125	0.25
Cape Mendocino, 1992	Shelter Cove Airport	513.7	C	7.0	26.5	0.238	0.20
Hector Mine, 1999	Hector	684.9	C	7.1	10.3	0.336	0.50
Düzce-Turkey, 1999	Lamont 1061	481	C	7.1	11.5	0.126	0.34
Düzce-Turkey, 1999	Bolu	326	D	7.1	12.0	0.785	0.32
Landers, 1992	Joshua Tree	379.3	C	7.3	11.0	0.288	0.70
Landers, 1992	Yermo Fire Station	353.6	D	7.3	23.6	0.223	0.28
Kocaeli-Turkey, 1999	Arcelik	523	C	7.5	10.6	0.217	0.17
Kocaeli-Turkey, 1999	Düzce	276	D	7.5	13.6	0.375	0.38
Chi-Chi-Taiwan, 1999	CHY025	277.5	D	7.6	19.1	0.160	0.50
Chi-Chi-Taiwan, 1999	CHY035	555.2	C	7.6	12.6	0.278	0.60
Friuli-Italy-01, 1976	Tolmezzo	424.8	C	6.5	15.0	0.386	0.26
San Fernando, 1971	Lake Hughes #4	821.7	B	6.6	19.4	0.192	0.15
Loma Prieta, 1989	Coyote Lake Dam	295	D	6.9	20.4	0.185	0.19
Northridge-01, 1994	Beverly Hills - 12520	545.7	C	6.7	12.4	0.594	0.25

[1] Average shear wave velocity of the upper 30m of soil
[2] Moment magnitude M_w
[3] Joyner-Boore distance (closest horizontal distance to the surface projection of the rupture plane)
[4] Period corresponding to peak spectral acceleration of the ground-motion record.

The buildings have been designed for the same forces (controlled by capping on period of vibration of the building); hence they have almost the same strength capacity, in either of the directions. The 4-storied building has the highest over-strength factor (Ω) as compared to the 8- and 12-storied buildings. The reason for this higher over-strength lies in the fact that the design of a 4-storied building is governed by gravity loads which imposes a higher load factor as

compared to earthquake load. Further, the ductility capacity of the considered building models is found out to be lesser in the transverse direction as compared to the longitudinal direction (Fig. 3.10), which can be attributed to the combined effect of the lesser redundancy and increased yield spectral displacement.
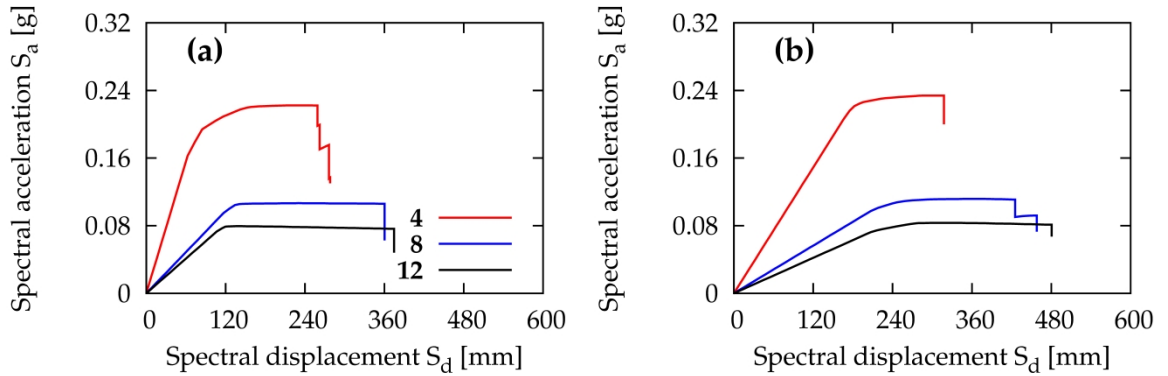
Fig. 3.10 Static capacity curves for considered building models: (a) in longitudinal direction; and (b) in transverse direction.

Table 3.8 Dynamic characteristics, structural strength and ductility parameters.

Building Model	Direction	T_1 (sec)	α_{m1} (%)	V_d (kN)	V_y (kN)	Ω	μ
4-storey	L	1.22	85	1360	3476	2.56	3.23
	T	1.75	81	1360	3635	2.67	1.73
8-storey	L	2.20	80	1750	3597	2.06	2.70
	T	2.90	80	1750	3712	2.12	1.82
12-storey	L	2.36	83	2110	4468	2.12	3.27
	T	3.38	81	2110	4534	2.15	2.06

L – longitudinal, T – transverse, α_{m1} – modal mass participation ratio corresponding to the fundamental mode of vibration.

The capacity curves obtained using the static and dynamic methods have a basic difference. In the case of dynamic capacity curves, the IM ordinates take into account the characteristics of the ground-motion records, as these are obtained from direct application of ground-motion records (Fig. 3.11b), whereas, in the case of the static method, the capacity curve is a characteristic of the structure alone (Fig. 3.11a), and does not represent the influence of ground-motion characteristics. Further, flattening of the static capacity curve represents yielding of the building, whereas, in the case of the dynamic capacity curve, it represents dynamic instability or collapse of the building. Contrary to the static capacity curves, yielding of the structure is not distinctly visible in the dynamic capacity curves.

To compare the static and dynamic capacity curves, a convolution of the static capacity curves with the demand spectrum is necessary. Dolsek and Fajfar (2007) suggested an approach called as Incremental N2 (or IN2) method, where an incremental static analysis using the N2 method (Fajfar 1999) is performed in order to obtain the capacity curve. Vamvatsikos and Cornell

(2006) developed an MS Excel workbook application "SPO2IDA tool" in order to convert the static capacity curve into approximate IDA results. However, this tool is applicable to low-rise buildings, which are regular in plan and elevation, and in which their response is dominated by first mode translational behaviour.
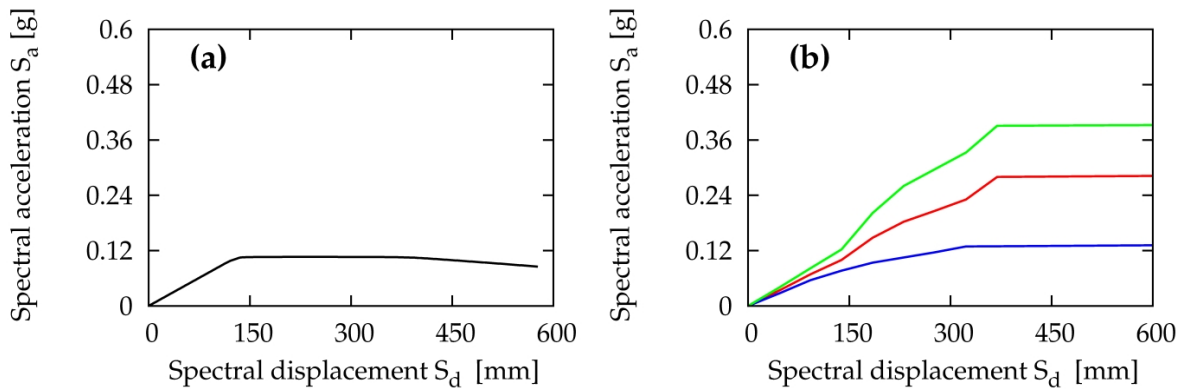
Fig. 3.11 Capacity curves for a building model derived by: (a) static; and (b) dynamic procedure.

In this study, a similar approach as suggested by Dolsek and Fajfar (2007) has been used to compare the static capacity curve with dynamic capacity curve. Figure 3.12 schematically illustrates the process of transformation. Here, any S_a value corresponding to a given value of S_d beyond the yield displacement on the transformed capacity curve, is obtained using a demand spectrum suitably scaled to result in the chosen value of inelastic S_d. For obtaining the inelastic S_d from the corresponding elastic S_d, the displacement modification method (DMM) of ASCE/SEI 41-13 (2013) has been used. In the displacement modification method (DMM), the inelastic S_d can be obtained directly from the corresponding elastic S_d using the modification factor (or inelastic displacement ratio). It can be noted that, depending on the period of the building, the elastic and inelastic S_d may differ by different magnitudes. Up to the structure's yield point, the transformed capacity curve follows the original capacity curve, and if the equal displacement principle is assumed to be valid (as is the case for most long-period structures), the convoluted capacity curve is simply an extension of the elastic portion of the original capacity curve, up to collapse.

Figures 3.13-3.15 present a comparison of the dynamic capacity curves with transformed (convoluted) capacity spectrum for the considered building models. The dynamic capacity curves have been presented in the form of 16th, 50th, and 84th percentile. It can be observed that, in each case, the transformed static capacity curves are very close to the 50th percentile (median) IDA curves, though the transformed capacity curves are overestimating the structures' capacities, as compared to the median IDA curves. Nevertheless, the transformed static

capacity curves are well within the 16th and 84th percentile IDA curves, except for one case. One of the primary reasons for this difference in collapse capacity obtained through two different procedures can be attributed to the spectral shape of the ground-motion records.
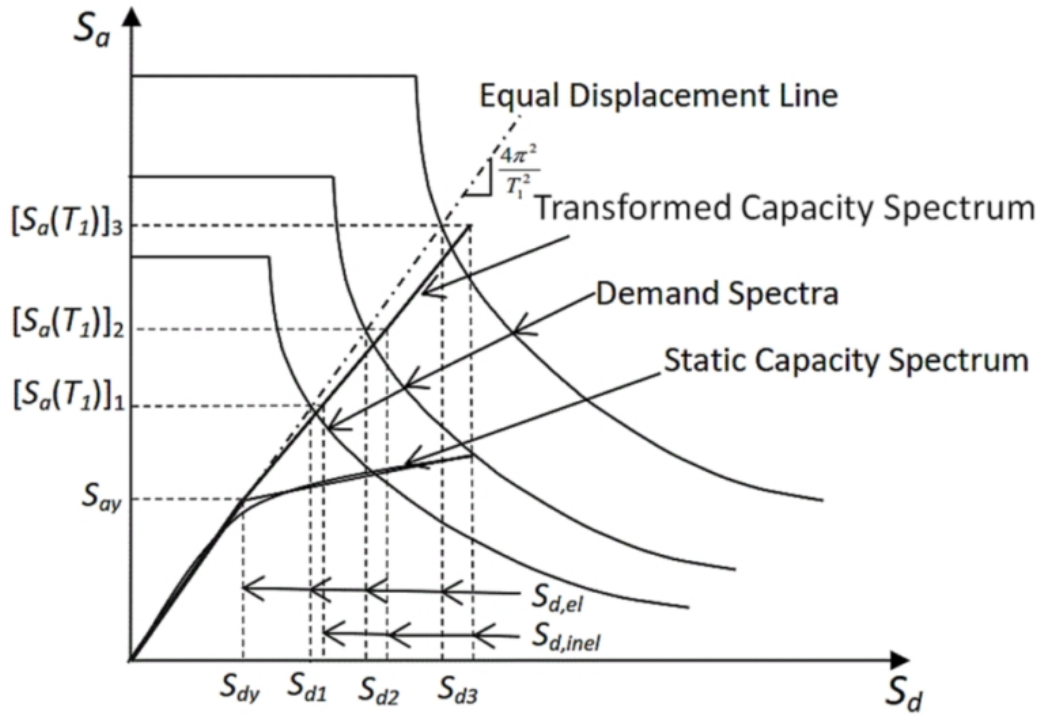
Fig. 3.12 Transformation of the static capacity curve using convolution with the demand.

Table 3.9 compares the roof drift ratio (RDR) at incipient collapse, as obtained from static and dynamic procedures. It can be observed that the RDR at the point of collapse, decreases with increasing building height. One of the primary reasons for this observation is that roof drifts are in general controlled by the deformations in lower storeys. With the increase in building height, the normalized axial force ratio on columns in the lower storeys increases, and thereby the plastic deformation capacity of columns reduces. This reduction in plastic rotation capacity of columns leads to reduced overall drift capacity of the building near collapse. Similar observations were also made by Haselton et al. (2011a). Further, the roof drift at incipient collapse, predicted by the static method is on the higher side as compared to the dynamic method. The reason for this increased roof drift capacity in the static method lies in the fact that the static method is based on the fundamental mode of vibration, which is unable to capture the contribution of higher modes (which are particularly important in drift contribution at the upper floors) and overestimates the drift capacity at incipient collapse.
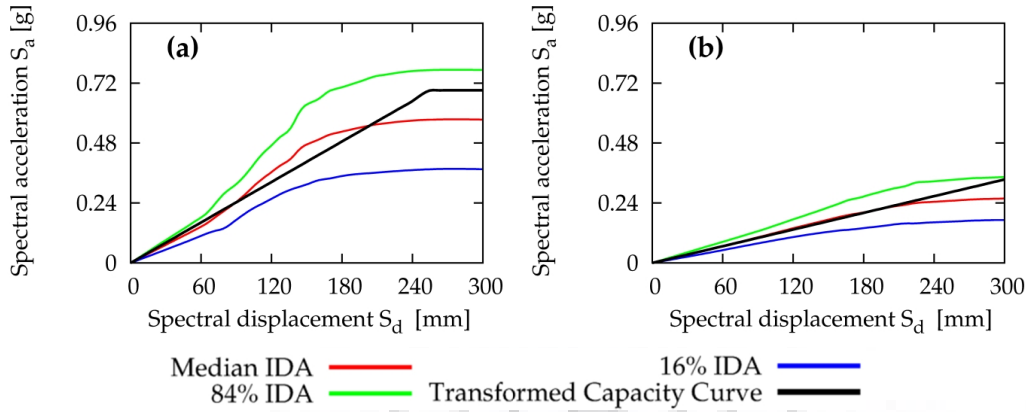
Fig. 3.13 Comparison of transformed static capacity curve with dynamic capacity curves for the 4-storied building: (a) in longitudinal direction; and (b) in transverse direction.
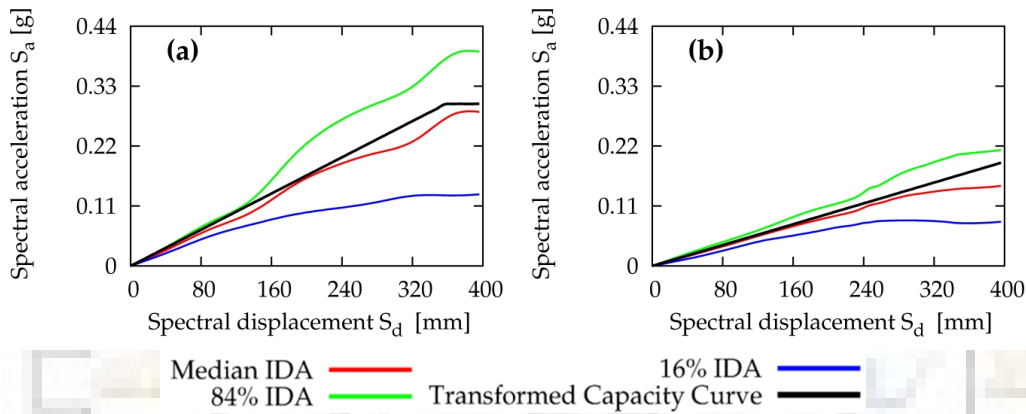
Fig. 3.14 Comparison of transformed static capacity curve with dynamic capacity curves for the 8-storied building: (a) in longitudinal direction; and (b) in transverse direction.
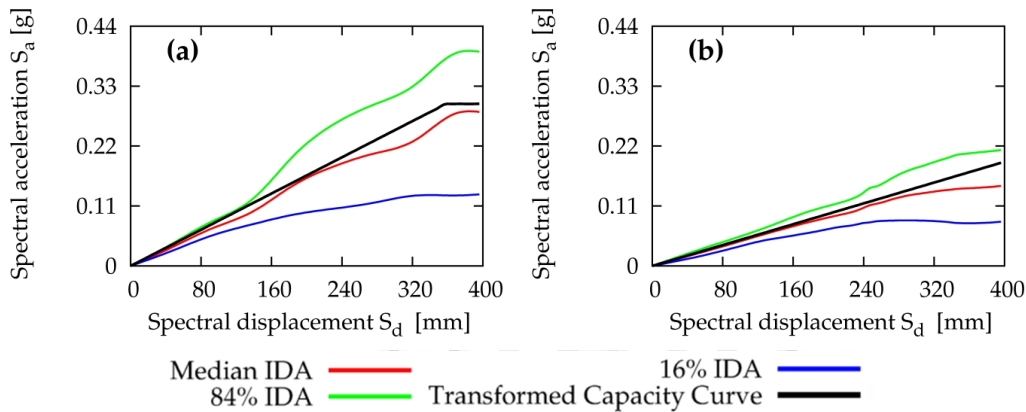
Fig. 3.15 Comparison of transformed static capacity curve with dynamic capacity curves for the 12-storied building: (a) in longitudinal direction; and (b) in transverse direction.

Table 3.9 Roof drift ratio (RDR) at collapse from static and dynamic procedures.

Building Model	Static RDR		Dynamic RDR	
	Longitudinal	Transverse	Longitudinal	Transverse
4-storey	0.024	0.030	0.023	0.027
8-storey	0.017	0.021	0.016	0.016
12-storey	0.012	0.016	0.011	0.011

3.11 SUMMARY

Various linear and non-linear methods for evaluation of seismic response of structures are presented. Advantages, weaknesses and limitations of both conventional and advanced pushover analyses methods are discussed. A comprehensive state-of-the-art on the application of non-linear static and non-linear dynamic procedure is presented along with component behaviour, failure modes and simulation of these failure modes and modelling of damping, selection and scaling of ground-motion records and its effect on structural response is also discussed. A state-of-the-art on comparative studies between non-linear static and dynamic procedures is also presented.

A comparative study on static and dynamic procedures has been conducted for Indian-code designed RC frame buildings. The conventional non-linear static and IDA are conducted on considered RC frame buildings. The derived static and dynamic capacity curves cannot be compared directly as the two curves are in different domains. In order to compare the static and dynamic capacity curves, the static capacity curve has been transformed using convolution with the demand spectrum and compared with the median dynamic capacity curve. The following observations have been made for the two sets of the capacity curves:

- It has been observed that the transformed static capacity curve closely follows the median dynamic capacity curves in the elastic range and slightly deviates in the inelastic range. This observation can be attributed to the fact that the transformed capacity curve is based on the fundamental mode of vibration; which captures the elastic response but as the inelasticity increases, the dynamic characteristics of the building get changed and the contribution of higher modes also becomes significant. Thereby, the transformed capacity curve starts deviating from median dynamic capacity curve.

- The transformed static capacity curve in general overestimates the structural collapse capacity. However, the transformed static capacity curve lies within the median and 84th percentile of the dynamic capacity curves. This observation can be primarily attributed to the fact that collapse capacity of a structure is dependent on the ground-motion record suite used in non-linear dynamic analyses, as it is strongly influenced by the spectral shape of the ground-motion records used.

4.1 INTRODUCTION

Today, the majority of national seismic building codes are based on a conventional 'Force-based design' (FBD) principle with the intended performance objective to ensure a 'No Collapse' ('Life Safety' in some of the codes) design target under the Maximum Considered Earthquake (MCE) ground-motion level. The FBD principle is based on prescriptions alone and does not provide any framework to ensure the intent of the respective seismic design code. To address this issue, the concept of 'Performance-based design' (PBD) was developed for existing buildings in its earlier developments (e.g. FEMA 273 1997). Later, the concept of PBD was extended for the seismic design of new buildings. During the past decade, the PBD methodology has gained wide popularity and has been updated continuously, with its documentation in FEMA 356 (2000), FEMA 440 (2005), FEMA P695 (2009) and FEMA P58 (2012). With these developments in the field of PBD, the research in seismic fragility analysis has also boosted significantly. In recent years, with the advancements in PBEE, and understanding of the uncertainties involved in different steps of design, it has been highlighted that the building's collapse risk need to be controlled (FEMA P695 2009; ASCE 7-10 2010 and NIST 2012) to ensure the "Life Safety" of the building occupants with a reasonable level of reliability. In line with this understanding, ASCE 7 (2010) adopted a risk-targeted design (RTD) framework based on various risk categories of structures. This framework targets a 10% probability of collapse for MCE ground-motions as the acceptance criteria for structures of risk category II (ASCE 7 2010).

In this chapter, methods to estimate the seismic vulnerability of buildings are reviewed. A numerical study on seismic fragility of Indian code-designed RC frame buildings with structural configurations SC A, SC B, and SC C (as identified in Chapter 2) is presented. A large fraction of India's building stock still consists of pre-code (designed for gravity loads alone) buildings, as also observed in the field surveys that had been conducted in Mussoorie and Nainital. Therefore, three different design levels are used in the numerical study that are representative of (i) pre-code buildings (designed for gravity loads alone), (ii) moderate-code buildings (designed as SMRF but non-conforming to strong-column weak-beam (SCWB)

design), and (iii) high-code buildings (designed as SMRF and also conforming to SCWB design). For each of the considered building models, the median collapse capacity, the typical collapse mechanisms, record-to-record variability (at collapse), and the collapse fragility curves are presented and compared.

4.2 METHODS OF SEISMIC VULNERABILITY ESTIMATION

The seismic vulnerability (or fragility) of a structure is generally defined as its susceptibility to experience damage, given a certain ground shaking intensity. It is expressed as a relationship between a parameter representing the ground-motion severity (e.g. intensity, PGA, spectral acceleration or spectral displacement etc.) and structural damage (expressed in terms of damage grades, maximum inter-storey drift ratio, or an average damage ratio). In order to represent seismic vulnerability, fragility curves and Damage Probability Matrices (DPMs) are the most commonly used formats. Both methods describe the conditional probability of exceeding different levels of damage at a given ground-motion intensity. Fragility curves express the data in a graphical format as a continuous curve, whereas DPMs express it numerically in terms of discrete values. For the development of vulnerability relations for different types of buildings, a number of approaches are available in literature (e.g. Calvi et al. 2006; D'Ayala et al. 2010; Meslem and D'Ayala 2012; D'Ayala et al. 2014a; Yepes-Estrada et al. 2016), ranging from those based on empirical damage data collected from past earthquakes to those based on the purely analytical simulations. The available methods of vulnerability assessment can broadly be classified into three generic groups: (i) empirical methods (e.g. Whitman et al. 1973; Spence et al. 1992; Hassan and Sozen 1997; Rossetto and Elnashai 2003; Yakut 2004; Jaiswal et al. 2011; Ioannou et al. 2015; Maqsood et al. 2016), (ii) analytical methods (e.g. Singhal and Kiremidjian 1996; Rossetto and Elnashai 2005), and (iii) hybrid methods (e.g. Kappos et al. 1995; Barbat et al. 1996; Kappos et al. 1998).

Empirical methods of vulnerability assessment are based on post-earthquake damage observations and are therefore considered to be the most realistic approach of vulnerability assessment for any particular region. These methods are mostly based on intensity scales as a measure of ground-motion severity. These intensity scales include Modified Mercalli Intensity (MMI; Wood and Neumann 1931), Medvedev-Sponheuer-Karnik (MSK; Sponheuer and Karnik 1964; Medvedev et al. 1965), European Macroseismic Scale (EMS-98; Grünthal et al.

1998) and the Parameterless scale of seismic intensity (PSI; Spence et al. 1991). However, the lack of adequate and reliable damage data for various building typologies, subjected to different earthquake intensities generally restricts the applicability of empirical methods. This is particularly true for lower shaking intensities, where structural and non-structural damage is difficult to be observed.

Considering the lack of sufficient empirical post-earthquake damage data, and excessive costs of experimental tests, analytical methods may be a more attractive approach for vulnerability assessment. These methods include 'Capacity Spectrum Method' (CSM; ATC 40 1996; FEMA 440 2005; Rossetto et al. 2016), 'Collapse-Based Method' (CBM; D'Ayala and Speranza 2002; Bernardini et al. 1990; Cosenza et al. 2005), 'Displacement-Based Method' (DBM; D'Ayala 2005; Crowley et al. 2004; Miranda 1999; Silva et al. 2013), 'Displacement Coefficient Method' (DCM; FEMA 356 2000; FEMA 440 2005), 'Incremental Dynamic Analysis' (IDA; Shome and Cornell 1999; Vamvatsikos and Cornell 2002) and 'Multiple Stripe Analysis' (MSA; Koopaee et al. 2017).

Earlier attempts to analytically assess the seismic fragility of buildings were primarily based on the non-linear static procedure (NSP; among others FEMA 2002; Penelis et al. 2003; Rossetto and Elnashai 2003; Rossetto and Elnashai 2005; Kappos et al. 2006; Barbat et al. 2008; Haldar and Singh 2009; D'Ayala et al. 2012; D'Ayala and Meslem 2013; D'Ayala et al. 2014b; Silva et al. 2014; Rossetto et al. 2016). In this non-linear static procedure, a structure's capacity spectrum (inelastic displacement) is utilized to identify the damage state of the structure (e.g. Barbat et al. 2008; Haldar and Singh 2009). In this procedure, the effect of period elongation associated with an inelastic structure is implicitly taken into account through the inelastic displacement ratio (IDR). However, the definition of structural collapse during NSP is still an ongoing research topic and a significant variation between different guidelines is reported (Kappos et al. 2006). For example, HAZUS (FEMA 2002) defines the collapse damage state as the damage state when 50% of the components reach the post-capping deformation point in the cyclic backbone curve, whereas FEMA P695 (FEMA 2009) defines the collapse point as the point where the static lateral force carrying capacity drops down to 80% of the maximum. Based on various shake-table test data on buildings, Dymiotis et al. (1999) observed that a maximum inter-storey drift ratio of 4% can be considered as a suitable collapse limit state for buildings.

More recent studies (e.g. Koopaee et al. 2017) on seismic fragility assessment are either based on a cumbersome multiple stripe analysis (MSA) (Kohrangi et al. 2016a; Kohrangi et al. 2016b; Koopaee et al. 2017) procedure or non-linear incremental dynamic analysis (IDA) procedure (i.e. Vamvatsikos and Cornell 2002; Zareian and Krawinkler 2007; Haselton and Deierlein 2007a; Zareian et al. 2010; Haselton et al. 2011a; Liel et al. 2011; Champion and Liel 2012; Ahmad et al. 2014; Burton et al. 2014; Xu et al. 2014; Balasubramnian et al. 2014; Eads et al. 2015, 2016; Zeng et al. 2016; Nassirpour et al. 2017). The MSA procedure requires different ground-motion record suites corresponding to different hazard levels (Kohrangi et al. 2016a; Koopaee et al. 2017) with site-specific motions. Therefore, it is quite demanding in selecting the ground-motion records, particularly when assessing the collapse fragility of a wide range of buildings. On the other hand, IDA analyses can be conducted with a general ground-motion record suite, selected based on advanced ground-motion selection methods discussed in Chapter 3 (e.g. CMS, CS, and GCIM). Both MSA and IDA procedures are based on non-linear dynamic procedure, and therefore explicitly take into account the effect of period elongation. In the case of NDP, structural collapse is defined as the point where a slight increment in IM leads to very large increments in the Damage Measure (DM) (Vamvatsikos and Cornell 2002). The main disadvantage of analytical methods is that these are computationally very challenging and time consuming, and therefore not suitable to be applied for a large area or country with widely varying construction practices. Further, it is very cumbersome task to simulate and replicate the real behaviour of structures under earthquake shaking with the available techniques of analytical modelling and the instability of the solution algorithm used "may lead to completely divergent results if not handled with caution" (Kappos et al. 2006).

The hybrid approach of vulnerability assessment is the combination of available empirical data with the results of numerical analysis and thus bridges the gap between the lack of empirical data and the uncertainties of the analytical estimation (Barbat et al. 2008). The main difficulty of hybrid methods is to calibrate analytical results using observed data, because the two sets of data have two different sources of uncertainty, and therefore cannot be compared directly.

Although India has suffered several devastating earthquakes (e.g. 1897 Great Assam earthquake, 1991 Uttarkashi earthquake, 1993 Killari earthquake, 1997 Jabalpur earthquake, 1999 Chamoli earthquake, 2001 Bhuj earthquake, 2005 Kashmir earthquake, 2011 Sikkim

earthquake, 2016 Manipur earthquake etc.) in the past, very few systematic post-earthquake damage surveys have been conducted. The quantity and quality of available data does not allow a proper analysis in depth. Further, the available damage data is also not in a format which is suitable for the development and calibration of reliable estimates of seismic vulnerability. Based on the available information for Indian earthquakes, Prasad (2009) has proposed intensity-based DPMs for Indian model buildings. In the absence of adequate empirical data, these need to be supported and supplemented by extensive analytical studies for different Indian model building types. Further, these DPMs are valid for buildings resting on flat land, as these do not account for irregular structural configuration of buildings in hilly regions.

An important step in developing fragility estimates (DPMs/fragility functions) consists in the definition of various 'damage states' and their corresponding threshold parameters. The definition of different damage state also varies significantly (e.g. Barbat et al. 2006; Kappos et al. 2006). In intensity scales, these damage states are defined in descriptive terms, while for fragility analysis these need to be defined in terms of engineering parameters (e.g. PGA, spectral acceleration, spectral displacement, etc.). The selection of an engineering demand parameter is dependent on the objective of response evaluation (Vamvatsikos and Cornell 2002). For example, to predict structural damage the maximum inter-storey drift can be an ideal choice, whereas non-structural damage may be best predicted either by using maximum interstorey drift or by peak floor acceleration demands.

In the present study, the IDA method of analytical fragility assessment has been adopted. In this method, the structural response, ranging from elastic response to the global dynamic instability, is captured under a suite of ground-motion records. In this methodology, 'collapse' has a clear definition, and it is defined as the 'damage state' when a slight increase in IM cause very large increase in DM (Vamvatsikos and Cornell 2002; Haselton et al. 2011a; Liel et al. 2011).

4.3 COLLAPSE MARGIN RATIO AND ACCEPTANCE CRITERION

The collapse margin ratio (CMR) is defined as the ratio of the median collapse capacity, $S_a\,(T, 5\%)_{\text{Median}}$ of the structure to the seismic demand corresponding to the MCE, $S_a\,(T, 5\%)_{\text{MCE,}}$ both computed at the fundamental period of the structure (FEMA P695 2009), given as:

$$CMR = \frac{S_a(T, 5\%)_{Median}}{S_a(T, 5\%)_{MCE}} \qquad (4.1)$$

Contrary to collapse fragility curve, the CMR does not take into account the uncertainties involved in the process (e.g. record-to-record variability and uncertainty in analysis of structure). Therefore, it only provides a partial picture of the collapse performance of a structure.

To take into account the inherent total variability in prediction of collapse of a structure, the acceptable CMR values in FEMA P695 have been provided based on total uncertainty. For the structures with total uncertainty of 0.50, acceptable CMR values higher than 1.90 and 1.52, are considered to be acceptable for 10% and 20% probabilities of collapse. On the other hand, for the structures with total uncertainty of 0.60, the acceptable CMR values increase to 2.16 and 1.66, for 10% and 20% probabilities of collapse. In other words, structures with higher total uncertainty require higher CMR to achieve acceptable collapse performance.

4.4 SEISMIC FRAGILITY ASSESSMENT AND ACCEPTANCE CRITERION

Seismic fragility curves are log-normal curves which represents the probability of reaching or exceeding certain damage state (ds) ('collapse' in the present study) for a given median estimate of an IM, and can be expressed in the functional form as:

$$P[C/IM] = \Phi\left[\frac{1}{\beta_T} \ln\left(\frac{IM}{\overline{IM}}\right)\right] \qquad (4.2)$$

where, $\overline{IM}$ is the median IM for collapse damage state, Φ is the normal cumulative distribution function, and β_T is the log-normal standard deviation of the IM for collapse damage state, which describes the total variability, taking into account the record-to-record variability (β_{RTR}), and modelling variability (β_M).

In the present study, the record-to-record variability (β_{RTR}) has been computed directly from the IDA results, considering collapse capacity to be log-normally distributed (Haselton et al. 2011b, Liel et al. 2011). The modelling variability, as also discussed in FEMA P695 (2009), is

dependent on prevalent construction practices, material of construction, design and detailing provisions, and the robustness and completeness of the analytical model used for the simulation of collapse. Realistic estimation of modelling variability requires huge computational efforts (Liel et al. 2009; Meslem and D'Ayala 2013). Currently, reliable estimates of modelling variability are not available in context of Indian code-designed buildings. In absence of reliable estimates of modelling variability for simulation of collapse of Indian code-designed buildings, the modelling variability from previous studies (Haselton and Deierlein 2007; Liel et al. 2009) based on a United States dataset has been adopted in the present study. Both, record-to-record variability (β_{RTR}) and modelling variability (β_M) are combined using the square-root-of-sum-of-squares (SRSS) technique (Haselton et al. 2011b, Liel et al. 2009) in order to obtain total variability (β_T) in the collapse fragility curves.

In the context of probabilistic performance assessment, FEMA P695 (2009) defines 10% average probability of collapse as a threshold value for an acceptable probability of collapse, for a performance group (e.g., group of buildings with varying heights, gravity loads and structural periods) of a structural system, under the occurrence of MCE ground-motions. The acceptable collapse probability for an individual building is higher, and the performance of a single building is considered to be satisfactory up to 20% probability of collapse, conditioned on the occurrence of MCE ground-motions. The buildings with even higher probability of collapse, for MCE ground-motions, are considered as outliers from that performance group and additional design measures need to be adopted to enhance the collapse performance of such buildings (FEMA P695 2009). In the present study, the same definition following FEMA P695 guidelines has been used in order to assess the collapse performance of hill buildings.

4.5 NUMERICAL STUDY

As highlighted in Chapter 2, both Mussoorie and Nainital have an abundance of RC buildings, predominantly of structural configurations SC A, SC B and SC C covering approximately 50% of the building stock. These typologies are studied in detail for their seismic behaviour and fragility assessment, using IDA. For this purpose, a representative generic building plan is chosen based on the observations made during the field survey (Fig. 3.9). In the present study, 34 generic RCMRF (reinforced-concrete moment-resisting frame) buildings (Table 4.1) of structural configurations, SC A, SC B and SC C with different dimensions in the two directions

have been considered. The considered buildings are representative of low- (2-storey), mid- (4-storey), and high-rise (8-storey) buildings in Indian Himalayas. The elevations of the typical building models in along-slope direction for 4-storey (mid-rise) buildings have been shown in Fig. 4.1. 2- and 8-storey buildings also have same elevation but have not been shown here for brevity.

For the numerical investigations, low- and mid-rise buildings of all the three design levels (viz. pre-, moderate- and high-code) have been considered, whereas high-rise buildings of high-code design level only have been studied. For all the considered building models, the storey height has been kept constant to 3.3 m, which was most commonly observed value during the field survey in the study area. In structural configurations SC B and SC C, the building's longer dimension (along length) has been kept parallel to the direction of the slope, whereas in structural configuration SC A, the building's orientation with respect to the slope direction does not have any significance, as slope-stability and topographic amplification are not being considered in the present study.

The 3-D building models have been created in the proprietary building analysis and design software ETABS 2016 (CSI 2016). Beams and columns are modelled using 3-D frame elements while slabs have been defined as rigid diaphragms. The cracked section properties of beams and columns are derived following ASCE 41 (2013) guidelines. Dead loads and live loads on the buildings have been assigned according to IS 875 Part 1 (1987a) and IS 875 Part 2 (1987b), respectively. All the buildings are designed following the provisions of Indian standards IS 1893 (2002), IS 1893 (2016), IS 13920 (1993) and IS 13920 (2016) for seismic zones IV / V, on soil type I (i.e., hard soil/rock) considering that competent hard rock is available in most parts of Mussoorie, and the effects of topographic/site amplification and slope instability are not being considered in the present study. P-delta effects are considered both in the analysis and the design.

The seismic design and performance of SMRF (special moment resisting frame) buildings designed as per Indian codes is influenced to a great extent by the capping on design period (Khose et al. 2012). The upper-bound design period for RC frame buildings as provided in IS 1893 is based on the building height from the ground level. For the design of the buildings resting on slopes (in case of both SC B and SC C), the upper-bound design period is considered

based on the building height above the uppermost foundation level (CED 39 2016; IS 1893 Part 1 2016). The buildings are denoted using the strings described in Chapter 2 (e.g. a pre-code building having structural configuration SC A with 2-storeys above the uppermost foundation level is abbreviated as AL-RC-R6).
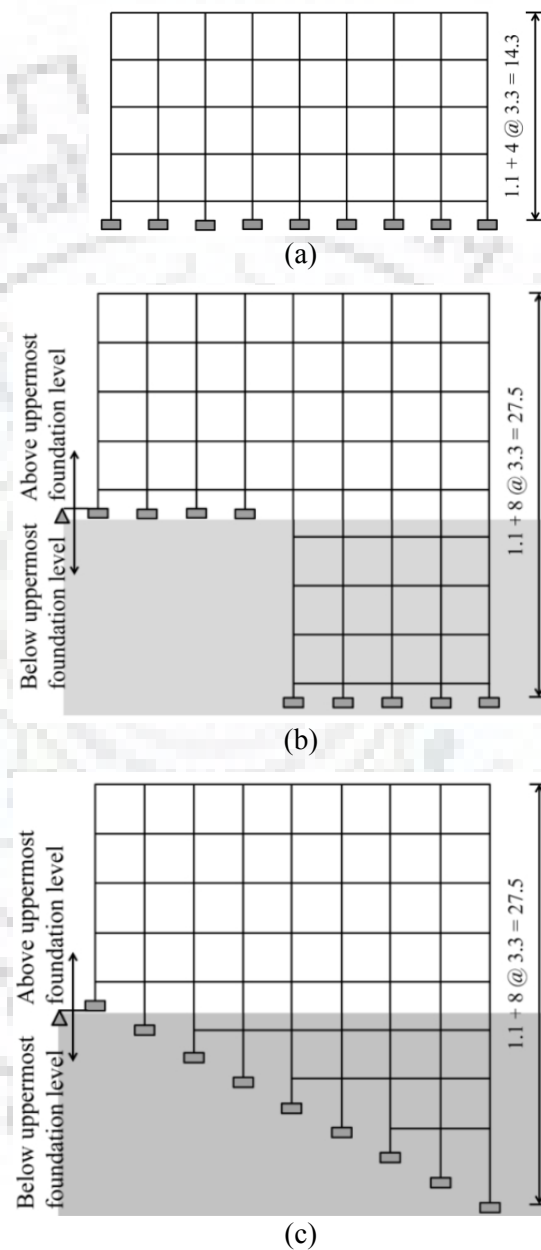
Fig. 4.1 Typical layouts of the investigated structural configurations: (a) elevation of a 4-storey building (SC A); (b) elevation of a 4-storey split-foundation (SF) building (SC B); and (c) elevation of a 4-storey step-back (SB) building (SC C). The gray-shaded area shows the building's portion below the uppermost foundation level. In case of SF buildings, the short-columns are of 1.1 *m* height, whereas in case of SB buildings, the short-columns are of 1.1 *m* and 2.75 *m* heights in successive storeys resting on the slope (refer to Fig. 4.1b and 4.1c).

Table 4.1 Details and member sizes of the considered building models. (All dimensions are in mm.)

Code Level	Building Model	Material Strength		T (s)	Design Base Shear Coefficient (*V/W*)	Beams	Columns	Short-columns
		Concrete (MPa)	Rebars (MPa)					
Pre-code	AL-RC-R6	20	415	1.47	-	230×300	300×300	-
	AM-RC-R6	20	415	2.89	-	230×300	300×300	-
	BL-RC-R6	20	415	1.57	-	230×300	300×300	300×300
	BM-RC-R6	20	415	3.00	-	230×300	300×300	300×300
	CL-RC-R6	20	415	1.78	-	230×300	300×300	300×300
	CM-RC-R6	20	415	3.08	-	230×300	300×300	300×300
Moderate-code	AL-RC-R6	40	500	1.00	0.060	300×300	350×350	-
	AM-RC-R6	40	500	1.50	0.044	300×400	350×350	-
	AL-RC-R6	40	500	1.00	0.090	300×300	350×350	-
	AM-RC-R6	40	500	1.50	0.065	300×400	350×350	-
	BL-RC-R6	40	500	1.05	0.060	300×300	350×350	350×350
	BM-RC-R6	40	500	1.51	0.044	300×400	350×350	350×350
	CL-RC-R6	40	500	1.07	0.060	300×300	350×350	550×550
	CM-RC-R6	40	500	1.49	0.044	300×400	350×350	600×600
High-code	AL-RC-R6	40	500	1.00	0.060	300×300	350×350	-
	AM-RC-R6	40	500	1.50	0.044	300×400	350×350	-
	AH-RC-R6	40	500	3.35	0.027	300×400	300×300, 350×350	-
	AL-RC-R6	40	500	1.00	0.090	300×300	350×350	-
	AM-RC-R6	40	500	1.50	0.065	300×400	350×350	-
	AH-RC-R6	40	500	3.35	0.040	300×400	300×300, 350×350	-
	BL-RC-R6	40	500	1.05	0.060	300×300	350×350	400×400
	BM-RC-R6	40	500	1.51	0.044	300×400	350×350	400×400
	BH-RC-R6	40	500	3.38	0.027	300×400	300×300, 350×350	400×400
	BL-RC-R6	40	500	1.03	0.090	300×300	350×350	450×450
	BM-RC-R6	40	500	1.49	0.065	300×400	350×350	450×450
	BH-RC-R6	40	500	3.30	0.040	300×400	300×300, 350×350	500×500
	CL-RC-R6	40	500	1.07	0.060	300×300	350×350	600×600, 450×450
	CM-RC-R6	40	500	1.52	0.044	300×400	350×350	650×650, 450×450
	CH-RC-R6	40	500	3.36	0.027	300×400	300×300, 350×350	650×650, 450×450
	CL-RC-R6	40	500	1.00	0.090	300×300	350×350	750×750, 450×450
	CM-RC-R6	40	500	1.49	0.065	300×400	350×350	800×800, 450×450
	CH-RC-R6	40	500	3.32	0.040	300×400	300×300, 350×350	800×800, 500×500

T is the average period of vibration of the building.

The details of building models, material strength, periods of vibration (arithmetic mean of the periods of vibration in the two principal directions of the building), design forces and obtained member sizes are summarized in Table 4.1. The member sizes have been obtained such that the reinforcement in columns is within the range of 1.5-4 % and in beams within 0.75-1.5 % on each face. Two different grades of concrete, 20 MPa for pre-code buildings and 40 MPa for moderate- and high-code buildings have been used, consistent with the typical construction practice in northern India. The typical spacing of stirrups in the potential plastic hinge regions is kept 200 mm in pre-code buildings whereas 100 mm in case of moderate- and high-code buildings, in both beams and columns. In the case of moderate-code buildings, the reinforcement in columns has been obtained from design forces; whereas in case of high-code buildings, the reinforcement in columns (obtained from design) has been increased further to achieve a SCWB ratio of 1.4. To compute the SCWB ratio, the nominal moment capacities for columns are computed at a factored axial force following the provisions of IS 13920 (2016), ACI 318 (2011) and ACI 318M (2014). Due to the shorter span of beams in the longitudinal direction, the investigated building models have slightly higher SCWB ratio in the longitudinal direction as compared to the transverse direction. Further, this difference in SCWB ratio is higher in the case of low-rise buildings designed for seismic zone IV, due to the relatively higher gravity loads effects.

It can be observed from Table 4.1, that for buildings of the same height above the uppermost foundation level and the same design level, the average periods of vibration are quite close for all the three structural configurations, justifying the use of this height for the classification of buildings (as considered in the Chapter 2) and for use in estimation of upper-bound design period. Accordingly, the design base shear coefficients (controlled by the upper-bound design period) of all the buildings of the same height above the uppermost foundation level are identical.

4.5.1 Non-Linear Modelling and Analysis

The lumped-plasticity (uniaxial moment plastic hinges and P-M-M interaction) hinges have been assigned at both ends of beams and columns, respectively. These hinges are capable of simulating the side-sway collapse mechanism associated with RC SMRF buildings (FEMA P695 2009). The strength deterioration effects are inherently considered in the ASCE 41 backbone curves as these were obtained from the cyclic envelopes (PEER ATC 72-1 2010;

LATBSDC 2014), whereas the degradation of stiffness and energy dissipation capacity is modelled explicitly using a degrading hysteresis model (also discussed in Chapter 3) based on cumulative energy dissipation in ETABS 2016 (CSI 2016). This hysteresis model has been calibrated with experimental results obtained by Dadi and Agarwal (2015). ASCE 41 defines backbone curves in which strength drops suddenly post-capping. However, such sudden drops are highly unrealistic and cause numerical instability problems in the solution algorithm (PEER ATC-72-1 2010; LATBSDC 2014). Therefore, a gradual reduction in strength as recommended in PEER ATC-72-1 (2010) and FEMA P58 (2012) has been used for the estimation of collapse capacity of the building models.

The stirrups spacing ratio and force-deformation (back-bone) curve parameters for typical beams and columns are presented in Table 4.2. The typical plastic rotation parameters are on the higher side in case of moderate-/high-code buildings as compared to pre-code buildings. This difference is due to the combined effect of ductile detailing (conforming) and low axial load ratio (due to increased member size) in case of moderate- and high-code buildings. The total amount of energy dissipated during inelastic excursions in a member is dependent on parameters θ_p (pre-capping plastic rotation capacity), θ_{pc} (post-capping plastic rotation capacity), f_1, f_2, and s_w. These parameters are dependent on the section details, such as stirrup area ratio, ratio of stirrup spacing to the effective depth of the section, shear span, and axial load ratio (Haselton et al. 2007). In the present study, the effect of section dimensions, reinforcement detailing and axial load ratio has been considered on θ_p and θ_{pc}, through the use of ASCE 41 plastic rotation parameters. On the other hand, parameters f_1, f_2, and s_w have been obtained from calibration with the experimental results. As these parameters are used to simulate the stiffness degradation and energy dissipation, these are also expected to be influenced by the axial load ratio and stirrup spacing (s) to depth (d) ratio (Haselton et al. 2007).

Table 4.2 Shear reinforcement details and plastic rotation capacities of typical members.

Member	$P/A_g f_c'$	s/d	θ_p	θ_{pc}
Beam (Non-conforming)	0.00	0.74	0.015	0.008
Beam (Conforming)	0.00	0.31	0.025	0.025
Column (Non-conforming)	0.35	0.80	0.008	0.000
Column (Conforming)	0.10	0.29	0.027	0.007

The member properties are presented for structural configuration SC C. θ_p and θ_{pc} represent the pre-capping and post-capping plastic deformation capacities, respectively. Here, s and d represent the transverse reinforcement spacing and section depth, respectively.

The building models considered in the present study have typical axial load ratios varying between 0-0.35 (Table 4.2), and the typical stirrup spacing to depth ratio of 0.70-0.80 in case of pre-code buildings, and between 0.27-0.35 in case of moderate- and high-code buildings. Therefore, the experiments conducted by Dadi and Agarwal (2015) and Dadi (2015) with zero axial load ratio and typical stirrup spacing (s) to depth (d) ratio of 1.13 and 0.35, in case of non-conforming and conforming beams, respectively, reasonably represent the range of parameters used in this study, particularly in absence of more specific information for the considered types of construction. The typical stirrup spacing to depth ratio is even smaller in case of short-columns in high-code buildings (particularly in structural configuration SC C), due to increased depth (Table 4.1). Therefore, these modelling parameters may differ in case of short-columns. This effect can be included in future studies, when sufficient experimental evidence on short-columns is available.

For all the buildings considered in the present study, shear failure has been modelled following ASCE 41 (2013) guidelines considering it a displacement-controlled action, and the shear strength has been computed based on section and transverse reinforcement details using shear strength model as per ASCE 41. Based on the recommendations by Li and Hwang (2016), a gradual reduction in the post-peak strength has been considered and shear failure has been assumed when the displacement exceeds the allowable limit specified in ASCE 41 (2013).

In order to investigate the dynamic response of the considered structural models, the IDA has been conducted under bi-directional (i.e., simultaneous application of two horizontal components of the ground-motions) excitation. In the present study, the far-field record suite (consisting of 22 pairs of ground-motion records) of FEMA P695 (2009) has been considered, and S_a (T, 5%) has been used as the scaling parameter as well as the main Intensity Measure (IM). It is important to consider that the structural models investigated in the present study have different periods of vibration along the two principal directions of the building. Therefore, the arithmetic mean of the periods corresponding to the fundamental translational modes of the two orthogonal directions has been used for computing S_a (T, 5%) following the guidelines of FEMA P58 (2012). In order to scale the bi-directional ground-motion records, the geometric mean of the spectral ordinates of individual components has been used. Collapse has been defined as the point where slight increment in the considered IM cause a large increase in DM (i.e., the maximum inter-storey drift ratio, representative of side-sway collapse). In order to

model damping effects, a Rayleigh damping of 5% has been assigned at periods corresponding to the lowest mode and the mode resulting in 95% cumulative mass participation.

4.6 DYNAMIC CAPACITY CURVES

IDA of the considered building models has been performed for the FEMA P695 far-field ground-motion record suite. Figures 4.2-4.4 present the dynamic capacity curves for the pre-code, moderate- and high-code 4-storey (mid-rise) buildings with structural configurations SC A, SC B, and SC C, respectively, designed for seismic zone IV. Results are presented in terms of the IM, i.e. S_a $(T, 5\%)$ vs. DM (θ_{Max}) curves for individual records, as well as the 16th, 50th (median), and 84th percentile dynamic capacity curves. Similar results have also been obtained for the other investigated building models but are not presented here for brevity. The corresponding median collapse capacities have been reported in Tables 4.3-4.6.

Table 4.3 presents the median collapse capacities in terms of S_a $(T, 5\%)$ for the pre-code building models investigated in this study. It can be observed that the pre-code buildings have very low collapse capacity, as these buildings were designed for gravity loads alone. In these pre-code buildings, the collapse capacity reduces by almost 30% and 50% in structural configuration SC C when compared with the corresponding structural configuration SC A, for low- and mid-rise buildings, respectively. The reason for this reduction can be attributed to the combined effect of the torsionally irregular structural configuration and shear failure of the short-columns. In all the investigated pre-code building models, CMR have been found out to be less than unity. The CMR reduces further, in the higher seismic zone (i.e., zone V) due to the increased seismic demand, while the capacity remains unchanged.

Table 4.4 presents the median collapse capacities in terms of S_a $(T, 5\%)$ for the moderate-code building models investigated in this study. It can be observed that although all the moderate-code building models having different structural configurations but the same height above the uppermost foundation level were designed for identical base shear coefficient (Table 4.1), the structural configuration SC A has the highest median collapse capacity as compared to SC B and SC C. The reduction in collapse capacity from SC A to SC C, in case of moderate-code buildings, has been observed to be up to 20%. The reason for this lies in the fact that SC A is subjected to flexural failure of beams and columns whereas SC B and SC C are also subjected

to the shear failure of short-columns, as these are very rigid and attract a major share of the corresponding storey shear.
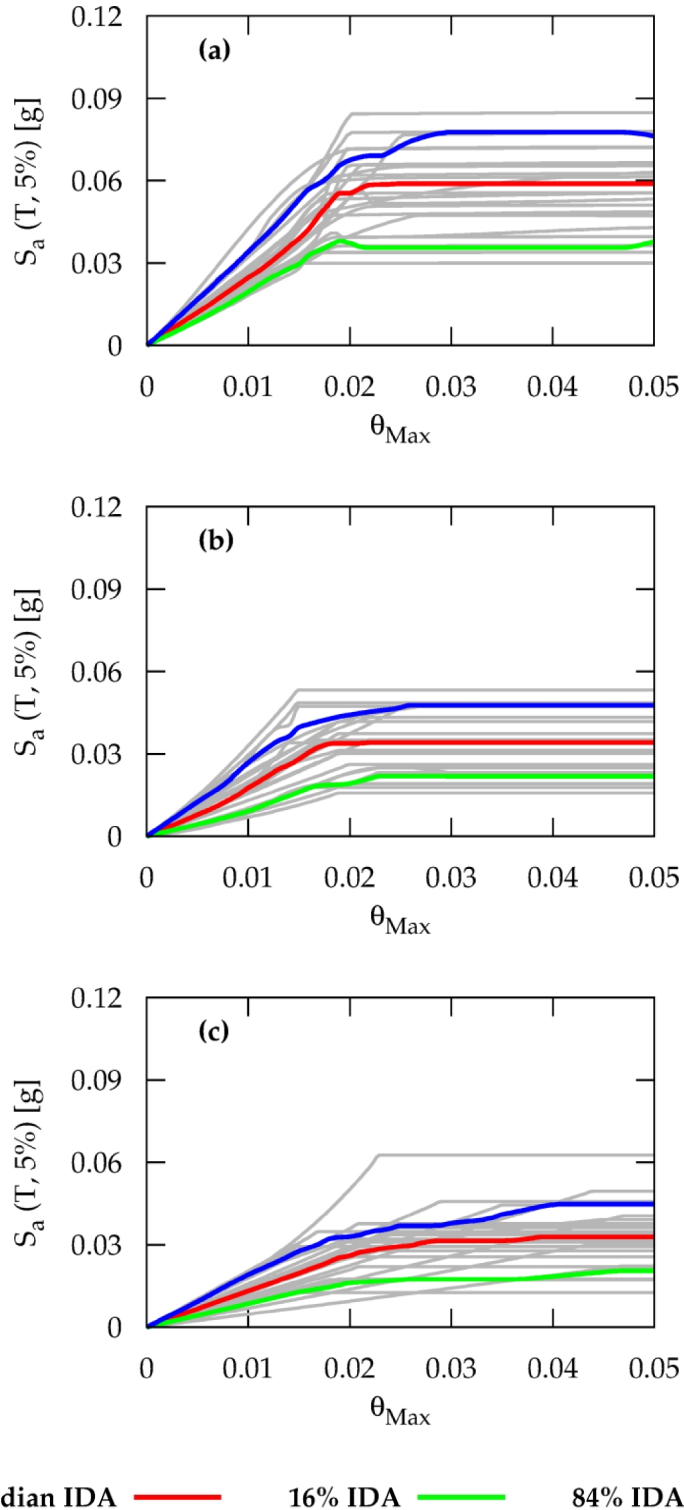
Fig. 4.2 Dynamic capacity curves for pre-code mid-rise buildings: (a) SC A; (b) SC B; and (c) SC C.

93
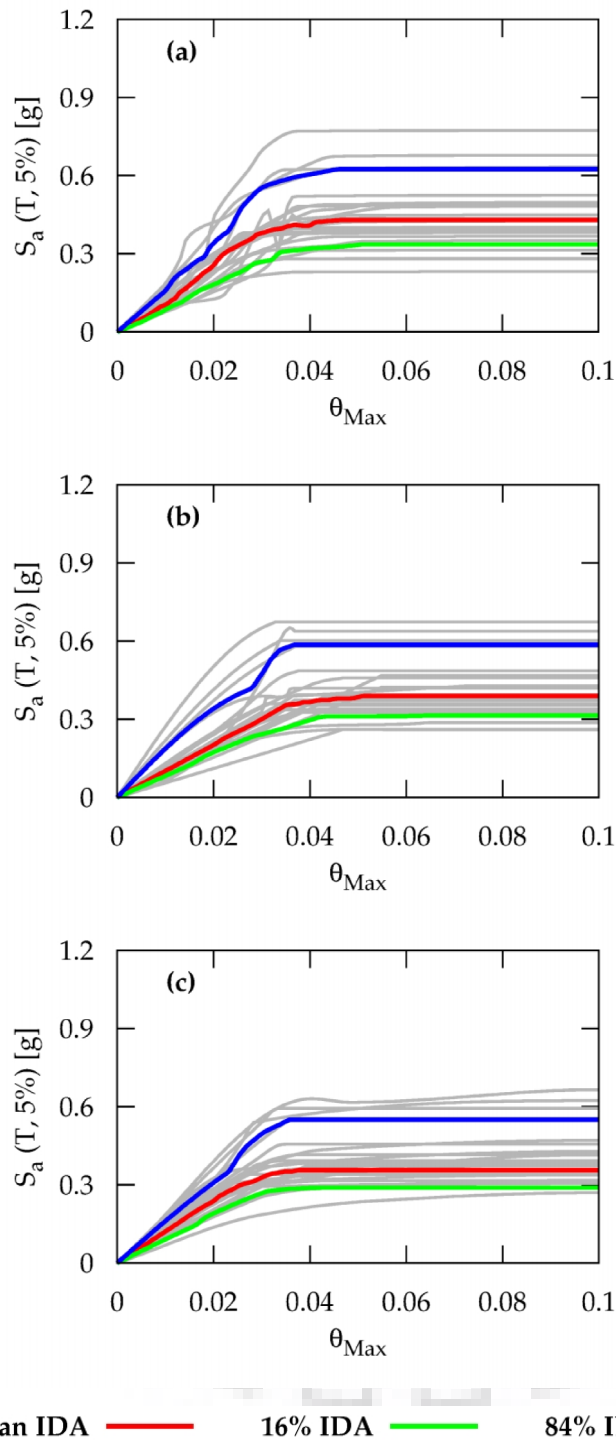
Fig. 4.3 Dynamic capacity curves for moderate-code mid-rise buildings: (a) SC A; (b) SC B; and (c) SC C.

Table 4.5 presents the median collapse capacities in terms of S_a (T, 5%) for the high-code building models investigated in this study. All the high-code building models in seismic zone IV, having different structural configurations but the same height above the uppermost

foundation level, were designed for identical base shear coefficient (Table 4.1). Further, the different building models in seismic zone V were designed for 50% higher base shear coefficient, in comparison with zone IV. However, the increase in the median collapse capacity of buildings designed for seismic zone V is only up to 10%, when compared with their counterparts designed for seismic zone IV.
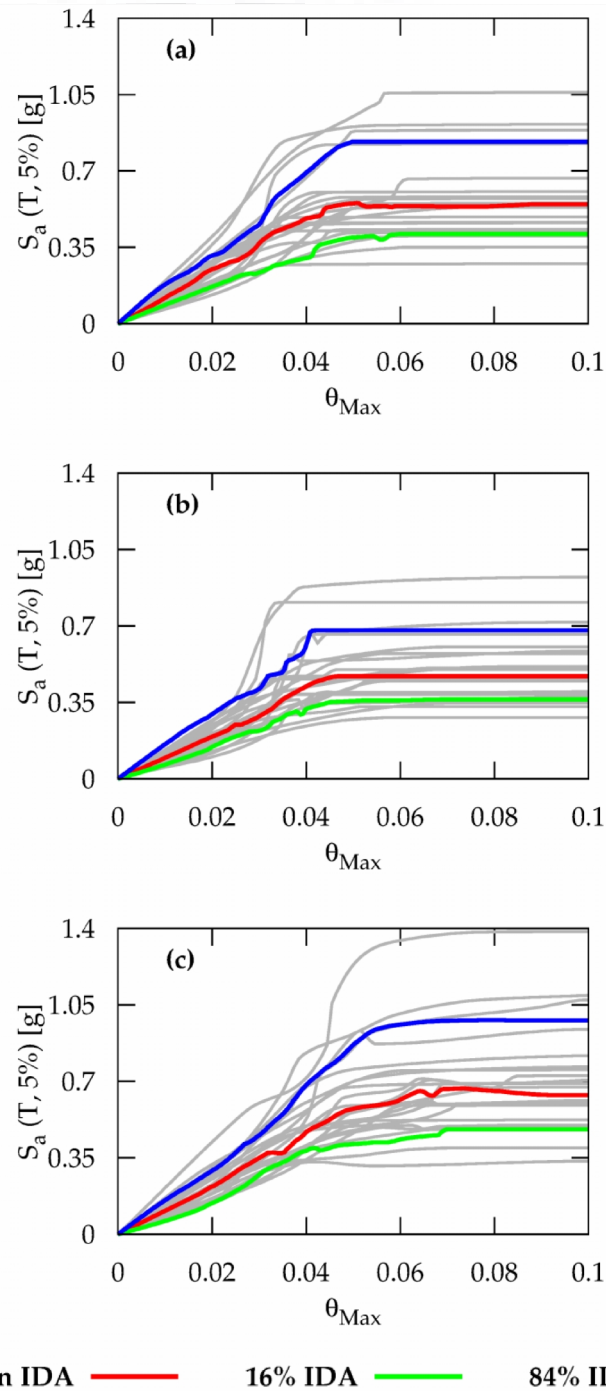
Fig. 4.4 Dynamic capacity curves for high-code mid-rise buildings: (a) SC A; (b) SC B; and (c) SC C.

95

Table 4.3 Collapse capacities and CMR of the considered pre-code buildings.

Building Model	Seismic Zone	S_a (D)	S_a (C)	CMR
AL-RC-R6	IV	0.163g	0.106g	**0.65**
AM-RC-R6	IV	0.083g	0.059g	**0.71**
BL-RC-R6	IV	0.153g	0.094g	**0.61**
BM-RC-R6	IV	0.080g	0.034g	**0.43**
CL-RC-R6	IV	0.135g	0.075g	**0.56**
CM-RC-R6	IV	0.078g	0.033g	**0.42**
AL-RC-R6	V	0.245g	0.106g	**0.43**
AM-RC-R6	V	0.125g	0.059g	**0.47**
BL-RC-R6	V	0.229g	0.094g	**0.41**
BM-RC-R6	V	0.120g	0.034g	**0.28**
CL-RC-R6	V	0.202g	0.075g	**0.37**
CM-RC-R6	V	0.117g	0.033g	**0.28**

S_a (D) - seismic demand for MCE hazard in terms of S_a, S_a (C) - median collapse capacity in terms of S_a, CMR values shown in bold shows failure of that particular building based on FEMA P695 acceptance criterion.

Table 4.4 Collapse capacities and CMR of the considered moderate-code buildings.

Building Model	Seismic Zone	S_a (D)	S_a (C)	CMR
AL-RC-R6	IV	0.240g	0.660g	2.75
AM-RC-R6	IV	0.160g	0.440g	2.75
AH-RC-R6	IV	0.072g	0.120g	**1.67**
AL-RC-R6	V	0.360g	0.790g	2.19
AM-RC-R6	V	0.240g	0.450g	**1.88**
AH-RC-R6	V	0.107g	0.090g	**0.84**
BL-RC-R6	IV	0.229g	0.586g	2.56
BM-RC-R6	IV	0.159g	0.387g	2.43
CL-RC-R6	IV	0.224g	0.543g	2.42
CM-RC-R6	IV	0.161g	0.360g	2.24

S_a (D) - seismic demand for MCE hazard in terms of S_a, S_a (C) - median collapse capacity in terms of S_a, CMR values shown in bold shows failure of that particular building based on FEMA P695 acceptance criterion.

Table 4.5 Collapse capacities and CMR of the considered high-code buildings.

Building Model	Seismic Zone	S_a (D)	S_a (C)	CMR
AL-RC-R6	IV	0.240g	0.930g	3.88
AM-RC-R6	IV	0.160g	0.550g	3.44
AH-RC-R6	IV	0.072g	0.150g	2.08
AL-RC-R6	V	0.360g	0.990g	2.75
AM-RC-R6	V	0.240g	0.600g	2.50
AH-RC-R6	V	0.107g	0.160g	**1.50**
BL-RC-R6	IV	0.229g	0.792g	3.46
BM-RC-R6	IV	0.159g	0.484g	3.04
BH-RC-R6	IV	0.071g	0.128g	**1.80**
BL-RC-R6	V	0.350g	0.803g	2.29
BM-RC-R6	V	0.242g	0.525g	2.17
BH-RC-R6	V	0.109g	0.110g	**1.01**
CL-RC-R6	IV	0.224g	0.932g	4.16
CM-RC-R6	IV	0.158g	0.671g	4.25
CH-RC-R6	IV	0.071g	0.136g	**1.92**
CL-RC-R6	V	0.360g	1.027g	2.85
CM-RC-R6	V	0.242g	0.600g	2.48
CH-RC-R6	V	0.108g	0.143g	**1.32**

S_a (D) - seismic demand for MCE hazard in terms of S_a, S_a (C) - median collapse capacity in terms of S_a, CMR values shown in bold shows failure of that particular building based on FEMA P695 acceptance criterion.

In case of high-rise buildings with structural configuration SC B and mid-rise buildings with SC C, a slight reduction in the median collapse capacity for seismic zone V has been observed when compared with the corresponding counterparts designed for seismic zone IV (Table 4.5). The reason for this difference can be attributed to the combined effect of inherent over-strength in the seismic design, the load redistribution mechanism in the inelastic range, and also the governing collapse mechanism for the individual ground-motion records. Further, in general the effect of structural configuration leads to a reduction in collapse capacity of about 10%-15% from SC A to SC C for low- and mid-rise buildings. However, in case of high-rise buildings with structural configuration SC B designed for seismic zone V, a 31% reduction in collapse capacity has been observed when compared with its counterparts having structural configuration SC A.

4.7 COLLAPSE MECHANISMS

In a suite of ground-motion records, the collapse mechanism varies from record-to-record due to significantly different ground-motion characteristics of individual records. Therefore, the collapse mechanisms which have been most frequently observed in the suite of 22 ground-motion records, considered in the present study, are presented in this section. The typical collapse mechanisms for mid-rise buildings only have been presented here.

Figure 4.5 presents the typical collapse mechanisms for mid-rise pre-, moderate-, and high-code buildings, with SC A. In case of the pre-code building, collapse occurs due to flexural failure of columns in the first storey (Fig. 4.5a) as well as due to shear-failure of columns in the upper storeys. In case of moderate-code building, only flexural failure of columns in the first storey has been observed (Fig. 4.5b). This column failure mechanism changes to combined beam-column failure mechanism in case of high-code buildings (Fig. 4.5c). Figure 4.6 presents the typical collapse mechanisms of mid-rise buildings, with SC B. In case of the pre-code buildings with SC B, collapse occurs due to flexural failure of the columns of the storey just above the uppermost foundation level (Fig. 4.6a) and the shear-failure has been observed in short-columns at the uppermost foundation level, as well as in the upper storeys. In case of both moderate- and high-code buildings, flexural failure of normal length columns and shear failure of short-columns in the storey at the uppermost foundation level has been observed. However,

the ground-motion intensity at which collapse occurs in moderate- and high-code buildings differs significantly.

(a)

(b)

(c)

● Flexural yielding   ● Flexural failure   ● Shear failure
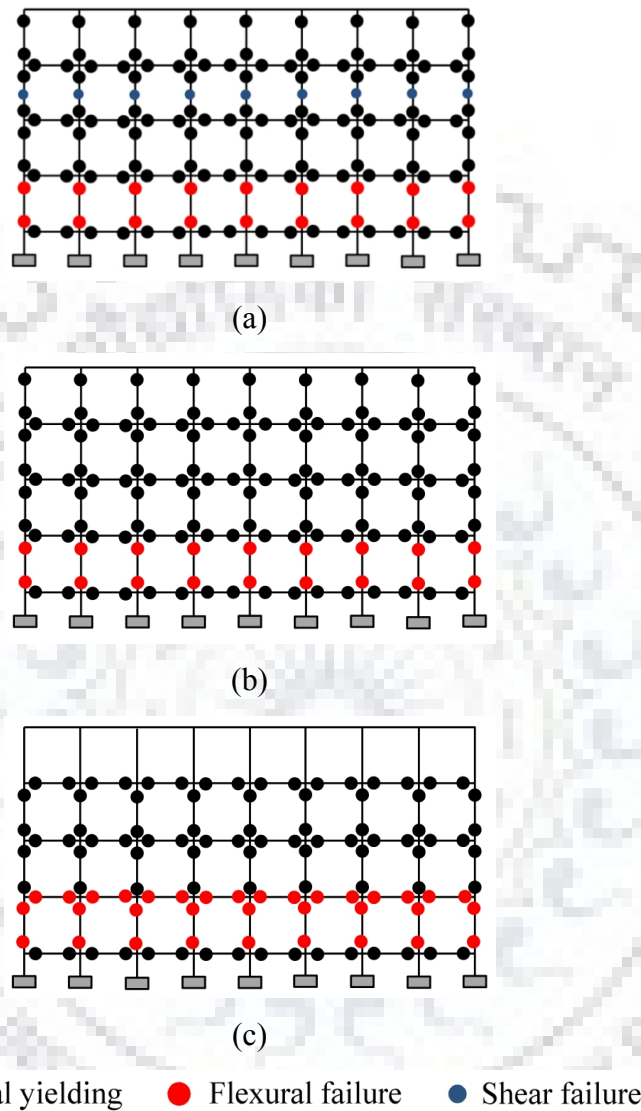
Fig. 4.5 Typical collapse mechanism for mid-rise buildings with SC A: (a) pre-code; (b) moderate-code; and (c) high-code building.

Figure 4.7 presents the typical collapse mechanisms of mid-rise buildings with SC C. In case of the pre-code building, collapse occurs due to flexural failure of the columns of the storey at the level of uppermost foundation and just above it (Fig. 4.7a). In addition, shear-failure in short-columns in the portion below the uppermost foundation level, and the columns of an upper storey has also been observed. The shear-failure in short-columns occurs sequentially, starting from the uppermost short-column and moving down the hill towards the lowermost short-column, leading to some sort of 'zippering effect'. In case of both moderate- and high-code

buildings, flexural failure at storey level just at the uppermost foundation level has been observed, along with shear failure of short-columns, in a sequential manner. However, the ground-motion intensity at which collapse occurs in moderate- and high-code buildings differs significantly.

(a)

(b)
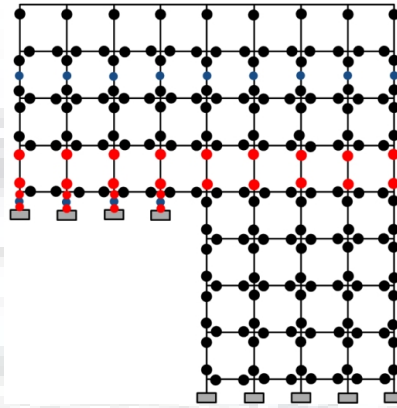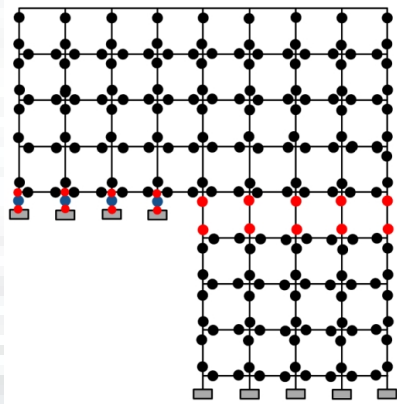
● Flexural yielding   ● Flexural failure   ● Shear failure

Fig. 4.6 Typical collapse mechanism for mid-rise buildings with SC B: (a) pre-code; and (b) moderate-/ high-code building.

The typical collapse mechanism observed in case of mid-rise buildings are consistently observed in case of low-rise buildings as well. Further, in case of high-code high-rise buildings (for all the three structural configurations, i.e., SC A, SC B, and SC C) the beam failure mechanism in multiple storeys along with the column yielding throughout the building height (except the upper storeys) has been observed. In both the structural configurations, SC B and SC C, the failure at storeys just at the level of the uppermost foundation and above it, has been observed. The reason for this failure at the uppermost foundation level can be attributed to the

significant torsional irregularity existing in that particular storey (shown later in the Chapter 7), in both the structural configurations, SC B and SC C.

(a)

(b)
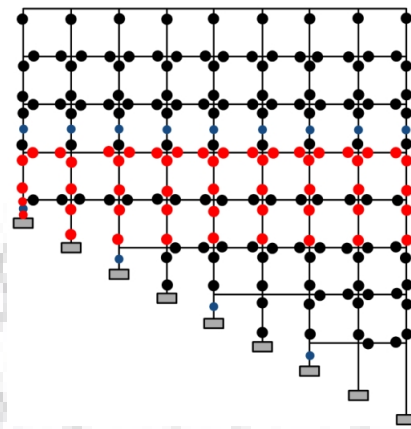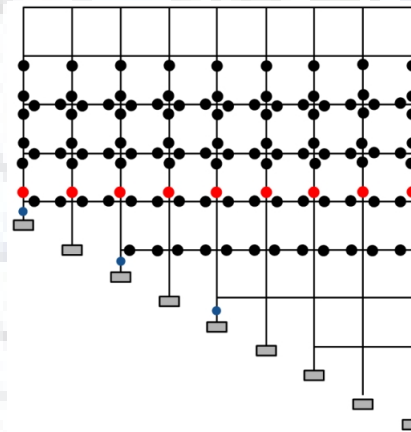
● Flexural yielding   ● Flexural failure   ● Shear failure

Fig. 4.7 Typical collapse mechanism for mid-rise buildings with SC C: (a) pre-code; and (b) moderate-/high-code building.

Although, both the moderate-code and the high-code buildings were designed for identical base shear coefficients, the high-code buildings have an enhanced collapse capacity as compared to the moderate-code buildings. This observation highlights the effect of SCWB design (in case of high-code buildings) on seismic collapse capacity of buildings. The presented observations suggest that, even when designing for a SCWB ratio of 1.4 (in case of high-code buildings), column hinging (yielding) cannot be avoided and observed to be consistent with findings of earlier studies (Dooley and Bracci 2001; Kuntz and Browning 2003). However, failure is governed by failure of beams in a storey, in the case of low- and mid-rise buildings, and failure

of beams in multiple storeys, in the case of high-rise buildings. The observed collapse mechanisms clearly indicate that there is still room for possible improvements in the capacity design procedure to involve the beams of all the storeys in the collapse mechanism. Such a failure mechanism is expected to enhance the collapse capacity of the building, further.

4.8 FRAGILITY CURVES

In order to develop the collapse fragility curves, the methodology presented in Section 4.4, has been used. Tables 4.6-4.8 present the variability parameters for the pre-, moderate- and high-code buildings, considered in the present study. β_{RTR} (S_a) has been computed based on standard deviation of natural logarithm of the observed collapse intensities (in terms of S_a) of different ground-motion records for a building model. The total variability β_T in collapse fragility curves, has been obtained by combining the β_{RTR} (S_a) and β_M using SRSS combination rule. It can be observed that for the entire set of building models investigated in the present study, the average value of β_{RTR} (S_a) and β_T (S_a) are of the order of 0.30 and 0.60, respectively. It is to be noted that β_M is expected to be slightly different in case of pre-, moderate- and high-code buildings. However, in the absence of reliable estimates of β_M in context of Indian-code designed buildings, the same value of β_M has been used in developing the fragility curves, irrespective of the design level of a building model.

Figure 4.8 compares the collapse fragility curves for low- and mid-rise buildings, representative of pre-, moderate- and high-code design levels, for all the considered structural configurations. These fragility curves have been plotted with the S_a (T, 5%), normalized by the corresponding S_a (T, 5%) at MCE, for seismic zone IV. S_a (T, 5%) at MCE has been obtained from IS 1893 Part 1 (2016) for seismic zone IV on rock site. This normalization of the fragility curves with S_a (T, 5%) at MCE, eliminates the effect of the building period, and therefore, the fragility curves for different buildings can be compared directly. It is clearly evident from Figure 4.8 that, pre-code buildings are highly vulnerable when compared with their counterpart moderate- and high-code buildings. Further, the collapse vulnerability of moderate-code buildings is also higher when compared with high-code buildings. However, the difference between collapse fragility of moderate- and high-code buildings is relatively very small when compared with the difference between pre- and moderate-code buildings.

Table 4.6 Variability parameters for the considered pre-code buildings.

Building Model	Seismic Zone	β_M	$\beta_{RTR}(S_a)$	$\beta_T(S_a)$
AL-RC-R6	IV	0.50	0.39	0.63
AM-RC-R6	IV	0.50	0.28	0.57
BL-RC-R6	IV	0.50	0.27	0.57
BM-RC-R6	IV	0.50	0.34	0.60
CL-RC-R6	IV	0.50	0.30	0.58
CM-RC-R6	IV	0.50	0.37	0.62
AL-RC-R6	V	0.50	0.39	0.63
AM-RC-R6	V	0.50	0.28	0.57
BL-RC-R6	V	0.50	0.27	0.57
BM-RC-R6	V	0.50	0.34	0.60
CL-RC-R6	V	0.50	0.30	0.58
CM-RC-R6	V	0.50	0.37	0.62

$\beta_{RTR}(S_a)$ - record-to-record variability in collapse capacity, when S_a is chosen as IM, $\beta_T(S_a)$ - total variability in the collapse capacity, when S_a is chosen as IM.

Table 4.7 Variability parameters for the considered moderate-code buildings.

Building Model	Seismic Zone	β_M	$\beta_{RTR}(S_a)$	$\beta_T(S_a)$
AL-RC-R6	IV	0.50	0.28	0.57
AM-RC-R6	IV	0.50	0.30	0.58
AH-RC-R6	IV	0.50	0.37	0.62
AL-RC-R6	V	0.50	0.32	0.59
AM-RC-R6	V	0.50	0.30	0.58
AH-RC-R6	V	0.50	0.30	0.58
BL-RC-R6	IV	0.50	0.20	0.54
BM-RC-R6	IV	0.50	0.27	0.57
CL-RC-R6	IV	0.50	0.32	0.59
CM-RC-R6	IV	0.50	0.30	0.58

$\beta_{RTR}(S_a)$ - record-to-record variability in collapse capacity, when S_a is chosen as IM, $\beta_T(S_a)$ - total variability in the collapse capacity, when S_a is chosen as IM.

Table 4.8 Variability parameters for the considered high-code buildings.

Building Model	Seismic Zone	β_M	$\beta_{RTR}(S_a)$	$\beta_T(S_a)$
AL-RC-R6	IV	0.50	0.28	0.57
AM-RC-R6	IV	0.50	0.32	0.59
AH-RC-R6	IV	0.50	0.31	0.59
AL-RC-R6	V	0.50	0.26	0.56
AM-RC-R6	V	0.50	0.31	0.59
AH-RC-R6	V	0.50	0.32	0.59
BL-RC-R6	IV	0.50	0.32	0.59
BM-RC-R6	IV	0.50	0.27	0.57
BH-RC-R6	IV	0.50	0.43	0.66
BL-RC-R6	V	0.50	0.30	0.58
BM-RC-R6	V	0.50	0.26	0.56
BH-RC-R6	V	0.50	0.32	0.59
CL-RC-R6	IV	0.50	0.38	0.63
CM-RC-R6	IV	0.50	0.33	0.60
CH-RC-R6	IV	0.50	0.30	0.58
CL-RC-R6	V	0.50	0.35	0.61
CM-RC-R6	V	0.50	0.34	0.60
CH-RC-R6	V	0.50	0.32	0.59

$\beta_{RTR}(S_a)$ - record-to-record variability in collapse capacity, when S_a is chosen as IM, $\beta_T(S_a)$ - total variability in the collapse capacity, when S_a is chosen as IM.

Figure 4.9 compares the collapse fragility curves for low-, mid- and high-rise buildings representative of high-code design level, for all the considered structural configurations, for seismic zone IV and V. It is evident from Figure 4.9 that the high-code buildings designed for seismic zone V are more vulnerable when compared with their counterparts designed for seismic zone IV. This observation can be attributed to the fact that the collapse capacity of a building is a function of both strength and ductility capacities. In case of buildings designed for seismic zone V, the strength of the buildings has been increased by 50% (due to increased design base shear coefficient), but the ductility capacity of the buildings designed for seismic zone V remain almost unchanged when compared with the buildings designed for seismic zone IV. These effects lead to an increase in the global collapse capacity of about 10% only (in contrary to a 50% increase in seismic demand). This observation is found out to be in good agreement with FEMA P695, where it has already been reported that collapse performance of a structural system is always governed by the higher seismic zone for which the structural system is permitted.
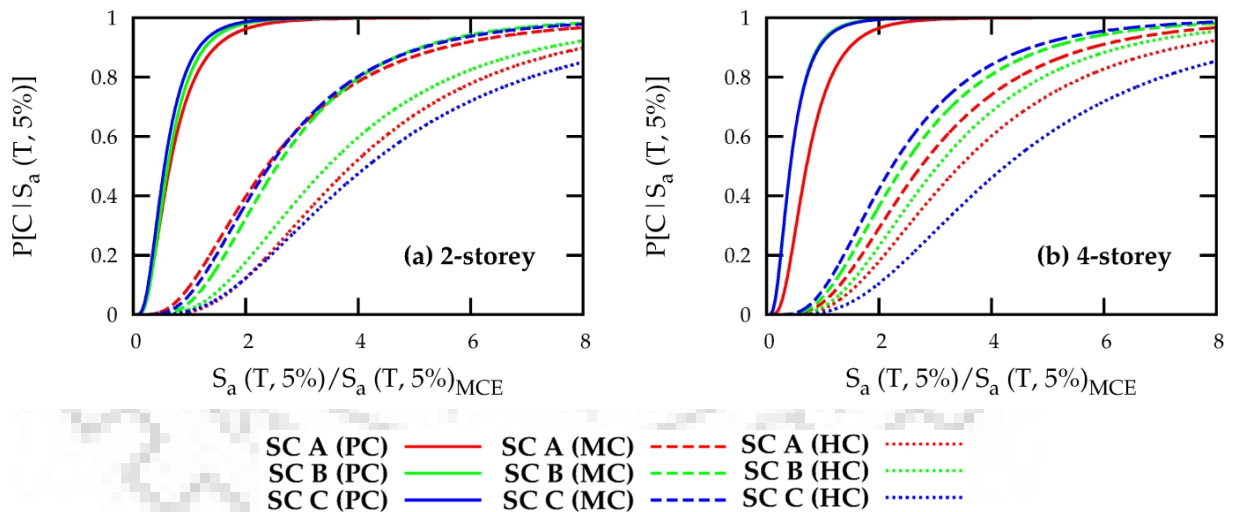
Fig. 4.8 Collapse fragility curves for different structural configurations of low- and mid-rise, pre- (PC); moderate- (MC); and high-code (HC) RC buildings, for seismic zone IV.

Tables 4.9-4.11 present the collapse probabilities for pre-, moderate- and high-code buildings investigated in this study. These collapse probabilities are computed for the MCE seismic demands obtained from IS 1893 Part 1 (2016) for seismic zones IV and V, at a rock site. It is very clear from the Table 4.9 that pre-code buildings have unacceptably high probabilities of collapse at MCE.
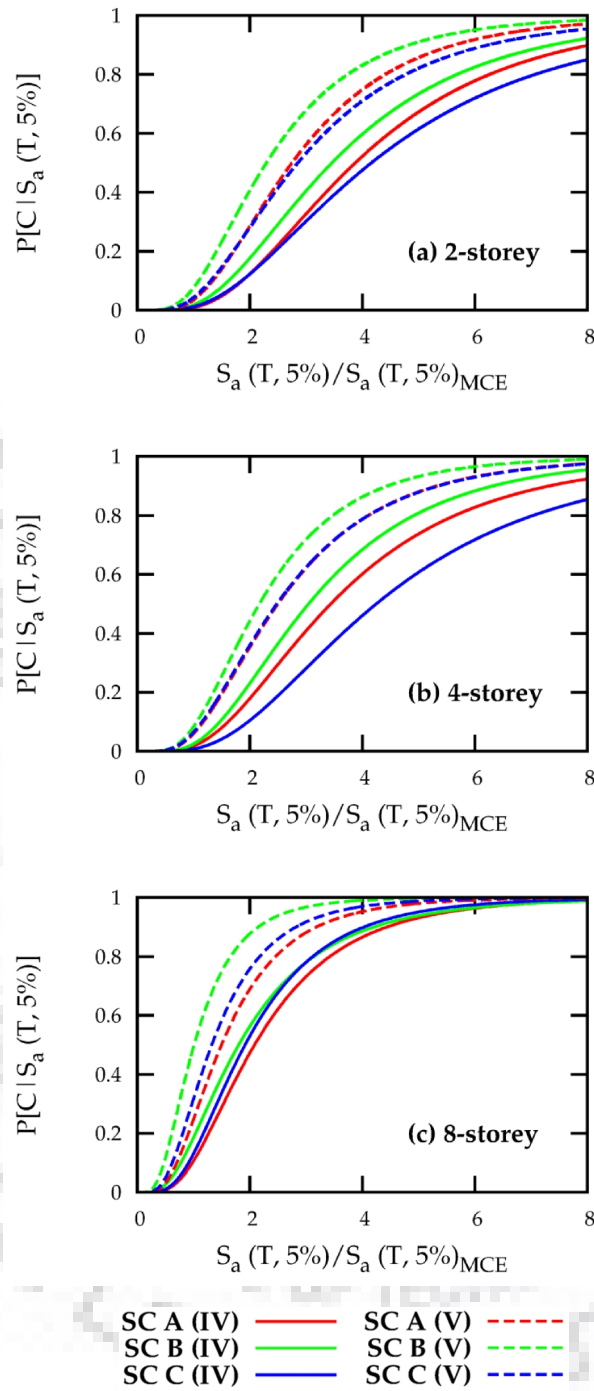
Fig. 4.9 Collapse fragility curves for different structural configurations of high-code RC buildings, for seismic zones IV and V.

The average probabilities of collapse for pre-code low- and mid-rise buildings are 80% and 86%, respectively, for seismic zone IV. These collapse probabilities reduce significantly in case of moderate-code buildings. The average probabilities of collapse for moderate-code low- and mid-rise buildings are 7% and 6%, respectively, for seismic zone IV.

Table 4.9 Collapse probabilities for the considered pre-code buildings.

Building Model	Seismic Zone	Collapse Probability (%) P[C/S_a]
AL-RC-R6	IV	**75**
AM-RC-R6	IV	**73**
BL-RC-R6	IV	**80**
BM-RC-R6	IV	**92**
CL-RC-R6	IV	**84**
CM-RC-R6	IV	**92**
AL-RC-R6	V	**91**
AM-RC-R6	V	**91**
BL-RC-R6	V	**94**
BM-RC-R6	V	**98**
CL-RC-R6	V	**96**
CM-RC-R6	V	**98**

P[C/S_a] - probability of collapse for MCE hazard, when S_a is chosen as IM. Collapse probability values shown in bold shows failure of that particular building based on FEMA P695 acceptance criterion.

Table 4.10 Collapse probabilities for the considered moderate-code buildings.

Building Model	Seismic Zone	Collapse Probability (%) P[C/S_a]
AL-RC-R6	IV	10
AM-RC-R6	IV	04
BL-RC-R6	IV	04
BM-RC-R6	IV	06
CL-RC-R6	IV	06
CM-RC-R6	IV	08

P[C/S_a] - probability of collapse for MCE hazard, when S_a is chosen as IM. Collapse probability values shown in bold shows failure of that particular building based on FEMA P695 acceptance criterion.

Table 4.11 Collapse probabilities for the considered high-code buildings.

Building Model	Seismic Zone	Collapse Probability (%) P[C/S_a]
AL-RC-R6	IV	01
AM-RC-R6	IV	02
AH-RC-R6	IV	11
AL-RC-R6	V	04
AM-RC-R6	V	06
AH-RC-R6	V	**25**
BL-RC-R6	IV	02
BM-RC-R6	IV	03
BH-RC-R6	IV	19
BL-RC-R6	V	08
BM-RC-R6	V	08
BH-RC-R6	V	**50**
CL-RC-R6	IV	01
CM-RC-R6	IV	01
CH-RC-R6	IV	13
CL-RC-R6	V	04
CM-RC-R6	V	07
CH-RC-R6	V	**32**

P[C/S_a] - probability of collapse for MCE hazard, when S_a is chosen as IM. Collapse probability values shown in bold shows failure of that particular building based on FEMA P695 acceptance criterion.

These collapse probabilities further reduce in case of high-code buildings. The average probabilities of collapse for high-code low- and mid-rise buildings are 1% and 2%,

respectively, for seismic zone IV and increase to 5% and 7%, respectively, for seismic zone V. Further, in case of high-code high-rise buildings, the average collapse probabilities are 14% and 36% in seismic zones IV and V, respectively.

In comparison to the acceptance criterion of FEMA P695, the high-rise buildings designed for seismic zone V, show a significantly poor performance since these buildings have unacceptably higher probabilities of collapse when compared with the acceptance criterion of 20% probability of collapse, conditioned on the occurrence of MCE earthquake. It is to be noted that the results presented in this Chapter do not account for the effect of spectral shape of ground-motion records used in IDA, which can lead to either under- or over-estimation in collapse capacity of the buildings. In order to make a definitive statement about collapse fragility, the effect of site and spectral shape of the ground-motion records on estimated collapse probabilities need to be considered. The effects are being presented in the next Chapter.

4.9 SUMMARY

Non-linear building models for a set of RC frame buildings with three different structural configurations SC A, SC B, and SC C have been developed. IDA has been conducted on the considered building models using a far-field ground-motion record suite. The effects of seismic design level (viz. pre-code, moderate-code and high-code) and seismic zone (viz. zone IV and zone V) on the collapse fragility of low-, mid- and high-rise RC frame buildings, designed for Indian codes have been studied. Based on the presented results, the following major observations can be made:

- The effect of structural configuration on collapse capacity and collapse fragility is more pronounced in pre-code buildings, as compared to moderate- and high-code buildings. The collapse capacity of pre-code buildings reduces up to 50% due to the irregular structural configuration. This reduction has been observed to be relatively smaller (only of the order of 10-20%) in case of moderate- and high-code buildings.

- In case of pre-code buildings, the typical failure mechanism includes the flexural failure of beams and columns, and shear failure of short-columns as well as normal height columns (at upper stories). On the other hand, in case of moderate- and high-code buildings, the flexural

failure of beams and columns along with the shear failure of short-columns has been observed.

- In all the high-code buildings considered in this study, yielding of columns could not be avoided even when using a SCWB ratio of 1.40, as recommended in the Indian seismic design code.

- In both the structural configurations SC B and SC C, the storey just above the uppermost foundation level has a significant torsional effect, leading to failure of that particular storey. This pattern of failure has been consistently observed in both SC B and SC C, irrespective of the building's design level.

- The far-field record suite of FEMA P695 resulted in average record-to-record variability of 0.30 at collapse under bi-directional excitation. This was observed for the wide range of building models and structural configurations investigated in this study, while choosing S_a as the IM.

- In case of low- and mid-rise buildings, pre-code design resulted in unacceptably high collapse probabilities varying from 73-98%, for MCE hazard level. These collapse probabilities reduce to a significant extent in case of moderate- and high-code buildings with corresponding collapse probabilities varying from 4-10% and 1-8%, respectively.

- In case of high-rise high-code buildings, the collapse probabilities vary from 11-50% for the MCE hazard level. These high-rise high-code buildings show significantly poor performance when compared with the acceptance criterion of FEMA P695, which specifies 20% probability of collapse as acceptable, conditioned on the occurrence of the MCE.

CHAPTER 5

SITE EFFECTS IN SEISMIC FRAGILITY ANALYSIS

5.1 INTRODUCTION

In the earlier developments of Performance-Based Earthquake Engineering (PBEE), the seismic fragility of a building was considered as being solely a function of the structure itself (e.g. FEMA 2002; Penelis et al. 2003; Kappos et al. 2006; Barbat et al. 2008; Haldar and Singh 2009; Kamatchi et al. 2008; Kamatchi et al. 2009; Kamatchi et al. 2010). Recent research (e.g. Baker and Cornell 2006; Haselton and Deierlein 2007a; Mousavi et al. 2011; Bojorquez and Iervolino 2011; Haselton et al. 2011a; Haselton et al. 2011b; Eads et al. 2015 and Eads et al. 2016), as also discussed in Chapter 3 demonstrates that the spectral shape of rarely occurring ground-motion records (e.g. caused by the MCE) is a key parameter in the collapse fragility assessment of structures. The spectral shape of an expected but rare earthquake foremost depends on the seismotectonic regime and the local geological conditions of the site as well as the hazard level of interest. Therefore, the collapse fragility of a structure cannot be developed independent of these conditions (Kohrangi et al. 2017c).

To take into account the site-specific effects in seismic fragility analysis, two representative sites 'Mussoorie' and 'Shillong' situated in seismic zones IV and V, respectively, as per current seismic zoning map of India (IS 1893 Part 1 2016) have been considered and investigated in the present Chapter. For both the considered sites, deterministic as well as probabilistic seismic hazard analyses have been conducted. The evaluated site-specific seismic hazard has been used to construct the Conditional Mean Spectrum (CMS) to obtain the expected spectral shape of the MCE earthquake, corresponding to the spectral period of interest. The computed CMS has been used as the demand spectrum, and the collapse probabilities have been computed for the building models investigated in Chapter 4. A comparison showing the effects of design level, and seismic zone on collapse fragility curves of RC frame buildings with different structural configurations has been presented.

In the later part of this Chapter, the CMS for the Mussoorie site has also been developed considering the near-field effects. The high-code buildings considered in Chapter 4 have been further investigated by applying the IDA procedure using two additional ground-motion record

suites of FEMA P695: (i) the record suite of near-field ground-motions without velocity pulses, and (ii) the record suite of near-field ground-motions with velocity pulses. A comparison of collapse probabilities with and without considering the near-field site effects for the Mussoorie site has also been presented.

5.2 CONDITIONAL MEAN SPECTRUM

Baker (2011) presented the concept of CMS which was developed primarily for the selection of ground-motion records. As also discussed in Chapter 3, a CMS provides the mean expected response spectrum at a site, conditioned on the occurrence of a target spectral acceleration value at the period of interest. The CMS is considered to be more realistic than a Uniform Hazard Spectrum (UHS), since a UHS represents the equal probability of exceedance of all the spectral ordinates, irrespective of the period of interest. The shape of the UHS is significantly different than the spectral shape of a typical MCE ground-motion record, at the site of interest (Baker 2011).

In the present study, CMS have been developed for both Mussoorie and Shillong sites. For the development of the CMS at the considered sites, the procedure as illustrated by Baker (2011) has been used. Both the Deterministic Seismic Hazard Analysis (DSHA) and the Probabilistic Seismic Hazard Analysis (PSHA) are considered to be an integral part of this procedure. The PSHA results in the target S_a at the period of interest, and the hazard deaggregation results in the governing earthquake characteristics, e.g. the event magnitude (M_w), the epicentral distance (R_s), and the epsilon (ε) at the period of interest. Parameter ε is defined as the number of standard deviations by which a given $\ln S_a$ value at a site differs from its mean predicted value derived from an attenuation model (or ground-motion prediction equation) for a given magnitude and distance. In a functional form, parameter epsilon (ε) can be expressed as:

$$\varepsilon(T) = \frac{\ln\left(S_a(T)\right) - \mu_{\ln S_a}(M_w, R_s, T)}{\sigma_{\ln S_a}(T)} \tag{5.1}$$

where, $\mu_{\ln S_a}(M_w, R_s, T)$ and $\sigma_{\ln S_a}(T)$ are the predicted mean and standard deviation of $\ln S_a(T)$ at the period of interest, and $\ln S_a(T)$ is the natural logarithm of the spectral acceleration of interest. The first two parameters can be obtained from attenuation models (e.g. Campbell and

Bozorgnia 2008, Boore and Atkinson 2008) based on the mean value of magnitude (here moment magnitude M_w) and epicentral distance (R_s) obtained from the hazard deaggregation, at the period of interest. The epsilon (ε) values at the periods other than the period of interest can be computed based on the cross-correlation coefficients reported in literature (e.g. Baker and Jayaram 2008). Using the computed parameters, the CMS can be developed following the procedure suggested by Baker (2011).

In the present study, for both Mussoorie and Shillong sites, the attenuation model developed by Campbell and Bozorgnia (2008) has been used to develop the CMS. To also include the near-field effects for the Mussoorie site, the attenuation model developed by Campbell and Bozorgnia (2014) has been used. In total three different sets of CMS have been developed for three different periods of interest (viz. 1.00 s, 1.50 s, 3.35 s), corresponding to the three building heights above the uppermost foundation (which controls the period of vibration in case of hill buildings). Tables 5.1-5.3 present the hazard deaggregation results for the sites of Mussoorie and Shillong and the corresponding CMS have been presented in Figs. 5.1-5.2. It can be observed from Tables 5.1 and 5.2, at both the sites Mussoorie and Shillong, that the spectral ordinates at different periods are controlled by a single governing earthquake.

Table 5.1 Hazard deaggregation results for Mussoorie site obtained from CB08 attenuation model.

T (s)	Moment Magnitude, M_w	Epicentral distance, R_s	Epsilon, ε
1.00	6.35	08	0.07
1.50	6.35	08	0.23
3.35	6.35	16	0.27

Table 5.2 Hazard deaggregation results for Shillong site obtained from CB08 attenuation model.

T (s)	Moment Magnitude, M_w	Epicentral distance, R_s	Epsilon, ε
1.00	7.70	32	0.64
1.50	7.70	32	0.72
3.35	7.70	32	1.00

Table 5.3 Hazard deaggregation results for Mussoorie site obtained from CB14 attenuation model, including near-field effects.

T (s)	Moment Magnitude, M_w	Epicentral distance, R_s	Epsilon, ε
1.00	6.85	16	0.51
1.50	6.85	16	0.52
3.35	6.85	16	0.58

The governing earthquake magnitude at the Shillong site has a magnitude, M_w = 7.70, in comparison to M_w = 6.85 and 6.35 for the Mussoorie site, with and without considering the

near-field effects, respectively. The ε values typically range from 0.07-0.27 for the Mussoorie site and 0.64-1.00 for the Shillong site. In the attenuation model, when the near-field effects are considered for Mussoorie site, the ε values increase and typically range between 0.51-0.58 (Table 5.3). For both the sites, ε values at all periods have been observed to be positive.
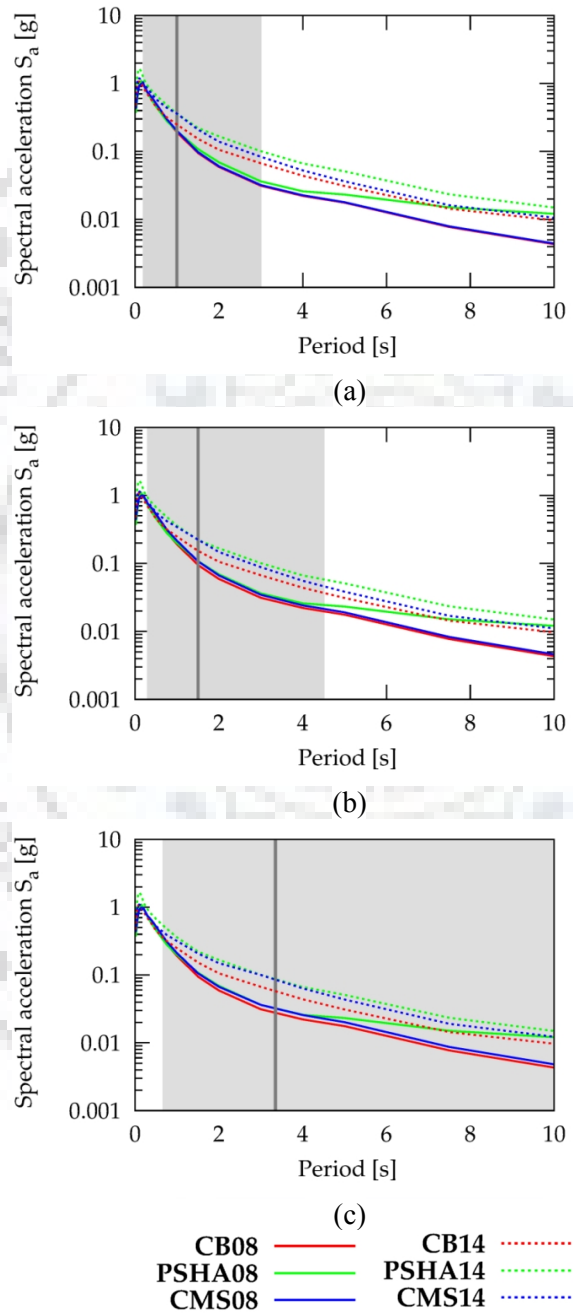
Fig. 5.1 Conditional Mean Spectra for the Mussoorie site for: (a) $T = 1.00$ s; (b) $T = 1.50$ s; and (c) $T = 3.35$ s. The suffix 08 indicates Campbell and Bozorgnia (2008) attenuation model (i.e. without near-field effects), and the suffix 14 indicates Campbell and Bozorgnia (2014) attenuation model (i.e. with near-field effects). The gray-shaded zone represents the period range between $0.2T$-$3T$.
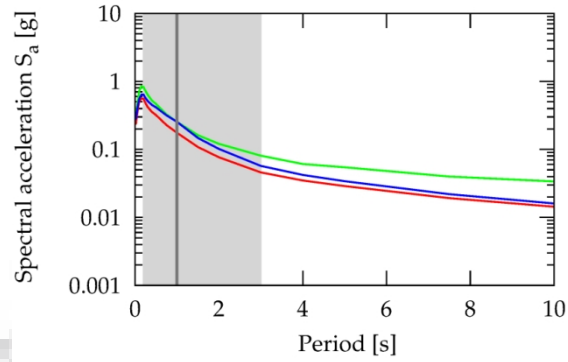
(a)
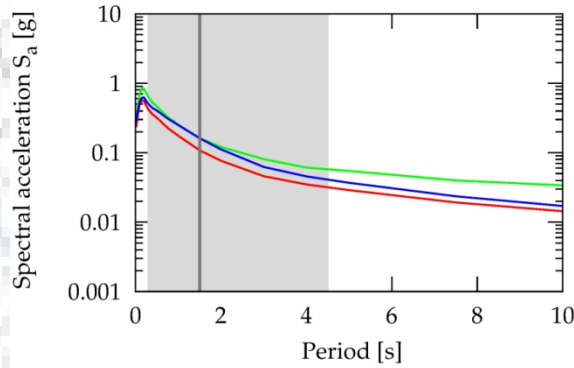
(b)
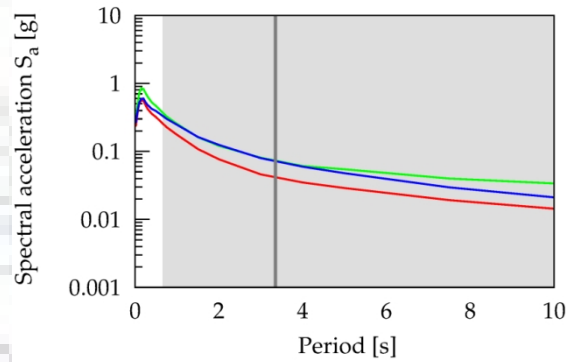
(c)

CB08 ———
PSHA08 ———
CMS08 ———

Fig. 5.2 Conditional Mean Spectra for the Shillong site for: (a) $T = 1.00$ s; (b) $T = 1.50$ s; and (c) $T = 3.35$ s. The suffix 08 indicates Campbell and Bozorgnia (2008) attenuation model (i.e. without near-field effects). The gray-shaded zone represents the period range between $0.2T$-$3T$.

Figure 5.1 presents a comparison of the 5%-damped response spectra obtained from the attenuation model (CB08 and CB14, corresponding to governing earthquake parameters), the PSHA, and the CMS for the Mussoorie site. The response spectra for the Mussoorie site have been presented for both the cases: (i) based on the attenuation model by Campbell and Bozorgnia (2008) without considering the near-field effects, and (ii) based on the attenuation

113

model by Campbell and Bozorgnia (2014) considering near-field effects. It is clearly evident from Fig. 5.1 that the CMS matches the PSHA estimate of the spectral acceleration at the period of interest, and at the other periods, it falls in between the PSHA and CB08/CB14 estimates of the spectral ordinates. Further, the consideration of the near-field effects leads to increased hazard for the Mussoorie site, to a significant extent (upto 2.6 times in long-period range, at $T = 3.35$ s).

Figure 5.2 presents a comparison of the 5%-damped response spectra obtained from the attenuation model (CB08, corresponding to governing earthquake parameters), the PSHA, and the CMS for the Shillong site. It is evident from Fig. 5.2 that the relative difference between the PSHA and the CB08 estimates of the spectral ordinates is higher in case of the Shillong site as compared to the Mussoorie site. This effect can also be corroborated with Tables 5.1 and 5.3, in which it can be seen that ε values are higher for the Shillong site when compared with the corresponding values for the Mussoorie site, in both the cases, i.e. without and with considering near-field effects.

5.3 EFFECT OF SPECTRAL SHAPE

In this section, the collapse capacity assessment results for the building models investigated in Chapter 4, for the far-field sites, (in seismic zones IV and V) have been presented after incorporating the spectral shape effects. Figures 5.3-5.5 present the dynamic capacity curves for the pre-, moderate-, and high-code mid-rise buildings with structural configurations SC A, SC B and SC C, respectively, designed for seismic zone IV. These results are similar to those presented in Chapter 4 (Figs. 4.2-4.4), except that a different intensity measure, i.e. $S_{a,avg}$ (0.2T-3T, 5%) has been chosen. This intensity measure takes into account the spectral shape in the period range 0.2T to 3T. The dynamic capacity curves for individual records, as well as the 16th, 50th (median), and 84th percentile are shown.

A comparison of Figs. 5.3-5.5 with Figs. 4.2-4.4 shows that while choosing $S_{a,avg}$ (0.2T-3T, 5%) as collapse IM, the record-to-record dispersion in collapse capacities reduces, significantly. Similar results have also been obtained for the other investigated building models, but are not presented here for brevity. The corresponding median collapse capacities have been reported in Tables 5.4-5.6. The collapse capacities have been reported both in terms of S_a (reproduced from

Chapter 4) and $S_{a,avg}$ and the corresponding MCE demands have been obtained from the code (IS 1893 Part 1 2016) response spectrum and the CMS, respectively. The procedure for computing seismic demand in terms of $S_{a,avg}$ (0.2T-3T, 5%), used in the present study, is an indirect procedure, since the hazard analysis has been conducted in terms of S_a (T, 5%), and $S_{a,avg}$ (0.2T-3T, 5%) has been obtained from the plot of S_a (T, 5%). However, Kohrangi et al. (2017b) have shown that this procedure leads to identical median $S_{a,avg}$ (0.2T-3T, 5%) values when compared with the case in which seismic hazard analysis is performed directly in terms of $S_{a,avg}$ (0.2T-3T, 5%).
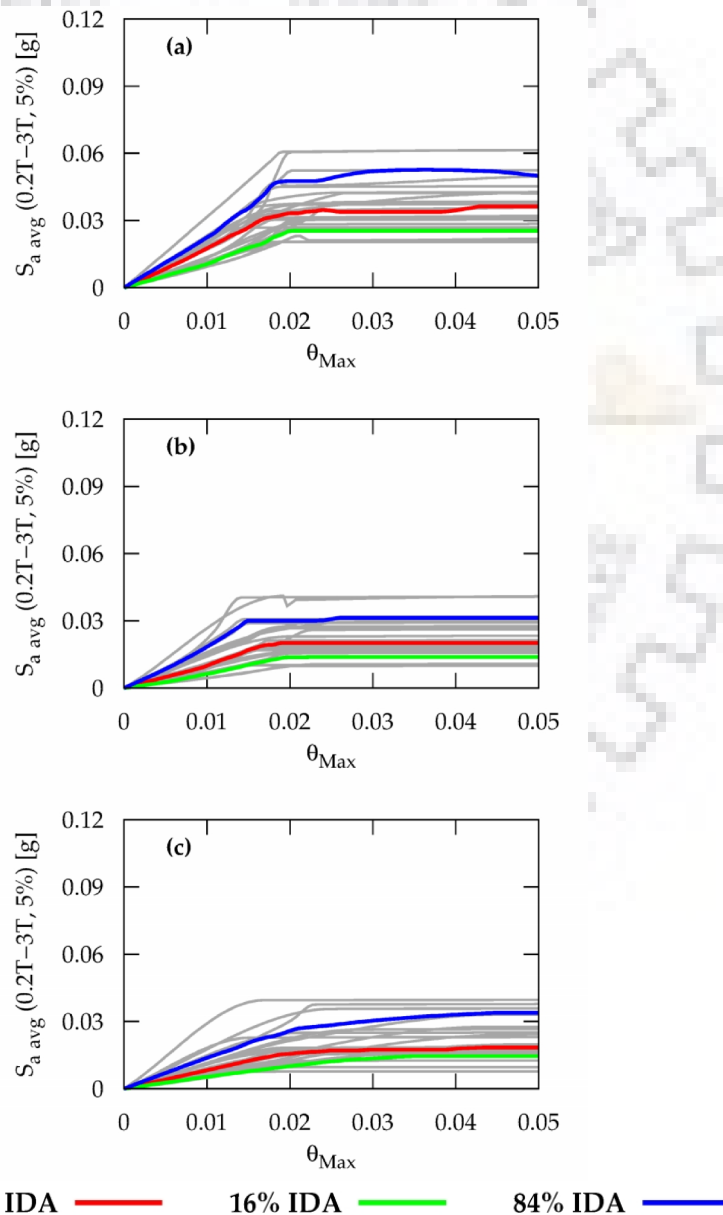
Fig. 5.3 Dynamic capacity curves for pre-code mid-rise buildings: (a) SC A; (b) SC B; and (c) SC C.
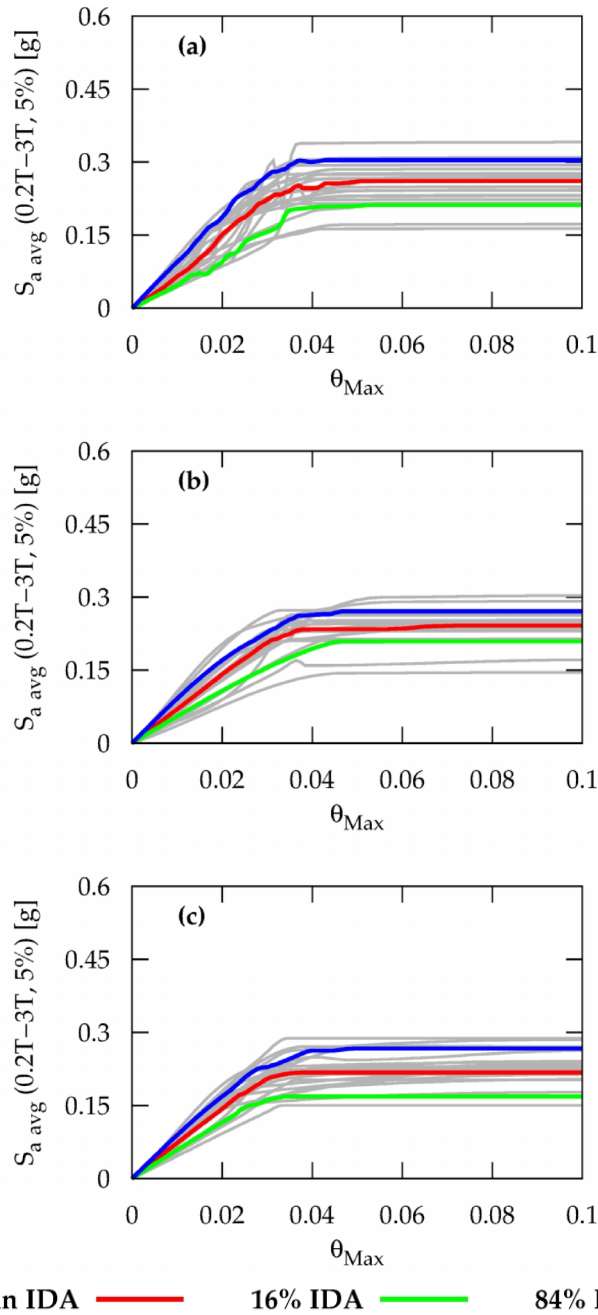
Fig. 5.4 Dynamic capacity curves for moderate-code mid-rise buildings: (a) SC A; (b) SC B; and (c) SC C.

The CMR has been computed earlier in Chapter 4 (Eq. 4.1), whereas the adjusted collapse margin ratio (ACMR) has been computed from the ratio of the collapse capacity to seismic demand, both computed in terms of $S_{a,avg}$ (defined as the geometric mean of spectral ordinates between a range of periods $0.2T$-$3T$, where, T is the average period of vibration). This method of directly computing ACMR is different than the conventional method of 'adjusting' the CMR for the effects of the spectral shape of the ground-motions chosen in the analysis (as presented

in FEMA P695). The major difference between the two metrics (CMR and ACMR) of collapse performance lies in the fact that ACMR accounts for the effect of site-specific spectral shape through $S_{a,avg}$ whereas CMR does not account for the same, as it is based on single ordinate of response spectrum. It is to be noted that the effect of spectral shape can vary from building to building, depending on the site conditions, the period of vibration, and ductility capacity of the building. In this section, the average values of ACMR have been compared with the corresponding values of CMR.
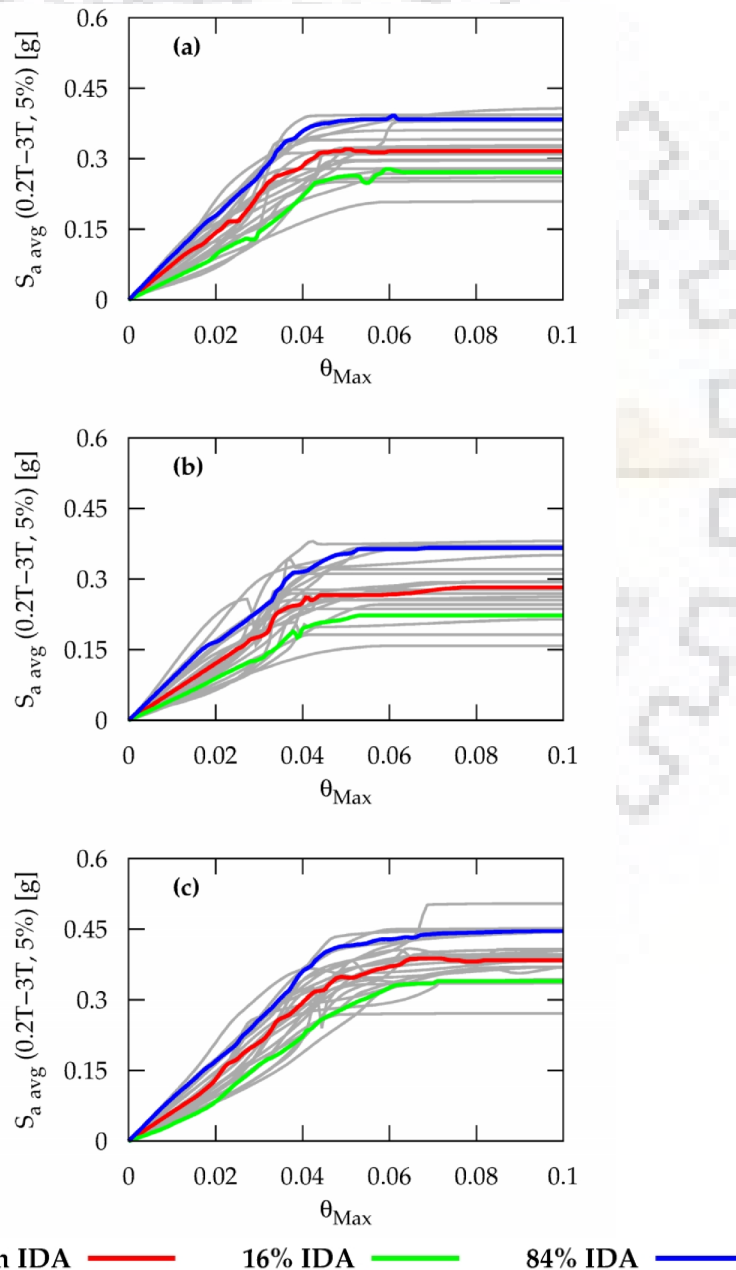
Fig. 5.5 Dynamic capacity curves for high-code mid-rise buildings: (a) SC A; (b) SC B; and (c) SC C.

Table 5.4 Collapse capacities and CMR of considered pre-code buildings.

Building Model	Seismic Zone	S_a(D)	S_a(C)	$S_{a,avg}$(D)	$S_{a,avg}$(C)	CMR	ACMR
AL-RC-R6	IV	0.163g	0.106g	0.067g	0.061g	0.65	0.91
AM-RC-R6	IV	0.083g	0.059g	0.022g	0.036g	0.71	1.64
BL-RC-R6	IV	0.153g	0.094g	0.066g	0.058g	0.61	0.88
BM-RC-R6	IV	0.080g	0.034g	0.021g	0.020g	0.43	0.95
CL-RC-R6	IV	0.135g	0.075g	0.060g	0.045g	0.56	0.75
CM-RC-R6	IV	0.078g	0.033g	0.021g	0.019g	0.42	0.90
AL-RC-R6	V	0.245g	0.106g	0.103g	0.061g	0.43	0.59
AM-RC-R6	V	0.125g	0.059g	0.054g	0.036g	0.47	0.67
BL-RC-R6	V	0.229g	0.094g	0.100g	0.058g	0.41	0.58
BM-RC-R6	V	0.120g	0.034g	0.052g	0.020g	0.28	0.38
CL-RC-R6	V	0.202g	0.075g	0.098g	0.045g	0.37	0.46
CM-RC-R6	V	0.117g	0.033g	0.050g	0.019g	0.28	0.38

S_a(D) - seismic demand for MCE hazard in terms of S_a, S_a(C) - median collapse capacity in terms of S_a, $S_{a,avg}$(D) - seismic demand for MCE hazard in terms of $S_{a,avg}$, and $S_{a,avg}$(C) - median collapse capacity in terms of $S_{a,avg}$.

Table 5.5 Collapse capacities and CMR of considered moderate-code buildings.

Building Model	Seismic Zone	S_a(D)	S_a(C)	$S_{a,avg}$(D)	$S_{a,avg}$(C)	CMR	ACMR
AL-RC-R6	IV	0.240g	0.660g	0.112g	0.455g	2.75	4.06
AM-RC-R6	IV	0.160g	0.440g	0.067g	0.259g	2.75	3.87
AH-RC-R6	IV	0.072g	0.120g	0.022g	0.076g	1.67	3.45
AL-RC-R6	V	0.360g	0.790g	0.154g	0.520g	2.19	3.38
AM-RC-R6	V	0.240g	0.450g	0.103g	0.260g	1.88	2.52
AH-RC-R6	V	0.107g	0.090g	0.054g	0.054g	0.84	1.00
BL-RC-R6	IV	0.229g	0.586g	0.112g	0.381g	2.56	3.40
BM-RC-R6	IV	0.159g	0.387g	0.067g	0.241g	2.43	3.60
CL-RC-R6	IV	0.224g	0.543g	0.112g	0.373g	2.42	3.33
CM-RC-R6	IV	0.161g	0.360g	0.067g	0.244g	2.24	3.64

S_a(D) - seismic demand for MCE hazard in terms of S_a, S_a(C) - median collapse capacity in terms of S_a, $S_{a,avg}$(D) - seismic demand for MCE hazard in terms of $S_{a,avg}$, and $S_{a,avg}$(C) - median collapse capacity in terms of $S_{a,avg}$.

It can be observed that the consideration of spectral shape effects lead to an increase in ACMR for the considered far-field sites, irrespective of the design level of the buildings. This observation can be attributed to the fact that the considered sites have 'positive ε' values (Tables 5.1-5.2) for the MCE hazard level which is higher than median 'ε' values (computed from CB08 attenuation model) of the ground-motion record suite at all periods of interest, which results in an increase in collapse capacity of the building models after adjusting for the spectral shape effects. The observed trends are consistent with previous investigations on collapse assessment which reported an increase in collapse capacity for 'positive ε' sites for the United States (e.g. Haselton et al. 2011b; FEMA P695 2009).

In case of the pre-code buildings, the average increase in the collapse capacity due to the spectral shape effects is 80% and 36% in seismic zones IV and V, respectively. In case of the moderate-code buildings, the average increase in the collapse capacity due to the spectral shape

effects is 52% and 36% in seismic zones IV and V, respectively. In case of the high-code buildings, the average increase in the collapse capacity due to the spectral shape effects is 63% and 41%, respectively.

Table 5.6 Collapse capacities and CMR of considered high-code buildings.

Building Model	Seismic Zone	S_a(D)	S_a(C)	$S_{a,avg}$(D)	$S_{a,avg}$(C)	CMR	ACMR
AL-RC-R6	IV	0.240g	0.930g	0.112g	0.660g	3.88	5.89
AM-RC-R6	IV	0.160g	0.550g	0.067g	0.320g	3.44	4.78
AH-RC-R6	IV	0.072g	0.150g	0.022g	0.100g	2.08	4.55
AL-RC-R6	V	0.360g	0.990g	0.154g	0.660g	2.75	4.29
AM-RC-R6	V	0.240g	0.600g	0.103g	0.360g	2.50	3.50
AH-RC-R6	V	0.107g	0.160g	0.054g	0.110g	1.50	2.04
BL-RC-R6	IV	0.229g	0.792g	0.112g	0.492g	3.46	4.39
BM-RC-R6	IV	0.159g	0.484g	0.067g	0.294g	3.04	4.39
BH-RC-R6	IV	0.071g	0.128g	0.022g	0.080g	1.80	3.64
BL-RC-R6	V	0.350g	0.803g	0.154g	0.520g	2.29	3.38
BM-RC-R6	V	0.242g	0.525g	0.103g	0.316g	2.17	3.07
BH-RC-R6	V	0.109g	0.110g	0.054g	0.070g	1.01	1.30
CL-RC-R6	IV	0.224g	0.932g	0.112g	0.602g	4.16	5.38
CM-RC-R6	IV	0.158g	0.671g	0.067g	0.382g	4.25	5.70
CH-RC-R6	IV	0.071g	0.136g	0.022g	0.092g	1.92	4.18
CL-RC-R6	V	0.360g	1.027g	0.154g	0.629g	2.85	4.08
CM-RC-R6	V	0.242g	0.600g	0.103g	0.367g	2.48	3.56
CH-RC-R6	V	0.108g	0.143g	0.054g	0.096g	1.32	1.78

S_a (D) - seismic demand for MCE hazard in terms of S_a, S_a (C) - median collapse capacity in terms of S_a, $S_{a,avg}$ (D) - seismic demand for MCE hazard in terms of $S_{a,avg}$, and $S_{a,avg}$ (C) - median collapse capacity in terms of $S_{a,avg}$.

In this study, the increase in collapse capacity (by accounting spectral shape through $S_{a,avg}$) has been observed to be of similar order when compared with the simplified method outlined in FEMA P695 for sites located in the United States. The simplified method outlined in FEMA P695 increases the collapse capacity in terms of S_a through a spectral shape factor (SSF), which results in an increase up to 37% and 61%, in collapse capacity for Seismic Design Category (SDC) C and D_{max}, respectively, which are equivalent to Indian seismic zones IV and V, respectively, based on the design spectral ordinates. This increase in collapse capacity is expected to affect the collapse fragility of the buildings significantly. Therefore, the effect of spectral shape on fragility of the investigated buildings has been studied in the next section.

5.4 FRAGILITY ANALYSIS WITH SPECTRAL SHAPE EFFECTS

In this section, the fragility curves for all the building models investigated in Chapter 4, for the far-field sites, in seismic zones IV and V have been presented after incorporating the spectral shape effects. Tables 5.7-5.9 present variability parameters for the pre-, moderate- and high-

code buildings, considered in the present study. The values reported in Tables 5.7-5.9 for β_{RTR} (S_a) have been reproduced from Chapter 4 for the sake of comparison, and the value of β_M has been taken uniform from the available literature, as discussed in the previous chapter. It can be observed that in case of the pre-code buildings, the β_{RTR} (S_a) values are in general on the lower side when compared to those obtained from β_{RTR} $(S_{a,avg})$, the corresponding average values being 0.33 and 0.35 (Table 5.7), respectively. On the other side, in case of both moderate- and high-code buildings, this trend gets reversed with the corresponding average values of β_{RTR} (S_a) and β_{RTR} $(S_{a,avg})$ being 0.30 and 0.24 (Table 5.8), respectively in case of moderate-code buildings, and 0.32 and 0.24 (Table 5.9), respectively in case of the high-code buildings.

Table 5.7 Variability parameters for the considered pre-code buildings.

Building Model	Seismic Zone	β_M	β_{RTR} (S_a)	β_{RTR} $(S_{a,avg})$	$\beta_T(S_a)$	$\beta_T(S_{a,avg})$
AL-RC-R6	IV	0.50	0.39	0.44	0.63	0.67
AM-RC-R6	IV	0.50	0.28	0.31	0.57	0.59
BL-RC-R6	IV	0.50	0.27	0.29	0.57	0.58
BM-RC-R6	IV	0.50	0.34	0.40	0.60	0.64
CL-RC-R6	IV	0.50	0.30	0.27	0.58	0.57
CM-RC-R6	IV	0.50	0.37	0.41	0.62	0.65
AL-RC-R6	V	0.50	0.39	0.44	0.63	0.67
AM-RC-R6	V	0.50	0.28	0.31	0.57	0.59
BL-RC-R6	V	0.50	0.27	0.29	0.57	0.58
BM-RC-R6	V	0.50	0.34	0.40	0.60	0.64
CL-RC-R6	V	0.50	0.30	0.27	0.58	0.57
CM-RC-R6	V	0.50	0.37	0.41	0.62	0.65

β_{RTR} (S_a) - record-to-record variability in collapse capacity, when S_a is chosen as IM, β_{RTR} $(S_{a,avg})$ - record-to-record variability in collapse capacity, when $S_{a,avg}$ is chosen as IM, β_T (S_a) - total variability in the collapse capacity, when S_a is chosen as IM, and β_T $(S_{a,avg})$ - total variability in the collapse capacity, when $S_{a,avg}$ is chosen as IM.

Table 5.8 Variability parameters for the considered moderate-code buildings.

Building Model	Seismic Zone	β_M	β_{RTR} (S_a)	β_{RTR} $(S_{a,avg})$	$\beta_T(S_a)$	$\beta_T(S_{a,avg})$
AL-RC-R6	IV	0.50	0.28	0.25	0.57	0.56
AM-RC-R6	IV	0.50	0.30	0.16	0.58	0.52
AH-RC-R6	IV	0.50	0.37	0.36	0.62	0.62
AL-RC-R6	V	0.50	0.32	0.29	0.59	0.58
AM-RC-R6	V	0.50	0.30	0.20	0.58	0.54
AH-RC-R6	V	0.50	0.30	0.34	0.58	0.60
BL-RC-R6	IV	0.50	0.20	0.16	0.54	0.52
BM-RC-R6	IV	0.50	0.27	0.16	0.57	0.52
CL-RC-R6	IV	0.50	0.32	0.24	0.59	0.55
CM-RC-R6	IV	0.50	0.30	0.18	0.58	0.53

β_{RTR} (S_a) - record-to-record variability in collapse capacity, when S_a is chosen as IM, β_{RTR} $(S_{a,avg})$ - record-to-record variability in collapse capacity, when $S_{a,avg}$ is chosen as IM, β_T (S_a) - total variability in the collapse capacity, when S_a is chosen as IM, and β_T $(S_{a,avg})$ - total variability in the collapse capacity, when $S_{a,avg}$ is chosen as IM.

The reason for this observation can be attributed to the fact that the pre-code buildings have very limited ductility. Therefore, these buildings are not subjected to a significant period

elongation in the non-linear range, prior to collapse, and hence the collapse response is better captured by S_a based on a single period of vibration (average of the first mode periods in the two orthogonal directions). Contrary to the pre-code buildings, the moderate- and high-code buildings are subjected to a significant period elongation, prior to collapse. Therefore, to capture the collapse response of these buildings, the consideration of spectral ordinates $S_{a,avg}$, in a period range around T, leads to a significant reduction in β_{RTR} ($S_{a,avg}$). However, this observation has been found to be limited to low- and mid-rise buildings.

Table 5.9 Variability parameters for the considered high-code buildings.

Building Model	Seismic Zone	β_M	β_{RTR} (S_a)	β_{RTR} ($S_{a,avg}$)	β_T (S_a)	β_T ($S_{a,avg}$)
AL-RC-R6	IV	0.50	0.28	0.21	0.57	0.54
AM-RC-R6	IV	0.50	0.32	0.15	0.59	0.52
AH-RC-R6	IV	0.50	0.31	0.27	0.59	0.57
AL-RC-R6	V	0.50	0.26	0.19	0.56	0.53
AM-RC-R6	V	0.50	0.31	0.17	0.59	0.53
AH-RC-R6	V	0.50	0.32	0.32	0.59	0.59
BL-RC-R6	IV	0.50	0.32	0.21	0.59	0.54
BM-RC-R6	IV	0.50	0.27	0.25	0.57	0.56
BH-RC-R6	IV	0.50	0.43	0.43	0.66	0.66
BL-RC-R6	V	0.50	0.30	0.21	0.58	0.54
BM-RC-R6	V	0.50	0.26	0.24	0.56	0.55
BH-RC-R6	V	0.50	0.32	0.33	0.59	0.60
CL-RC-R6	IV	0.50	0.38	0.21	0.63	0.54
CM-RC-R6	IV	0.50	0.33	0.15	0.60	0.52
CH-RC-R6	IV	0.50	0.30	0.26	0.58	0.56
CL-RC-R6	V	0.50	0.35	0.23	0.61	0.55
CM-RC-R6	V	0.50	0.34	0.20	0.60	0.54
CH-RC-R6	V	0.50	0.32	0.33	0.59	0.60

β_{RTR} (S_a) - record-to-record variability in collapse capacity, when S_a is chosen as IM, β_{RTR} ($S_{a,avg}$) - record-to-record variability in collapse capacity, when $S_{a,avg}$ is chosen as IM, β_T (S_a) - total variability in the collapse capacity, when S_a is chosen as IM, and β_T ($S_{a,avg}$) - total variability in the collapse capacity, when $S_{a,avg}$ is chosen as IM.

In case of high-rise buildings, both S_a and $S_{a,avg}$ lead to comparable β_{RTR} (S_a) and β_{RTR} ($S_{a,avg}$), which can be attributed to a relatively longer period of the high-rise buildings (also explained later in this Chapter). The use of $S_{a,avg}$ as an IM not only accounts for the spectral shape but also leads to a reduction in aleatoric uncertainty in the collapse fragility curves, particularly for the low- and the mid-rise buildings. This observation is found out to be in agreement with earlier studies on 2D buildings subjected to uni-directional excitations (Eads et al. 2015; 2016). The observed trends have direct implication in the seismic design of buildings, particularly for ductile buildings. As evidenced, $S_{a,avg}$ leads to a reduced β_{RTR} ($S_{a,avg}$), which means that a lesser number of dynamic analyses will be required, while choosing $S_{a,avg}$ as an IM when compared with S_a, to achieve the same confidence in predicting structural collapse. The reduction in

number of the dynamic analyses is typically of the order of 25% (based on average reduction in record-to-record variability) in case of ductile buildings even with horizontal and vertical irregularities (e.g. hill buildings), subjected to bi-directional excitations.

Figure 5.6 compares the collapse fragility curves for the low- and the mid-rise buildings, representative of pre-, moderate- and high-code design levels, for all the considered structural configurations. These fragility curves are plotted with $S_{a,avg}$ (0.2T-3T, 5%), normalized by the corresponding $S_{a,avg}$ (0.2T-3T, 5%) at MCE for Mussoorie (seismic zone IV), computed for the far-field site. It is clearly evident from Figure 5.6 that the pre-code buildings are extremely vulnerable when compared with the moderate- and high-code buildings. Further, the collapse fragility of the moderate-code buildings is also higher when compared with the high-code buildings. However, the difference between collapse fragility of the moderate- and the high-code buildings is relatively small when compared with the pre- and moderate-code buildings.
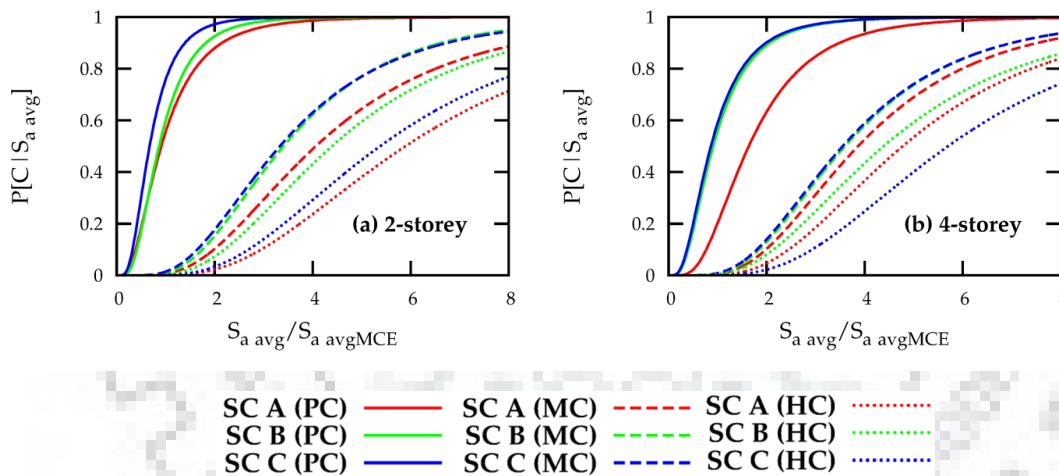
Fig. 5.6 Collapse fragility curves for different structural configurations of low- and mid-rise, pre- (PC); moderate- (MC); and high-code (HC) RC buildings, for seismic zone IV.

Figure 5.7 compares the collapse fragility curves for the low-, mid- and high-rise buildings representative of the high-code design level, for all the considered structural configurations, for both the Mussoorie (zone IV) and Shillong (zone V) sites. It is evident from Figure 5.7 that the high-code buildings located at Shillong site are more vulnerable when compared with their counterparts located at the Mussoorie site. Further, the effect of seismic zone is more pronounced in high-rise (8-storey) buildings. Tables 5.10-5.12 present the collapse probabilities for the pre-, moderate- and high-code buildings investigated in this study, after adjusting for spectral shape effects through $S_{a,avg}$. The collapse probabilities using $S_{a,avg}$ as the IM, have been

computed based on the seismic demands obtained from the CMS (constructed in Section 5.2), for far-field site conditions, both for the Mussoorie and the Shillong site, whereas, the collapse probability estimates based on S_a have been reproduced from Chapter 4, for the purpose of comparison.
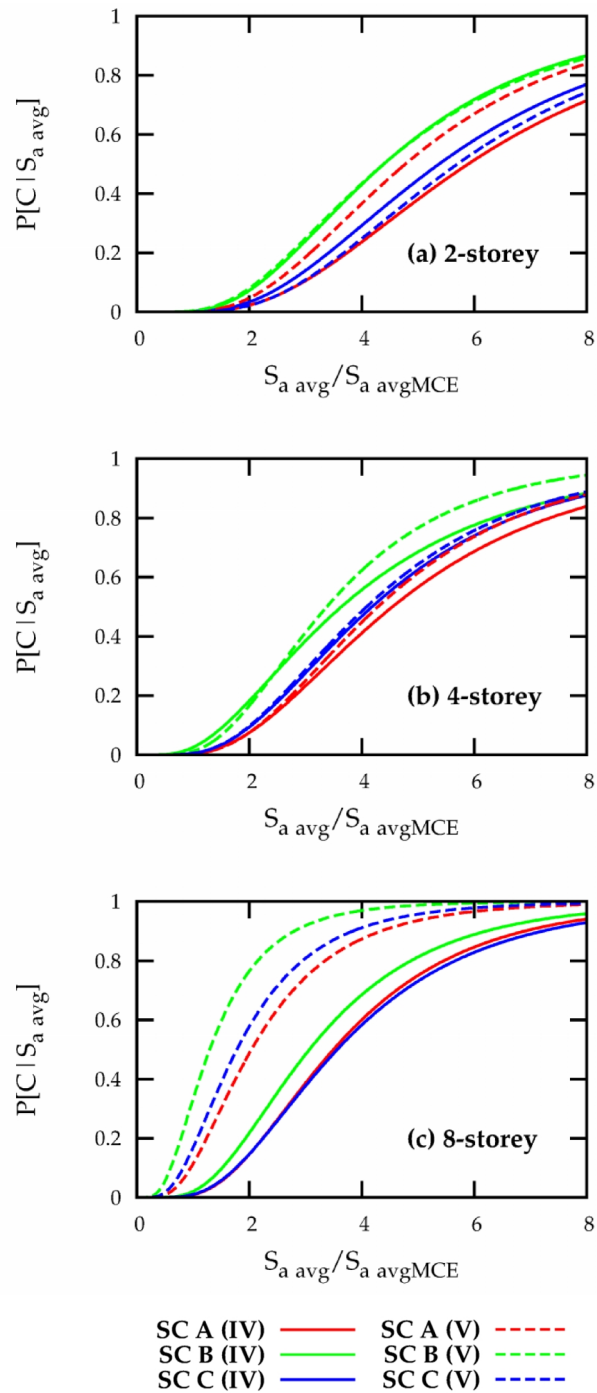
Fig. 5.7 Collapse fragility curves for different structural configurations of high-code RC buildings, for seismic zones IV and V.

Table 5.10 Collapse probabilities at MCE hazard for the considered pre-code buildings.

Building Model	Seismic Zone	Collapse Probability (%) P[C/S_a]	Collapse Probability (%) P[C/$S_{a,avg}$]
AL-RC-R6	IV	**75**	**56**
AM-RC-R6	IV	**73**	**21**
BL-RC-R6	IV	**80**	**60**
BM-RC-R6	IV	**92**	**56**
CL-RC-R6	IV	**84**	**76**
CM-RC-R6	IV	**92**	**59**
AL-RC-R6	V	**91**	**78**
AM-RC-R6	V	**91**	**76**
BL-RC-R6	V	**94**	**84**
BM-RC-R6	V	**98**	**94**
CL-RC-R6	V	**96**	**93**
CM-RC-R6	V	**98**	**95**

P[C/S_a] and P[C/$S_{a,avg}$] represent the probabilities of collapse for MCE hazard while choosing S_a and $S_{a,avg}$ as IM's, respectively. Collapse probability values shown in bold shows failure of that particular building based on FEMA P695 acceptance criterion.

Table 5.11 Collapse probabilities at MCE hazard for the considered moderate-code buildings.

Building Model	Seismic Zone	Collapse Probability (%) P[C/S_a]	Collapse Probability (%) P[C/$S_{a,avg}$]
AL-RC-R6	IV	10	01
AM-RC-R6	IV	04	01
BL-RC-R6	IV	04	01
BM-RC-R6	IV	06	01
CL-RC-R6	IV	06	02
CM-RC-R6	IV	08	01

P[C/S_a] and P[C/$S_{a,avg}$] represent the probabilities of collapse for MCE hazard while choosing S_a and $S_{a,avg}$ as IM's, respectively. Collapse probability values shown in bold shows failure of that particular building based on FEMA P695 acceptance criterion.

Table 5.12 Collapse probabilities at MCE hazard for the considered high-code buildings.

Building Model	Seismic Zone	Collapse Probability (%) P[C/S_a]	Collapse Probability (%) P[C/$S_{a,avg}$]
AL-RC-R6	IV	01	01
AM-RC-R6	IV	02	01
AH-RC-R6	IV	11	01
AL-RC-R6	V	04	01
AM-RC-R6	V	06	01
AH-RC-R6	V	**25**	11
BL-RC-R6	IV	02	01
BM-RC-R6	IV	03	01
BH-RC-R6	IV	19	03
BL-RC-R6	V	08	01
BM-RC-R6	V	08	02
BH-RC-R6	V	**50**	**33**
CL-RC-R6	IV	01	01
CM-RC-R6	IV	01	01
CH-RC-R6	IV	13	01
CL-RC-R6	V	04	01
CM-RC-R6	V	07	01
CH-RC-R6	V	**32**	17

P[C/S_a] and P[C/$S_{a,avg}$] represent the probabilities of collapse for MCE hazard while choosing S_a and $S_{a,avg}$ as IM's, respectively. Collapse probability values shown in bold shows failure of that particular building based on FEMA P695 acceptance criterion.

In case of the pre-code buildings, the collapse fragility has been observed to be significantly higher even after adjusting for the spectral shape effects. Further, in case of both the moderate- and the high-code buildings, the collapse probabilities of the investigated building models is observed to be satisfactory when compared with the FEMA P695 criterion of 10% average probability of collapse, conditioned on the occurrence of the MCE ground-motions. On the other hand, in case of the high-code high-rise buildings, the performance is satisfactory in seismic zone IV and unsatisfactory in seismic zone V. In case of the high-code high-rise buildings in seismic zone V, the collapse probabilities have been observed to be higher (particularly in case of structural configuration B) than the acceptance criterion of 20% probability of collapse for individual buildings, conditioned on the occurrence of MCE, even after adjusting for the effect of spectral shape. The presented results suggest a need to consider the effect of structural configuration (particularly in high-rise buildings) in seismic design to achieve satisfactory performance.

5.5 NEAR-FIELD EFFECTS ON COLLAPSE FRAGILITY

In order to investigate the effect of near-field site conditions, only high-code buildings designed for seismic zone IV have been included in the numerical investigations (Table 4.1). The Indian seismic design code (IS 1893 Part 1 2016) does not distinguish between near- and far-field sites. Therefore, seismic design of building models designed for the near- and far-field sites does not differ (buildings have been designed for the same base shear coefficient as presented in Table 4.1). Modelling and analysis of the considered buildings have been conducted using the procedure presented in Section 4.5. In order to study the near-field site effects on seismic collapse fragility, two different ground-motion record suites have been considered: (i) the near-field ground-motion record suite without velocity pulse, and (ii) the near-field ground-motion record suite with velocity pulse. Both these near-field record suites consist of 14 pairs of ground-motion records as identified in the FEMA P695 project. IDA has been conducted on the considered building models following the methodology presented in Section 4.5, and the collapse fragility curves accounting for the spectral shape have been developed and presented.

5.5.1. Dynamic Capacity Curves

Figure 5.8 presents the dynamic capacity curves for the high-code mid-rise building model with SC A, designed for seismic zone IV (Mussoorie site), obtained from two different suites of

near-field ground-motion records (Figs. 5.8(a)-(b)). The capacity curves are presented in terms of $S_{a,avg}$ versus maximum inter-storey drift ratio, for individual ground-motion pair, as well as the 16th, 50th (median), and 84th percentile curves. Similar results have been obtained for other building models, but not presented here for the sake of brevity.

Median IDA ———   16% IDA ———   84% IDA ———
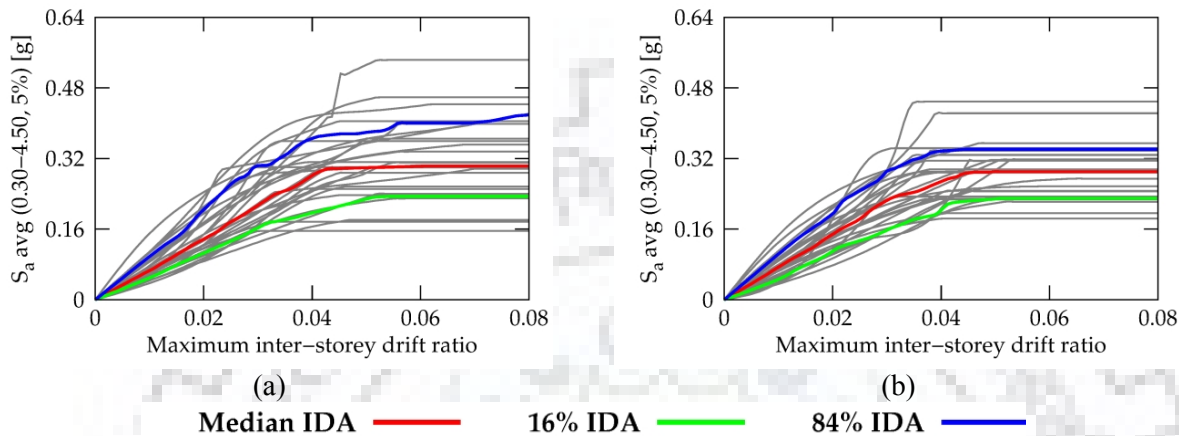
Fig. 5.8 Dynamic capacity curves for high-code mid-rise building: (a) near-field ground-motion record suite without velocity pulses; and (b) near-field ground-motion record suite with velocity pulses.

Table 5.13 presents the median collapse capacities of the building models investigated in this study in terms of both the IM's, i.e. S_a and $S_{a,avg}$. Figure 5.9 presents the 5%-damped acceleration spectra at collapse of the low-, mid- and high-rise building models with structural configuration SC A. The figure shows the median spectra for three different ground-motion record suites (the far-field suite used for investigation earlier in Chapter 4 and the near-field ground-motion record suites with and without velocity pulses), and all the ground-motion record suites combined together. The shaded gray zone in Figure 5.9 represents the range of period (between periods $0.2T$-$3T$) which is influential to the seismic response at collapse of the corresponding building model.

A comparison of Table 5.6 with Table 5.13 indicates that the difference in the collapse capacity in terms of S_a, estimated using different ground-motion record suites, is relatively higher for low- and mid-rise buildings, as compared to the high-rise buildings. This observation can be attributed to the fact that S_a is based on spectral ordinate at a single period. However, the response of a multi-storey building (even in elastic range) is affected by spectral ordinates at multiple periods. In addition, the near-collapse response of a building is governed by its elongated period, and S_a does not include any information about it. This observation is in agreement with earlier studies (Mousavi et al. 2011; Eads et al. 2015; 2016). Further, S_a based

on a single spectral ordinate also does not include any information about the pulse-period (Luco and Cornell 2007; Tothong and Luco 2007; Tothong and Cornell 2008; Eads et al. 2015, 2016). In contrary to S_a, the difference in collapse capacities in terms $S_{a,avg}$ reduces significantly in all three sets of the ground-motion records, particularly for low- and mid-rise buildings. It is evident from Figure 5.9 that the median collapse capacity obtained in terms of $S_{a,avg}$ is almost the same for all the record suites. The reason for this observation lies in the fact that $S_{a,avg}$ (0.2T-3T, 5%) is based on spectral ordinates at multiple periods. Therefore, it captures the effect of higher modes of vibration, the effect of period elongation of an inelastic structure, the effect of velocity-pulse (if present, in the periods influential to structural response), and hence the spectral shape. However, this difference in collapse capacities in terms of $S_{a,avg}$ increases to some extent in case of high-rise buildings, when compared with the corresponding difference in collapse capacities in terms of S_a.

Table 5.13 Collapse capacities and CMR of considered high-code buildings, for near-field ground-motion suite.

Building Model	Record Suite	S_a (D)	S_a (C)	$S_{a,avg}$ (D)	$S_{a,avg}$ (C)	CMR	ACMR
AL-RC-R6	NF (NP)	0.240g	1.100g	0.218g	0.651g	4.58	2.99
AM-RC-R6	NF (NP)	0.160g	0.470g	0.136g	0.310g	2.94	2.28
AH-RC-R6	NF (NP)	0.072g	0.160g	0.048g	0.080g	2.22	1.67
BL-RC-R6	NF (NP)	0.229g	0.776g	0.218g	0.479g	3.39	2.20
BM-RC-R6	NF (NP)	0.159g	0.440g	0.136g	0.287g	2.77	2.11
BH-RC-R6	NF (NP)	0.071g	0.135g	0.048g	0.060g	1.90	1.25
CL-RC-R6	NF (NP)	0.224g	0.946g	0.218g	0.614g	4.22	2.82
CM-RC-R6	NF (NP)	0.158g	0.631g	0.136g	0.382g	3.99	2.81
CH-RC-R6	NF (NP)	0.071g	0.163g	0.048g	0.074g	2.30	1.54
AL-RC-R6	NF (P)	0.240g	0.850g	0.218g	0.630g	3.54	2.89
AM-RC-R6	NF (P)	0.160g	0.440g	0.136g	0.290g	2.75	2.13
AH-RC-R6	NF (P)	0.072g	0.160g	0.048g	0.080g	2.22	1.67
BL-RC-R6	NF (P)	0.229g	0.704g	0.218g	0.539g	3.07	2.47
BM-RC-R6	NF (P)	0.159g	0.431g	0.136g	0.320g	2.71	2.35
BH-RC-R6	NF (P)	0.071g	0.163g	0.048g	0.070g	2.30	1.46
CL-RC-R6	NF (P)	0.224g	0.803g	0.218g	0.635g	3.58	2.91
CM-RC-R6	NF (P)	0.158g	0.520g	0.136g	0.349g	3.29	2.57
CH-RC-R6	NF (P)	0.071g	0.158g	0.048g	0.073g	2.23	1.52

NF (NP) – near-field suite without velocity pulse, NF (P) – near-field suite with velocity pulse, S_a (D) - seismic demand for MCE hazard in terms of S_a, S_a (C) - median collapse capacity in terms of S_a, $S_{a,avg}$ (D) - seismic demand for MCE hazard in terms of $S_{a,avg}$, and $S_{a,avg}$ (C) - median collapse capacity in terms of $S_{a,avg}$.

In order to investigate the difference in collapse capacities in terms of $S_{a,avg}$ for high-rise buildings, Fig. 5.10 presents the 5%-damped displacement spectra at collapse for the high-rise building models with structural configuration SC A, for all the three different ground-motion record suites considered in the present study (the far-field suite investigated in Chapter 4 and

the near-field ground-motion record suites with and without velocity pulses used in the present chapter). The shaded gray zone in Figure 5.10 represents the range between periods $0.2T$-$3T$ of the corresponding building model, which is influential to its seismic response at collapse.
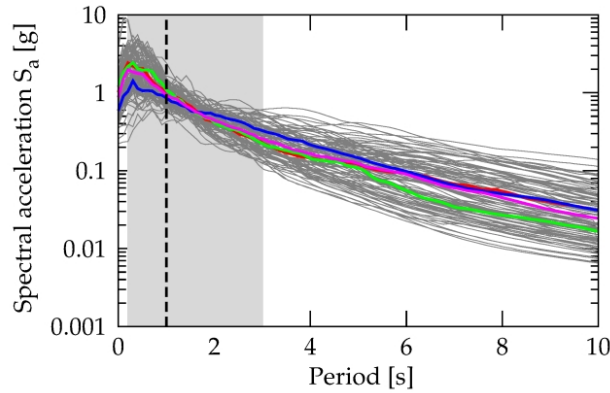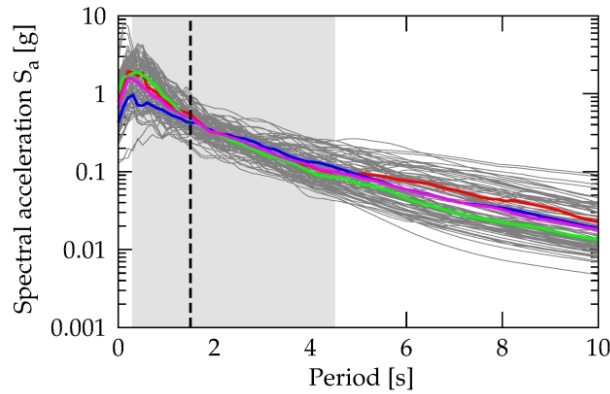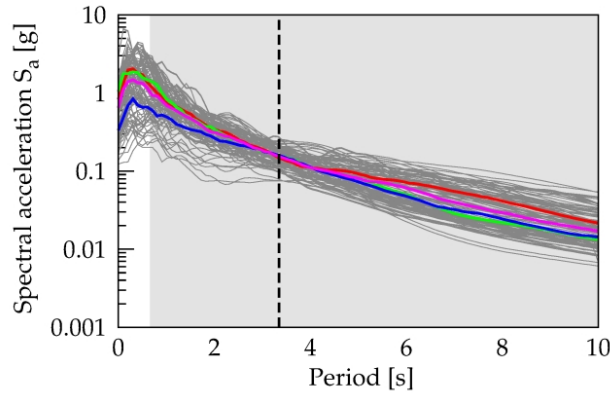
Fig. 5.9 Comparison of acceleration spectra of the scaled ground-motion records at collapse state: (a) 2-storey building (SC A); (b) 4-storey building (SC A); and (c) 8-storey building (SC A). (The vertical line represents arithmetic mean of the periods corresponding to the fundamental translational modes of the two orthogonal directions; the gray-shaded zone represents the period range between $0.2T$-$3T$ for the corresponding building model).
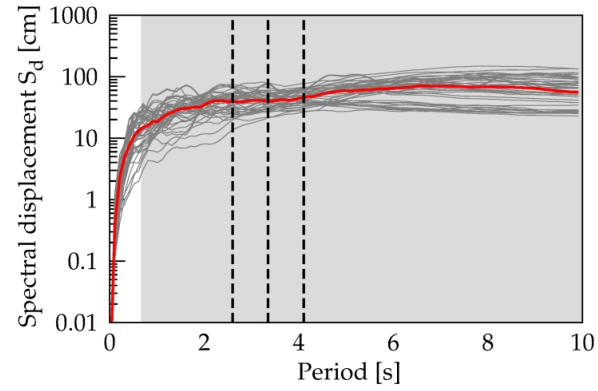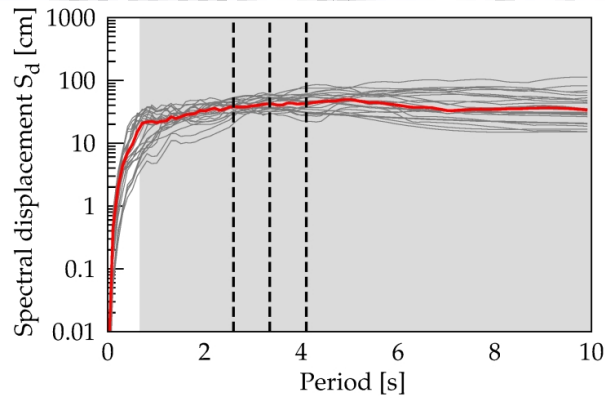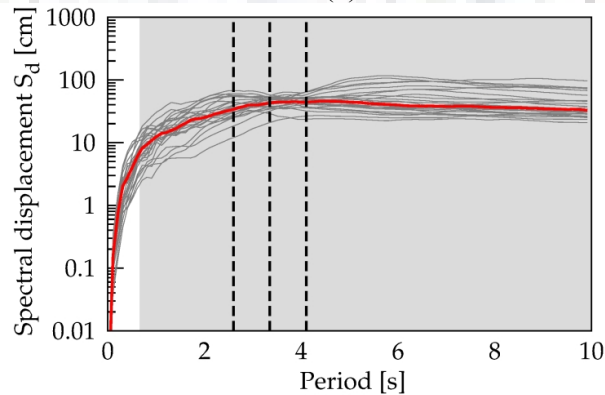
Fig. 5.10 Comparison of displacement spectra of the scaled ground-motion records at collapse: (a) 8-storey building (SC A) with the far-field record suite; (b) 8-storey building (SC A) with the near-field record suite without velocity pulse; and (c) 8-storey building (SC A) with the near-field record suite with velocity pulse. (The outer dotted vertical lines show the periods in the fundamental translational modes of the two orthogonal directions, and the central line shows the arithmetic mean of these two periods; the gray-shaded zone represents the period range between $0.2T$-$3T$ for the corresponding building model).

It can be observed that the building period falls in the so-called 'displacement-controlled spectral range' and the median displacement spectrum of all the three suites of ground-motion

records is almost flat in the influence period range of the building. Further, for the periods higher than T, which are particularly more influential to the collapse response in the non-linear range, this displacement is almost constant. This displacement can be easily predicted through a single spectral ordinate, S_a. Therefore, the observed collapse capacity for high-rise buildings is almost identical in terms of S_a.

The presented results clearly highlight the advantage of using $S_{a,avg}$ as an IM, as compared to S_a. Past research (Liel and Champion 2012; Champion and Liel 2012) has shown that, for near-field sites with forward directivity effects, the collapse capacity (in terms of S_a) of a building model is dependent on the expected period of the pulse (T_{pulse}) at the site. Further, this pulse has also a probability distribution associated with it, and with increase in distance from the fault, the probability of occurrence of the pulse reduces. Therefore, while using S_a as an IM, in collapse fragility analysis for the near-field sites, the building fragility function becomes dependent on the pulse-period as well as on the distance of the site from the fault. On the other hand, the use of $S_{a,avg}$ as an IM, makes collapse capacity of a building model independent of the ground-motion suite, the pulse-period, as well as the site. Further, this approach neither requires any information regarding the pulse-period nor the probability of occurrence of the pulse. Therefore, $S_{a,avg}$ can be considered as a suitable choice for seismic fragility assessment of a class of buildings, with varying heights, periods of vibrations and site conditions (i.e., near-field/far-field). However, the fragility analysis using $S_{a,avg}$ as IM requires a site-specific seismic hazard analysis in order to compute the seismic hazard in terms of $S_{a,avg}$, which can be carried out using the methodology suggested in literature (e.g. Baker and Jayaram 2008; Kohrangi et al. 2017a; Kohrangi et al. 2017b; Kohrangi et al. 2017c).

5.6 FRAGILITY ANALYSIS FOR NEAR-FIELD SITES

Table 5.14 presents the variability parameters for the high-code buildings subjected to the near-field ground-motion records. It can be observed that in case of the low- and mid-rise buildings, in general, $S_{a,avg}$ leads to a reduced dispersion as compared to S_a. In case of high-rise buildings, S_a leads to a reduced dispersion as compared to $S_{a,avg}$. These observations are consistent with the findings in the earlier section dealing with the far-field ground-motion record suite. This trend has been observed consistently for both the no-pulse, and the pulse-like ground-motion record suites.

Table 5.14 Variability parameters for the considered high-code buildings, for near-field ground-motion suite.

Building Model	Record Suite	β_M	β_{RTR} (S_a)	β_{RTR} ($S_{a,avg}$)	β_T (S_a)	β_T ($S_{a,avg}$)
AL-RC-R6	NF (NP)	0.50	0.25	0.17	0.56	0.53
AM-RC-R6	NF (NP)	0.50	0.31	0.29	0.59	0.58
AH-RC-R6	NF (NP)	0.50	0.25	0.27	0.56	0.57
BL-RC-R6	NF (NP)	0.50	0.20	0.21	0.54	0.54
BM-RC-R6	NF (NP)	0.50	0.29	0.33	0.58	0.60
BH-RC-R6	NF (NP)	0.50	0.37	0.43	0.62	0.66
CL-RC-R6	NF (NP)	0.50	0.15	0.14	0.52	0.52
CM-RC-R6	NF (NP)	0.50	0.25	0.25	0.56	0.56
CH-RC-R6	NF (NP)	0.50	0.27	0.23	0.57	0.55
AL-RC-R6	NF (P)	0.50	0.26	0.22	0.56	0.55
AM-RC-R6	NF (P)	0.50	0.29	0.21	0.58	0.54
AH-RC-R6	NF (P)	0.50	0.25	0.30	0.56	0.58
BL-RC-R6	NF (P)	0.50	0.20	0.23	0.54	0.55
BM-RC-R6	NF (P)	0.50	0.25	0.16	0.56	0.52
BH-RC-R6	NF (P)	0.50	0.25	0.33	0.56	0.60
CL-RC-R6	NF (P)	0.50	0.23	0.19	0.55	0.53
CM-RC-R6	NF (P)	0.50	0.31	0.19	0.59	0.53
CH-RC-R6	NF (P)	0.50	0.23	0.31	0.55	0.59

β_{RTR} (S_a) - record-to-record variability in collapse capacity, when S_a is chosen as IM, β_{RTR} ($S_{a,avg}$) - record-to-record variability in collapse capacity, when $S_{a,avg}$ is chosen as IM, β_T (S_a) - total variability in the collapse capacity, when S_a is chosen as IM, and β_T ($S_{a,avg}$) - total variability in the collapse capacity, when $S_{a,avg}$ is chosen as IM.

Figure 5.11 compares the collapse fragility curves for the low-, mid-, and high-rise buildings, designed for seismic zone IV, for the near- and far-field suites of the ground-motion records, and for all the considered structural configurations. These fragility curves are plotted with $S_{a,avg}$ normalized by the corresponding $S_{a,avg}$ at MCE, obtained from the corresponding site-specific CMS. It is evident from Fig. 5.11 that the considered buildings are more vulnerable at the near-field sites when compared with the far-field sites. Further, the near-field site effect has been observed to be more pronounced in case of the high-rise building as compared to the low- and the mid-rise buildings. For all the building heights investigated in this study, the structural configuration SC B has been observed to be the most vulnerable.

The increased seismic fragility of SC B can be attributed to the fact that for the elastic response, SC C has higher normalized eccentricity ratio when compared with the corresponding SC B structural configuration. With the progress in yielding of the elements at the flexible edge (downhill side columns), the relative eccentricity in case of SC B increases more significantly as compared to SC C, at the floor just above the uppermost foundation level. This effect leads to higher torsional effects in SC B in the inelastic range (due to shifting of centre of rigidity toward uphill side), for which SC B buildings were not designed. This effect leads to a

significant reduction in median collapse capacity for SC B, as compared to the SC C, even though both were designed for identical base shear coefficients. The observed trends for normalized floor eccentricity and reduction in median collapse capacity are quite consistent among all the investigated SC B and SC C building models.
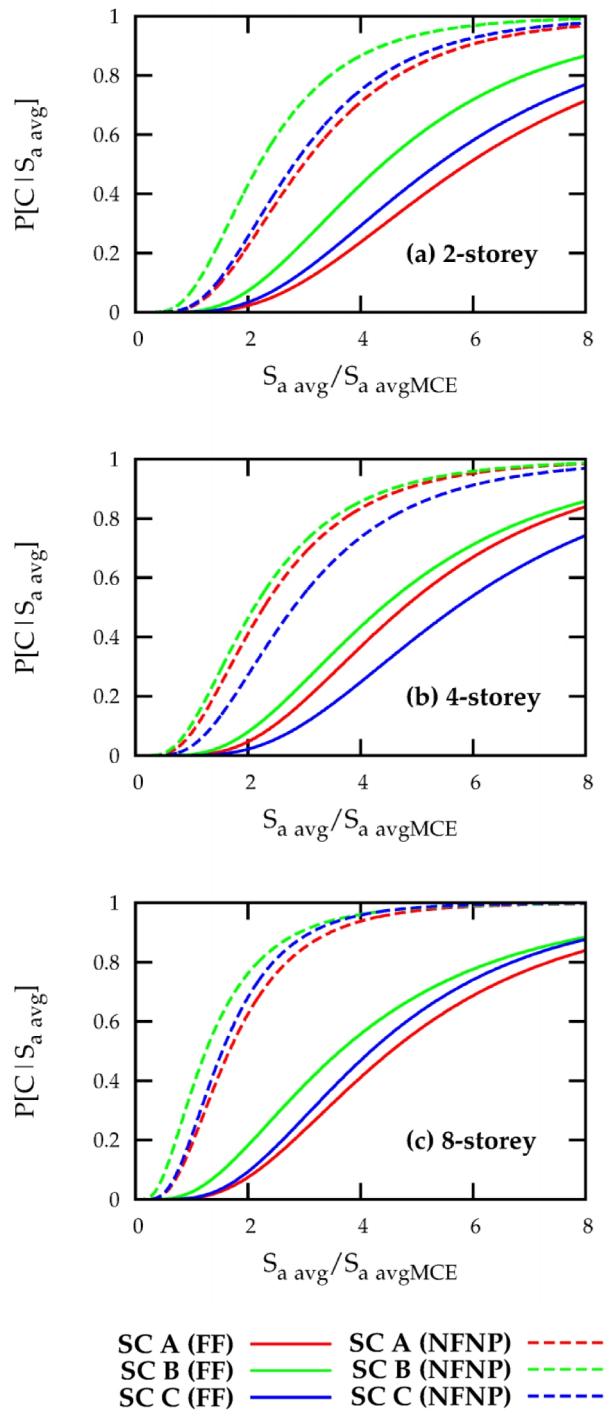
Fig. 5.11 Comparison of collapse fragility curves for buildings designed for seismic zone IV for far-field (FF) and near-field site (NFNP) without velocity pulse.

Table 5.15 presents a comparison of collapse probabilities of the considered buildings at the near- and the far-field sites, after incorporating spectral shape effects. In computation of the collapse probabilities for near-field sites, the median collapse capacity and record-to-record variability have been obtained corresponding to near-field ground-motions without velocity pulses, since hazard analyses presented in Section 5.2 included near-source effects, without considering forward-directivity effects. It can be observed that buildings located at the far-field sites have an average 1% probability of collapse at the MCE hazard level (reproduced from section 5.4). This average probability of collapse increases to 12% for the near-field sites without velocity pulses. The collapse performance of the high-rise buildings, in the near-field sites has been observed to be significantly poor even in case of high-code buildings designed for seismic zone IV, with the typical average probability of collapse being of the order of 26% at MCE, as compared to the corresponding average value of 2% probability of collapse for the far-field site. This collapse probability is likely to increase further, for buildings located in the near-field sites, in seismic zone V.

Table 5.15 Collapse probabilities for the considered high-code buildings, for near- and far-field sites.

Building Model	Record Suite	Collapse Probability (%) $P[C/S_{a,avg}]$*	Collapse Probability (%) $P[C/S_{a,avg}]$
AL-RC-R6	NF (NP)	02	01
AM-RC-R6	NF (NP)	08	01
AH-RC-R6	NF (NP)	19	01
BL-RC-R6	NF (NP)	07	01
BM-RC-R6	NF (NP)	11	01
BH-RC-R6	NF (NP)	**37**	03
CL-RC-R6	NF (NP)	02	01
CM-RC-R6	NF (NP)	03	01
CH-RC-R6	NF (NP)	**22**	01

$P[C/S_{a,avg}]$* and $P[C/S_{a,avg}]$ represent the probabilities of collapse for MCE hazard, at near- and far-field sites, respectively. Collapse probability values shown in bold shows failure of that particular building based on FEMA P695 acceptance criterion.

Major national seismic design codes (ASCE 7-10 2010; NZS 2006) recognize the damage potential of the near-field ground-motion records and recommend amplification factors for seismic design of buildings. For example, ASCE 7-10 (2010) provides amplification factors for the acceleration- and the velocity-controlled ranges of response spectra for the seismic design of buildings located in the near-field sites, depending on the distance between the site and the fault. On similar lines, NZS code (NZS 1170.4 2004) also recommends an amplification in design forces for the near-field sites depending on the expected pulse-period at the site. The presented results clearly suggest the need for consideration of site-specific conditions in the seismic design of buildings. However, such provisions are currently not included in the Indian

seismic design code (IS 1893 Part 1 2016) and should be included in future revisions to have an acceptable collapse performance, even in case of high-rise hill buildings.

5.7 SUMMARY

In order to take into account the effect of spectral shape, the Conditional Mean Spectra for the Mussoorie and the Shillong sites have been developed, and the collapse probabilities without and with spectral shape effects have been compared. The collapse probabilities for the near- and far-field sites have also been compared. The major observations made from this Chapter are:

- The inclusion of near-field effects leads to a significant increase in seismic hazard for the Mussoorie site. The increase in seismic hazard (in terms of S_a) is of the order of 1.70, 2.10 and 2.60 times at periods of 1.00 s, 1.50 s and 3.35 s, respectively.

- The consideration of the spectral shape for the far-field sites lead to an increase in the collapse capacity of the buildings (due to a 'positive ε') at both Mussoorie and Shillong sites. The average increase in the collapse capacity is about 80% in case of the pre-code buildings, 52% in case of the moderate-code buildings, and 63% in case of the high-code buildings.

- In case of the pre-code buildings, S_a leads to smaller β_{RTR} when compared to $S_{a,avg}$ due to the limited ductility of such buildings. On the other hand, in case of the moderate- and the high-code buildings, $S_{a,avg}$ leads to smaller β_{RTR} (in low- and mid-rise buildings) when compared to S_a, due to the significant period elongation prior to collapse.

- In case of the high-code high-rise buildings, $S_{a,avg}$ leads to almost equal (or higher, in some cases) β_{RTR} when compared to S_a.

- In case of the pre-code low- and mid-rise buildings, the average probabilities of collapse reduce to 64%, and 45%, respectively, due to spectral shape effect, as compared to the corresponding unadjusted values of 80% and 86%, respectively, for seismic zone IV.

- In case of the high-code, low- and mid-rise buildings, the average probabilities of collapse reduce to 1%, as compared to the corresponding unadjusted values of 1% and 2%, respectively, for seismic zone IV, 5% and 7%, respectively, for seismic zone V.

- In case of the high-code high-rise buildings, the average collapse probabilities reduce to 2% and 20%, respectively, as compared to the corresponding unadjusted values of 14% and 36%, respectively, in seismic zones IV and V.

- S_a leads to significantly different collapse capacity for different ground-motion record suites (viz. the far-field record suite, the near-field record suite without velocity pulses and the near-field record suite with velocity pulses) in comparison with $S_{a,avg}$, particularly in low- and mid-rise buildings. This observation highlights that S_a representing spectral ordinate at a single period is unable to capture the effects of higher modes, period elongation and the velocity-pulse.

- At far-field site, the investigated buildings have an average collapse probability of 1% at MCE. This average collapse probability at MCE increases to 12% at near-field site. This increase in collapse probability is quite significant for high-rise buildings (up to 37% probability of collapse) leading to a significant increase in average probability of collapse for buildings located on the near-field site. This observation underscores the need to include special design provisions for the near-field sites in order to have an acceptable collapse performance.

CHAPTER 6

FLOOR RESPONSE OF REGULAR BUILDINGS

6.1 INTRODUCTION

The components which are supported by the building structure but do not contribute to gravity or lateral load resistance are termed as non-structural components (NSCs). The seismic vulnerability of non-structural components (NSCs) has been reported during numerous earthquakes in the past, i.e. 1964 Alaska (Ayers et al. 1973); 1971 San Fernando (Whitman et al. 1973); 1989 Loma Prieta (Soong 1990; Rihal 1992); 1994 Northridge (Reitherman and Sabol 1995; Phipps 1997); 2010 Darfield (Dhakal 2010), 2010 Chile (Miranda et al. 2012) and 2011 Sikkim (Murthy et al. 2012b; EERI 2012), even though the structural performance of most buildings was deemed to be satisfactory. The damage to NSCs is not solely related to economic losses, but severe damage to NSCs can cause life-threatening situations for building occupants. Further, the seismic safety of a building's NSCs is important for its post-earthquake operability. Consequently, it is a crucial element in the framework of Performance-Based Earthquake Engineering (PBEE) both for ordinary (e.g. residential) buildings as well as for buildings of greater importance (i.e., hospitals, fire stations, power plants).

The NSCs may consist of furniture, equipment, partition walls, curtain wall system, electrical equipment, bookcases and many other items. The NSCs may be grouped into three main categories, namely (i) architectural components, (ii) mechanical and electrical equipments, and (iii) building contents. The NSCs are sensitive to large floor accelerations, velocities and displacements. Floor acceleration becomes an important parameter for those components (e.g., ceilings, light fixtures etc.) which are sensitive to inertia forces whereas inter-storey drift becomes an important parameter for those components (e.g., walls, pipings etc.) which are sensitive to drifts. It has been observed in the past, that the damage to non-structural components are sensitive to either floor acceleration or inter-storey drift and hence can be classified under two main categories as (i) acceleration sensitive non-structural components (AS-NSCs), and (ii) drift sensitive non-structural components (DS-NSCs). There is also a third category of NSCs which are sensitive to both acceleration and drift. In this Chapter, the methods to evaluate the floor acceleration demands are reviewed and a state-of-the-art is presented in context of the seismic design of light-weight acceleration-sensitive NSCs. In the

later part of this Chapter, a numerical study is conducted to study the floor response of NSCs mounted on structural configuration SC A. Correlation of floor accelerations with PGA, PFA and GRS is studied and the critical parameters affecting the floor response are identified. Based on the identified parameters affecting the floor acceleration response, spectral amplification functions are developed. The developed floor spectral amplification functions can be used to predict the floor acceleration demands on NSCs directly from the GRS, provided, the dynamic characteristics (periods and mode shapes), the location of NSC within the supporting structure, and level of inelasticity (ductility demand) of the supporting structure are known.

6.2 PAST STUDIES ON ASSESSMENT OF FLOOR ACCELERATION DEMANDS IN BUILDINGS

In order to determine the response of acceleration-sensitive NSCs, two major approaches are available in literature, viz. coupled analysis and decoupled analysis. The application of a particular approach depends on the dynamic interaction between the supporting structure (i.e. the building structure) and the NSC. Generally, the dynamic interaction between the supporting structure and the NSC can be ignored if the mass of the NSC is negligible in comparison to the supporting structure (Amin et al. 1971; Singh and Ang 1974), hence simplifying the analysis of NSCs significantly. In this simplified approach, the response of the building at any given floor is obtained independent of the NSC and is applied as an input motion to the NSC. This approach is termed as decoupled analysis, since the two systems, viz. the supporting structure and the NSC, are treated independently. The floor response is usually expressed in terms of an acceleration response spectrum, while the approach is also known as Floor Response Spectrum (FRS) method. However, it was found that this method may produce overly conservative results if the NSCs possess significant mass as compared to the supporting structure (Toro et al. 1989). In this section a review of some of the major available approaches for determination of floor response spectra in both elastic and inelastic buildings is presented.

The seismic design of NSCs based on floor response started in the early 1970's. Since then, a significant number of research attempts have been made by various groups in order to study the effect of dynamic characteristics of both the supporting structure and the NSC (e.g., Taghavi and Miranda 2005). Further, crucial issues identified in past research are the effect of damping of the NSC (e.g., Medina et al. 2006), amplification of peak floor acceleration (PFA) along the

height of the building (e.g., Singh et al. 2006a, b), and the effect of degree of inelasticity of the supporting structure (e.g., Rodriguez et al. 2002).

Biggs and Roesset (1970), Amin et al. (1971) and Singh and Ang (1974) proposed methods for deriving the floor acceleration spectrum directly from the ground acceleration spectrum. "Although simple in concept and somewhat rational, these methods were quickly recognized to be impractical" (Villaverde 1997) since these methods required lengthy numerical integrations. A summary of the state-of-the-art of the seismic design of NSCs was presented by Villaverde (1997). He identified the main limitation of the earlier methods as being based on the assumption that both the supporting structure and NSC purely respond in the elastic range.

Taghavi and Miranda (2005) proposed a simplified approach in order to estimate the peak floor acceleration (PFA) along the height of the building. The approach was based on the dynamic characteristics (first three modes of vibration) of equivalent continuum structures that consisted of a flexural and a shear beam, interconnected by axially rigid links. However, this model was also limited to linear elastic buildings. Singh et al. (2006a, b) studied the difference between the recorded accelerations and those calculated by code provisions for rigid as well as flexible NSCs. They observed significant differences in the recorded acceleration values when compared with code provisions due to the building's irregularity, the ground-motion characteristics, and the higher mode effects. They further demonstrated that for taller buildings, the acceleration demand at the level of the roof suddenly increases due to the whiplashing effect in the higher modes. They proposed a simplified method to account for this whiplashing effect. Kumari and Gupta (2007) proposed a modal combination rule in order to estimate PFA demands for linear elastic buildings.

Lin and Mahin (1985) highlighted that a significant reduction in floor accelerations can be achieved if the inelastic behaviour of the supporting structure is taken into account. Similar observations were also made by Rodriguez et al. (2002), Medina et al. (2006), Chaudhuri and Villaverde (2008), Chaudhuri and Hutchinson (2011), Weiser et al. (2013), Lucchini et al. (2014) and Flores et al. (2015). Villaverde (2006) proposed an approximate method to determine the non-linear seismic response of NSCs that are attached to supporting structures which are exhibiting inelastic response. This method requires consideration of the geometric characteristics, masses and the target ductility of both the NSC and the supporting structure to

which it is connected to, in addition to the fundamental period of the supporting structure and the elastic design response spectrum.

Petrone et al. (2015a) compared the floor response of elastic and inelastic buildings as obtained from time-history analyses, with the EN 1998 provisions. They observed that the EN 1998 formulation overestimates the acceleration demands on NSCs with periods close to the fundamental period of the supporting structure and significantly underestimates the floor acceleration demands corresponding to higher modes. Further, they highlighted an urgent need to include the effect of ductility demand in the evaluation of floor spectra. Further, Chaudhuri and Hutchinson (2011) added that increased inelasticity leads to larger participation of higher modes of vibration.

Politopoulos and Feau (2007), Oropeza et al. (2010), Sullivan et al. (2013), Vukobratović and Fajfar (2015) and Vukobratović (2015) studied the effect of inelasticity on the floor spectrum for single-degree-of-freedom (SDOF) structures that have different periods of vibration, damping values and hysteretic models. Calvi and Sullivan (2014) extended their study to multiple-degree-of-freedom (MDOF) structures responding in the elastic range. They proposed a simplified modal combination approach for estimation of acceleration spectra on upper floors and accounted for limited filtering of the ground-motion input that occurs on lower floors. They also underlined future research needs to predict floor spectra of the MDOF structures responding inelastically. Vukobratović (2015) extended the study to inelastic MDOF structures, using a modal combination procedure in combination with the N2 method (to predict ductility demand). He found that ductility has significant influence on the floor spectral acceleration, not only in the fundamental mode, but in some cases also in higher modes.

Sharp peaks in the floor acceleration spectrum were observed (Medina et al. 2006; Sankaranarayanan and Medina 2007; Oropeza et al. 2010; Weiser et al. 2013; Lucchini et al. 2014; Petrone et al. 2015b; and Vukobratović and Fajfar 2015) when the NSCs period of vibration coincides with the supporting structure's period of vibration. This effect was also observed corresponding to higher modes, in the case of buildings having significant contribution of higher modes in seismic response. Petrone et al. (2015b) considered the peaks in the floor response spectra, corresponding to higher modes, and modified the floor spectral shape of EN 1998 (CEN 2004) using a piece-wise formulation to have a flat plateau covering all the

peaks corresponding to the fundamental and higher modes. The researchers recommended the use of a normalized period (T_p/T_1) for expressing the amplification factor, where T_p is the NSCs period of vibration and T_1 is the natural period of the supporting structure.

Vukobratović (2015) observed that in the case of inelastic supporting structures, the peak values in floor spectra corresponding to the first mode are smaller than the corresponding peak values for elastic supporting structures. A significant effect of higher modes was observed at lower floors of MDOF supporting structures. However, the modes of very high frequencies do not exhibit peaks in the floor spectrum corresponding to their respective periods. Further, in the case of elasto-plastic models, the peaks occur close to the elastic period, whereas for degrading models, these peaks shift towards higher periods, with increasing inelasticity. Weiser et al. (2013) studied the effect of inelasticity on floor acceleration demands for code-designed steel moment-resisting frame buildings. They observed that the amplification of PFA reduces with an increase in the period of vibration as well as with the inelasticity of the supporting structure. They proposed simplified expressions in order to consider the amplification of PFA along the height of the buildings. The effect of inelasticity in the PFA amplification was accounted for through the effective period (T_{eff}). They also proposed an approach to derive the floor acceleration spectrum from the ground acceleration spectrum using a spectral amplification function. However, the proposed spectral amplification function does not include the effect of inelasticity; further studies are recommended to take into account the complex effect of mode shape on the floor amplification along the height of the building.

Lucchini et al. (2014) studied the floor response of bare and infilled RC frame buildings. They observed that current code-compliant models, which do not account for inelasticity, overestimate the PFA and underestimate the peaks of the floor acceleration spectrum. Recently, Lucchini et al. (2016) performed a detailed study of a 6-storey RC frame to develop a probabilistic model for estimating the seismic demand on NSCs. They have observed that the peak spectral accelerations in the impact zone of a natural mode depend on earthquake intensity, whereas the variation of the peak spectral accelerations along the height "does not significantly change with the increase of the earthquake intensity." The recent developments in the context of floor accelerations consist of multimode methods to predict the floor acceleration demands (Pan et al. 2017a, b), uniform hazard floor spectrum (Lucchini et al. 2017a) and the probabilistic models considering the variabilities in the floor response (Lucchini et al. 2017b).

6.3 FLOOR SPECTRUM IN SEISMIC DESIGN CODES

Most of the national seismic building design and retrofitting codes (i.e., ASCE 41-13 2013, EN 1998 2004, and NZS 1170.5 2004) consider the amplification of floor acceleration along the height of the building with a linearly increasing profile. This linearly increasing profile is based on the assumption that the response of the building is dominated by the fundamental mode of the supporting structure, which can be approximated as linear. However, this assumption is not valid for taller buildings or buildings with significant contributions from higher modes of vibration.

Figure 6.1 compares the existing floor acceleration models of few major national codes and documents, i.e., FEMA P750 (2009), EN 1998 (CEN 2004), IS 1893: Part 1 (Draft Version) and NZS 1170.5 (2004). Except for NZS 1170.5, all provisions consider a linear variation of floor acceleration right up to the top of the building, whereas NZS 1170.5 considers a linear variation up to a height of 12 m or up to 20% of the building height, whichever is larger, and constant floor acceleration above that. Further, out of the considered models, the floor amplification model of IS 1893 (Draft) provides the lowest amplification factor (i.e. 2, at roof level), whereas Eurocode provides the roof level amplification factor of 2.5 while FEMA P750 (and also ASCE 41-13 2013 and ASCE 7-10 2010) and NZS 1170.5 provide a maximum floor amplification of 3. In addition to the floor acceleration, the response of the NSC primarily depends on two parameters, viz. damping ratio of the NSC and frequency tuning between the NSC and the floor motion. Current code provisions take into account the frequency tuning using a component amplification factor (a_p).

Figure 6.2 compares the two different models of component amplification factor (a_p) as provided by different codes. IS 1893 (Draft) as well as ASCE 41-13 and ASCE 7-10 (not shown in Fig. 6.2) provide a uniform component amplification factor ($a_p = 2.5$; Fig. 6.2a) which may be too conservative for a wide range of periods, as it is based on the peak value of the floor response spectrum. This becomes also evident when compared with other codes (Fig. 6.2b). NZS 1170.5 (2004) assumes a component amplification factor (a_p) as a function of period of vibration of the NSC only, and reduces the value drastically for NSCs having periods longer than 1.5 s.
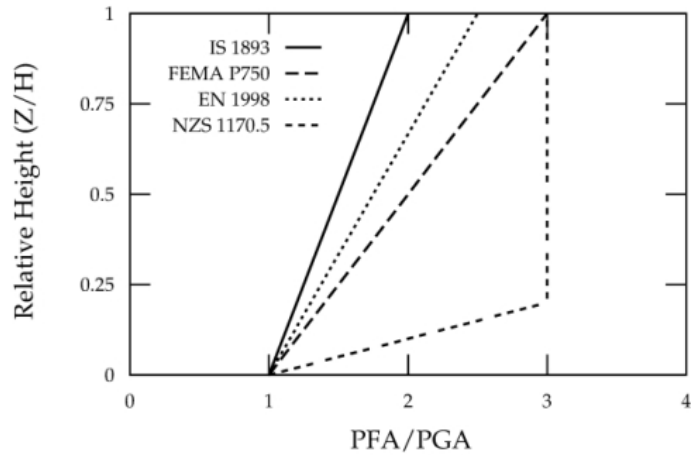
Fig. 6.1 Comparison of PFA profiles along the height of the building as provided in different codes and documents. (In case of NZS 1170.5, the PFA profile has been plotted for buildings taller than 60 *m;* for buildings shorter than 12 *m* it coincides with the PFA profile of FEMA P750, and for intermediate heights it is in between the two).
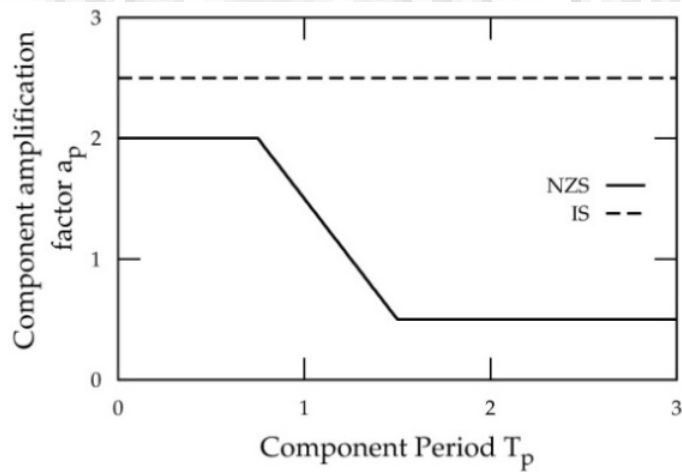
(a) Component period model
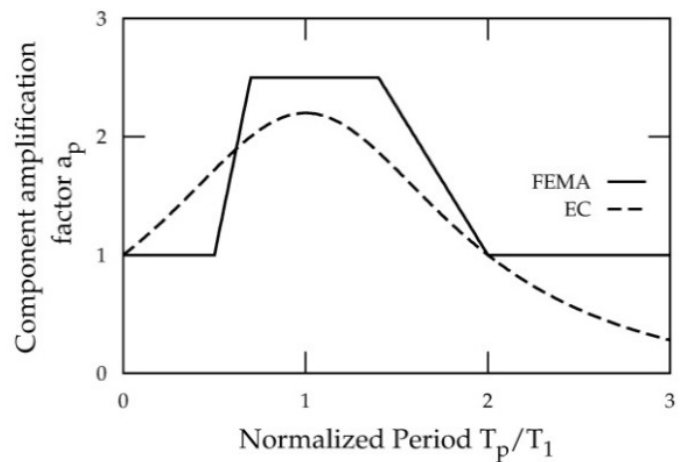
(b) Normalized period model

Fig. 6.2 Comparison of component amplification factor (a_p) model of different codes.

Both, FEMA P750 (2009) and EN 1998 (2004) consider the effect of frequency tuning between the NSC and the supporting structure by providing a model for a_p in terms of normalized period (T_p/T_1). Both the models show a peak corresponding to T_p/T_1 equal to unity, and the value of a_p reduces significantly for NSCs having periods different than the fundamental period of the supporting structure. FEMA P750 (2009) provides a multi-linear model for component amplification factor (a_p) varying between 1.0 and 2.5 (Fig. 6.2b) depending on the normalized period (T_p/T_1), and having a plateau between normalized periods 0.7 to 1.4. On the other hand, EN 1998 (2004) assumes a parabolic distribution (Fig. 6.2b). Further, for flexible NSCs mounted on short-period buildings, with normalized periods (T_p/T_1) exceeding 2, the EN 1998 (2004) model estimates the lowest seismic demand on the NSC, as compared to other codes.

The seismic design methodology of the current codes (EN 1998, CEN 2004; ASCE 7-10, 2010; NZS 1170.5, 2004; and IS 1893 Draft) for NSCs has four major limitations: (i) these code models completely ignore the ground-motion characteristics (spectral shape), (ii) the component amplification factors do not account for the dynamic characteristics (i.e., periods of vibration and mode shapes) of the supporting structure, (iii) the tuning between supporting structure and NSC is accounted for in a relatively simpler manner, (the provisions may be conservative or non-conservative depending on the location of the NSC within the structure and the ratio of the period of vibration of NSC to the supporting structure), and (iv) the inelasticity of the supporting structure is completely ignored although it is designed to respond inelastically under strong earthquakes.

Further, the current design practice for NSCs does not comply with a performance-based seismic design framework, since the effect of ductility demand and hence the targeted performance of the building is completely ignored in the design of NSCs. Past studies identified different parameters controlling the seismic floor response in multi-storey buildings. However, a comprehensive model for predicting floor response taking into account all the crucial parameters is lacking. The present study examines the correlation of floor spectral shape with different ground-motion parameters (PGA, PFA and GRS) and attempts to develop floor spectral amplification models which takes into account the characteristics of the ground-motion records through GRS, dynamic characteristics (periods and mode shapes) and level of inelasticity (ductility demand) of the supporting structure, and tuning between the NSC and the supporting structure.

6.4 NUMERICAL STUDY: FLOOR RESPONSE OF REGULAR BUILDINGS

In the present study, a set of five generic reinforced-concrete frame buildings (2-, 4-, 4S- 8- and 12-storied) with identical plan shape (Fig. 3.9) as presented in Chapter 3 are considered. Table 6.1 provides an overview of the dynamic characteristics of the considered building set, representing a fairly wide period range ($T_1 = 0.31$ s to 3.38 s). All the buildings, except for 4S, were designed using the normal member sizes as per relevant Indian codes and the periods have been obtained considering cracked section stiffness, according to the ASCE/SEI 41-06 (2007) guidelines. All these periods, even for the 2-storey building, lie beyond the constant acceleration plateau, in the so-called 'long-period' or 'velocity-controlled' range of the design response spectrum. In order to also include a short-period building (having a fundamental period that lies within the constant acceleration plateau of the design response spectrum), another 4-storey short-period building (4S) is considered, for which the stiffness of all the members in the 4-storey building was fictitiously increased by a factor of 16, without any change in the strength. This stiffening of the structure results in analytically obtained periods of 0.31 s and 0.44 s in the longitudinal and transverse directions, respectively.

Table 6.1 Dynamic characteristics of the considered building models.

	Building Description	Period of Vibration (s)			Period Ratio		Modal Mass Participation Ratio (%)		
N	Direction	First mode (T_1)	Second mode (T_2)	Third mode (T_3)	T_2/T_1	T_3/T_1	α_{m1}	α_{m2}	α_{m3}
4S	Longitudinal	0.31	0.10	0.06	0.32	0.19	84	11	4
	Transverse	0.44	0.13	0.07	0.30	0.16	81	13	5
2	Longitudinal	0.58	0.20	-	0.34	-	90	10	-
	Transverse	0.77	0.22	-	0.29	-	86	14	-
4	Longitudinal	1.22	0.40	0.23	0.33	0.19	85	10	4
	Transverse	1.75	0.53	0.26	0.30	0.15	81	12	5
8	Longitudinal	2.20	0.79	0.46	0.36	0.21	80	12	3
	Transverse	2.90	0.99	0.58	0.34	0.20	80	11	4
12	Longitudinal	2.36	0.78	0.45	0.33	0.19	83	9	3
	Transverse	3.38	1.12	0.64	0.33	0.19	81	10	4

N - no. of stories, S – short-period, α_{m1}, α_{m2} and α_{m3} - modal mass participation ratios corresponding to the first, second and third modes of vibration in a given direction of excitation.

In order to consider the inelastic behaviour, uniaxial moment plastic hinges and P-M-M interaction hinges have been assigned at both ends of the beams and columns, respectively. The idealized force-deformation curve of ASCE/SEI 41-06 (2007) has been assigned to each plastic hinge. These modelling parameters provided in ASCE 41-06 are already adjusted to account for

the cyclic strength deterioration effects, as explained in PEER/ATC 72-1 (2010). A Rayleigh damping of 5% is assigned at periods corresponding to the fundamental and the third (fundamental and second in case of the 2-storey building) modes (resulting 95% cumulative mass participation in the direction under consideration) of vibration. (The terms 'fundamental [1st] mode', 'second mode' and 'third mode' used throughout this thesis indicate the consecutive modes in order of decreasing mass participation in a principal direction and not the consecutive modes [with increasing period] of the 3D building as a whole).

All the considered model buildings have more than 80% mass participation in the fundamental mode, and up to 14% in the second mode (Table 6.1). It is interesting to note that the ratio of the second mode period to the first mode period is close to 0.3 and that of the third mode period to the first mode period is close to 0.2, in all the cases (Table 6.1). This observation is not specific to the chosen set of buildings, and similar observations were also made by other researchers (Chaudhuri and Hutchinson 2011; Weiser et al. 2013). This observation can be used to simplify the floor amplification model, where the periods in the higher modes of the supporting structure can be expressed as constant fractions of the fundamental period.

6.4.1 Ground-Motion Records and Consideration of Structural Inelasticity

The ground-motion records used to study the floor response have been presented in Table 3.8. It can be observed that the ground-motion suite has an average period corresponding to peak spectral acceleration, T_{peak} of 0.32 s, which is closest to the fundamental period of vibration of the short-period building (4S) in the longitudinal direction. This period corresponding to peak spectral acceleration (T_{peak}) has been used to categorize the buildings as short- and long-period buildings. The buildings having a fundamental period shorter than or close to T_{peak} can be considered as short-period buildings, whereas buildings having periods longer than T_{peak} can be considered as long-period buildings. In case of a code-based design spectrum, the corner period (i.e., the intersection between the constant spectral acceleration plateau and the velocity-controlled range, generally denoted as T_c) can be considered as the predominant period of ground-motion (Miranda 1993; Gazetas 2006).

For a given structural model, the major component (i.e., the horizontal component with higher PGA) of each ground-motion has been applied along both the principal directions of the building, separately. The ground-motion is scaled to multiple intensities based on the spectral

acceleration at the fundamental period of the building S_a (T_1, 5%) in the considered direction. The structural inelasticity is considered through a strength ratio (R) defined as:

$$R = \frac{S_a(T_1, 5\%)}{S_{ay}}$$

(6.1)

where, S_a (T_1, 5%) is the 5%-damped elastic spectral acceleration of the scaled ground-motion at the building's fundamental period T_1, and S_{ay} is the spectral acceleration at yielding, which is obtained from a non-linear static analysis of the building (e.g., using the method of ASCE/SEI 41-13 2013). In the present study, the strength ratio (R) is preferred over ductility demand (μ), as it can be obtained relatively easily. In the case of design of new buildings, it can be estimated, approximately, using the following correlation with behaviour factor (also known as 'response reduction factor') as illustrated in Fig. 6.3.

$$R = \frac{q}{\Omega}$$

(6.2)

where, q is the behaviour factor and Ω is the over-strength factor (ASCE 7 2010). The over-strength factor may vary with the design code used and local construction practices.
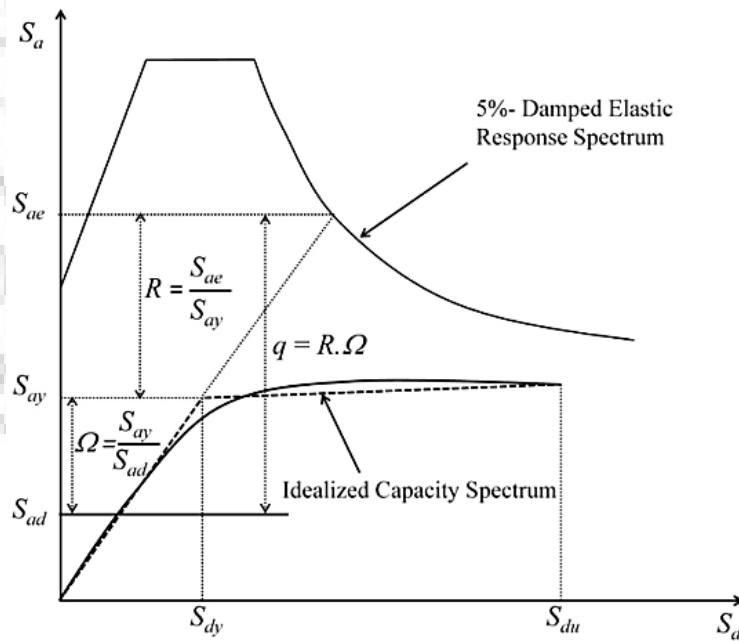
Fig. 6.3 Schematic diagram illustrating relationship between behaviour factor, q, strength ratio, R, and over-strength factor, Ω. (S_{ad} - design spectral acceleration, S_{ay} - spectral acceleration at yielding, S_{ae} - elastic spectral acceleration demand, S_{dy} - spectral displacement at yielding, and S_{du} - spectral displacement at ultimate point).

For RC frame buildings designed for the Indian code, the over-strength factor has been found to be about 2 (Khose et al. 2012). In the absence of an available estimate or for accurate estimation of R, a non-linear static analysis of the designed building is recommended.

6.4.2 Results and Discussion: Amplification of Floor Acceleration

All the five buildings have been analyzed for the major components of 30 ground-motions applied in both directions, separately, and scaled to seven levels of seismic intensity, represented by the elastic case and different values of R (from 1.0 to 3.5). In each of the considered building models, the PFA demands have been studied at four different heights, i.e., at $0.25H$, $0.50H$, $0.75H$ and H; where, H is the height of the building above ground level. Figures 6.4 and 6.5 compare the existing PFA models of major national codes, i.e., ASCE 41 (2013), EN 1998 (2004), NZS 1170.5 (2004) and IS 1893 Draft with the median PFA demands as obtained from non-linear dynamic analyses using a suite of 30 ground-motion records, for each of the considered building models. Following observations can be made from Figs. 6.4 and 6.5:

- For the elastic response of the supporting structure, the ASCE 41 and NZS 1170.5 models are conservative for short-period (4S) buildings, whereas EN 1998 predicts closest to the numerically obtained PFA/PGA profile. On the other hand, IS 1893 has been found to be non-conservative for this building. For intermediate- and long-period buildings (4-, 8-, and 12-storied building), all code models predict conservative estimates with ASCE 41 and NZS 1170.5 being the most conservative and IS 1893 the least conservative.

- For the 4-storied buildings (short- as well as long-period), the shape of the numerically obtained PFA/PGA profiles is close to the linear profiles assumed by different codes, since the response of the supporting structure is dominated by the fundamental mode of vibration.

- With the increase in building height (for 8- and 12-storied buildings), the variation of PFA/PGA along the height starts changing, which can be approximated as linear for lower floors (up to $0.25H$), is almost constant at intermediate floors ($0.25H$-$0.75H$) and increases rapidly near the roof (at levels above $0.75H$) due to the whiplashing effect of higher modes. Similar observation has also been made by Rodriguez et al. (2002), Singh et al. (2006a, b) and Lucchini et al. (2014).
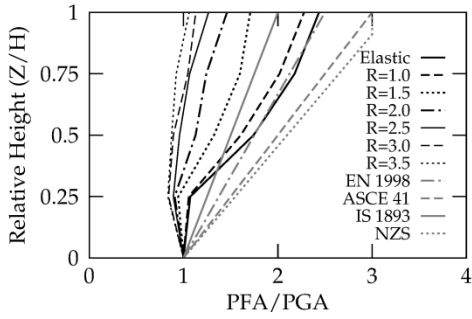
(a) 4-storied short-period building
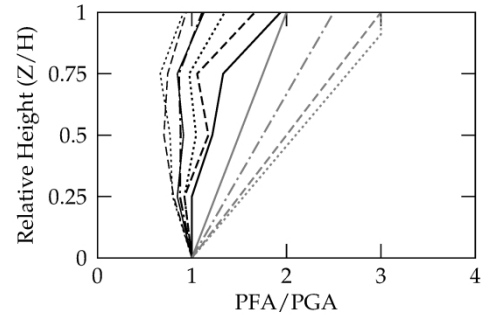
(b) 4-storied intermediate-period building
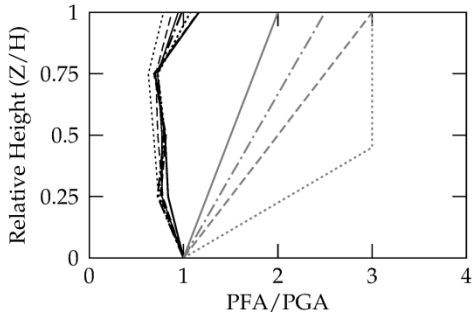
(c) 8-storied long-period building
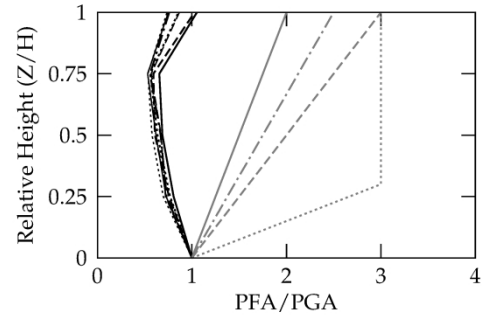
(d) 12-storied long-period building

Fig. 6.4 Median PFA for longitudinal direction (L) as obtained from IDA and predicted by different code models. Results corresponding to 2-storey building model has not been presented for brevity.
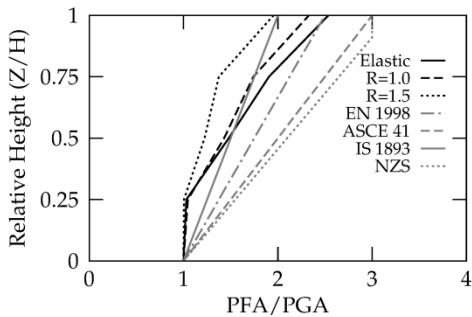
(a) 4-storied short-period building
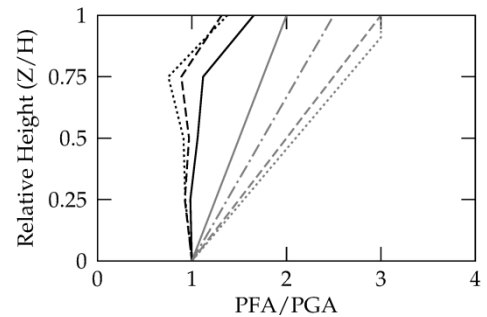
(b) 4-storied intermediate-period building
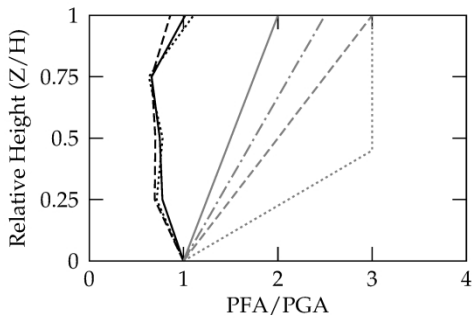
(c) 8-storied long-period building
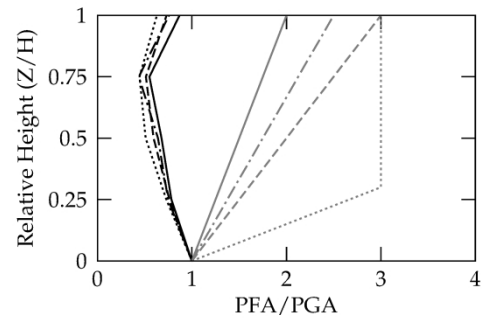
(d) 12-storied long-period building

Fig. 6.5 Median PFA for transverse direction (T) as obtained from IDA and predicted by different code models. Results corresponding to 2-storey building model has not been presented for brevity.

Table 6.2 presents the fundamental period of vibration of the considered building models and the median PFA/PGA at the roof level as obtained from non-linear dynamic analyses. It is interesting to note that the trend clearly suggests that the PFA/PGA ratio is almost constant in the short-period range and reduces with increase in period of vibration of the supporting structure in the intermediate- and long-period ranges. The reduction in PFA/PGA ratio with increased period was also observed by Weiser et al. (2013) for steel frame buildings with fundamental periods of vibration T_1 longer than 1 s. Further, for the 12-storied building in transverse direction ($T_1 = 3.38$ s), this ratio has been found out to be less than unity, even under pure elastic response. For larger strength ratios ($R = 3.50$) the floor amplification reduces significantly. In this case, only the values in longitudinal direction have been presented, since the buildings showed collapse in transverse direction due to lesser redundancy. The median PFA/PGA value at roof level is close to unity for short-period buildings and less than unity for intermediate- and long-period buildings (Table 6.2). This can be understood by the fact that the increased strength ratio (and hence the ductility demand) results in increased hysteretic energy dissipation and elongation of the effective period of vibration of the supporting structure. Further, the effect of strength ratio is more pronounced in the short-period building, as compared to the intermediate- and long-period buildings.

Table 6.2 Median PFA/PGA ratio at the roof level for strength ratio, elastic and $R = 3.50$.

Building Description		T_1	(PFA/PGA)$_{Roof}$	(PFA/PGA)$_{Roof}$
N	Direction	(s)	Elastic	$R = 3.50$
4S	Longitudinal	0.31	2.44	1.06
	Transverse	0.44	2.54	-
2	Longitudinal	0.58	2.02	1.05
	Transverse	0.77	1.80	-
4I	Longitudinal	1.22	1.94	0.91
	Transverse	1.75	1.66	-
8L	Longitudinal	2.20	1.16	0.79
	Transverse	2.90	1.02	-
12L	Longitudinal	2.36	1.05	0.74
	Transverse	3.38	0.87	-

N - no. of stories, S - short period, I - intermediate period, L - long period, and dash indicates collapse of the building model.

6.4.3 Results and Discussion: Floor Response Spectra

Figures 6.6-6.8 present the median 5%-damped floor spectrum profiles obtained at the center of mass (coinciding with the geometric center in the present case of symmetric buildings). These floor spectrum profiles are shown at two different relative heights (0.5 H and H) for the 4-storey, 8-storey and 12-storey buildings in the longitudinal direction. The presented floor

spectra are normalized by Peak Floor Acceleration (PFA), Peak Ground Acceleration (PGA) and the ground acceleration spectrum ($S_{AG}(T)$).

(a) Normalized with PFA, $Z/H = 0.50$

(b) Normalized with PFA, $Z/H = 1.00$

(c) Normalized with PGA, $Z/H = 0.50$

(d) Normalized with PGA, $Z/H = 1.00$

(e) Normalized with S_{AG}, $Z/H = 0.50$

(f) Normalized with S_{AG}, $Z/H = 1.00$
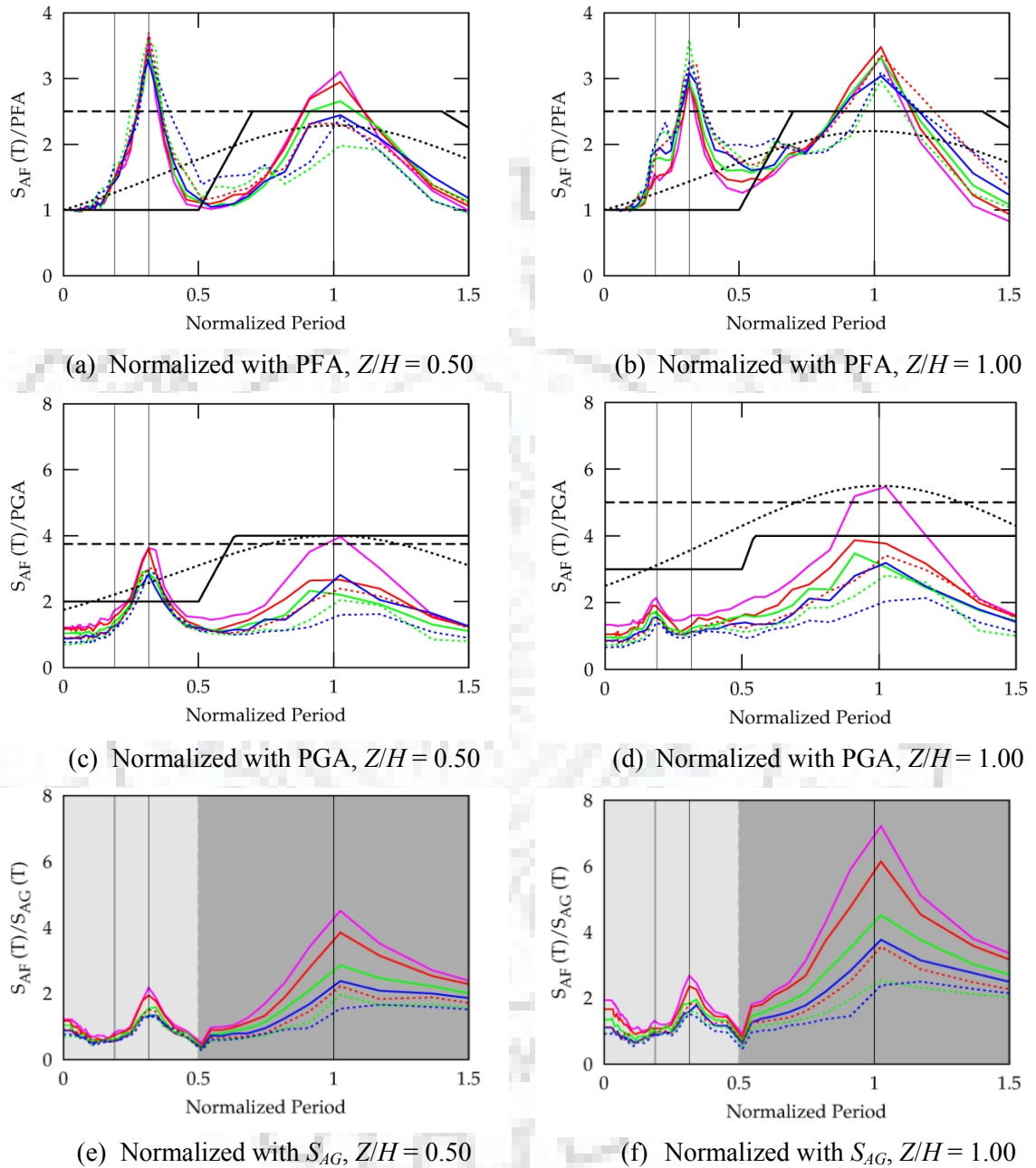
Elastic —	R=1.5 —	R=2.5 —	R=3.5 ····	FEMA P750 —
R=1.0 —	R=2.0 —	R=3.0 —	IS1893 – –	EN1998 ····

Fig. 6.6 Median floor response spectra at mid-height ($Z/H = 0.5$) and at roof level ($Z/H = 1.0$) of the 4-storey building subjected to 30 ground-motions in longitudinal direction, normalized by PFA, PGA and corresponding ground spectrum ($S_{AG}(T)$), for different strength ratios. (The three vertical lines represent the periods of vibration corresponding to the third, second and first modes of vibration, consecutively, in the longitudinal direction).
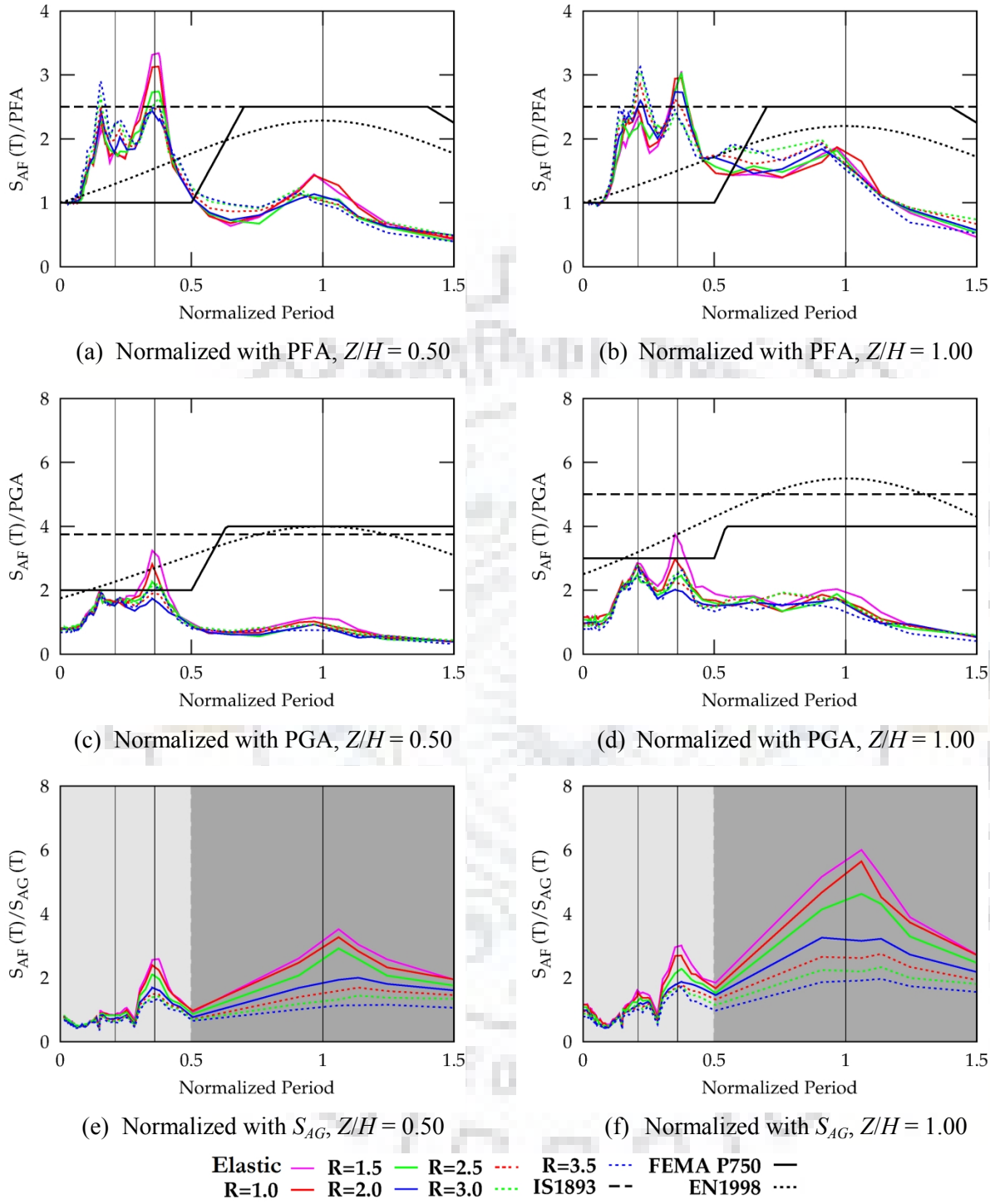
Fig. 6.7 Median floor response spectra at mid-height ($Z/H = 0.5$) and at roof level ($Z/H = 1.0$) of the 8-storey building subjected to 30 ground-motions in longitudinal direction, normalized by PFA, PGA and corresponding ground spectrum ($S_{AG}(T)$), for different strength ratios. (The three vertical lines represent the periods of vibration corresponding to the third, second and first modes of vibration, consecutively, in the longitudinal direction).

(a) Normalized with PFA, $Z/H = 0.50$

(b) Normalized with PFA, $Z/H = 1.00$

(c) Normalized with PGA, $Z/H = 0.50$

(d) Normalized with PGA, $Z/H = 1.00$

(e) Normalized with S_{AG}, $Z/H = 0.50$

(f) Normalized with S_{AG}, $Z/H = 1.00$

| Elastic — | R=1.5 — | R=2.5 — | R=3.5 ···· | FEMA P750 — |
| R=1.0 — | R=2.0 — | R=3.0 — | IS1893 – – | EN1998 ···· |
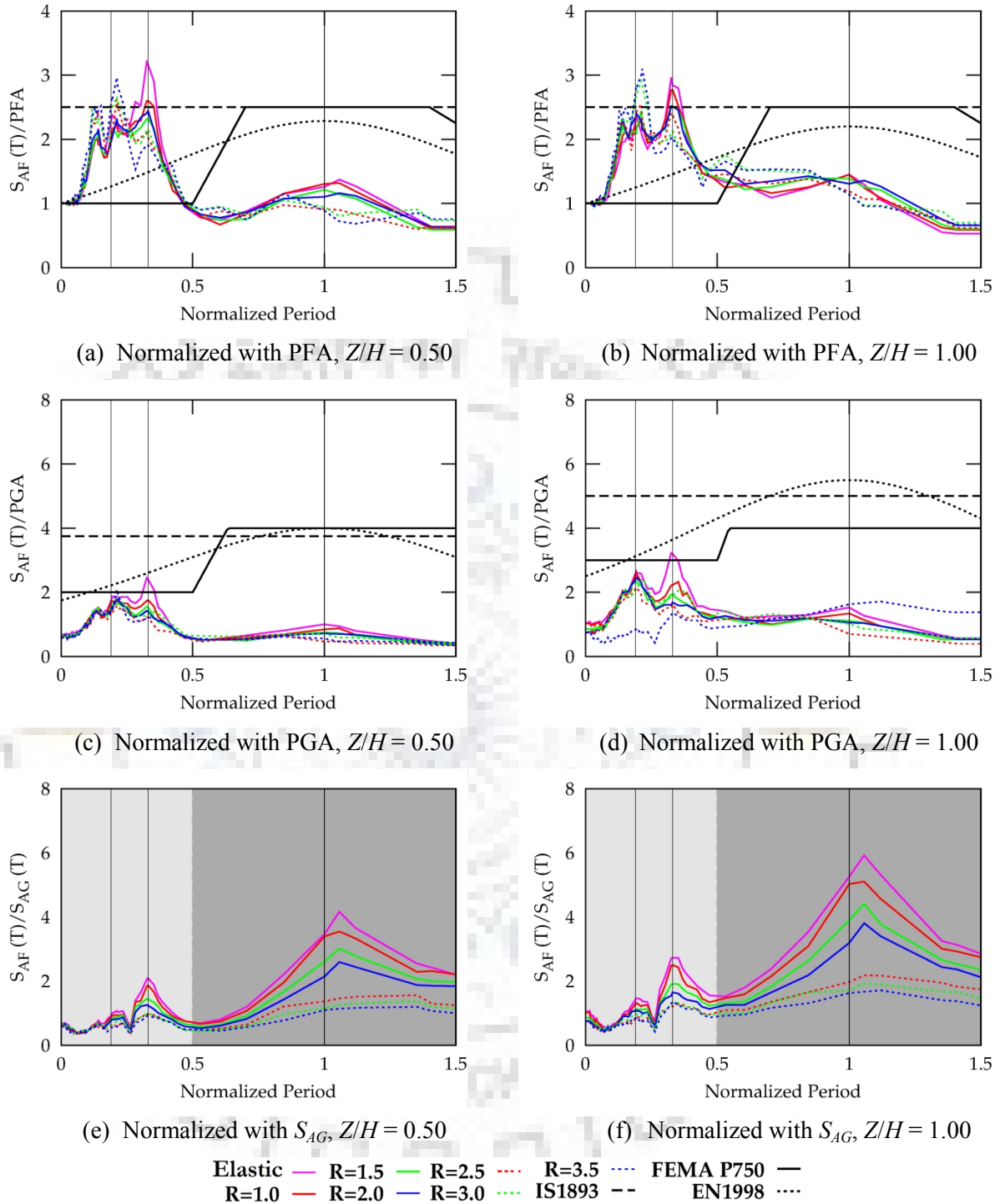
Fig. 6.8 Median floor response spectra at mid-height ($Z/H = 0.5$) and at roof level ($Z/H = 1.0$) of the 12-storey building subjected to 30 ground-motions in longitudinal direction, normalized by PFA, PGA and corresponding ground spectrum ($S_{AG}(T)$), for different strength ratios. (The three vertical lines represent the periods of vibration corresponding to the third, second and first modes of vibration, consecutively, in the longitudinal direction).

The floor spectrum normalized by PFA (Figures 6.6(a) and 6.6(b)) represents the component amplification factor, a_p. Sharp peaks are observed in floor spectral shapes, corresponding to different modes of vibration of the building. The peak values of the normalized floor spectra are much higher than the maximum value of 2.5 recommended in most of the considered codes. The code models significantly underestimate component amplification (a_p), in the vicinity of the first two modes of vibration of the supporting structure. Further, the peak corresponding to the second mode of vibration is higher than (at $0.5H$) or nearly equal (at H) to that corresponding to the first mode, and is relatively insensitive (in comparison to the peak corresponding to the fundamental mode) to the strength ratio, R. On the other hand, the code models completely ignore the peak in a_p corresponding to the second mode of the supporting structure.

Figures 6.6(c) and 6.6(d) present floor spectra normalized by PGA. The peak value of the median normalized spectral acceleration at the roof level is of the order of 5.5 for the elastic case and reduces as the building starts responding inelastically. These normalized spectra represent the combined effect of floor amplification and component amplification in the code models, and depend on characteristics (spectral shape) of the ground-motion and its amplification by the supporting structure. The corresponding values in IS 1893, FEMA P750, EN 1998, and NZS 1170.5 are 5, 4, 5.5, and 6, respectively. (Please note that in case of FEMA P750, it is controlled by the upper limit of 4).

It is interesting to note that the code models, which are quite non-conservative in terms of component amplification (a_p), result in reasonably close estimates of the combined effect of floor amplification (PFA/PGA) and component amplification ($a_p = S_{AF}(T)$/PFA), as compared to the peak median estimates at the fundamental period of the elastic supporting structure (please compare Figures 6.6(a) and 6.6(b) with 6.6(c) and 6.6(d)). This indicates that the non-conservative model for component amplification in the design codes is compensated by the overly conservative model for floor amplification, resulting in peak values of component spectral acceleration, which are in reasonable agreement with the numerical results. However, at mid-height of the building, the code models (except for IS 1893) are non-conservative in the vicinity of the second mode period of the supporting structure, as these models ignore the effect of higher modes of vibration. On the other hand, the IS 1893 model, being based on uniform component amplification, results in conservative estimates of acceleration demands on NSCs,

for the whole range of periods. Figures 6.6(e) and 6.6(f) present floor spectra (S_{AF} (T)) normalized by the respective ground spectrum (S_{AG} (T)). These curves directly represent the spectral amplification factors as a function of normalized period. The peak corresponding to the second mode of vibration is less prominent in these curves, as compared to Figures 6.6(a) and 6.6(b). The reason for this, lies in the shapes of the ground response spectra, which have their peak in the short-period range (i.e., towards higher modes of vibration of buildings). When the floor spectrum is normalized with the corresponding ground response spectrum, this effect is compensated resulting in lower peaks corresponding to the higher modes. It can be observed that as the strength ratio increases, the spectral amplification factors reduce. For a given strength ratio, a higher reduction in the spectral amplification factor has been observed in the vicinity of the fundamental mode of vibration as compared to the higher modes of vibration. A possible explanation to this observation is that since the response of the supporting structure is dominated by the fundamental mode of vibration, the supporting structure dissipates a larger amount of energy through it, leading to a larger corresponding reduction. The dark gray- and light gray-shaded areas in Figures 6.6(e) and 6.6(f) represent the impact zones of the fundamental and the higher modes of vibration, respectively.

Figure 6.9 shows the same results for the 4-storey short-period building (4S), where Figs. 6.9(c) and 6.9(d) present floor spectra normalized by PGA. The median values of peak normalized floor spectral acceleration for the elastic case are much higher (of the order of 10.5 at the roof level) for this building. This indicates that for short-period buildings, where the predominant ground-motion period (T_{peak}) is closer to the supporting structure's fundamental period of vibration (T_1), current code models may significantly underestimate the floor accelerations. Further, the peak corresponding to the second mode of vibration diminishes significantly (almost disappears), in this case. A similar observation, in the case of elastic stiff supporting structures, has also been made by Vukobratović (2015): "It was also observed that there were practically no peaks related to the modes with very high frequencies, i.e. with frequencies above the frequency at which spectral acceleration practically returns to zero period acceleration."

Figure 6.10 compares the coefficients of variation (COV) of the floor spectra normalized by the respective PGA, PFA and ground response spectrum, for the considered thirty earthquake time histories (Table 3.8). It is to be noted here that the horizontal axis in Fig. 6.10 represents the

period of vibration of the NSC. The COV is shown at different relative heights and for different levels of inelasticity.

(a) Normalized with PFA, $Z/H = 0.50$

(b) Normalized with PFA, $Z/H = 1.00$

(c) Normalized with PGA, $Z/H = 0.50$

(d) Normalized with PGA, $Z/H = 1.00$

(e) Normalized with S_{AG}, $Z/H = 0.50$

(f) Normalized with S_{AG}, $Z/H = 1.00$

| Elastic —— | R=1.5 —— | R=2.5 —— | R=3.5 ···· | FEMA P750 —— |
| R=1.0 —— | R=2.0 —— | R=3.0 —— | IS1893 – – | EN1998 ···· |
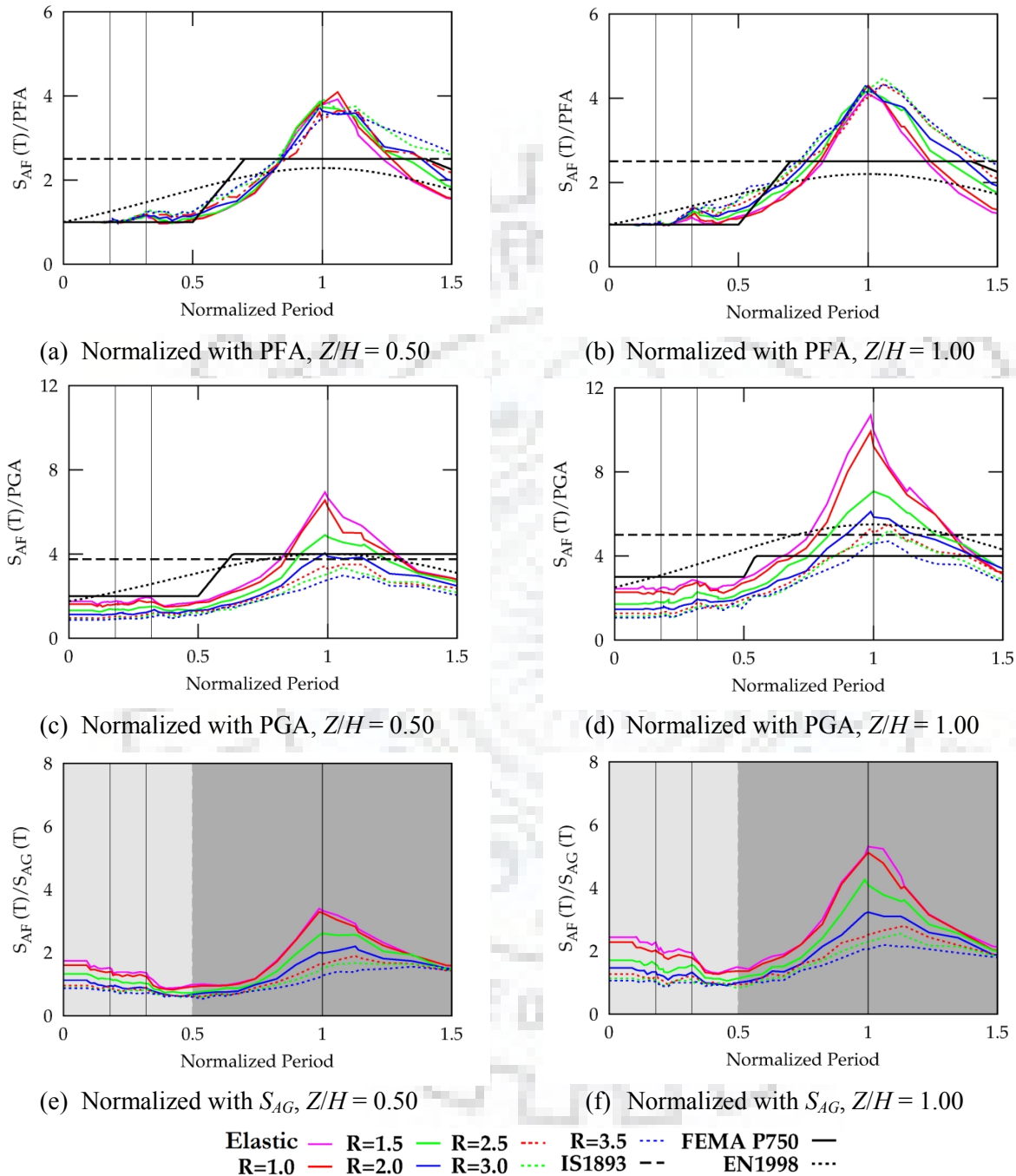
Fig. 6.9 Median floor response spectra at mid-height ($Z/H = 0.5$) and at roof level ($Z/H = 1.0$) of the 4-storey short-period building (4S) subjected to 30 ground-motions in longitudinal direction, normalized by PFA, PGA and corresponding ground spectrum (S_{AG} (T)), for different strength ratios. (The three vertical lines represent the periods of vibration corresponding to third, second and first modes of vibration, consecutively, in the longitudinal direction).
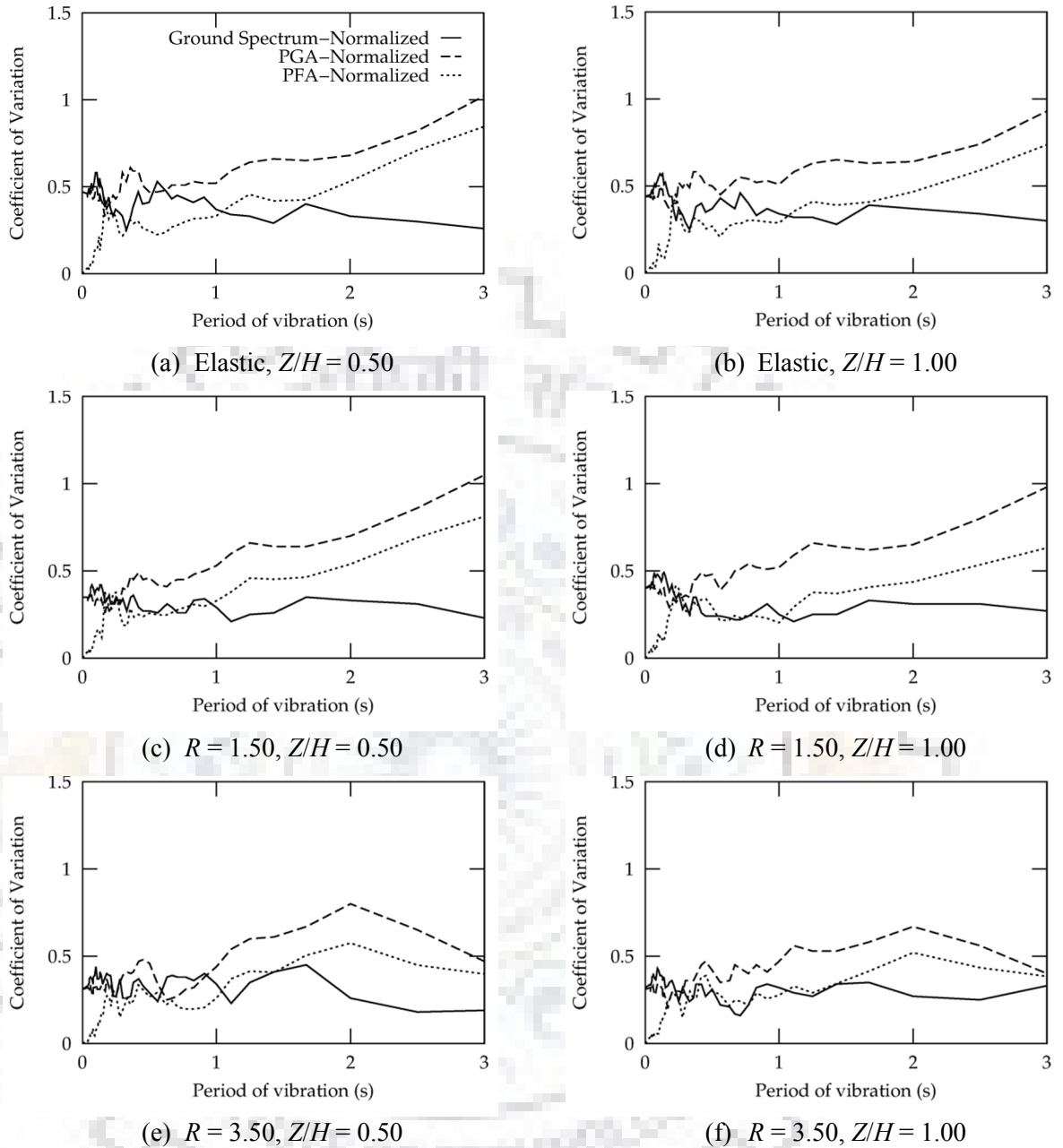
Fig. 6.10 Coefficients of variation (COV) of floor spectral ordinates obtained from 30 ground-motion records, normalized by PGA, PFA and ground acceleration spectrum ($S_{AG}(T)$). The results are presented for the 4-storey building having period of vibration 1.22 s in longitudinal direction.

The results are shown here for the longitudinal direction of the 4-storey building ($T_1 = 1.22$ s). It is observed that for any given period of vibration, inelasticity and relative height, the normalization with respect to PGA has a higher COV as compared to the normalization with respect to ground response spectrum. Further, the normalization with respect to PGA leads to an increase in COV in the long-period range (for the period greater than fundamental period of vibration of the supporting structure) whereas the normalization with respect to ground

157

spectrum leads to more or less uniform COV for the whole period range (Fig. 6.10). This underlines the fact that the floor response spectrum is better correlated with the ground response spectrum, in comparison to the PGA. The normalization with PFA leads to the lowest COV in the very short-period range (i.e. for very rigid NSCs), but the COV increases in the long-period range, significantly. Further, it is to be noted that PFA is not an independent input parameter as it, in turn, depends on the ground-motion and usually obtained as a function of PGA. This dependence on PGA will lead to further increased variability, even in the short-period range, which is of the same order as in the case of a floor spectral acceleration close to zero period, when normalized with PGA.

These observations highlight the importance of the ground-motion characteristics in generating the floor spectra. The need for the use of the ground response spectrum to generate the floor spectrum has already been expressed by Weiser et al. (2013). The theoretical background and importance of ground response spectra to generate the floor response spectra has been presented by Jiang et al. (2015). It has been shown that the floor response spectra can be considered as amplified ground response spectra (Jiang et al. 2015). Hence, in the present study, the floor response of elastic and inelastic RC buildings has been studied, in terms of the amplification factor with respect to the ground spectral acceleration, $S_{AG}(T)$.

6.4.3.1 Spectral Amplification Factors

Figure 6.11 presents the variation of the spectral amplification factor corresponding to the first two natural periods in both directions of the considered buildings, normalized by the corresponding mode shape along the building height (i.e. dividing the amplification factor value at the considered natural period and a particular floor level by the ordinate of the normalized mode shape at that particular floor level. The term 'normalized mode shape' here represents the mode shape with its maximum ordinate as unity). It is expected that the mode shape of an inelastic supporting structure may change with the level of inelasticity. However, Lucchini et al. (2016) have shown that the effect of inelasticity on mode shapes of the building is insignificant and (for regular buildings) "elastic deformed shape is a reasonable proxy for the inelastic one." The different solid lines in the figure represent the longitudinal direction of excitation in different buildings and the dotted lines correspond to the transverse direction of the same buildings.
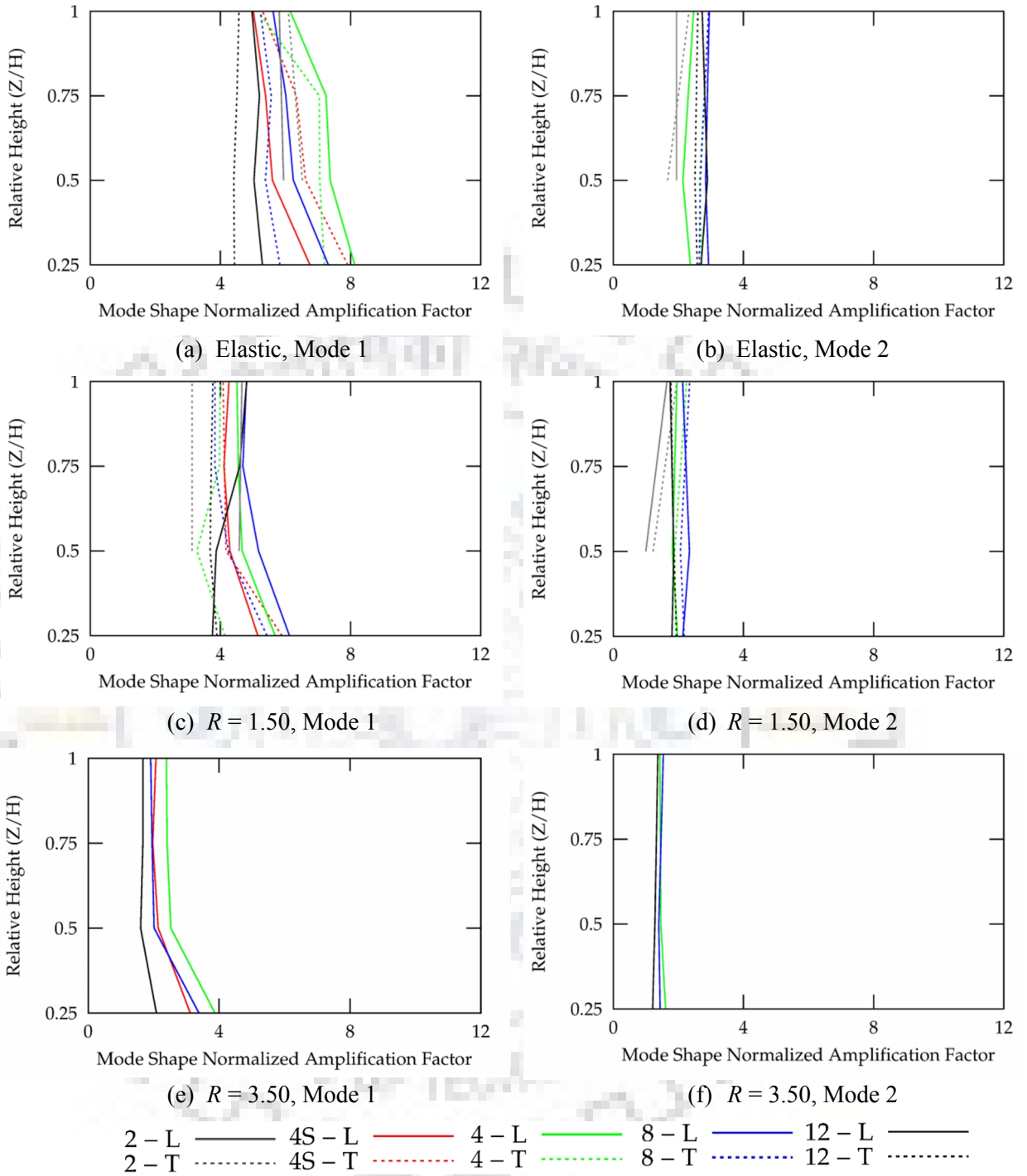
Fig. 6.11 Variation of amplification factors normalized by mode shape, along the height of the building. (Different lines represent different buildings considered. In case of 2-storey building, these factors are available at $0.5H$ and H only. The decreasing number of curves with increasing strength ratios indicates collapse of some of the buildings at the considered intensity level. L and T indicate longitudinal and transverse directions, respectively).

It can be observed from the figure that the spectral amplification pattern, after normalizing with the respective mode shape, can be approximated as a vertical line. This vertical line pattern has

been observed to correspond to both the fundamental as well as the second mode of vibration. In fact, the difference in the normalized spectral amplification factors for different buildings reduces as the strength ratio increases, and in the case of the second mode. These observations indicate that the variation of peak (corresponding to natural periods) spectral amplification of motion, along the building height, can be approximated by the corresponding mode shape. However, as explained by Lucchini et al. (2016) this observation may be specific to the chosen set of buildings which are regular in plan and elevation, and it needs to be examined further for other types of buildings.

Figure 6.12 presents median spectral amplification factors corresponding to the fundamental and second modes of vibration for the considered buildings. The different buildings are indicated by their corresponding period of vibration.

(a) 1st Mode

(b) 2nd Mode
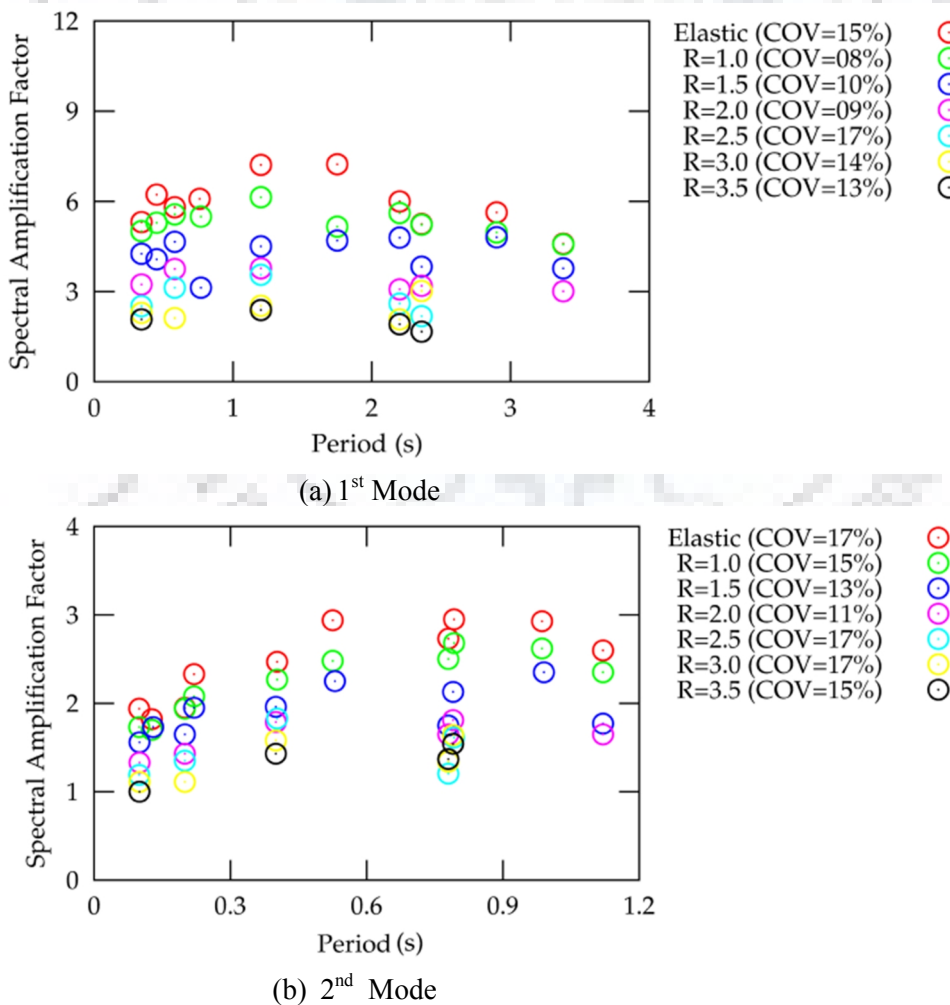
Fig. 6.12 Amplification factors (at roof level) for the considered building models with different strength ratios. (The number of circles for higher strength ratios is reduced due to collapse of some buildings).

These spectral amplification factors are distributed within a COV of the order of 17%, indicating that these can be approximately considered as independent of the building's period of vibration. The same observation has also been made by Weiser et al. (2013) for spectral amplification factors under elastic response for steel buildings. Further, the maximum values of median spectral amplification factors corresponding to the fundamental and second modes of vibration at the roof level are of the order of 7.50 and 3.00, respectively, which are the same as proposed by Weiser et al. (2013).

6.4.4 Proposed Model: Amplification of Floor Acceleration

Weiser et al. (2013) observed that the amplification of the peak floor acceleration along the height of the building depends on the period of the building and the level of inelasticity (strength ratio). Similar observations have been made in the present study; and the following expression for the amplification function (A_0) at zero period is proposed based on envelope values of median estimates:

For elastic response,
$$1 \le A_0 = 1 + \left(\frac{2.5 - T_1}{T_1} \right) \frac{Z}{H} \le 3.0 \tag{6.3}$$

and for inelastic response ($R \ge 1$),
$$1.0 \le A_0 = 1.0 + \left(\left(\frac{T_1 - 2.5}{3T_1} \right) R + \left(\frac{8.75 - 3.5T_1}{3T_1} \right) \right) \frac{Z}{H} \le 1.0 + \left(\frac{7 - 2R}{3} \right) \frac{Z}{H} \tag{6.4}$$

where, T_1 is the fundamental period of vibration of the building for the direction under consideration, R is the strength ratio as defined earlier, Z is the height from the base to the floor at which the response spectrum is being constructed, and H is the total height of the building from its base.

Equations (6.3) and (6.4) have been developed based on the median PFA demands observed in the present study. It has been observed that the PFA demand at the level of roof is almost constant in short-period range and decreases with increase in period of vibration as well as strength ratio of the supporting structure. Further, for supporting structures with a period of vibration greater than 2.5 s, the median PFA demand has been found to be lesser than the PGA,

even under an elastic response of the supporting structure. As the considered building models are low- to mid-rise, the response of these buildings is dominated by the fundamental mode of vibration. Hence, a linear variation of PFA demand from bottom to top has been considered. A similar observation was also made by Weiser et al. (2013) and Eq. (6.3) is actually the same as proposed by Weiser et al. (2013) for steel buildings exhibiting an elastic response. In addition to these observations, an upper bound (to control the predicted PFA demand for short-period buildings within the observed limit) and a lower bound (to have some conservativeness in the proposed model) have also been recommended based on the observations in the present study. The proposed model has been developed considering the fact that under elastic response of the supporting structure, the PFA/PGA ratio is almost constant for short-period buildings (Table 6.2), and reduces with increase in the fundamental period of vibration of the supporting structure up to 2.50 s. The maximum amplification at the level of the roof (A_0) for the short-period buildings has been considered as equal to 3, as observed in the present study and proposed in ASCE 41 and NZS 1170.5. In this study, for the 8-storied supporting structure with fundamental period of vibration, $T_1 = 2.36$ s, the PFA/PGA ratio has been found out to be closer to unity (i.e. 1.06, see Table 6.2). Hence, the proposed model considers amplification of PFA demands at the roof level of buildings with period of vibration up to 2.50 s under elastic response. For buildings with periods of vibration greater than 2.50 s, the model results in PFA values equal to PGA and independent of strength ratio, R, indicating that a de-amplification of PFA in inelastically responding long-period buildings has been ignored, for conservativeness.

Figure 6.13 compares the median PFA/PGA ratios at the roof level as obtained from non-linear dynamic analyses using a suite of 30 ground-motion records. It can be observed that the proposed model is conservative in the short- and long-period ranges for all strength ratios defined for the present study. For $R = 3.50$, the proposed model predicts the (PFA/PGA)$_{Roof}$ to be equal to unity (not shown in figure) and independent of period of vibration of the supporting structure.

6.4.5 Proposed Model: Amplification of Floor Spectrum

Based on the observations made in the previous sections, identification of different parameters governing the floor response, and the results obtained from the numerical study, a comprehensive spectral amplification model is proposed. The proposed model consists of floor

amplification functions to estimate the floor response spectrum at any given level, directly from the ground response spectrum, if the building's first two mode shapes, and corresponding periods of vibration and strength ratio, are known. The proposed functions have been developed to capture the peaks corresponding to the first two modes of vibration. The proposed functions have some similarity with the model recommended by EN 1998 (CEN 2004) for determination of floor spectral acceleration demand on NSCs.
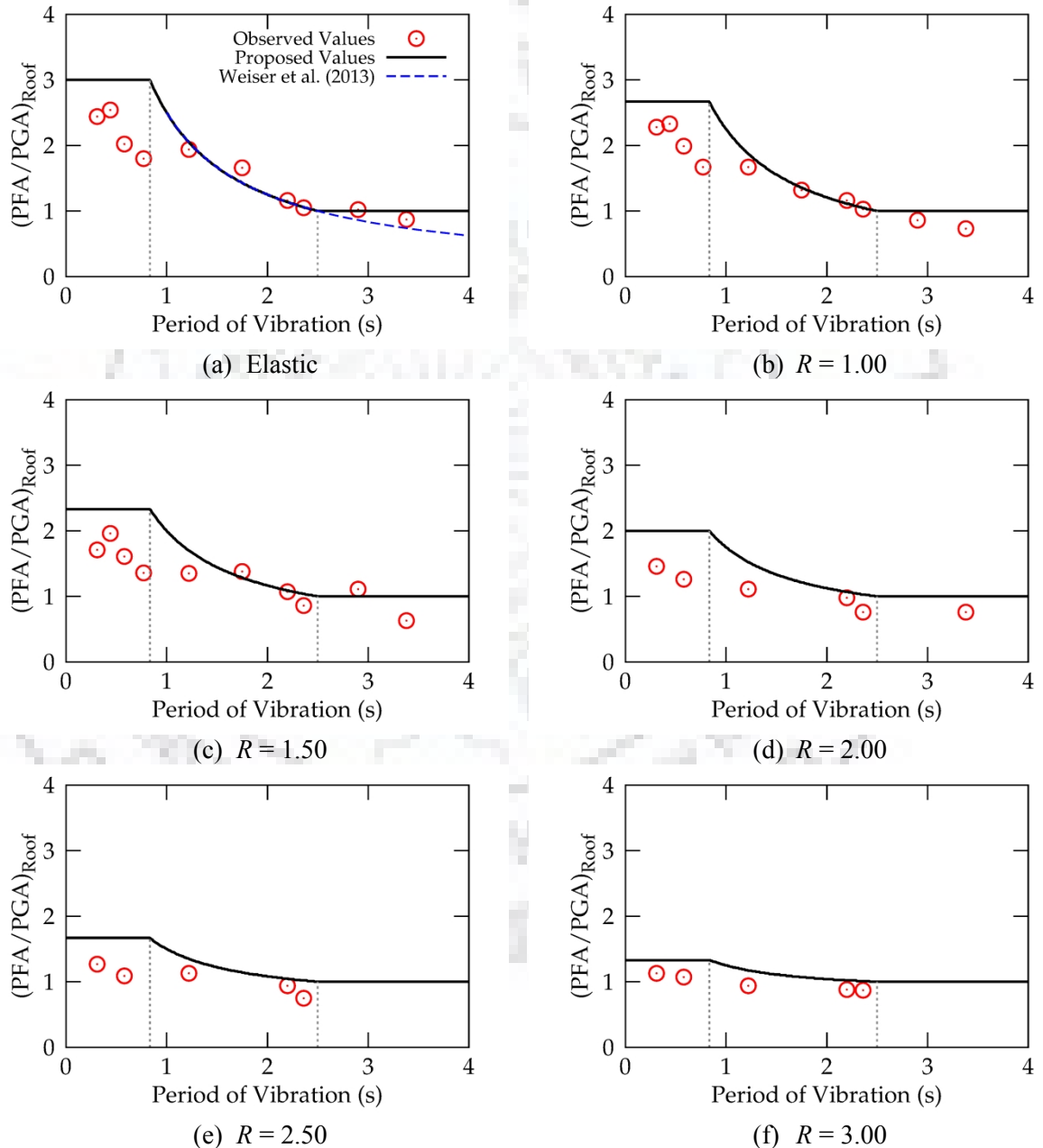
Fig. 6.13 Comparison of median PFA/PGA ratios at the roof level, as obtained from IDA and as predicted by the proposed model.

However, it has two basic differences from the EN 1998 model. Firstly, the proposed model considers a constant plateau and single peak for short-period buildings and two peaks for long-period buildings (Fig. 6.14) instead of a single peak as in the case of the EN 1998 model. These peaks are bounded within impact zones of fundamental and second modes of vibration. For periods outside the impact zones, the model amplifies the ground spectrum by constant factors. Secondly, the EN 1998 model is based on PGA; whereas, the proposed spectral amplification function is based on ground response spectrum.

Figure 6.14 presents the proposed spectral amplification functions for short- and long-period buildings. These amplification functions can be used along with the design response spectrum as well as with the site-specific ground response spectrum, and account for the ground-motion characteristics, frequency tuning between the site (ground-motion) and the supporting structure, as well as tuning between the supporting structure and the NSC. These spectral amplification functions are derived based on impact zones of different modes of vibration of the building. As observed from Figs. 6.6-6.9, the normalized period, $T_p/T_1 = 0.5$ more or less acts like a boundary between the impact zones of the fundamental and the higher modes. Similar demarcation has also been suggested by Sankarnarayanan and Medina (2007).
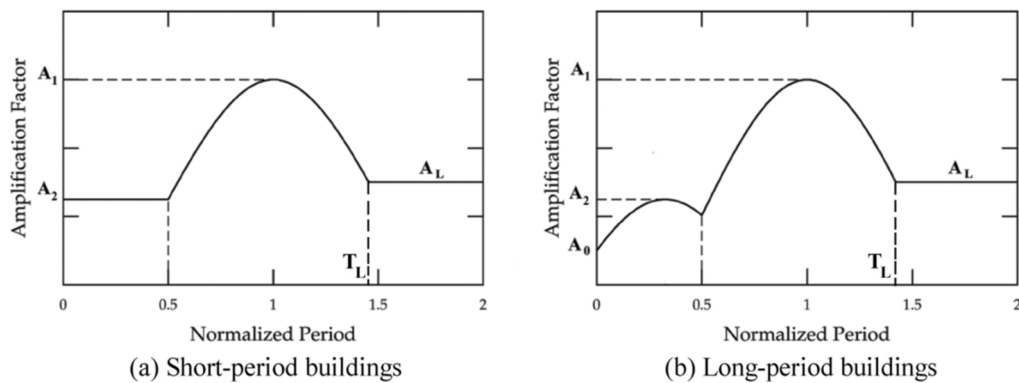
Fig. 6.14 Proposed spectral amplification functions.

For short-period buildings, the amplification factor within the impact zone of second and higher modes of vibration can be reasonably considered as constant (Fig. 6.9). On the other hand, in the case of long-period buildings, sharp peaks are observed corresponding to the first two modes of vibration (Figs. 6.6-6.8). In the proposed function, these peaks have been represented by separate parabolic functions within the impact zone of each mode. The impact zone of the second mode (including the effect of higher modes which cause local smaller peaks) has been

considered between the normalized periods 0 and 0.5, whereas the impact zone of the fundamental mode starts from the normalized period 0.5 and continues up to the point of intersection with the long-period amplification factor (A_L), which is assumed to be constant, for both short- and long-period buildings. Based on the results of the numerical study, the floor spectral amplification function for median response has been developed.

The peak values of the amplification function, corresponding to the first and second modes, at i^{th} floor, can be obtained as:

For elastic response,

$$A_1 = 7.50\left(\frac{\phi_{1,i}}{\phi_{1,roof}}\right) \geq 1.00 \tag{6.5}$$

$$A_2 = 3.00\left(\frac{\phi_{2,i}}{\phi_{2,roof}}\right) \geq 1.00 \tag{6.6}$$

and for inelastic response ($R \geq 1$),

$$A_1 = 7.50\left(\frac{\phi_{1,i}}{\phi_{1,roof}}\right)\left(0.95R^{-0.65}\right) \geq 1.00 \tag{6.7}$$

$$A_o \leq A_2 = 3.00\left(\frac{\phi_{2,i}}{\phi_{2,roof}}\right)\left(0.90R^{-0.25}\right) \geq 1.00 \tag{6.8}$$

where, A_1 and A_2 are the spectral amplification factors corresponding to the first and second modes of vibration and A_0 is as defined earlier (Eq. 6.3); $\phi_{1,i}$ and $\phi_{1,roof}$ are the first mode shape coefficients at i^{th} floor and roof, respectively; $\phi_{2,i}$ and $\phi_{2,roof}$ are the second mode shape coefficients at i^{th} floor and roof, respectively; and R is the strength ratio as defined in Eq. 6.2.

Equations (6.5) and (6.6) are derived from the envelope of the median peak spectral amplification factors obtained in the present study and observations made from Figure 6.11, whereas Eqs. (6.7) and (6.8) have been developed using regression of the peak median spectral amplification factors rounded off to the nearest higher multiple of 0.50, for different strength

ratios in the considered building models. Equations (6.7) and (6.8) result in a goodness of fit equal to 0.97 and 0.87, respectively, to the observed median peak spectral amplification factors.

Knowing the values of A_0, A_1, and A_2, the median amplification function can be obtained using Eqs. (6.9) - (6.11) as:

for $0 < T_p/T_1 < 0.5$,

$$A(T_p) = \frac{C_1}{1 + \left(\dfrac{T_2}{T_1} - \dfrac{T_p}{T_1}\right)^2} - C_2 \geq 1.00 \qquad (6.9)$$

for $0.5 < T_p/T_1 < T_L$

$$A(T_p) = \frac{C_3}{1 + \left(1 - \dfrac{T_p}{T_1}\right)^2} - C_4 \qquad (6.10)$$

for $T_p/T_1 > T_L$,

$$A(T_p) = A_L = 1 + 2\frac{Z}{H} \leq A_1 \qquad (6.11)$$

where, T_1 and T_2 are the periods of vibration of the building corresponding to the first and second mode, respectively; T_p is the period of vibration of the NSC; A_L is the long-period amplification factor; T_L is the normalized period beyond which the spectral amplification function has been assumed to be constant. The constants C_1, C_2, C_3 and C_4 can be obtained using the known values of the amplification function $A(T_p)$ at specific values of period, T_p (i.e. at $T_p = 0$, T_2, $0.5T_1$, and T_1).

Equations (6.9) and (6.10) are similar in shape to the EN 1998 formulation for determination of peak floor spectral acceleration in which peaks in floor response spectra are accounted for by two parabolic functions corresponding to the fundamental and second modes of vibration (although EN 1998 formulation considers only a single peak corresponding to the fundamental mode of vibration). Equation (6.11) has been obtained from the envelope of the median elastic response of the supporting structure at different relative heights, since the effect of inelasticity becomes insignificant for NSCs having a period sufficiently longer than the fundamental period of the supporting structure. Further, as shown by Vukobratović and Fajfar (2016), in case of NSCs having period much longer than the fundamental period of the supporting structure, the floor spectral acceleration tends to converge to the ground spectral acceleration, irrespective of the floor level. Therefore, Eq. (6.11) produces conservative estimates of the peak floor spectral

acceleration demand for long-period NSCs. An upper limit on the periods of NSCs up to 5 s or 2 times of the fundamental period of the supporting structure (whichever is smaller) has been recommended for applicability of the proposed model. For NSCs with even longer periods, the proposed function may yield too conservative estimates at upper floors.

It is important to note here that Eqs. (6.3), (6.5), (6.6), and (6.11) have been obtained from numerical analyses of elastic buildings' models, whereas Eqs. (6.4), (6.7), and (6.8) have been obtained from the inelastic models. Further, in the inelastic models, $R = 1$ does not represent the corresponding elastic case (before first yield), rather it indicates yielding of a significant number of structural elements, and hence the equations derived from inelastic models should not be expected to converge (at $R = 1$) to those obtained from the elastic models.

Figure 6.15 compares the proposed spectral amplification function (shaded area) with the numerically obtained median spectral amplification factors at the roof level. The spectral amplification functions are compared for short-period as well as long-period buildings. Under severe inelastic response ($R = 3.5$), the buildings show collapse in the transverse direction due to lesser redundancy. Hence, only the results from the longitudinal direction are presented.

It can be noted from Eqs. (6.3) - (6.11) that only A_0 depends on the supporting structure's period of vibration, whereas A_1 and A_2 are independent of supporting structures' period. As the curves shown in Fig. 6.15 correspond to buildings with different periods of vibration, the proposed amplification function for long-period buildings has been shown with A_0 corresponding to a 4-storey building ($T_1 = 1.22$ s) only, in order to keep the number of curves small for the sake of clarity in the figure, whereas for a short-period building, the upper bound on A_0 governs the floor amplification. For other long-period buildings, the proposed function will be only slightly different for normalized periods close to zero. It can be observed that the proposed amplification function takes into account the effect of higher modes as well as structural inelasticity. It can be understood from Fig. 6.15 that the parabolic shape of the spectral amplification function widens the peaks as opposed to the sharp peaks corresponding to the building's natural modes of vibration, obtained from the numerical analyses. This, at least to some extent, caters to the uncertainty and 'period shift' associated with the effective period of vibration of an inelastic supporting structure.

(a) Elastic, $Z/H = 1.00$

(b) Elastic, $Z/H = 1.00$

(c) $R = 1.50$, $Z/H = 1.00$

(d) $R = 1.50$, $Z/H = 1.00$

(e) $R = 3.50$, $Z/H = 1.00$

(f) $R = 3.50$, $Z/H = 1.00$
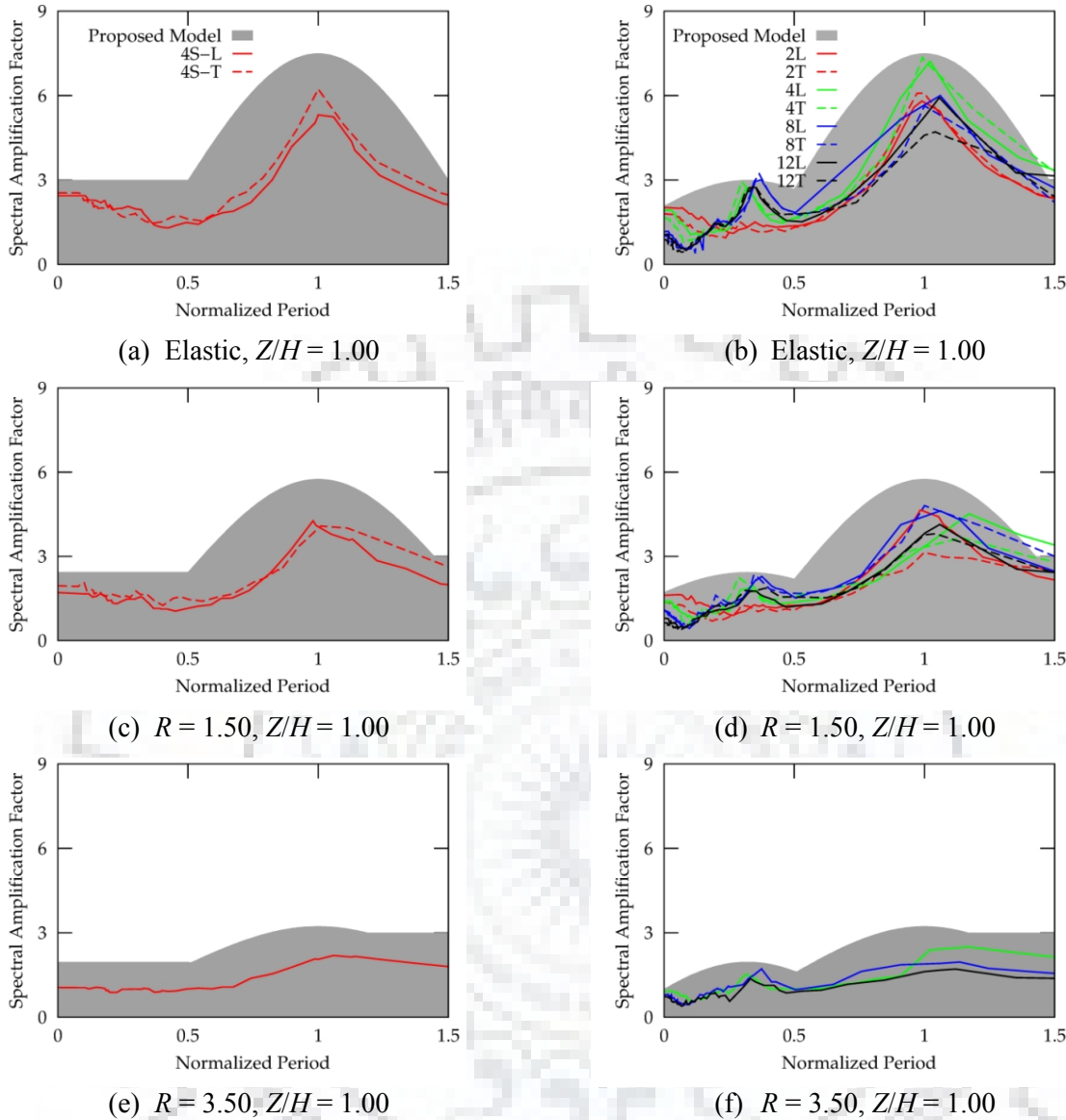
Fig. 6.15 Comparison of the proposed amplification functions with the numerically obtained spectral amplification factors. (L and T indicate longitudinal and transverse directions, respectively. For long-period buildings, the value of A_0 corresponding to the 4-storey building having period of vibration 1.22 s in longitudinal direction, has been used to plot the proposed amplification function, in order to keep the number of curves within reasonable limit for clarity in the figure).

6.4.6 Validation of Proposed Spectral Amplification Functions

In order to validate the proposed spectral amplification functions, non-linear dynamic analyses using spectrum-compatible time histories were performed on a 4-storey short-period building (4S) and a long-period (8-storey) RC frame building (both described and used in the present study) as well as on a 15-storey tall RC frame-shear wall building (15SW, which was not used to derive the spectral amplification factors in the present study). The details of the frame

buildings have already been provided in this Chapter earlier, whereas for the frame-shear wall building, these can be found in Surana et al. (2016).

Three ground-motion records, with a PGA close to 0.36g (i.e. expected MCE hazard level in seismic zone V in India) have been selected from the PEER Database (PEER 2011) and made compatible with the MCE design spectrum of the Indian seismic code (IS 1893 Part 1 2016) using the software WAVEGEN (Mukherjee and Gupta 2002). This software is based on a wavelet transform method for spectrum-compatibility, minimizing the distortions to the original recorded motions. The purpose of considering spectrum-compatible ground-motions is to enable a direct comparison with the code-based design floor response spectrum, and to test the proposed amplification function for a set of ground-motions with entirely different characteristics, than those used to derive it. Table 6.3 presents the details of the original records which are made spectrum-compatible. Figure 6.16 presents the comparison of the spectrum-compatible records with the 5%-damped elastic design response spectrum on Type I soil (rock) as per IS 1893 Part 1 (2016).

Table 6.3 Ground-motion records for non-linear time-history analyses using spectrum-compatible time histories.

Event	Station	$V_{s,30}$ (m/s)	NEHRP site	M_w	R_{jb} (km)	PGA (g)
Imperial Valley (H-E11140)	El Centro Array #11	196	D	6.5	12.5	0.38
Superstition Hills (B-ICC000)	El Centro Imp. Co.	192	D	6.5	18.2	0.36
Chi-Chi, Taiwan (CHY101)	CHY101	259	D	7.6	10.0	0.38
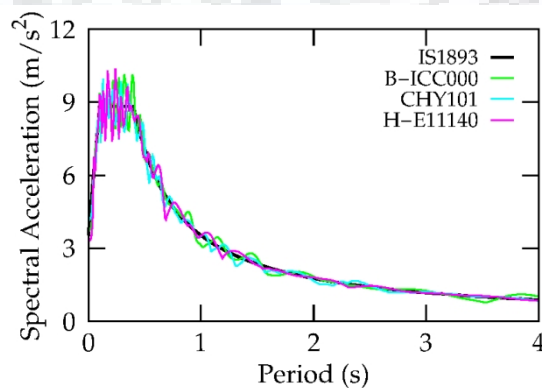
Fig. 6.16 Response spectra of selected ground-motion records made compatible with the MCE spectrum of Indian seismic code, IS 1893 Part 1 (2016).

It can be observed that for the 4-storied short-period building model (4S) (T_1 = 0.31 s), the proposed model produces conservative estimates of PFA demand in the lower half and fairly

accurate estimates of the PFA demand in the upper half of the building height as compared to the PFA demands obtained from spectrum-compatible time-history analyses (Fig. 6.17). For this building, under elastic response, the ASCE 41 and NZS 1170.4 predict PFA demands in close agreement with those obtained from spectrum-compatible time-history analyses and whereas the IS 1893 and EN 1998 under-predicts the PFA demands. For increased strength ratio, the code models (ASCE 41 and NZS 1170.4) are overly conservative, whereas the proposed model, due to taking into account the effect of inelasticity, predicts the PFA demands with reasonable accuracy (Fig. 6.17).
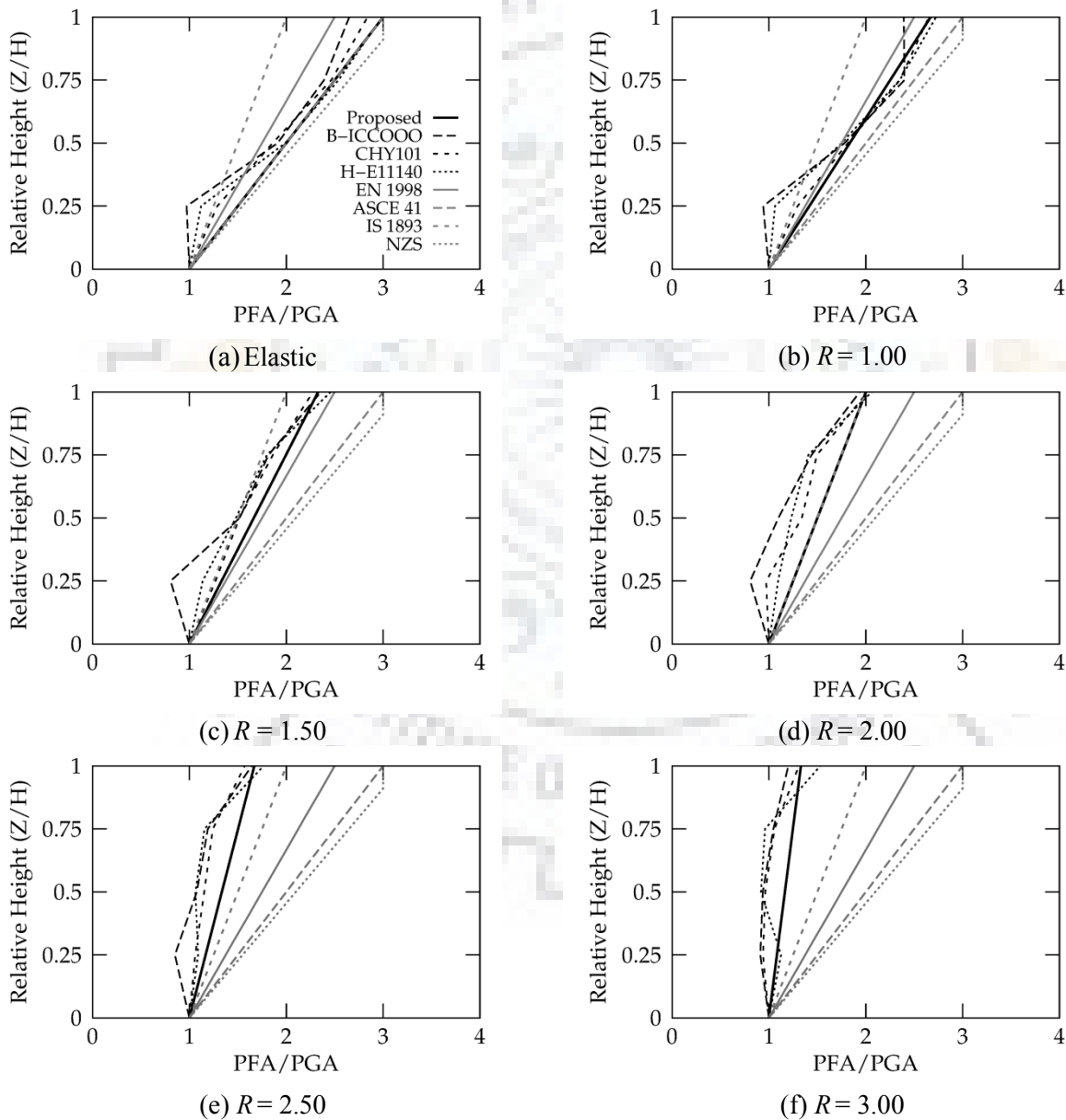
Fig. 6.17 Comparison of the PFA demands obtained from spectrum-compatible time-history analyses, predicted by the proposed model, and as obtained from major seismic design codes for 4S building.

For the 4-storied intermediate-period (4I) (T_1 = 1.22 s) building, the proposed model predicted PFA demands reasonably close to those obtained from spectrum-compatible time-history analyses, whereas the code models (IS 1893, ASCE 41, EN 1998 and NZS 1170.4) produce highly conservative estimates of PFA demands throughout the height of the building and for all strength ratios. Similar observations are also made for 8-storied building (8L) (Fig. 6.18). Further, PFA demand profiles as obtained from spectrum-compatible time-history analyses of 4-storied short-period building (4S) are close to linear, whereas for the 4-storied intermediate-period (4I) and 8-storied long-period (8L) building, the PFA/PGA ratio vary linearly in the bottom quarter, is almost constant in the middle half and linearly increases in the upper quarter due to the previously described whiplashing effect of higher modes.
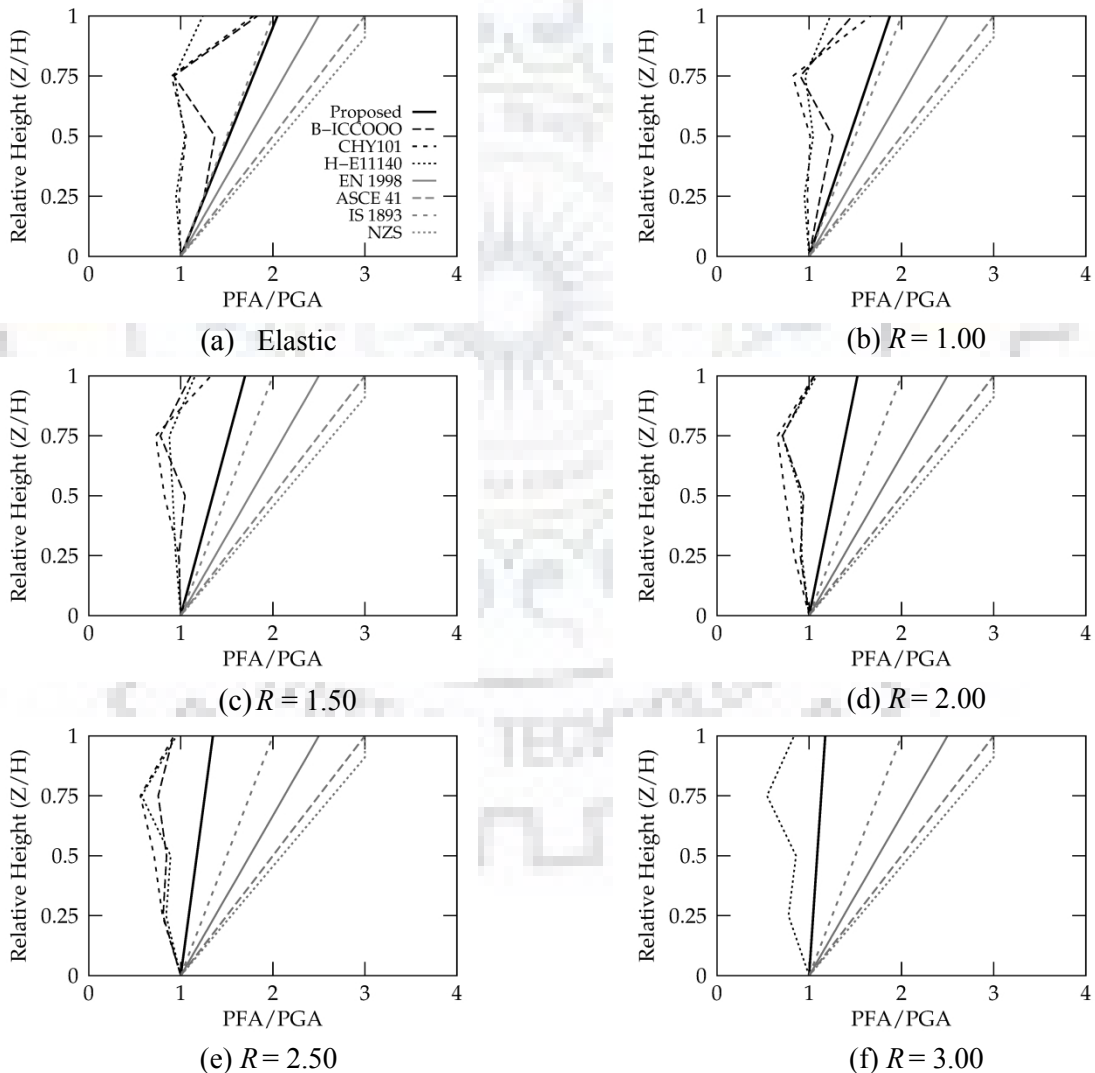
Fig. 6.18 Comparison of the PFA demands obtained from spectrum-compatible time-history analyses, predicted by the proposed model, and as obtained from major seismic design codes for 4-storey building.
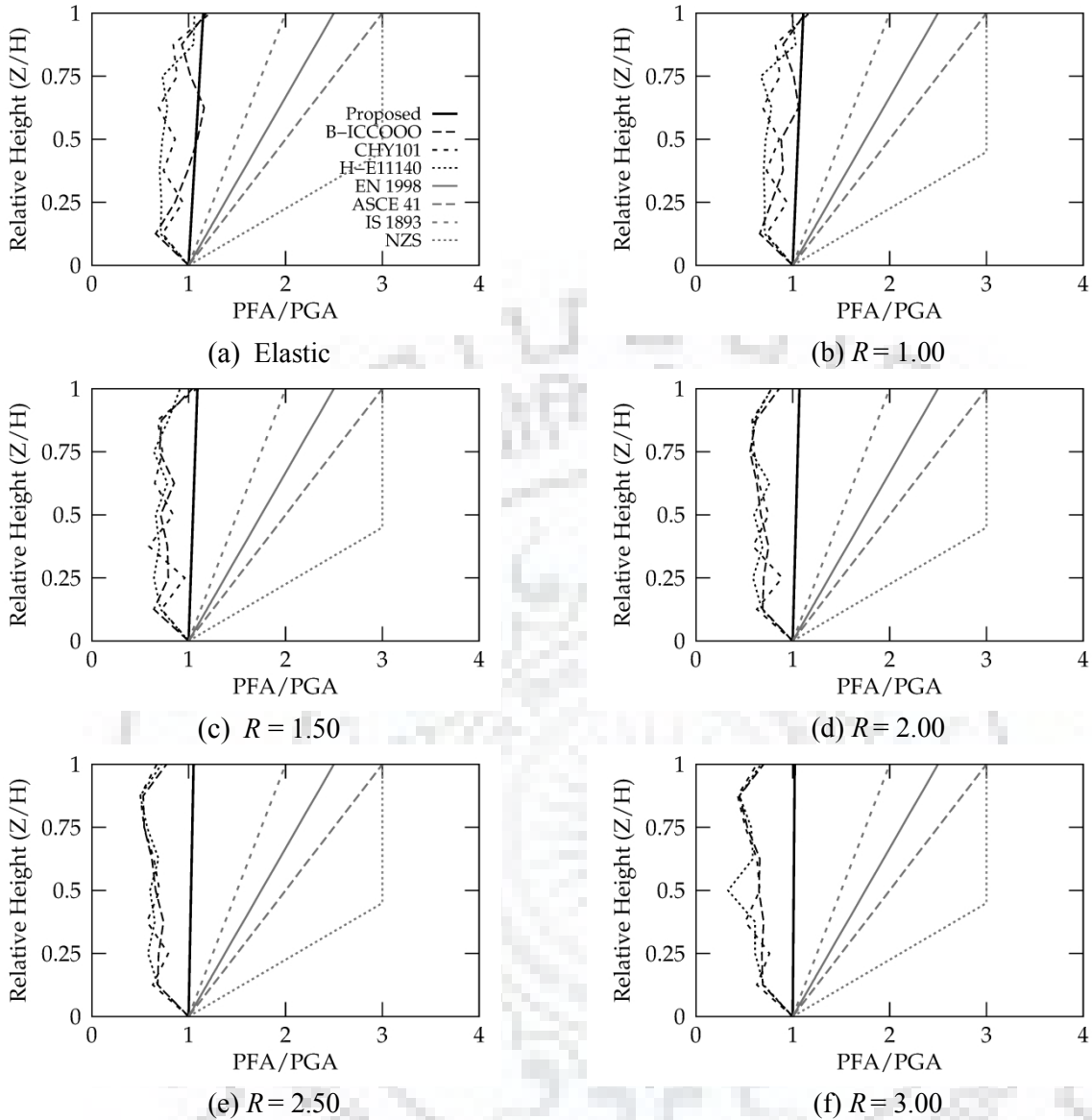
Fig. 6.19 Comparison of the PFA demands obtained from spectrum-compatible time-history analyses, predicted by the proposed model, and as obtained from major seismic design codes for 8-storey building.

The proposed model, though being based on the linear profile from bottom to top, produces conservative estimates throughout the entire height of the building for all strength ratios. However, this conservatism is much lesser as compared to the code models (Fig. 6.19).

Figures 6.20-6.21 presents a comparison of the floor spectra constructed using the proposed amplification function, with those obtained from the time-history analyses using spectrum-compatible records, and the models proposed by Weiser et al. (2013), Petrone et al. (2015b) and the design codes. The floor response spectra have been compared at the roof level as well as near the mid-height of the building, where higher mode response is more significant. It is

important to note here that the spectral amplification model proposed by Weiser et al. (2013) was developed for steel buildings with a fundamental period of vibration greater than 1s. Hence, the Weiser et al. model is not shown in the case of the short-period building '4S' (T_1 = 0.31 s). Further, the proposed function as well as the Weiser et al. (2013) model were developed for frame buildings and their comparison with the results of shear wall building '15 SW' is not strictly valid due to the difference in the deformed shapes.

In the case of 4-storey short-period building (4S), the codes' (EN 1998 and FEMA P750) models are non-conservative in the impact zone of the fundamental mode of the building. This non-conservatism is very significant in case of the elastic supporting structure, and reduces in case of the inelastic building (Fig. 6.20). The model proposed by Petrone et al. (2015b) is non-conservative for the elastic peak response in the impact zone of the fundamental mode of the building, but produces conservative estimates in comparison with the inelastic response (R = 3.50). The proposed model produces closest estimates in elastic as well as inelastic cases for this short-period building.
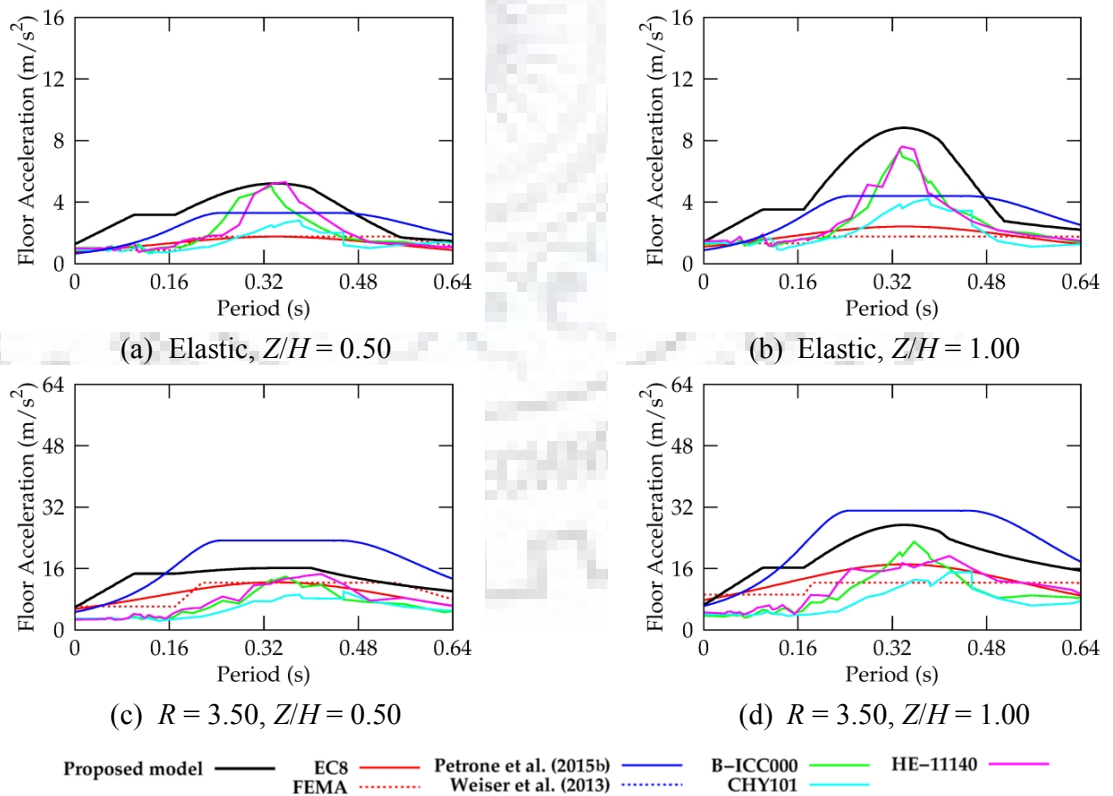
Fig. 6.20 Comparison of floor spectra for 4-storey short-period building obtained using the proposed function with those obtained from spectrum-compatible time-history analyses, from model by Petrone et al. (2015b), and from design codes.

For the 8-storey building, the code models are too conservative, even for an elastic response, for the periods close to and longer than the fundamental period of the building (Fig. 6.21). This conservatism further increases with an increase in the strength ratio. On the other hand, these models are non-conservative for predicting the floor spectral acceleration in the impact zone of higher modes, particularly in the elastic case. For predicting the floor spectral acceleration in the impact zone of higher modes, the model proposed by Petrone et al. (2015b) is reasonably accurate as it takes into account the peaks corresponding to higher modes, but it is also significantly conservative in the impact zone of fundamental mode particularly for the inelastic supporting structure.
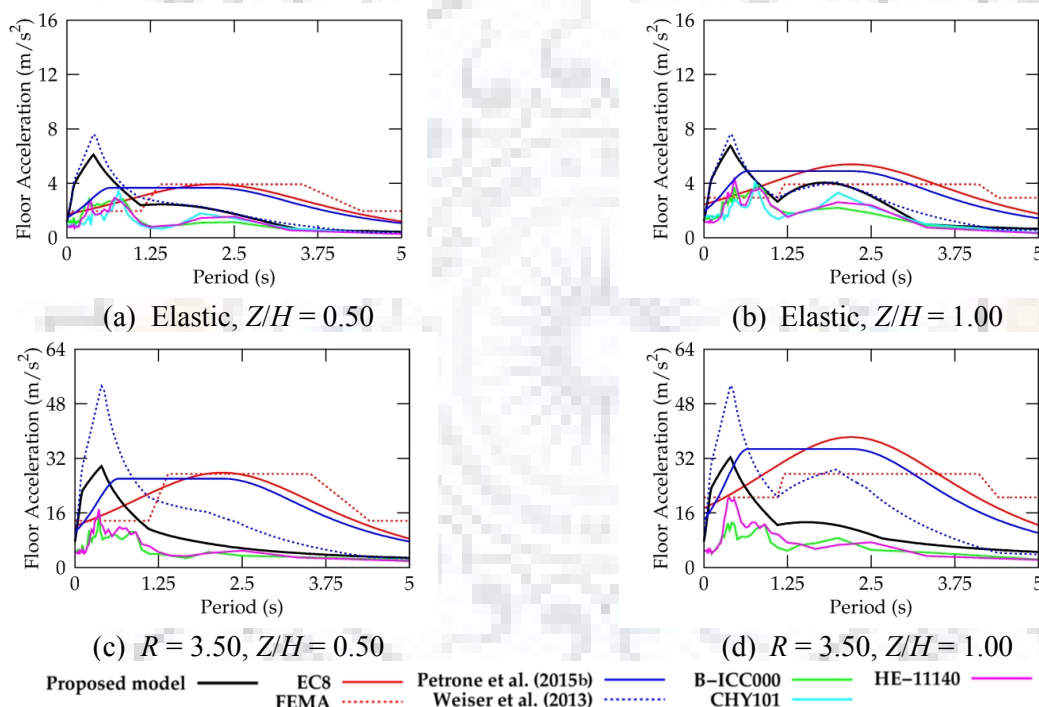
Fig. 6.21 Comparison of floor spectra for 8-storey building obtained using the proposed function with those obtained from spectrum-compatible time-history analyses, from models by Weiser et al. (2013) and Petrone et al. (2015b), and from design codes.

These observations can be attributed to the fact that these models are based on the amplification of PFA along the height of the building and utilize a fixed spectral shape (component amplification factor). The dependence of the floor response spectrum on the ground response spectrum is completely ignored in these models. Further, as identified in the previous research and the present study, the amplification of PFA is also dependent on the supporting structure's period of vibration and reduces with an increase in the period of vibration, whereas code models do not account for the period of vibration of the supporting structure.

The model proposed by Weiser et al. (2013) predicts floor spectral acceleration very close to the numerical results for elastic response of the supporting structure but predicts significantly conservative floor spectral accelerations for an inelastic supporting structure. The proposed amplification function predicts the floor response spectra closest to the numerical results in the whole of the spectral range, and for both elastic as well as inelastic supporting structures. In the elastic case, the proposed amplification function and the Weiser et al. (2013) model predict close results. The reason for this lies in the fact that both the models have the same spectral amplification factors at the roof, corresponding to the fundamental and second modes of vibration. The slight difference observed between the two models can be attributed to the following two facts: (1) the proposed model utilizes parabolic functions, whereas the Weiser et al. (2013) model is based on a multi-linear spectral amplification function; and (2) the model proposed by Weiser et al. (2013) utilizes a constant spectral amplification factor (independent of mode shape of the supporting structure) corresponding to the second mode of vibration. Further, the model proposed by Weiser et al. (2013) does not account for inelasticity of the supporting structure, and thereby produces very conservative floor spectral acceleration demands for inelastic supporting structures.

For the 15-storey frame-shear wall building (15SW), the relative performance of all the models is similar to that in the case of the 8-storey building, except that the proposed (median) amplification function is slightly non-conservative for some of the time histories (Fig. 6.22), in the impact zone of the second mode. Nevertheless, it is predicting the closest estimates to the numerical results, among all the considered models.

The proposed amplification function predicts the floor response spectra in good agreement with the spectrum-compatible time-history analyses, for short-period as well as long-period buildings, in the whole spectral range, and for all the considered values of strength ratio, R. The proposed method is much more comprehensive than the available models, as it takes into account the ground-motion characteristics, dynamic characteristics of the building (both periods and mode shapes), strength ratio of the building, and period of vibration of the NSC. It is interesting to note that although the proposed floor amplification functions have been developed using a numerical study on RC frame buildings, these predicts a reasonably accurate floor response of the considered RC frame-shear wall (dual system) building, justifying the

underlying principle i.e. the use of dynamic characteristics of the supporting structure and ground-motion characteristics in predicting the floor response spectrum.

(a) Elastic, $Z/H = 0.50$ (b) Elastic, $Z/H = 1.00$

(c) $R = 3.50$, $Z/H = 0.50$ (d) $R = 3.50$, $Z/H = 1.00$

| Proposed model —— | EC8 —— | Petrone et al. (2015b) —— | B–ICC000 —— | HE–11140 —— |
| | FEMA ·········· | Weiser et al. (2013) ·········· | CHY101 —— | |
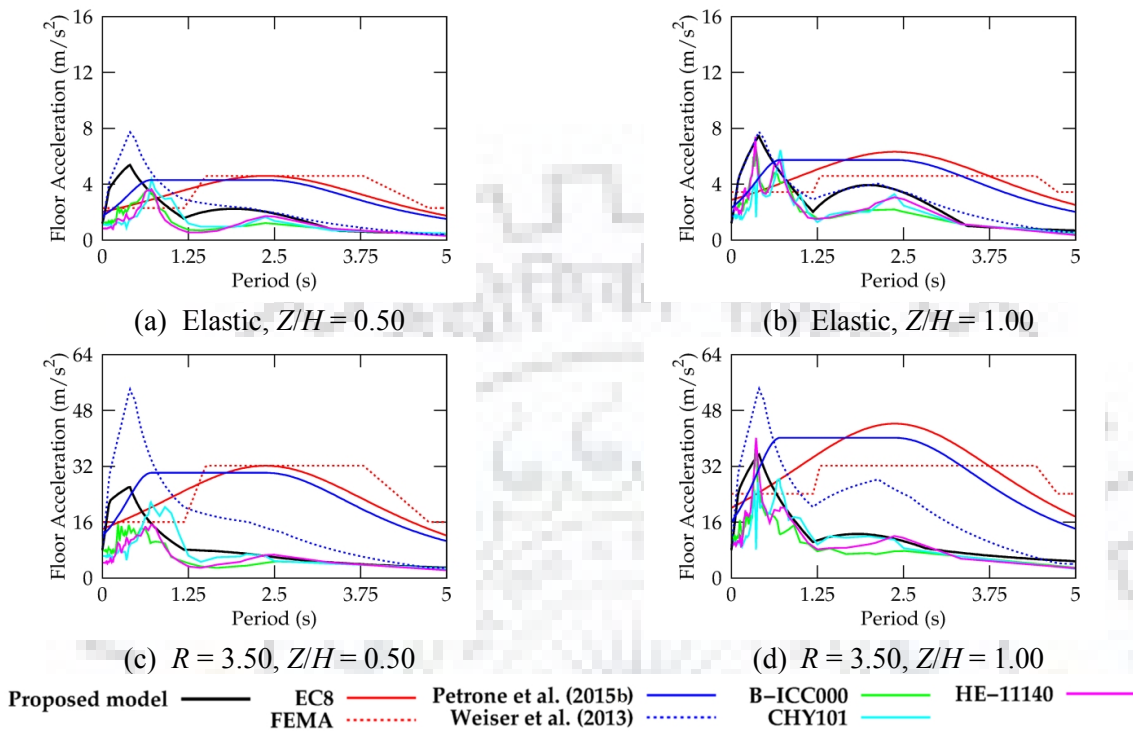
Fig. 6.22 Comparison of floor spectra for 15-storey shear-wall building obtained using the proposed function with those obtained from spectrum-compatible time-history analyses, from models by Weiser et al. (2013) and Petrone et al. (2015b), and from design codes.

6.5 SUMMARY

A-state-of-the-art on performance of the non-structural components has been presented. IDA was performed on a set of RC frame building models in order to obtain the floor response considering the different levels of inelasticity. The peak floor acceleration demands are studied for different levels of inelasticity. In order to identify critical parameters affecting the floor response, the floor response was normalized by three different normalization schemes, viz. normalization with respect to PGA, PFA, and $S_{AG}(T)$. The following observations are made:

- It is observed that PFA reduce with increase in period of vibration of the supporting structure as well as inelasticity, resulting the code profiles to be very conservative (ASCE 41, EN 1998, NZS 1170.5 and IS 1893 Draft) for long-period buildings and non-conservative (IS 1893 Draft and EN 1998) for short-period buildings. For higher level of inelasticity ($R = 3.50$), the PFA at the level of roof is observed to be even lesser than PGA.

- A PFA demand prediction model is developed and validated, which takes into account the effect of period of vibration as well as inelasticity of the supporting structure.

- It is observed that the normalization of floor spectrum, with respect to $S_{AG}(T)$ leads to the least coefficient of variation as compared to the normalization with respect to PGA and PFA, indicating that floor response spectrum is better correlated to $S_{AG}(T)$ than PGA and PFA.

- The spectral amplification factors corresponding to the fundamental and second modes of vibrations, for a given level of inelasticity, vary with the structure's period within a COV of the order of 17%; hence can be assumed to be independent of the period of vibration. Further, the spectral amplification factors along the height approximately follow the elastic mode shapes.

- Based on these observations, spectral amplification functions are developed. The proposed spectral amplification functions can be used with a code-based design response spectrum as well as a site-specific response spectrum to construct the floor spectrum. The proposed method is more comprehensive than available models as it takes into account the ground-motion characteristics, the dynamic characteristics of the building (both periods and mode shapes), the level of inelasticity expected in the building, and the period of vibration of the NSC.

- The proposed spectral amplification functions were validated using spectrum-compatible time-history analyses of short- and long-period buildings, including a frame-shear wall building, and compared with the design code models. It was observed that the current code models under-predict the floor response in case of short-period buildings under elastic response, and highly over-predict in case of long-period buildings. Further, these models do not consider the peaks corresponding to higher modes of vibration. The proposed model overcomes these limitations, since it takes into account the peaks corresponding to fundamental and second mode of vibration as well as the inelasticity of the structure. The proposed amplification function is particularly useful for performance based design as it can be used to develop design floor response spectra that are consistent with the targeted performance of the building structure.

CHAPTER 7

FLOOR RESPONSE OF IRREGULAR BUILDINGS

7.1 INTRODUCTION

As described in earlier chapters, the hill buildings have irregular structural configurations resulting in significantly different dynamic characteristics (periods and mode shapes) when compared with their counterparts resting on flat land. It has already been identified in the earlier studies (e.g., Lucchini et al. 2014) as well as in the previous Chapter (Chapter 6) that the dynamic characteristics play a crucial role in predicting floor acceleration demands. Further, the hill building structural configurations have torsional irregularity in cross-slope direction, which is further expected to influence the floor acceleration demand. Therefore, it becomes necessary to study the floor acceleration demands in hill building structural configurations.

In this Chapter, a state-of-the-art on floor acceleration demand prediction in context of irregular buildings is presented. A numerical study on low-, mid-, and high-rise SC B and SC C structural configurations is conducted to study the effect of structural configuration and torsional irregularity on the floor acceleration demand. Based on the observations and identified parameters governing the floor response of SC B and SC C structural configurations, floor acceleration demand prediction models are developed.

7.2 PAST STUDIES ON FLOOR ACCELERATIONS IN IRREGULAR BUILDINGS

Contrary to regular buildings, very few studies have focused on floor response of irregular buildings (Mohammed et al. 2008; Aldeka et al. 2014a; Aldeka et al. 2014b; Aldeka et al. 2015). Mohammed et al. (2008) carried out experimental investigations on NSCs mounted on stiffness- and mass-eccentric torsionally yielding supporting structures using shake table tests. It was reported that the torsional yielding of the supporting structure has significant implications for de-amplification of near tuned secondary system response. Aldeka et al. (2014a, b) studied the effect of ground type (site class) and eccentricity ratios on the seismic response of NSCs mounted on asymmetric inelastic RC buildings. It was observed that the NSCs attached to the flexible sides of taller buildings were more affected by torsional behaviour as compared to shorter buildings. The floor acceleration demand on the flexible side

(FL) was observed to be, on average, 42% higher as compared to that at the centre of rigidity (CR). They also observed that the increase in torsional behaviour resulted in increased accelerations for NSCs mounted on the flexible side (Aldeka et al. 2015). They further concluded that EN 1998-1 predictions were underestimated by 36% and 28.2%, for site class A and E, respectively, for NSCs attached to the flexible side under tuned conditions. Later on, it was attributed to the fact that the EN 1998-1 model does not take into account the floor amplification caused by torsional response of the supporting structure (Aldeka et al. 2014b, 2015). In addition, the torsional amplification factors (defined as the ratio of peak component acceleration of the NSC at the FL to that at the CR) were found to be well correlated with the floor rotation as well as angular accelerations (Aldeka et al. 2014b, 2015).

7.3 NUMERICAL STUDY: FLOOR RESPONSE OF IRREGULAR HILL BUILDINGS

In the present study, a set of SC B and SC C reinforced-concrete (RC) frame buildings with identical plan shapes (as shown in Figs. 3.9 and 4.1) are investigated. The heights of these model buildings are 2-, 4-, and 8-storeys, respectively, representing the low-, mid-, and high-rise building stock in hilly regions of northern India. Based on previous studies (Singh et al. 2012) and also observations made in Chapter 4, the supporting structure's height above the uppermost foundation level has been considered to define the number of storeys of hill buildings. It is based on the observation that only the building portion above the uppermost foundation level participates in the fundamental mode of vibration. Therefore, period and mode shape corresponding to the fundamental mode of a hill building are observed to be very close to those of a building resting on flat land with number of storeys same as the building height above the uppermost foundation level. The same definition consistent with previous sections (Section 4.5) has been adopted in the present study. The storey height is set constant to 3.30 m.

The 3D structural models are created in the integrated building analysis and design software ETABS 2016 (CSI 2016). Beams and columns are modelled using frame elements while the slabs are modelled as rigid diaphragms. The cracked section properties of both RC beams and columns are derived following the ASCE/SEI 41-13 (2013) guidelines. Dead loads and live loads on the buildings are assigned according to IS 875 Part 1 (1987a) and IS 875 Part 2 (1987b), respectively. The buildings are designed as special moment resisting frames (SMRF)

according to the Indian standards IS 456 (2000) and IS 1893 Part 1 (2016) for seismic zone V on soil type I (rock and hard soil). P-delta effect is also considered in the analysis and the design.

7.3.1 Dynamic Characteristics of the Considered Buildings

Table 7.1 provides an overview of the dynamic characteristics (periods and modal mass participation ratio) of the considered SC B and SC C structural configurations. It can be observed that both the SC B and the SC C structural configurations have uncoupled modes of vibration in the two orthogonal directions. It is interesting to note that the ratio of the second mode period to the first mode period is close to 0.3 which is consistent with the findings of earlier studies on regular frame buildings (Chapter 6), except for the case of the 2-storey SC B building (BL-RC-R6; Table 7.1), in which there is a coupled vibration of the portions above and below the uppermost foundation level.

Table 7.1 Dynamic characteristics of the considered building models.

Building Model		Period of Vibration (s)			Period Ratio		Modal Mass Participation Ratio (%)		
String	Direction	First mode (T_1)	Second mode (T_2)	k^{th} mode (T_k)	T_2/T_1	T_k/T_1	α_{m1}	α_{m2}	α_{mk}
BL-RC-R6	Along-slope	0.84	**0.75**[*]	**0.75**[*]	0.89	0.89	08	**61**[#]	**61**[#]
	Across-slope	1.23	**0.99**[*]	**0.99**[*]	0.80	0.80	07	**61**[#]	**61**[#]
BM-RC-R6	Along-slope	1.20	0.38	0.56	0.32	0.47	47	07	25
	Across-slope	1.78	0.51	0.73	0.29	0.41	44	10	25
BH-RC-R6	Along-slope	2.55	0.88	0.48	0.35	0.19	58	07	18
	Across-slope	4.05	1.26	0.64	0.31	0.16	58	06	18
CL-RC-R6	Along-slope	0.81	0.26	0.17	0.32	0.21	38	04	39
	Across-slope	1.20	0.36	0.31	0.30	0.26	38	22	16
CM-RC-R6	Along-slope	1.19	0.38	0.13	0.32	0.11	52	06	26
	Across-slope	1.78	0.52	0.25	0.29	0.14	52	08	16
CH-RC-R6	Along-slope	2.57	0.89	0.11	0.35	0.04	61	08	17
	Across-slope	4.07	1.27	0.22	0.31	0.05	61	08	06

α_{m1}, α_{m2} and α_{mk} - modal mass participation ratios corresponding to the fundamental, second and k^{th} modes of vibration in a given direction of excitation. The kth mode represents the significant mode of vibration of the building portion below the uppermost foundation level. * - period of the combined mode of vibration (both the building portions, below and above the uppermost foundation level, vibrating together). # - modal mass participation corresponding to the combined mode of vibration.

Figure 7.1 presents the normalized mode shapes of the 2- and 8-storey SC B and SC C structural configurations. The considered building models have significantly different modes of vibration when compared with buildings resting on flat land. In the first two modes, only the building portion above the uppermost foundation level vibrates, resulting in almost identical periods and mode shapes for the first two modes of vibration in case of SC B and SC C

181

structural configurations. The lower portion (below the uppermost foundation level) in case of both the buildings contributes only to a certain higher mode which is represented by index k (since its number varies from building to building) in Table 7.1 and Fig. 7.1. The observed trends are consistent among all building models investigated in this study, except for the 2-storey SC B building. In case of the 2-storey SC B building (BL-RC-R6), the portions below and above the uppermost foundation vibrate in a combined mode (Fig. 7.1a) resulting in a significantly different period ratio and mass participation corresponding to the second mode of vibration, when compared with other building models investigated in this study. This observation can be attributed to the fact that the stiffnesses of the building portions below and above the uppermost foundation are closer in case of the 2-storey SC B building (BL-RC-R6), as compared to the other buildings, and the two portions vibrate in harmony with each other. This trend is not observed in case of the 2-storey SC C building (CL-RC-R6), since its portion below the uppermost foundation is relatively rigid, due to the presence of ground-connected columns in each storey below the uppermost foundation level.
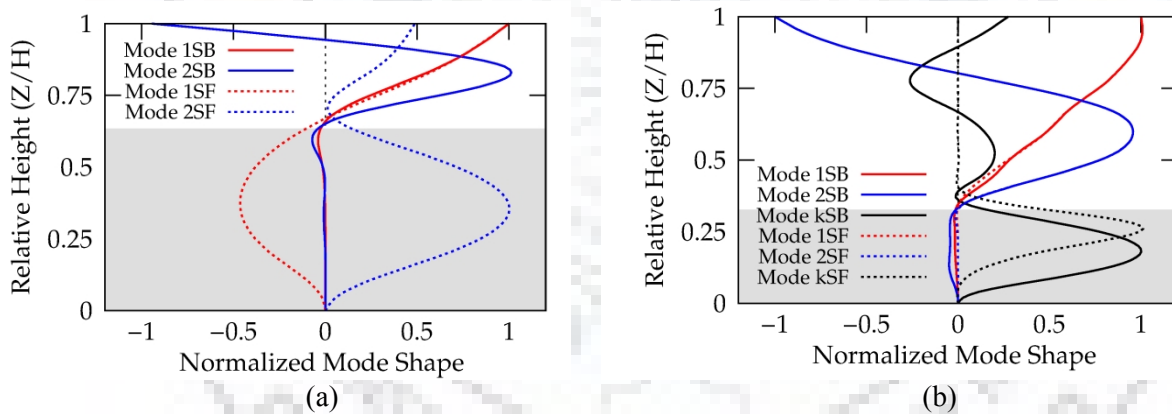
Fig. 7.1 Comparison of mode shapes between SC B and SC C structural configurations: (a) 2-storey building; and (b) 8-storey building. (The gray-shaded area shows the building portion below the uppermost foundation level).

7.3.2 Torsional Irregularity in Considered Structural Configurations

In order to quantify the effect of torsion, seismic design codes define either the ratio of maximum to minimum/average inter-storey drift (ASCE 7 2010; IS 1893 Part 1 2002; IS 1893 Part 1 2016) or the distance between the CR and the CM, i.e. floor eccentricity (EN 1998 2004). In case of multi-storey buildings, two different definitions of CR are available (Basu and Jain 2007). In the first case, the CR is defined by a set of points located on each floor through which

the application of the lateral load profile would not cause rotation of any floor. In the second case, the CR is represented for a single floor such that the application of lateral load at this point would not cause any rotation of that floor, while the other floors may rotate (Basu and Jain 2007). ASCE 7 (2010) defines a building to be torsionally irregular if the ratio of maximum to average inter-storey drift exceeds 1.20. On the other hand, according to the provisions of EN 1998-1, torsional irregularity is said to exist if the normalized eccentricity (defined as the ratio of floor eccentricity, e to torsional radius, r) exceeds a value of 0.30.

In this study, the single floor definition of CR has been adopted to compute the eccentricity of the considered supporting structures at different floor levels. Figure 7.2 presents the variation of normalized floor eccentricity (e/b, where b is the dimension of the floor, normal to the seismic excitation) along the height of the considered SC B and SC C buildings. As these building models do not have any eccentricity in the along-slope direction, the e/b ratio is presented for the across-slope direction only. It can be observed that in case of the SC C building, each storey below the uppermost foundation level has significant torsional effects due to presence of short-columns on the uphill side in each storey, while the maximum torsional effects occur in the storey just above the uppermost foundation level. On the other hand, in case of the SC B building, only the storey just above the uppermost foundation has significant torsional effects due to the presence of short-columns in that particular storey (Fig. 4.1b and 4.1c). The observed trends and the range of eccentricity are consistent among all the building models investigated in this study.

7.3.3 Analysis Methodology

In order to investigate the floor response of the considered structural models, bi-directional linear time-history analyses have been performed using the suite of 22 far-field recorded ground-motions, as identified in the FEMA P695 (2009) project. To conduct time-history analyses, both the horizontal components of a ground-motion record are applied simultaneously, along the two orthogonal directions (i.e., along- and across-slope). To model damping effects in time-history analyses, a Rayleigh damping of 5% has been assigned at periods corresponding to the first mode and the mode resulting in a total of 95% cumulative mass participation in both the directions. The floor acceleration demands in each building are evaluated at two locations (CR and FL) on each floor.
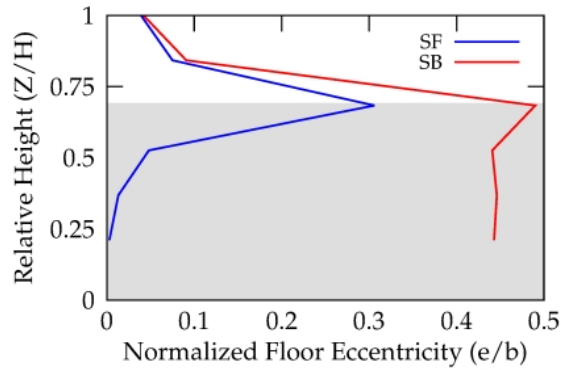
(a) 2-storey buildings
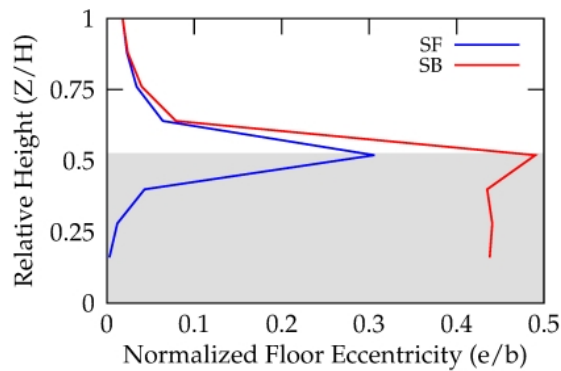
(b) 4-storey buildings
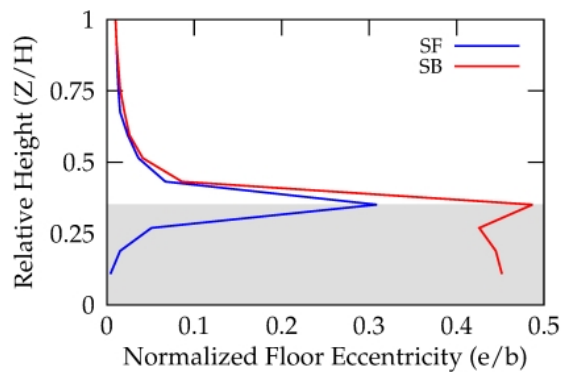
(c) 8-storey buildings

Fig. 7.2 Comparison of floor eccentricities of the considered SC B (SF) and SC C (SB) structural configurations. (The gray-shaded area shows the building portion below the uppermost foundation level).

7.4 RESULTS AND DISCUSSION

All the six building models have been analyzed for both horizontal components of the 22 ground-motion records that were applied simultaneously in the two orthogonal directions (i.e., along- and across-slope). Figure 7.3 compares the variation of median PFA/PGA ratio with two different code models. It can be observed that both FEMA P750 (and also ASCE 7) and EN

1998-1 significantly underestimate the PFA, particularly in the building portion below the uppermost foundation level, for both SC B and SC C structural configurations. The reason for this observation can be attributed to the fact that code models for predicting PFA are based on the assumptions that the building response is dominated by the fundamental mode of vibration and it can be assumed to be varying linearly along the height of the building. However, in both SC B and SC C structural configurations, the building portion below the uppermost foundation level does not participate in the fundamental mode of vibration, but vibrates in a higher (indicated as k^{th} mode, in this study) mode of vibration. Thereby, current code models are unable to capture the PFA demands in the building portion below the uppermost foundation level.
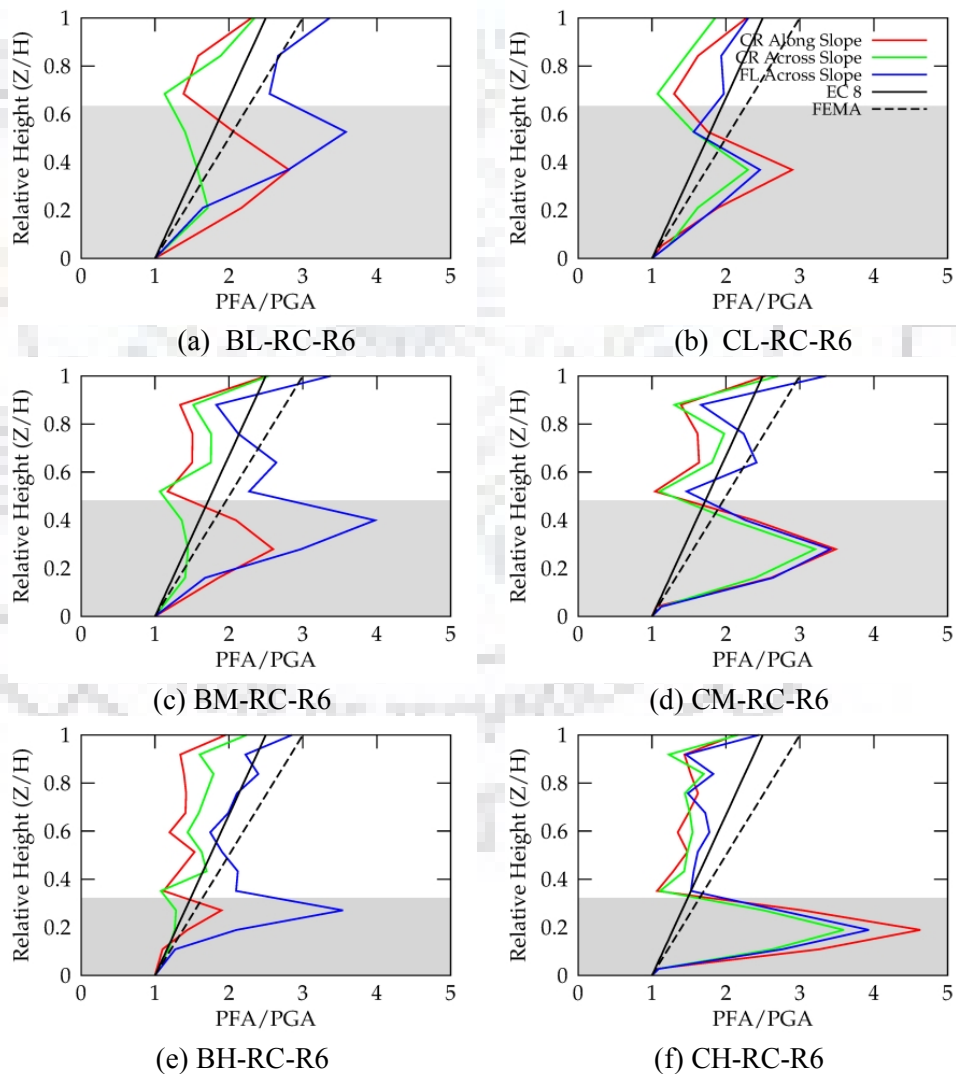
Fig. 7.3 Comparison of the ratio of PFA/PGA for SC B and SC C structural configurations with current code models. (The gray-shaded area shows the building portion below the uppermost foundation level).

185

For the building portion above the uppermost foundation level, the code models are reasonably accurate in predicting the floor acceleration demand at the CR, while these slightly underestimate the floor acceleration demand at FL, in some cases, particularly at the roof level. This occurs due to the combined effects of torsion and whiplashing of higher modes. It is interesting to note that the variation of PFA/PGA below the uppermost foundation level has a shape similar to the kth mode shape of vibration, for both SC B and SC C structural configurations (Figs. 7.1 and 7.3). The PFA demand is observed to be the highest at the same floor, where the kth mode has the highest ordinate. This provides an important insight that the kth mode shape of the SC B and SC C structural configurations can be utilized in predicting the floor accelerations below the uppermost foundation level. Further, the maximum value (occurring at the floor level having maximum ordinate in the kth mode shape) of median PFA in the portion below the uppermost foundation level is observed to be equal to 4 times PGA.

Figure 7.4 presents a comparison of the 5%-damped median Floor Response Spectrum (FRS) profiles for the 4-storey SC C structural configuration (CM-RC-R6) with those obtained from EN 1998-1 and FEMA P750 models. The presented FRS are normalized by Peak Floor Acceleration (PFA), Peak Ground Acceleration (PGA), and Ground Response Spectrum (GRS) and shown for cross-slope direction at the FL. Similar results have also been obtained for the along-slope direction and other buildings. The FRS normalized by PFA (Figures 7.4a-d) represents the component amplification factor, a_p. Sharp peaks are observed in the FRS, corresponding to modes of vibration of the building, contributing at the floor level under consideration. The peak values of the FRS normalized by PFA, corresponding to the fundamental mode of vibration, are within the maximum value of 2.5 recommended in FEMA P750 (and also in ASCE 7). However, the code models significantly underestimate the component amplification (a_p), near periods of higher modes of vibration of the supporting structure, as these models completely ignore the peak in FRS corresponding to higher modes of vibration. This observation is in good agreement with the previous studies on regular multi-storey buildings (e.g., Weiser et al. 2013; Lucchini et al. 2014). Further, the component amplification (a_p) at the FL of a lower floor ($Z/H = 0.28$), is approximately 50% higher than the corresponding value at the CR, under tuned condition with second and k^{th} modes of vibration. This increase in component amplification at the FL can be attributed to significant torsional effects in lower storeys, in case of SC C structural configuration.

Figures 7.4(e-h) present the FRS normalized by the PGA. The peak value of the PGA-normalized FRS is of the order of 12 (corresponding to the kth mode, at $Z/H = 0.28$) and 11 (corresponding to the second mode, at $Z/H = 1.00$). These normalized spectra represent the combined effect of PFA amplification and component amplification in the code models, and depend on the spectral shape of the ground-motion record and its amplification by the supporting structure, and therefore also depend on the dynamic and torsional characteristics of the supporting structure. These code models are found to be fairly accurate in the vicinity of the fundamental mode of vibration but are highly non-conservative in the vicinity of the higher modes of vibration, at both CR and FL.

Figures 7.4(i-l) present the FRS normalized by the respective GRS of the horizontal component of ground-motion in the direction under consideration. These curves directly represent the spectral amplification factors as a function of normalized period. Contrary to the FRS normalized by the PFA (Fig. 7.4(a-d)) or PGA (Fig. 7.4(e-h)), the peaks corresponding to the higher modes of vibration are less prominent in these curves, due to the characteristic spectral shape of GRS, which have their peaks in the short-period range. It is interesting to note that, at the CR in lower floors, a more or less constant amplification is observed in the whole period range of the FRS, when normalized by GRS. This indicates that the original shape of the GRS is retained in the portion below the uppermost foundation level, except under tuned condition with the kth mode of vibration, where a local peak occurs. This peak gets significantly amplified (up to 4 times) at the FL of the floor having the peak ordinate of the kth mode shape and found to be higher in case of SC C structural configurations as compared to SC B structural configurations.

The increased amplification in SC C structural configuration, as compared to SC B structural configuration can be attributed to relatively higher torsional effects in the SC C structural configuration, due to increased floor eccentricities. Interestingly, except at the periods close to the kth mode of vibration, the FRS at both CR and FL converge (Fig. 7.4i). The observed trends in amplification pattern are similar in case of SC B structural configurations also (BM-RC-R6; Fig. 7.5), but the effect of torsional amplification of floor acceleration is less pronounced in case of SC B structural configuration due to reduced eccentricity (Fig. 7.2).
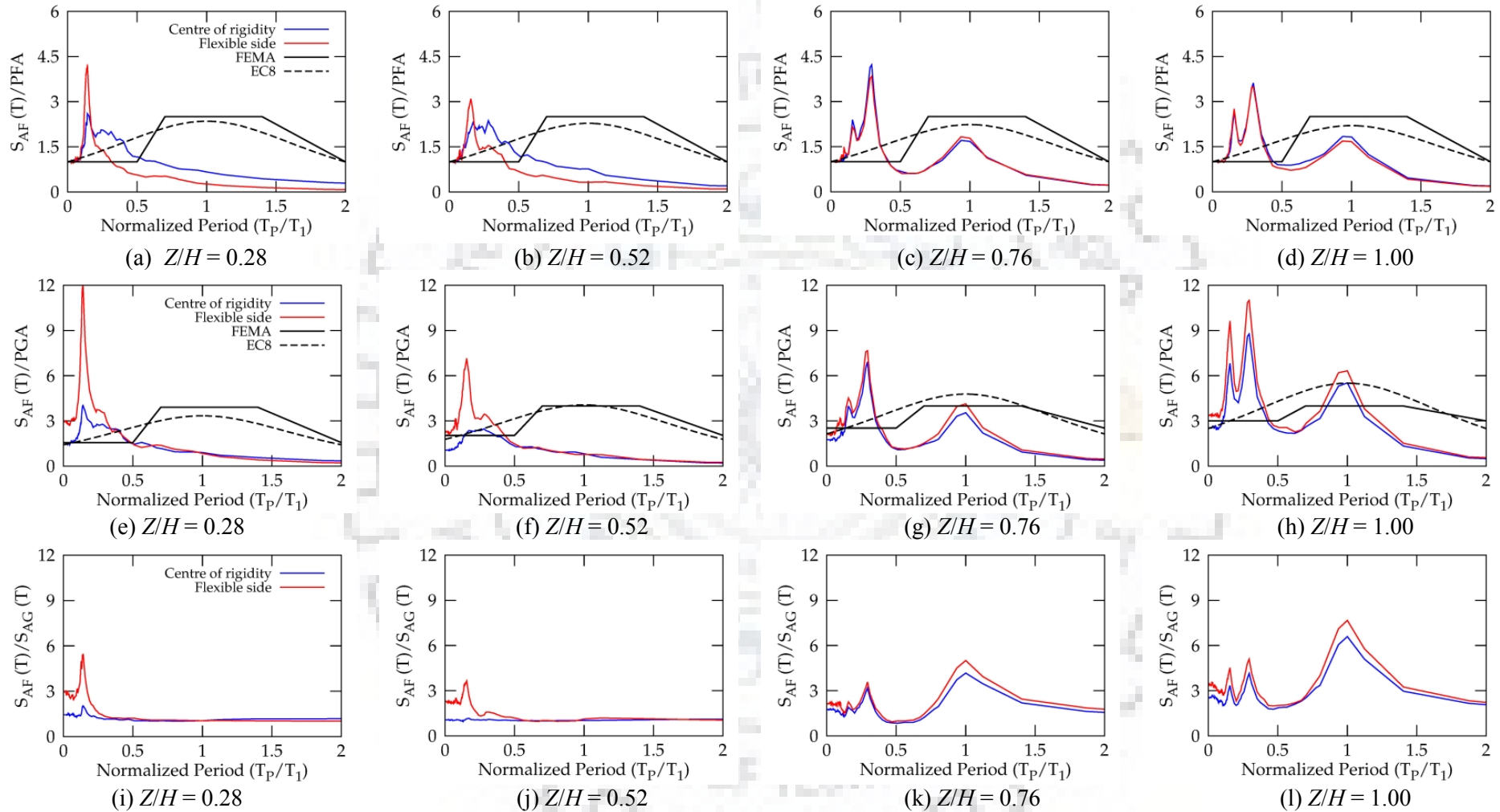
Fig. 7.4 Comparison of the median 5%-damped floor spectrum profiles with current code models when normalized by PFA, PGA and GRS, for 4-storey building with SC C structural configuration (CM-RC-R6).

(a) $Z/H = 0.28$ (b) $Z/H = 0.52$ (c) $Z/H = 0.76$ (d) $Z/H = 1.00$

(e) $Z/H = 0.28$ (f) $Z/H = 0.52$ (g) $Z/H = 0.76$ (h) $Z/H = 1.00$

(i) $Z/H = 0.28$ (j) $Z/H = 0.52$ (k) $Z/H = 0.76$ (l) $Z/H = 1.00$
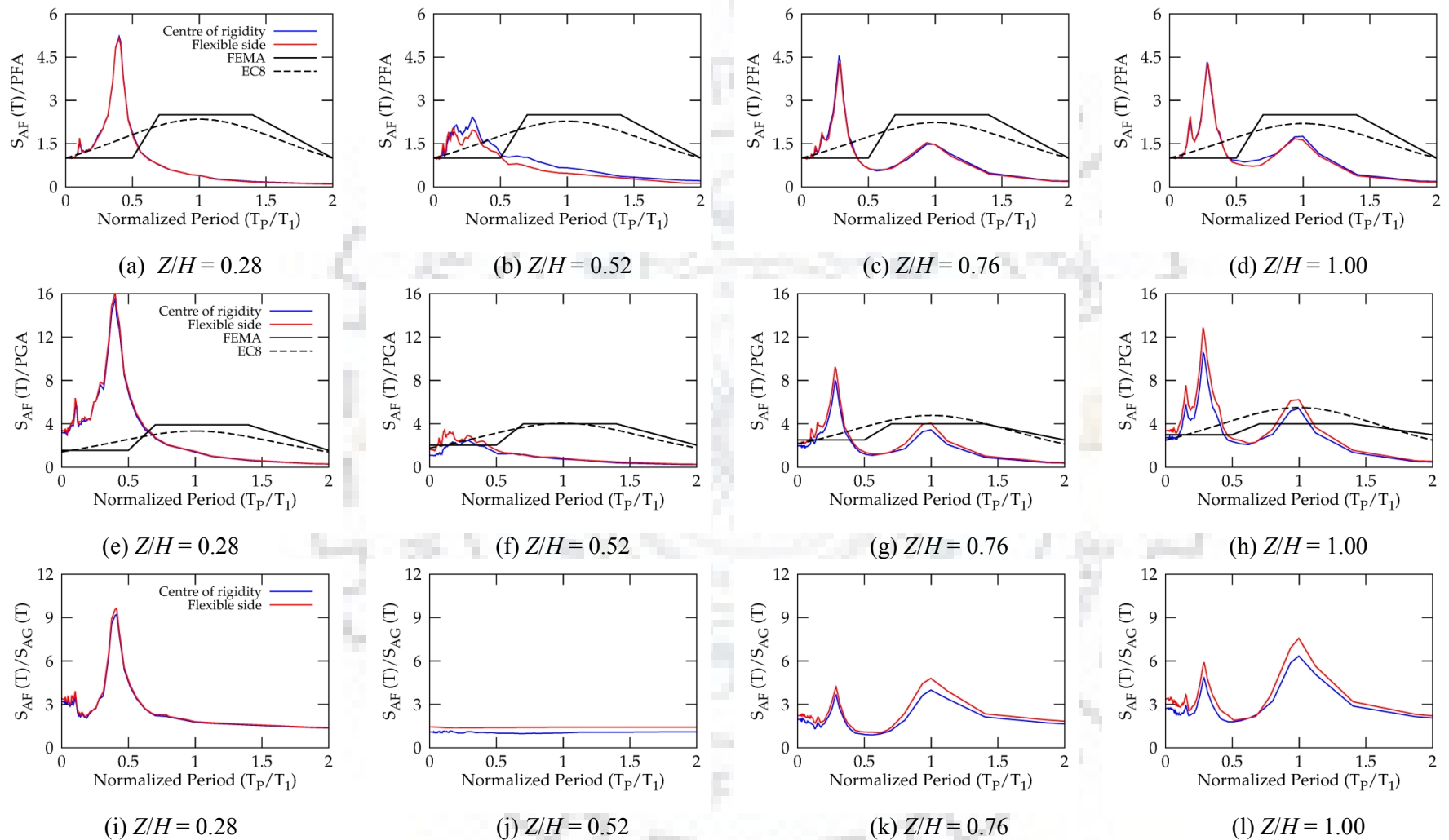
Fig. 7.5 Comparison of the median 5%-damped floor spectrum profiles with current code models when normalized by PFA, PGA and GRS, for 4-storey building with SC B structural configuration (BM-RC-R6).
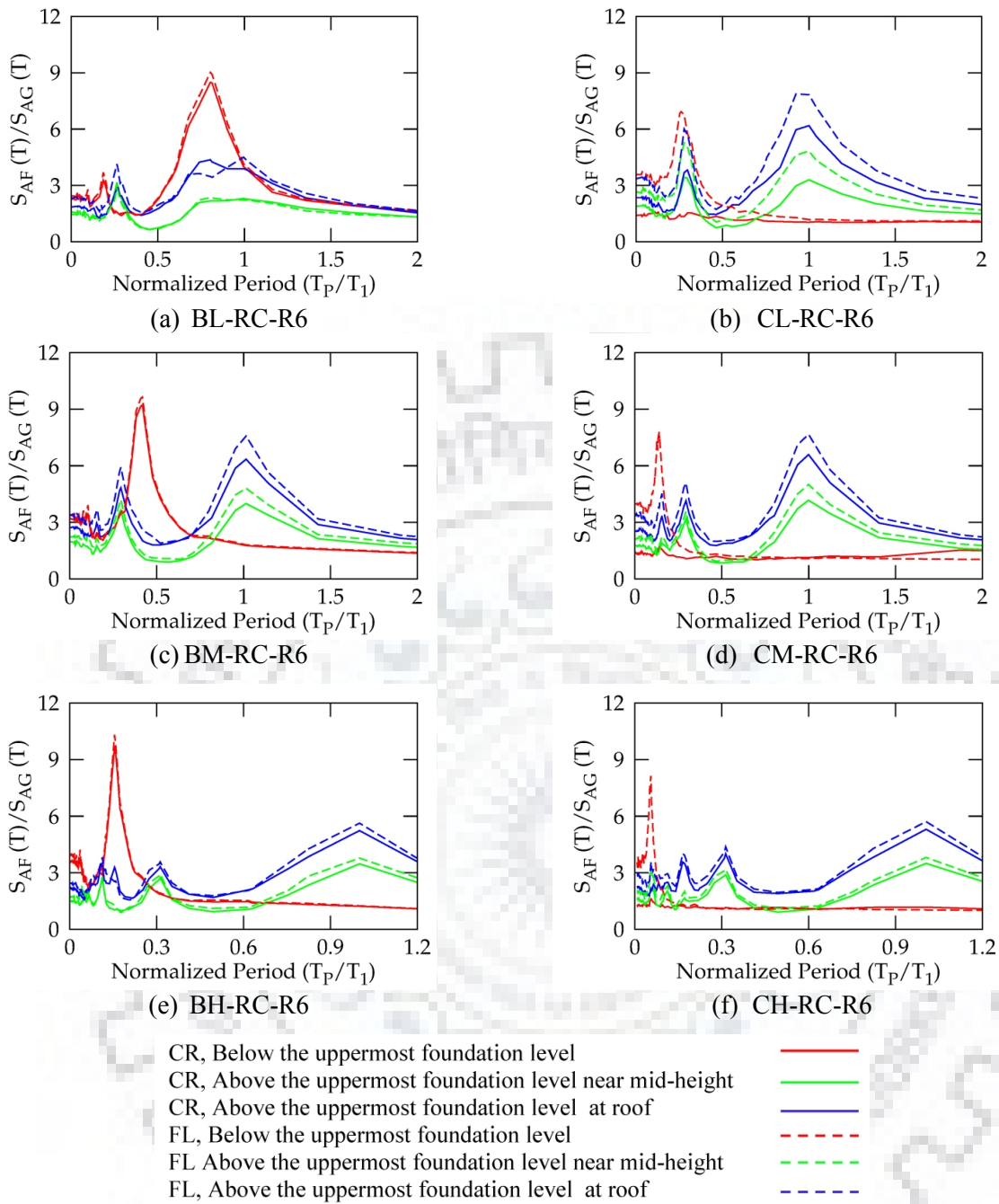
Fig. 7.6 Comparison of the median 5%-damped floor spectra normalized by GRS, for the considered building models.

Figure 7.7 compares the coefficients of variation (COV) of the FRS normalized by the respective PGA, PFA and GRS, for the considered 22 ground-motion records. The COV is shown at two different relative heights (i.e., Z/H = 0.52 and 1.00) for the 4-storey SC B and SC C structural configurations. It is observed that, in general, for any given period of vibration of the NSC, the prediction of floor accelerations through PGA has a higher COV as compared to the GRS. This observation is consistent among all the investigated buildings and also found to be in agreement with the findings on regular RC frame buildings with structural configuration

SC A, presented in the previous chapter. Hence, the floor response of the considered hill buildings has also been studied in terms of the amplification factor with respect to the GRS.
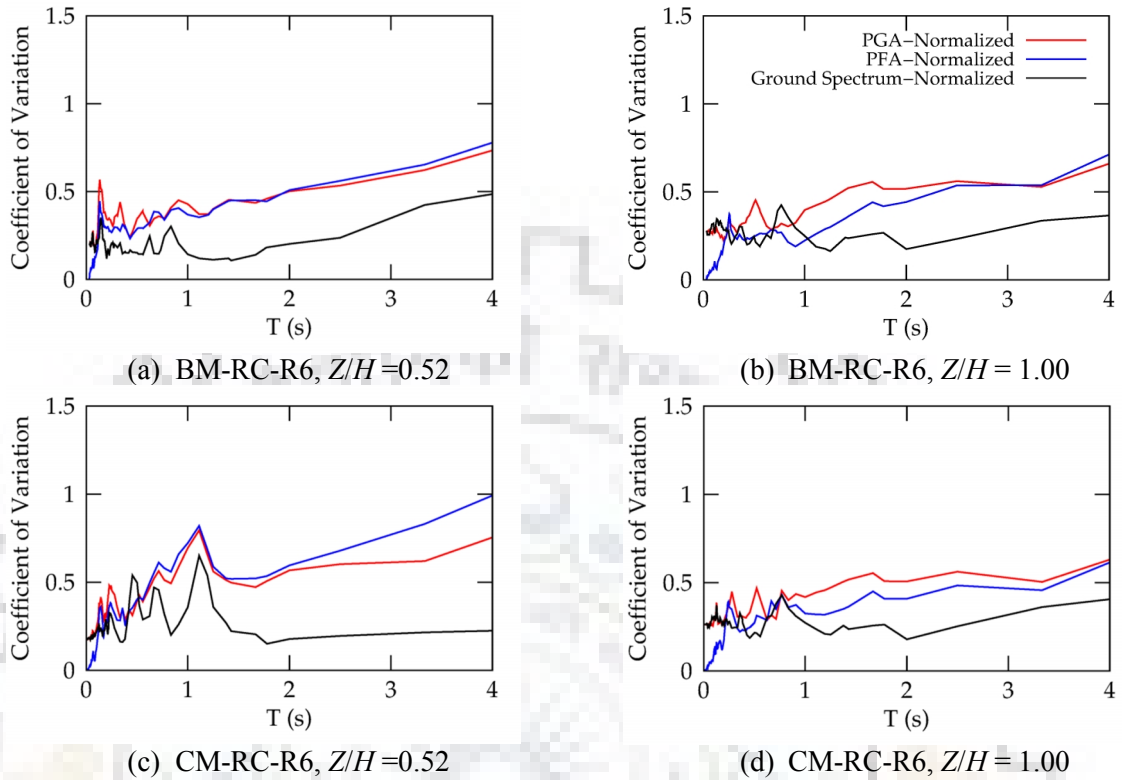
Fig. 7.7 Comparison of coefficient of variation in FRS of 22 ground-motion records normalized by PFA, PGA and GRS, for 4-storey building with SC B and SC C structural configurations. The FRS (in cross-slope direction) at FL are utilized to compute the coefficient of variation.

7.4.1 Spectral Amplification Factors

Figure 7.8 presents the variation of the spectral amplification factors corresponding to the fundamental and the kth modes of vibration in both directions (along- and across-slope) at the CR and at the FL, for all the considered hill buildings, normalized by the corresponding mode shape along the building height (i.e. dividing the amplification factor value at the considered natural period and a particular floor level by the ordinate of the normalized mode shape at that particular floor level. Here, the term 'normalized mode shape' represents the mode shape with its maximum ordinate as unity). It is to be noted that only the building portion above the uppermost foundation level vibrates in the fundamental mode of vibration (Fig. 7.1). Therefore, spectral amplification factors corresponding to fundamental mode are presented only for the building portion above the uppermost foundation level. In similar manner, the building portion below the uppermost foundation only participates in k^{th} mode of vibration. Therefore, spectral amplification factors corresponding to k^{th} mode are presented only for the building portion below the uppermost foundation level.

(a) 2-storey buildings, 1st Mode

(b) 2-storey buildings, k^{th} Mode

(c) 4-storey buildings, 1st Mode

(d) 4-storey buildings, k^{th} Mode

(e) 8-storey buildings, 1st Mode

(f) 8-storey buildings, k^{th} Mode

SF CR Along Slope —— SB CR Along Slope ——
SF CR Across Slope – – – SB CR Across Slope – – –
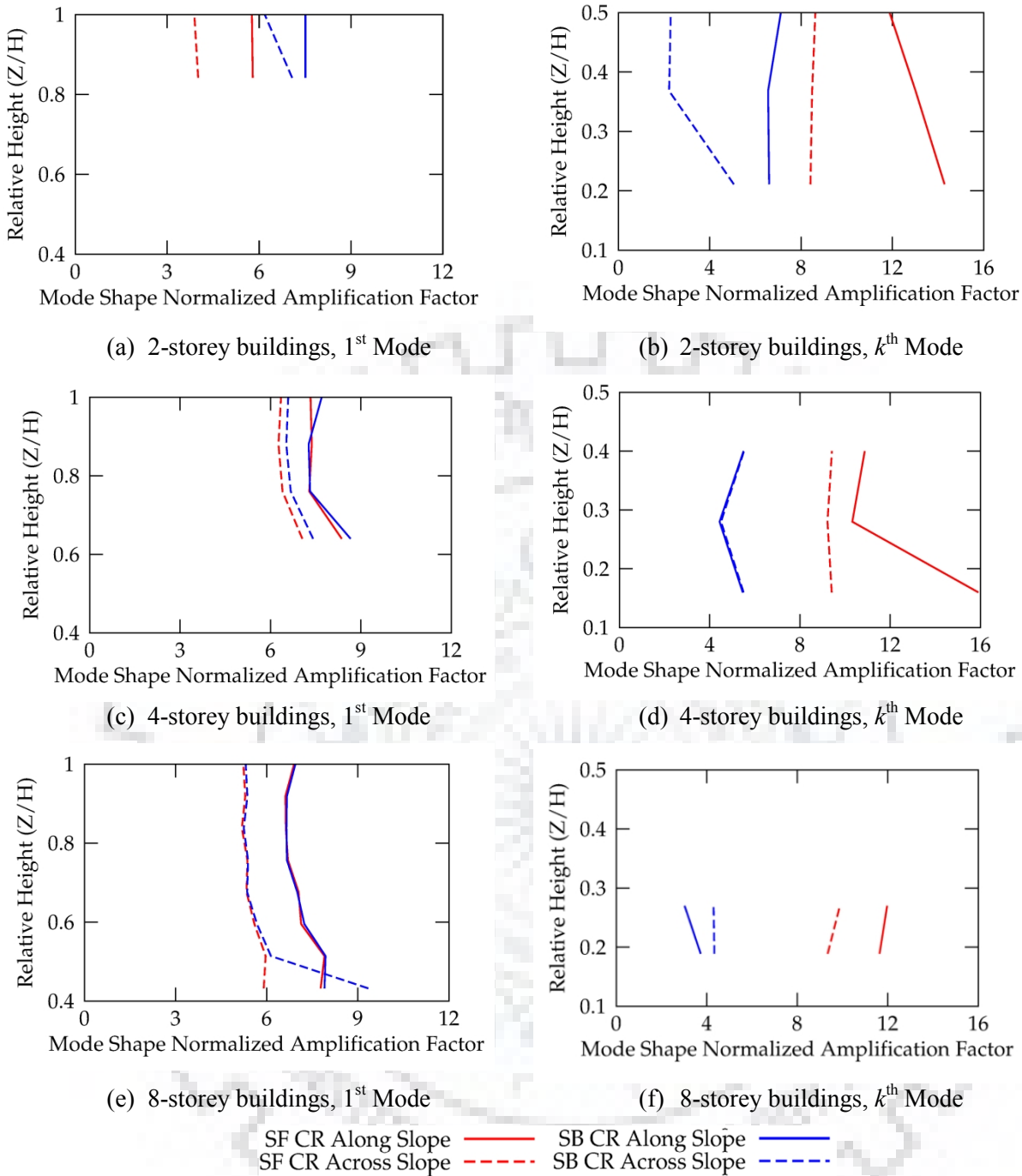
Fig. 7.8 Mode shape normalized spectral amplification factors corresponding to the fundamental and k^{th} modes of vibration of the considered SF (SC B) and SB (SC C) buildings. (The building portion above the uppermost foundation level only is shown, as the first mode does not contribute at the floors below the uppermost foundation level. The building portion below the uppermost foundation level only is shown, as the kth mode does not contribute at the floors above the uppermost foundation level).

It can be observed from the figure that the median spectral amplification pattern, after normalizing with the respective mode shape, can be approximated as a vertical line. This vertical line pattern has been observed corresponding to the fundamental, the second as well as the kth mode of vibration for all the considered buildings. These observations indicate that the variation of peak spectral amplification in the FRS (corresponding to the natural periods) along

the building height can be approximated by the corresponding mode shape (for the fundamental, the second and the kth mode of vibration). This observation is consistent with previous studies on regular frame buildings (Lucchini et al. 2016) as well as results presented in Chapter 6.

Figure 7.9 presents the median spectral amplification factors normalized by the mode shape, corresponding to the fundamental, second, and k^{th} modes of vibration at the CR of the considered SC B and SC C structural configurations, at the different floor levels. These spectral amplification factors corresponding to the fundamental, the second and the kth mode of vibration are distributed with COV of 16%, 20% and 32%, respectively. The median values of the mode shape normalized spectral amplification factors are 6.60, 4.00 and 9.10 and the envelope values are 7.50, 5.00 and 12.00, corresponding to the fundamental, the second and the kth mode of vibration, respectively.
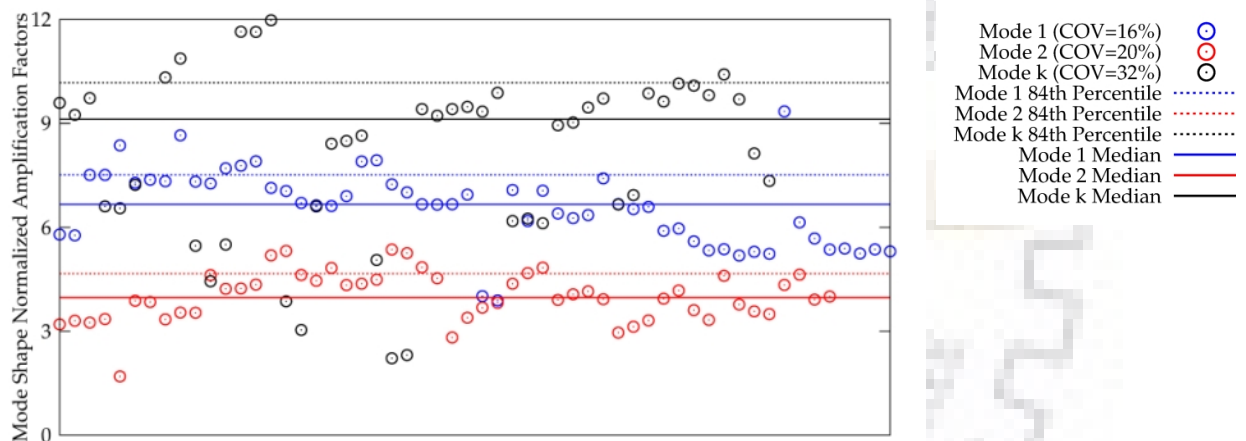
Fig. 7.9 Distribution of the mode shape normalized spectral amplification factors corresponding to the fundamental, the second, and the kth mode of vibration of the considered buildings. (The spectral amplification factors corresponding to the 1st and 2nd modes are shown only for the building portion above the uppermost foundation level whereas the spectral amplification factors corresponding to k^{th} mode are shown only for the building portion below the uppermost foundation level).

The observed values of spectral amplification factors corresponding to the fundamental and second modes of vibration are in general agreement with the findings of previous studies on steel and RC frame buildings and the corresponding reported spectral amplification factors are 7.50 and 3.00, respectively (Weiser et al. 2013). The scatter in spectral amplification factors corresponding to the kth mode of vibration is relatively higher (COV = 32%) as compared to the fundamental and second modes of vibration. Further, in case of SC B structural configurations, spectral amplification corresponding to the kth mode of vibration is relatively on the higher side (with an envelope value of 12, in either of the two directions) as compared to SC C structural configurations (with an envelope value of 5 and 3, in along- and across-slope directions,

respectively). This difference in the spectral amplification corresponding to the kth mode of vibration in SC B and SC C structural configurations can be attributed to the difference in the relative flexibility of the building portion below the uppermost foundation level, in SC B and SC C structural configurations.

7.4.2 Effect of Torsion on Floor Acceleration Response

To study and quantify the effect of torsion on the floor acceleration response in across-slope direction, the FRS are computed at the CR and at the FL, for each of the investigated building models. The torsional acceleration amplification factor (TAF) (θ_T), defined as the ratio of the median spectral amplification at the FL to that at the CR, is computed for each of the three modes of the vibration. Figure 7.10 (a, c, e) presents the variation of the TAF along the height of the building for all the considered building models, corresponding to the fundamental, the second and the kth mode of vibration.

It can be observed that torsional amplification can cause up to 50% increase in floor acceleration demands corresponding to the fundamental and second modes of vibration (except for very few cases in case of second mode of vibration, where it can be up to 300%). As the fundamental and the second mode of vibration do not contribute at lower floors (below the uppermost foundation level), the TAF corresponding to these two modes is close to unity at smaller Z/H (Fig. 7.10a, c and e), whereas it is higher than unity at the upper floors. On the other hand, the TAF corresponding to the kth mode of vibration is significant in the building portion below the uppermost foundation level, and it can cause up to 100% increase in floor acceleration demands (except a very few cases, where it can be as large as 400%). This observation can be attributed to the fact that the considered SC B and SC C structural configurations have significant torsional irregularities in the building portion below the uppermost foundation level (Fig. 7.2). These observations highlight that NSC mounted on of SC B and SC C hill building configurations are subjected to significant torsional amplification effects and the extent of torsional amplification varies along the height, depending on the contributing mode and floor eccentricity. Therefore, an engineering demand parameter to quantify torsional amplification in floor accelerations is required.

It has already been identified (Aldeka et al. 2014a; Aldeka et al. 2014b; Aldeka et al. 2015) that torsional amplification in floor response is strongly correlated with floor rotation. Therefore, to consider the effect of torsion in a simplified manner, a simple parameter, termed as 'torsional drift amplification ratio' (TDR, δ) and defined as the ratio of the displacement at the FL to the

CR, under the seismic action, is used in this study. The advantage of using TDR lies in the fact that it inherently captures the torsional response of the floor and it can be easily computed from 3D dynamic analysis of the hill building. To study the effect of torsional amplification in floor response through TDR, another parameter torsional amplification ratio, η defined as the ratio of TAF (θ_T) to TDR (δ) is explored here.
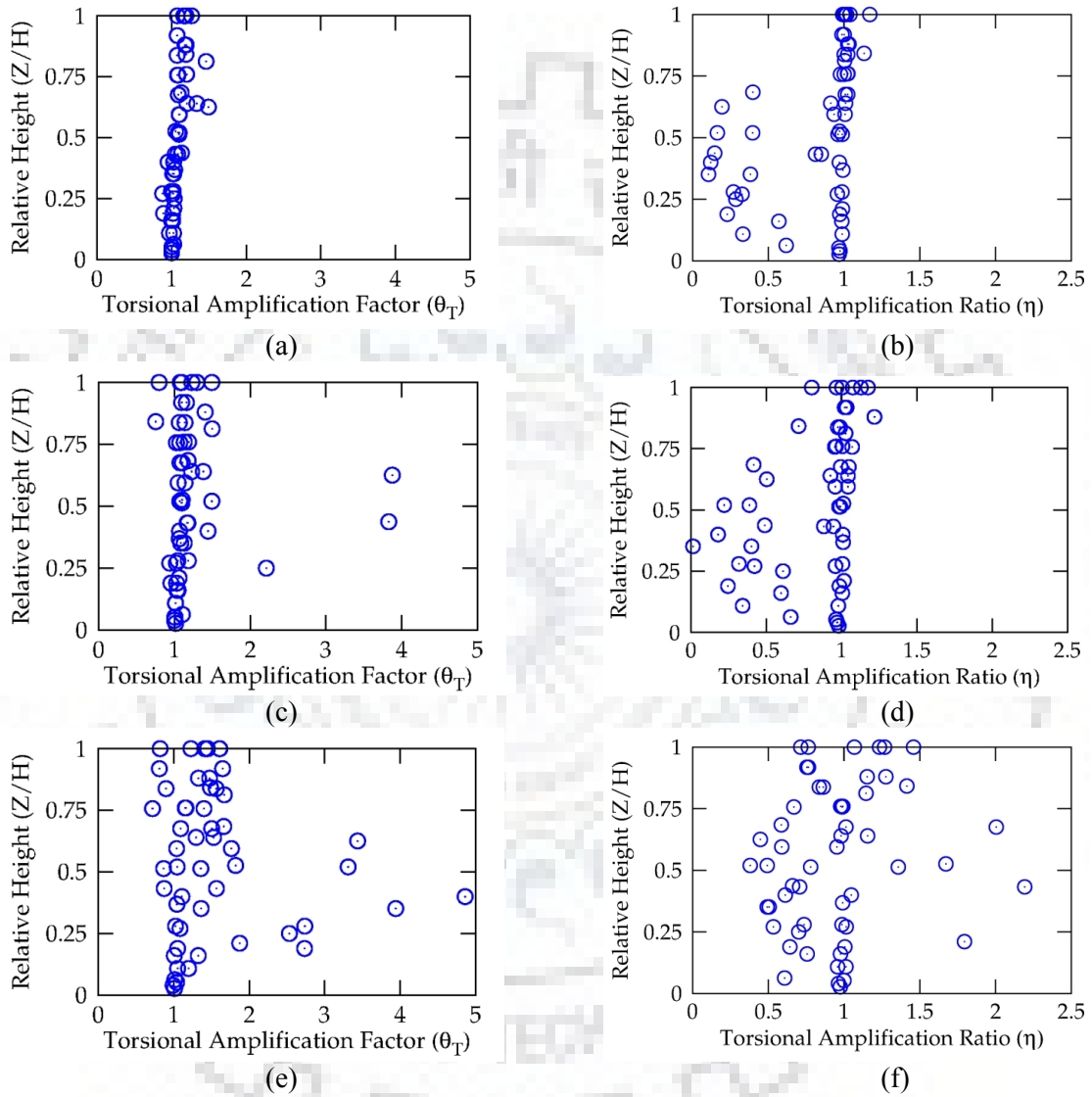
Fig. 7.10 Torsional amplification factor and torsional amplification ratio, corresponding to different modes of vibration of the considered SC B and SC C hill building configurations.

Figure 7.10 (b, d and f) presents the variation of the torsional amplification ratio, η for all the considered building models corresponding to the fundamental, the second and the kth mode of vibration. It is important to note here that TDR is obtained from 3D dynamic analysis; therefore it represents the combined effect of all modes of vibration. It can be observed that the use of the parameter η to predict the torsional floor amplification is fairly accurate in case of the fundamental, the second and the kth mode of vibration (except for a few cases, corresponding to

the kth mode of vibration, and these cases, in particular, correspond to floor levels where the kth mode of vibration has insignificant contribution) with corresponding median values close to unity, in each case. Accordingly, in the subsequent section the torsional amplification effects are considered in terms of TDR (δ).

7.4.3 Proposed Spectral Amplification Functions

Based on the observations made in the previous sections, identification of different parameters governing floor response, and the results obtained from the numerical study, a comprehensive SAF is proposed for SC B and SC C structural configurations. From the proposed SAF, FRS at any floor level can be obtained directly from the GRS, if the building's dynamic characteristics (i.e. mode shapes and periods) and the TDR (δ) are known.

The proposed functions have been developed to capture the peaks corresponding to the first two modes of vibration in the portion above the uppermost foundation level of SC B and SC C hill buildings (Fig. 7.11a). In the building portion below the uppermost foundation level, the proposed model captures the peak corresponding to the kth mode of vibration (Fig. 7.11b). The proposed functions have similarity with the FRS model proposed for regular buildings in the previous chapter, however, this model has a single peak (corresponding to k^{th} mode of vibration) for building portion below the uppermost foundation level. This peak is bounded within impact zones of the kth mode of vibration. For periods outside the impact zone, the model amplifies the GRS by a constant factor depending on the relative height of the floor under consideration.

As observed from Fig. 7.4 (k and l), for the building portion above the uppermost foundation level (i.e., Z/H between 0.76 and 1.00), the normalized period, $T_p/T_1 = 0.5$ acts like a boundary between the impact zones of the fundamental and the higher modes. This demarcation, similar to the regular buildings studied in the previous chapter, is also observed consistently among all the building models investigated in this chapter. In the proposed SAF, the peaks have been represented by separate parabolic functions within the impact zone of each mode. The impact zone of the second mode has been considered between the normalized periods 0 and 0.5, whereas the impact zone of the fundamental mode starts from the normalized period 0.5 and continues up to the point of intersection with the long-period amplification factor (A_L), which is assumed to be constant, depending on the relative height of the floor under consideration. On the other hand, the impact zone of the kth mode of vibration has been considered up to the period at which it becomes equal to the long-period amplification factor.
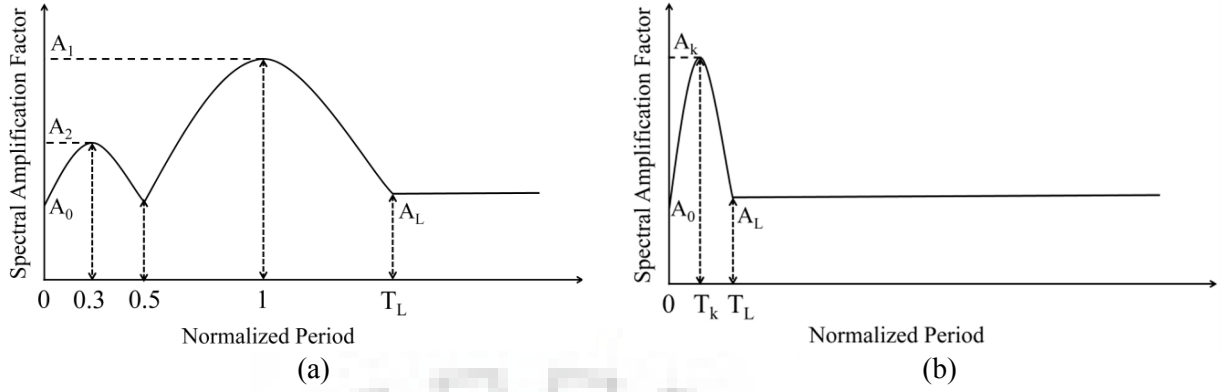
Fig. 7.11 Proposed SAF for SC B and SC C hill buildings: (a) For the building portion above the uppermost foundation level; and (b) for the building portion below the uppermost foundation level.

Based on the results of the numerical study, the SAF for predicting median response has been developed. Based on the observations made in the previous sections, the following expressions for the amplification function (A_0) at zero period are proposed. Equations (7.1) and (7.2) have been developed based on the envelope of the median PFA demands observed for SC B and SC C structural configurations, respectively.

For the building portion above the uppermost foundation level:

$$A_0 = 1 + 2 \times \left(\frac{\phi_{1,i}}{\phi_{1,max}} \right) \leq A_1 \qquad (7.1)$$

and for the building portion below the uppermost foundation level:

$$A_0 = 1 + 3 \times \left(\frac{\phi_{k,i}}{\phi_{k,max}} \right) \leq A_k \qquad (7.2)$$

where, $\phi_{1,i}$ and $\phi_{1,max}$ are the fundamental mode shape coefficients at the ith floor and the corresponding maximum value over all floors, for building portion above the uppermost foundation level, in the direction under consideration; $\phi_{k,i}$ and $\phi_{k,max}$ are the kth mode shape coefficients at the ith floor and the corresponding maximum value over all floors, for building portion below the uppermost foundation level, in the direction under consideration.

The peak values of the amplification function, corresponding to the fundamental, the second and the kth mode of vibration, at i^{th} floor, can be obtained as:

for both SC B and SC C structural configurations:

$$A_1 = 7.50 \times \left(\frac{\delta_{j,i}}{\delta_{cr,i}} \right) \times \left(\frac{\phi_{1,i}}{\phi_{1,max}} \right) \geq 1.00 \qquad (7.3)$$

197

for SC B and SC C structural configurations:

$$A_2 = 5.00 \times \left(\frac{\delta_{j,i}}{\delta_{cr,i}}\right) \times \left(\frac{\phi_{2,i}}{\phi_{2,max}}\right) \geq 1.00 \qquad (7.4)$$

for SC B structural configuration:

$$A_k = 12.00 \times \left(\frac{\delta_{j,i}}{\delta_{cr,i}}\right) \times \left(\frac{\phi_{k,i}}{\phi_{k,max}}\right) \geq 1.00 \qquad (7.5)$$

for SC C structural configuration (along-slope):

$$A_k = 5.00 \times \left(\frac{\delta_{j,i}}{\delta_{cr,i}}\right) \times \left(\frac{\phi_{k,i}}{\phi_{k,max}}\right) \geq 1.00 \qquad (7.6)$$

for SC C structural configuration (across-slope):

$$A_k = 3.00 \times \left(\frac{\delta_{j,i}}{\delta_{cr,i}}\right) \times \left(\frac{\phi_{k,i}}{\phi_{k,max}}\right) \geq 1.00 \qquad (7.7)$$

where, A_1, A_2 and A_k are the spectral amplification factors corresponding to the fundamental, the second and the kth mode of vibration; $\delta_{j,i}$ is the displacement of jth element (located at a particular distance from CR) at i^{th} floor, $\delta_{cr,i}$ is the displacement at the CR of the ith floor, $\phi_{1,i}$ and $\phi_{1,max}$ are as defined earlier, $\phi_{2,i}$ and $\phi_{2,max}$ are the second mode shape coefficient at the ith floor and the corresponding maximum value over all floors, for building portion above the uppermost foundation level, in the direction under consideration; $\phi_{k,i}$ and $\phi_{k,max}$ are as defined earlier. In each of the equations (7.3-7.7), a lower-bound value of unity is imposed since no de-amplification of seismic ground-motion is observed, at CR and FL on any floor level, among all the investigated building models.

Equations (7.3-7.7) are derived from the envelopes of the median peak spectral amplification factors obtained in the present study. Knowing the values of A_0, A_1, A_2, and A_k, the median amplification function for the building portion above the uppermost foundation level can be obtained using Eqs. (7.8) - (7.10) as:

for $0 < T_p/T_1 < 0.5$,
$$A(T_p) = \frac{C_1}{1 + \left(\frac{T_2}{T_1} - \frac{T_p}{T_1}\right)^2} - C_2 \qquad (7.8)$$

for $0.5 < T_p/T_1 < T_L$
$$A(T_p) = \frac{C_3}{1 + \left(1 - \dfrac{T_p}{T_1}\right)^2} - C_4 \qquad (7.9)$$

for $T_p/T_1 > T_L$,
$$A(T_p) = A_L = 1 + 2\frac{Z}{H} \leq A_1 \qquad (7.10)$$

and for the building portion below the uppermost foundation level:

for $0 < T_p/T_1 < T_L$,
$$A(T_p) = \frac{C_5}{1 + \left(\dfrac{T_k}{T_1} - \dfrac{T_p}{T_1}\right)^2} - C_6 \qquad (7.11)$$

for $T_p/T_1 > T_L$,
$$A(T_p) = A_L = 1 + 2\frac{Z}{H} \qquad (7.12)$$

where, T_1, T_2 and T_k are the periods of vibration of the building corresponding to the fundamental, the second and the kth mode of vibration, respectively, in the direction under consideration; T_p is the period of vibration of the NSC; A_L is the long-period amplification factor; T_L is the normalized period beyond which the SAF has been assumed to be constant. The constants C_1, C_2, C_3, C_4, C_5, and C_6 can be obtained using the known values of the amplification function $A(T_p)$ at specific values of period, T_p (i.e., at $T_p = 0$, T_2, $0.5T_1$, T_1, 0 and T_k). Equations (7.10) and (7.12) have been obtained from the envelope of the median spectral amplification for long-period range, at different relative heights. Further, as identified in previous studies (Vukobratovic and Fajfar 2015), as discussed earlier in Chapter 6, in case of those NSCs that are having periods much longer than the fundamental period of the supporting structure, the FRS tends to converge to the GRS, irrespective of the floor level. Therefore, equations (7.10) and (7.12) can produce conservative estimates of the peak floor spectral acceleration demand for very long-period NSCs. The proposed SAF is developed considering FRS up to 5 s. Therefore, considering the observations from previous studies (Vukobratovic and Fajfar 2015), an upper limit on the periods of NSCs up to 5 s or 2 times of the fundamental period of the supporting structure (whichever is smaller) is recommended for applicability of the proposed model. For NSCs with even longer periods, the proposed SAF may yield too conservative estimates of the floor accelerations.

Figure 7.12 compares the proposed SAF (gray-shaded areas) with the numerically obtained median spectral amplification factors at different relative heights of the considered SC B and SC C structural configurations.
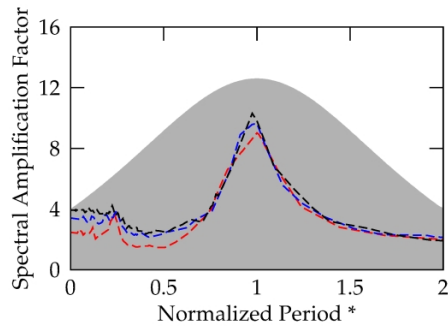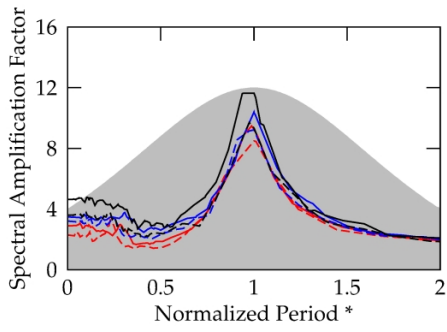
(a) Below uppermost foundation level, CR, SC B   (b) Below uppermost foundation level, FL, SC B
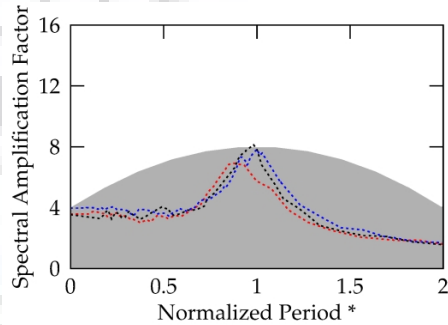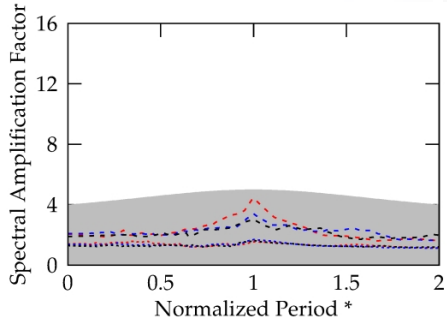
(c) Below uppermost foundation level, CR, SC C   (d) Below uppermost foundation level, FL, SC C
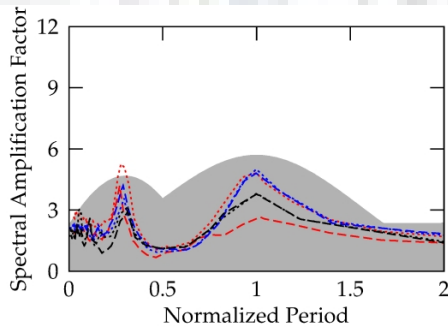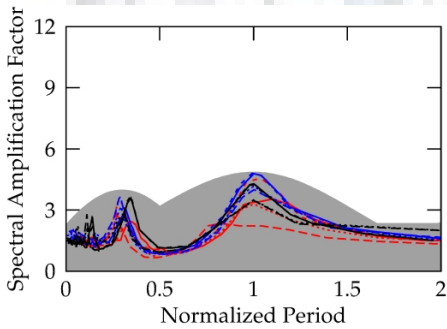
(e) Near mid-height, CR   (f) Near mid-height, FL

(g) At roof, CR   (h) At roof, FL

2SF Along Slope	4SF Along Slope	8SF Along Slope
2SF Across Slope	4SF Across Slope	8SF Across Slope
2SB Along Slope	4SB Along Slope	8SB Along Slope
2SB Across Slope	4SB Across Slope	8SB Across Slope
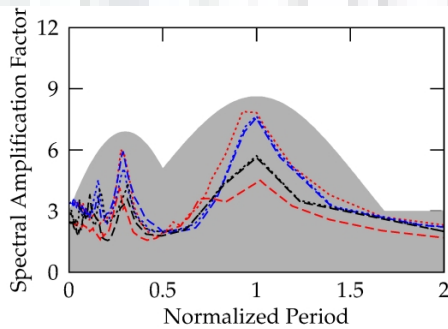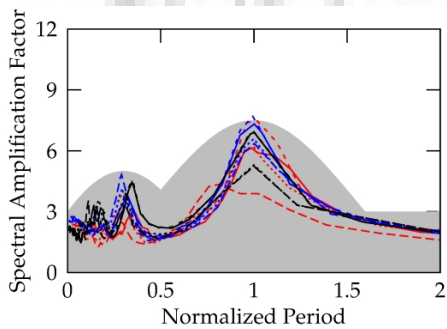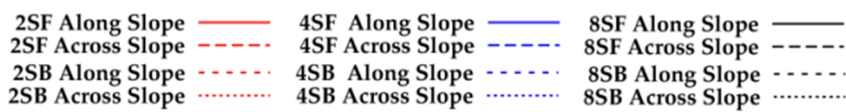
Fig. 7.12 Comparison of the proposed spectral amplification functions for SC B and SC C hill buildings, with median spectral amplification factors obtained from time-history analyses on individual buildings at the CR and the FL. (SF – split-foundation, SB – step-back, *indicates normalization is carried out with the period of the kth mode of vibration).

200

For the building portion below the uppermost foundation level, the SAF are compared at a floor level where the kth mode shape has the maximum ordinate so that all buildings can be compared simultaneously. On the other hand, for the building portion above the uppermost foundation level, the spectral amplification factors are compared at roof level and near mid-height (here the height is measured above the uppermost foundation level, where the mode shape coefficients and the corresponding TDR are almost identical, due to similar torsional effects).

It can be observed that the proposed functions take into account the dynamic characteristics (periods and mode shapes) and torsional response of the hill buildings, in the portions below and above the uppermost foundation level. Further, as discussed in Chapter 6, the parabolic shape of the proposed functions also caters to the uncertainty associated in the estimation of the period of vibration of the hill building, due to modelling uncertainties.

7.4.4 Validation of Proposed Spectral Amplification Functions

In order to validate the proposed SAF, linear dynamic analyses using spectrum-compatible time histories were conducted on 8-storey SC B and SC C building models. Three ground-motion records are made compatible with the design spectrum of the Indian seismic code (IS 1893 Part 1 2016) using the software WAVEGEN (Mukherjee and Gupta 2002). The details of these records are given in Table 6.3.

Figures 7.13 and 7.14 present a comparison of the FRS constructed using the proposed SAF with those obtained from the time-history analyses and the design codes, at the CR and FL in both along- and across-slope directions. The FRS have been compared at three different locations along the height of the building, i.e. portion below the uppermost foundation level (where the kth mode shape coefficient is maximum), near mid-height (where, both the fundamental and second modes are significant) and at the roof level (where the normalized fundamental and second mode shape coefficients are unity).

It can be observed from Figures 7.13 and 7.14 that for both the 8-storey SC B and SC C hill buildings, the code models are too conservative for normalized periods greater than 0.50, irrespective of the location of the NSC along the height of the building and on the floor plan (i.e., at CR or at FL). On the other hand, the code models are non-conservative under near tuned conditions corresponding to the second and the kth mode of vibration, throughout the height of the building. This non-conservatism in current code models is significantly higher, particularly at lower floors (i.e., Z/H = 0.19 and 0.27, for SC B and SC C buildings,

respectively). The observed trends can be explained by the fact that code models are based on the amplification of PFA along the height of the building and utilize a fixed spectral shape (component amplification factor). The dependence of the FRS on the dynamic characteristics, the GRS, and the TDR is completely ignored in these models.

The proposed amplification function predicts the FRS in good agreement with the spectrum-compatible time-history analyses, for both SC B and SC C hill buildings, in the whole spectral range. The proposed SAF to predict floor accelerations is much more comprehensive than the currently available models, as it takes into account the dynamic characteristics of the building (both periods and mode shapes), TDR, GRS, and the tuning between the supporting structure and the NSC.

The proposed model has been developed considering the elastic response of the supporting structure. However, the supporting structures are designed to respond inelastically during severe earthquakes. In such cases, the proposed model will yield conservative estimates of the floor acceleration demands. However, the level of conservatism in the proposed model is much lesser than that of the current code models, particularly at the lower floors. Further, it is to be noted that the proposed model predicts the floor accelerations in the two orthogonal directions independently. In reality, the buildings are subjected to simultaneous action of the two horizontal components of the seismic ground-motion. Therefore, in order to design NSC using the proposed method, the directional combination (vector sum) is necessary.
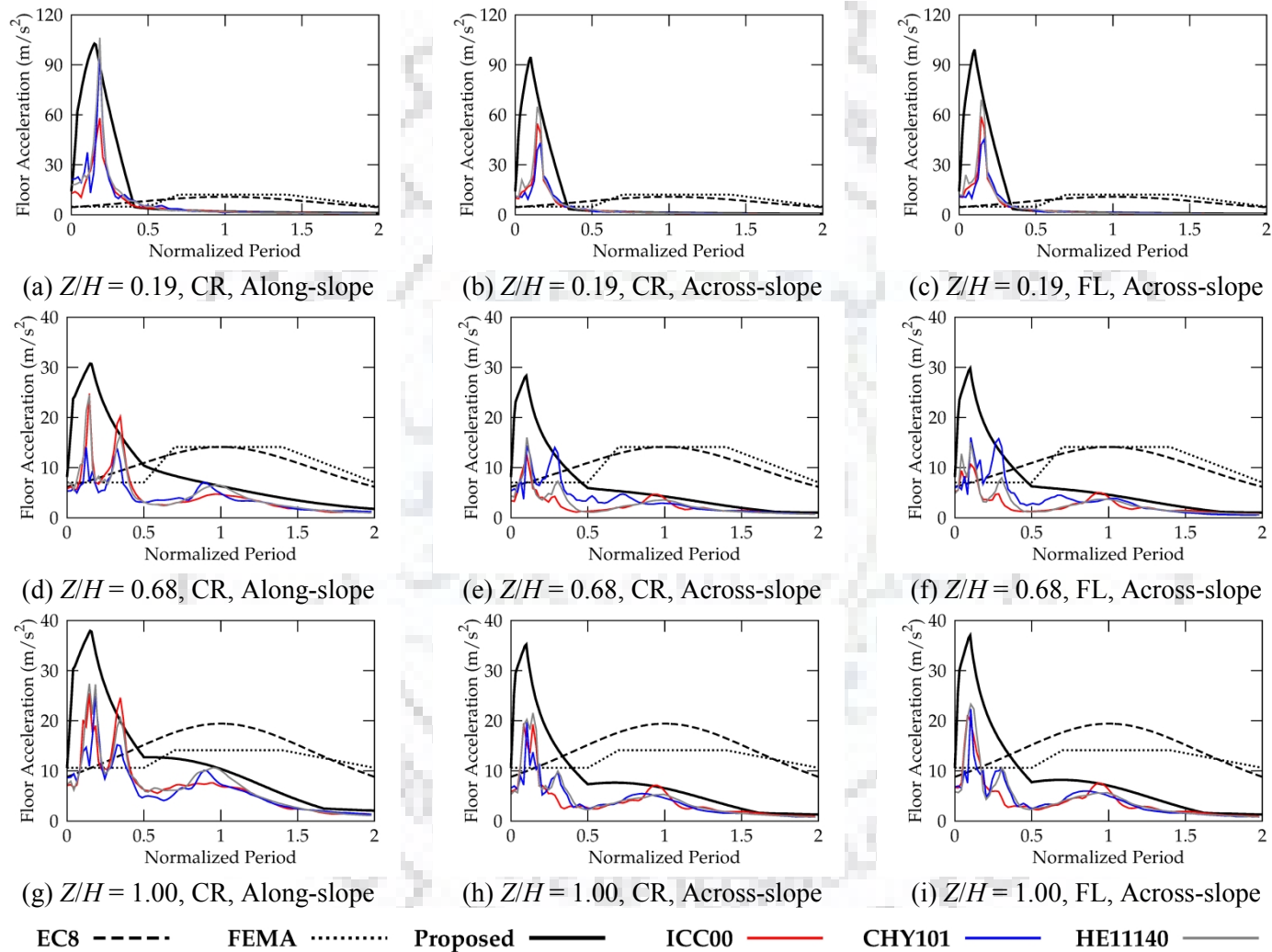
Fig. 7.13 Comparison of the FRS obtained from the proposed model with those obtained from code models and spectrum-compatible time-history analyses for SC B hill building (BH-RC-R6).

(a) $Z/H = 0.27$, CR, Along-slope   (b) $Z/H = 0.27$, CR, Across-slope   (c) $Z/H = 0.27$, FL, Across-slope

(d) $Z/H = 0.68$, CR, Along-slope   (e) $Z/H = 0.68$, CR, Across-slope   (f) $Z/H = 0.68$, FL, Across-slope

(g) $Z/H = 1.00$, CR, Along-slope   (h) $Z/H = 1.00$, CR, Across-slope   (i) $Z/H = 1.00$, FL, Across-slope

EC8 -----   FEMA ··········   Proposed ——   ICC00 ——   CHY101 ——   HE11140 ——
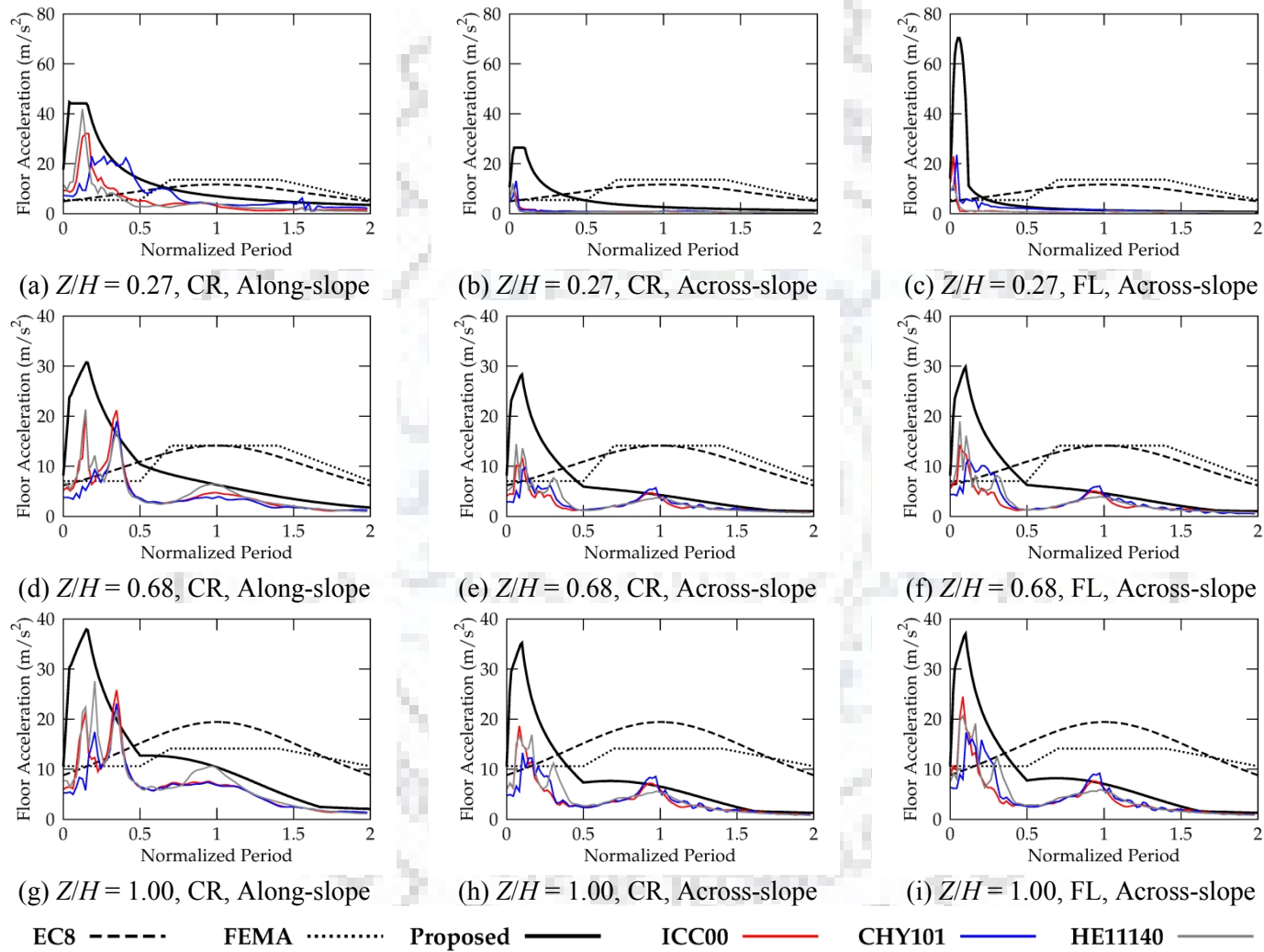
Fig. 7.14 Comparison of the FRS obtained from the proposed model with those obtained from code models and spectrum-compatible time-history analyses for SC C hill building (CH-RC-R6).

7.5 SUMMARY

A state-of-the-art on seismic demand estimation for the acceleration sensitive non-structural components mounted on irregular buildings has been presented. Linear dynamic analyses were performed on a set of RC frame hill building models in order to obtain the floor response. The peak floor acceleration and the floor acceleration response spectra are studied along the height of the building. In order to identify critical parameters affecting the floor response, the floor response was normalized using three different normalization schemes, viz. normalization with respect to PGA, PFA, and $S_{AG}(T)$. The following observations are made:

- The floor acceleration demand in the building portion below the uppermost foundation level is controlled by a higher mode of vibration (denoted by k^{th} mode, in the present study). This mode varies depending on the structural configuration of the building.

- It has been observed that both EN 1998-1 and FEMA P750 models underestimate the PFA demands in hill-side buildings, with SC B and SC C structural configurations, particularly in the building portion below the uppermost foundation level. FEMA P750 model is fairly accurate in predicting the PFA demands in the building portion above the uppermost foundation level, whereas the EN 1998-1 model is found out to be non-conservative in the building portion above the uppermost foundation level as well, particularly, at the FL near roof level. These observations can be attributed to the combined effect of the peculiar dynamic characteristics and the torsional amplification in the hill buildings.

- Similar to the regular buildings, the normalization with respect to GRS leads to the lowest COV as compared to the normalization with respect to PGA or PFA, even in case of SC B and SC C structural configurations.

- The peak spectral amplification factors corresponding to the fundamental, the second and the kth mode of vibration approximately follow the corresponding mode shapes along the height of the building.

- The torsional acceleration amplification in floor response is found out to be proportional to the torsional displacement amplification, which is an approximate indicator of the torsional response (rotation) of the floor, about the CR.

- Comprehensive spectral amplification functions have been developed taking into account the dynamic and torsional characteristics of the supporting structure, which provide fairly accurate acceleration demands in hill buildings with SC B and SC C structural configurations.

CHAPTER 8

CONCLUSIONS AND
RECOMMENDATIONS FOR FUTURE WORK

8.1 CONCLUSIONS

Extensive field surveys were conducted in the two test beds 'Mussoorie' and 'Nainital', both located in seismic zone IV as per the current seismic zonation map of India. A building typology classification scheme for hilly regions has been developed. To study the effect of different structural configurations on collapse fragility of RC frame buildings, three different structural configurations prevalent in hilly regions of Indian Himalayas with varying heights and design levels representative of pre-code, moderate-code, and high-code have been studied using IDA. In addition, the effects of seismic zone and near-field site on collapse fragility of high-code buildings have also been studied. Comprehensive spectral amplification functions have been developed for seismic design of light-weight NSCs mounted on RC hill buildings. The developed spectral amplification functions can be used to construct the design floor spectrum if a building's dynamic characteristics, input ground-motion characteristics and torsional displacement amplification ratio are known. The major conclusions of the presented research work are as follows:

- The structural configurations of the buildings in hilly regions have been observed to be significantly different as compared to the flat terrain. Therefore, the structural configuration should also be considered in the building typology classification and earthquake loss assessment studies in hilly regions.

- It has been observed that structural configurations SC A, SC B and SC C are predominantly used in both the test beds. In total, the structural configurations SC A, SC B and SC C cover approximately 95% of the building stock in both the test beds.

- In both the test beds, RC buildings have been observed to be in abundance and cover approximately 50% of the building stock. A majority of these buildings are observed to be either pre- or low-code buildings. In addition, moderate-code buildings have also been observed but their percentage in the total building stock is relatively small.

- In both the test beds, low-rise buildings have been observed to be in abundance, with the typical storey ratio (N_b/N_a) of 0.50, 1.00 and 2.00.

- In Mussoorie city, majority of the buildings are located on very mild to moderate slopes ranging from 0-45 degrees. However, the number of buildings located on steep slopes with angles varying form 60-90 degrees, is also significant.

- A methodology to compare static and dynamic capacity curves has been presented for regular symmetric buildings. The presented methodology is based on transformation of static capacity curve with the demand spectrum. It has been observed that the transformed capacity curve closely follows the median dynamic capacity curves in the elastic range and slightly deviates in the inelastic range.

- It has been observed that the transformed static capacity curve, in general, overestimates the structural collapse capacity. However, the transformed static capacity curve lies within the median and 84th percentile of the dynamic capacity curves.

- The effect of structural configuration on collapse capacity and collapse fragility has been observed to be more pronounced in case of pre-code buildings, as compared to moderate- and high-code buildings. The collapse capacity of pre-code buildings reduces up to 50% due to the irregular structural configuration in hilly regions. This reduction has been observed to be relatively small (only of the order of 10-20%) in case of moderate- and high-code buildings.

- In case of pre-code buildings, the typical failure mechanism includes the flexural failure of beams and columns, and shear failure of short-columns (in storey just at the level of the uppermost foundation) as well as normal height columns (in upper stories). On the other hand, in case of moderate- and high-code buildings, the flexural failure of beams and columns along with the shear failure of short-columns has been observed (in storey just at the level of the uppermost foundation). In case of structural configuration SC C, a sequential (zippering) failure of short-columns has been observed starting from the uphill side, in all buildings irrespective of the design level.

- In all the high-code buildings conforming to SCWB design, the column hinging cannot be avoided even when a SCWB ratio of 1.40, as recommended in the Indian seismic design

208

code, is used. Therefore, to avoid column hinging an even higher SCWB ratio should be considered.

- In both the structural configurations SC B and SC C, the storey just above the uppermost foundation level has a significant torsional effect, leading to failure of that particular storey. This mode of failure has been consistently observed in both SC B and SC C, irrespective of the seismic design level of the building. The observed failure pattern is quite similar to what has been observed after Sikkim earthquake of 2011, in which a building with structural configuration SC B suffered severe damage at the storey just above the uppermost foundation level.

- The far-field record suite of FEMA P695 under bi-directional excitation resulted in (on average) β_{RTR} of 0.30 (at collapse) while choosing S_a as the IM, for the wide range of building models and structural configurations investigated in this study.

- S_a, as the IM, is unable to capture the effects of higher modes, period elongation and the velocity-pulse, and leads to significantly different collapse capacities for different ground-motion record suites (viz. the far-field, the near-field without velocity pulse and the near-field with velocity pulse) as compared to $S_{a,avg}$, particularly in case of low- and mid-rise buildings.

- In case of the pre-code buildings, S_a leads to a reduced β_{RTR} when compared to $S_{a,avg}$ due to the limited ductility of such buildings. On the other hand, in case of the moderate- and the high-code buildings, in general, $S_{a,avg}$ leads to a reduced β_{RTR} when compared to S_a, as it considers the effect of higher modes of vibration as well as period elongation of an inelastic structure, which is particularly more important near collapse.

- In case of low- and mid-rise buildings, pre-code design resulted in unacceptably high collapse probabilities (upto 98%). These collapse probabilities reduce by a significant extent in case of moderate- and high-code buildings, with corresponding collapse probabilities varying from 4-10% and 1-8%, respectively, for the MCE hazard. In case of high-rise high-code buildings, the collapse probabilities vary from 11-50%, for the MCE hazard.

- The consideration of the spectral shape effects leads to an increase in the collapse capacity of the buildings due to a positive value of 'epsilon' at both 'Mussoorie' and 'Shillong' sites. This effect leads to an increase in collapse capacity upto 80%, underlining the importance of

spectral shape effects in the fragility analysis. This also highlights that collapse capacity is site dependent.

- The buildings designed for seismic zone V have been observed to be more vulnerable as compared to their counterparts designed for seismic zone IV. This observation can be attributed to the fact that increase in design force by 50% (from zone IV to zone V) resulted in only about 10% increase in collapse capacity, as the collapse capacity is not only a function of strength but also ductility; and the ductility of the SMRF buildings is almost identical in both the zones. Except in case of high-rise buildings in seismic zone V, the collapse probability of all high-code buildings has been found to be satisfactory for far-field sites, when compared with the criterion of FEMA P695.

- The buildings located at the far-field site in Mussoorie have, on an average, 1% probability of collapse at MCE. This average probability of collapse increases to 12% after consideration of near-field effects, showing significantly higher vulnerability of buildings located at near-field sites.

- It has been observed that PFA demand reduces with increase in period of vibration of the supporting structure as well as inelasticity. For higher level of inelasticity, the PFA demand even at the level of roof is observed to be lesser than PGA.

- It has been observed that code models under-predict the floor response in case of short-period buildings under elastic response, and highly over-predict in case of long-period buildings, particularly in case of inelastic response. Further, these models do not consider the peaks in floor response spectra, corresponding to higher modes of vibration.

- It has been observed that the floor response spectrum is better correlated to ground response spectrum rather than PGA, as used in current seismic design codes. This observation is valid for all the considered structural configurations.

- The spectral amplification factors corresponding to the fundamental and second modes of vibrations, for a given level of inelasticity, vary with the structure's period within a COV upto 17%, in case of SC A and 32%, in case of SC B and SC C; and hence can be assumed to be independent of the period of vibration. Further, the spectral amplification factors approximately follow the corresponding elastic mode shapes along the height, for all the considered structural configurations.

- In case of structural configurations SC B and SC C, the floor acceleration demand in the building portion below the uppermost foundation level is controlled by a higher mode of vibration.

- It has been observed that both EN 1998-1 and FEMA P750 models underestimate the PFA demands in hill buildings, with SF and SB structural configurations, particularly in the building portion below the uppermost foundation level. FEMA P750 model is fairly accurate in predicting the PFA demands in the building portion above the uppermost foundation level, whereas the EN 1998 model is found out to be non-conservative in the building portion above the uppermost foundation level as well, particularly on the flexible (down-hill) side, near the roof level. These observations can be attributed to the combined effect of the change in dynamic characteristics of the hill buildings due to structural configuration, and the torsional amplification in across-slope direction.

- The torsional amplification of acceleration at a floor has been found to be proportional to the torsional displacement ratio, which is an approximate indicator of the rotation of the floor, about the CR.

- A PFA demand prediction model has been developed considering the effect of the period of vibration as well as inelasticity of the supporting structure. The developed model has been validated for buildings with different periods of vibration and inelasticity. The developed model predicted the PFA demands in reasonable agreement with the spectrum-compatible time-history analyses for buildings of varying heights and inelasticity.

- Comprehensive spectral amplification functions have been developed for short- and long-period buildings. The proposed spectral amplification function can be used with a code-based design response spectrum as well as a site-specific response spectrum to construct the design floor response spectrum.

- The proposed method is more comprehensive than available models as it takes into account the ground-motion characteristics, the dynamic characteristics of the building (both periods and mode shapes), the level of inelasticity expected in the building, and the period of vibration of the NSC. Even though the proposed floor amplification function has been developed using a numerical study on RC frame buildings only, it predicts the floor response of the RC frame-shear wall (dual system) building also with reasonable accuracy.

211

- The developed spectral amplification functions for SC A have been modified taking into account the peaks corresponding to the fundamental, the second and the kth mode of vibration of the supporting structure for structural configurations SC B and SC C. The developed spectral amplification functions have been validated and can predict acceleration demands in hill buildings more accurately, as compared to the current code models.

8.2 RECOMMENDATIONS FOR FUTURE WORK

- The present study has been conducted to study the effect of structural configurations on seismic vulnerability of buildings in hilly regions. The slope-stability and topographic amplification effects (depending on the geometry of the slope and relative location of the building on slope) are other crucial issues, which are not considered in the present study. Therefore, the future studies are recommended considering slope-building interaction and topographic amplification effects.

- The present study is based on analytical simulation of the seismic behaviour and vulnerability, which needs to be validated by experimental results. Therefore, large scale tests of RC frame hill buildings with regular and irregular structural configurations are required to be undertaken.

- The present study has been conducted based on a representative plan shape, chosen from a field survey. It needs to be extended for other plan shapes as well.

- The present study has been conducted on RC bare frame hill buildings. The effect of presence of infills on seismic vulnerability of hill buildings needs to be studied.

- The floor acceleration demand prediction model developed for SC B and SC C hill buildings in the present study needs to be extended considering the inelastic response of the supporting structure. Further, the effect of near-field ground-motions on floor acceleration demands needs to be investigated.

REFERENCES

1. ACI (American Concrete Institute) (2011). Building code requirements for structural concrete and commentary. ACI 318, Farmington Hills, Michigan, United States.

2. ACI (American Concrete Institute) (2014). Building code requirements for structural concrete and commentary. ACI 318M, Farmington Hills, Michigan, United States.

3. Afarani, M. H. C., and Nicknam, A. (2012). Seismic response of mass irregular steel moment resisting frames according to performance levels from IDA approach. *Gazi University Journal of Science*, 25, 751-760.

4. Ahmad, N., Ali, Q., Crowley, H., and Pinho, R. (2014). Earthquake loss estimation of residential buildings in Pakistan. *Natural Hazards*, 73, 1889-1955.

5. Albanesi, T., Biondi, S., and Petrangeli. M. (2002). Pushover analysis: An energy based approach. *In the Proceedings of the 12*[th] *European Conference on Earthquake Engineering*, Paper 605. Elsevier Science Ltd.

6. Aldeka, A. B., Dirar, S., Chan A. H. C., and Martinez-Vazquez, P. (2015). Seismic response of non-structural components attached to reinforced concrete structures with different eccentricity ratios. *Earthquakes and Structures*, 8, 1069-1089.

7. Aldeka, A. B., Chan, A. H. C., and Dirar, S. (2014a). Response of non-structural components mounted on irregular RC buildings. *Earthquakes and Structures*, 7, 351-372.

8. Aldeka, A. B., Dirar, S., Martinez-Vazquez, P., and Chan, A. H. C. (2014b). Influence of ground type on the seismic response of non-structural components integrated on asymmetrical RC buildings. *Australian Earthquake Engineering Society*, Lorne, Victoria.

9. Algermissen, S. T., Rinehart, W. A., Dewey, J., Steinbrugge, K. V., Degenkolb, H. J., Cluff, L. S., McClure, F. E., Gordon, R. F., Scott, S., and Lagorio, H. J. (1972). *A study of earthquake losses in the San Francisco bay area: Data and analysis*. Washington, D.C.: Office of Emergency Preparedness and National Oceanic and Atmospheric Administration.

10. American Society of Civil Engineers (ASCE) (2005). Minimum design loads for buildings and other structures. ASCE/SEI 7-05 Standard, Reston, Virginia, United States.

11. American Society of Civil Engineers (ASCE) (2007). Seismic rehabilitation of existing buildings. ASCE/SEI 41-06 Standard, Reston, Virginia, United States.

12. American Society of Civil Engineers (ASCE) (2010). Minimum design loads for buildings and other structures. ASCE/SEI 7-10 Standard, Reston, Virginia, United States.

13. American Society of Civil Engineers (ASCE) (2013). Seismic evaluation and retrofit of existing buildings. ASCE/SEI 41-13, Reston, Virginia, United States.

14. Amin, M., Hall, W. N., and Kasawara, R. (1971). Earthquake response of multiply connected light secondary systems by spectrum methods. *In the Proceedings of ASME 1st National Congress on Pressure Vessels and Pipings*, New York, 103-129.

15. Anagnostopoulos, S. A., Providakis, C., Salvarieschi, P., Athanasopoulos, G., and Bonacina, G. (2008). Seismocare: An efficient GIS tool for scenario-type investigations of seismic risk of existing cities. *Soil Dynamics and Earthquake Engineering*, 28, 73–84.

16. Aslani, H. (2005). *Probabilistic earthquake loss estimation and loss deaggregation in buildings*. Ph.D. Dissertation, Stanford University, Stanford, California.

17. ATC (Applied Technology Council) (1996). Seismic evaluation and retrofit of concrete buildings: Volume 1. ATC 40, Redwood City, California, United States.

18. Ay, B. O., and Akkar, S. (2012). A procedure for ground motion selection and scaling for nonlinear response of simple structural system. *Earthquake Engineering and Structural Dynamics*, 41, 1693-1707.

19. Ayers, J. M., Sun, T. Y., and Brown, F. R. (1973). *Non-structural damage to buildings, The Great Alaska Earthquake of 1964: Engineering*. National Academy of Science, Washington, D.C.

20.   Baker, J. W. (2011). Conditional mean spectrum: Tool for ground-motion selection. *Journal of Structural Engineering*, ASCE, 137, 322-331.

21.   Baker, J. W., and Cornell, C. A. (2005). A vector valued ground motion intensity measure consisting of spectral acceleration and epsilon. *Earthquake Engineering and Structural Dynamics*, 34, 1193-1217.

22.   Baker, J. W., and Cornell, C. A. (2006). Spectral shape, epsilon and record selection. *Earthquake Engineering and Structural Dynamics*, 35, 1077-1095.

23.   Baker, J. W., and Cornell, C. A. (2008a). Vector-value intensity measures incorporating spectral shape for prediction of structural response. *Journal of Earthquake Engineering*, 12, 534-554.

24.   Baker, J. W., and Cornell, C. A. (2008b). Vector-valued intensity measure for pulse like near fault ground motions. *Engineering Structures*, 30, 1048-1057.

25.   Baker, J. W., and Jayaram, N. (2008). Correlation of spectral acceleration values from NGA ground motion models. *Earthquake Spectra*, 24, 299-317.

26.   Bal, I. E., Crowley, H., Pinho, R., and Gülay, G. (2008). Detailed assessment of structural characteristics of Turkish RC building stock for loss assessment models. *Soil Dynamics and Earthquake Engineering*, 28, 914–932.

27.   Balasubramnian, S. R., Rao, K. B., Meher Prasad, A., Goswami, R., and Anoop, M. B. (2014). A methodology for development of seismic fragility curves for URBS buildings. *Earthquakes and Structures*, 6, 611-625.

28.   Barbat, A. H., Pujades, L. G., and Lantada, N. (2008). Seismic damage evaluation in urban areas using the capacity spectrum method: Application to Barcelona. *Soil Dynamics and Earthquake Engineering*, 28, 851-865.

29.   Barbat, A. H., Yépez Moya, F., and Canas, J. A. (1996). Damage scenarios simulation for seismic risk assessment in urban zones. *Earthquake Spectra*, 12, 371-394.

30.   Basu, D., and Jain, S. K. (2007). Alternative method to locate centre of rigidity in asymmetric buildings. *Earthquake Engineering and Structural Dynamics*, 36, 965-973.

31. Bertero, V. V., and Collins, R. G. (1973). *Investigation of the failures of the Olive View Stair Towers during the San Fernando earthquake and their implications on seismic design*. Vol. UCB/EERC-73/26 Earthquake Engineering Research Center, University of California, Berkeley, pp. 276.

32. Beyer, K., and Bommer, J. J. (2006). Relationships between median values and between aleatory variabilities for different definitions of the horizontal component of motion. *Bulletin of the Seismological Society of America*, 96, 1512-1522.

33. Beyer, K., and Bommer, J. J. (2007). Selection and scaling of real accelerograms for bi-directional loading: A review of current practice and code provisions. *Journal of Earthquake Engineering*, 11:S1, 13-45.

34. Bianchini, M., Diotallevi, P., and Baker, J. W. (2009). Prediction of inelastic structural response using an average of spectral accelerations. *In the Proceedings of 10th International Conference on Structural Safety and Reliability* (ICOSSAR09), Osaka, Japan.

35. Biddah, A., and Ghobarah, A. (1999). Modelling of shear deformation and bond slip in reinforced concrete joints. *Structural Engineering and Mechanics*, 7, 413-432.

36. Biggs, J., and Roesset, J. (1970). *Seismic analysis of equipment mounted on massive structure. Seismic Design for Nuclear Power Plants*, MIT Press, Cambridge, 319-343.

37. BIS (Bureau of Indian Standards) (1987a). Indian standard – Code of practice for design loads (other than earthquake) for buildings and structures (Dead loads), IS 875 Part 1. New Delhi, India.

38. BIS (Bureau of Indian Standards) (1987b). Indian standard – Code of practice for design loads (other than earthquake) for buildings and structures (Live Loads), IS 875 Part 2. Bureau of Indian Standards, New Delhi, India.

39. BIS (Bureau of Indian Standards) (1993). Ductile detailing of reinforced concrete structures subjected to seismic forces – Code of practice, IS 13920. Bureau of Indian Standards, New Delhi, India.

40. BIS (Bureau of Indian Standards) (2000). Indian Standard – Plain and reinforced concrete, Code of practice, IS 456. Bureau of Indian Standards, New Delhi, India.

41. BIS (Bureau of Indian Standards) (2002). Indian standard criteria for earthquake resistant design of structures, Part 1: General provisions and buildings (Fifth revision), IS 1893 Part 1. Bureau of Indian Standards, New Delhi.

42. BIS (Bureau of Indian Standards) (2013). Seismic evaluation and strengthening of existing reinforced concrete buildings – Guidelines. Bureau of Indian Standards, New Delhi, India.

43. BIS (Bureau of Indian Standards) (2016). Ductile design and detailing of reinforced concrete structures subjected to seismic forces – Code of practice – IS 13920. Bureau of Indian Standards, New Delhi, India.

44. BIS (Bureau of Indian Standards) (2016). Indian standard criteria for earthquake resistant design of structures, Part 1: General provisions and buildings (Sixth revision) IS 1893 Part 1. Bureau of Indian Standards, New Delhi.

45. Bojorquez, E., and Iervolino, I. (2011). Spectral shape proxies and nonlinear structural response. *Soil Dynamics and Earthquake Engineering*, 31, 996-1008.

46. Bojorquez, E., Iervolino, I., Salazar, A. R., and Ruiz, S. E. (2012). Comparing vector valued intensity measures for fragility analysis of steel frames in the case of narrow band ground motion. *Engineering Structures*, 45, 472-480.

47. Bommer, J. J., and Alarcon, J. E. (2006). The prediction and use of peak ground velocity. *Journal of Earthquake Engineering*, 10, 1-31.

48. Boore, D. M., and Atkinson, G. M. (2008). Ground-motion prediction equations for the average horizontal component of PGA, PGV, and 5%-damped PSA at spectral periods between 0.01s and 10.0s. *Earthquake Spectra*, 24, 99-138.

49. Bousias, S. N., Verzeletti, G., Fardis, M. N., and Gutierrez, E. (1995). Load path effects in column biaxial bending with axial loads. *Journal of Engineering Mechanics*, 596-605.

50. Bradley, B. A. (2010). A generalized conditional intensity measure approach and holistic ground-motion selection. *Earthquake Engineering and Structural Dynamics*, 39, 1321-1342.

51. Bradley, B. A. (2012). A ground motion selection algorithm based on generalized conditional intensity measure approach. *Soil Dynamics and Earthquake Engineering*, 40, 48-61.

52. Brown, P. C., and Lowes, L. N. (2006). Fragility functions for modern reinforced concrete beam-column joints. *Earthquake Spectra*, 23, 263-289.

53. Brzev, S., Scawthorn, C., Charleson, A., and Jaiswal, K. (2012). GEM basic building taxonomy, version 1.0, GEM ontology and taxonomy global component project. Available from http://www.nexus.globalquakemodel.org/gemontology-taxonomy/posts/updated-gem-basic-building-taxonomy-v1.0.

54. Burt, J. E., and Barber, G. M. (1996). *Elementary Statistics for Geographers*. Guilford Press, New York, NY.

55. Burton, H., and Deierlein, G. G. (2014). Simulation of seismic collapse in nonductile reinforced concrete frame buildings with masonry infills. *Journal of Structural Engineering*, ASCE, 140, A4014016, 1-10.

56. Calvi, G. M., Pinho, R., Magenes, G., Bommer, J. J., Restrepo-Vélez, L. F., and Crowley, H. (2006). Development of seismic vulnerability assessment methodologies over the past 30 years. *ISET Journal of Earthquake Technology*, 43, 75-104.

57. Calvi, P. M., and Sullivan, T. J. (2014). Estimating floor spectra in multiple degree of freedom systems. *Earthquakes and Structures*, 7, 17-38.

58. Campbell, K. W., and Bozorgnia, Y. (2008). NGA ground motion model for the geometric mean horizontal component of PGA, PGV, PGD, and 5% damped linear elastic response spectra for periods ranging from 0.01 to 10 s. *Earthquake Spectra*, 24, 139-171.

59. Campbell, K. W., and Bozorgnia, Y. (2014). NGA west 2 ground motion model for the average horizontal components of PGA, PGV, and 5% damped linear acceleration response spectra. *Earthquake Spectra*, 30, 1087-1115.

60. Campos Costa, A., Sousa, M. L., Carvalho, A., and Coelho, E. (2010). Evaluation of seismic risk and mitigation strategies for the existing building stock: Application of LNECloss to the metropolitan area of Lisbon. *Bulletin of Earthquake Engineering*, 8, 119–134.

61. Catlan, A., Climent, A. B., and Cahis, X. (2010). Selection and scaling of earthquake records in assessment of structures in low-to-moderate seismicity zones. *Soil Dynamics and Earthquake Engineering*, 30, 40-49.

62. CED 39 (2016). Indian standard criteria for earthquake resistant design of structures, Part 1: General provisions and buildings (Sixth Revision). Bureau of Indian Standards, New Delhi.

63. Census (2011), Census of India. Available from http://www.citypopulation.de/php/ india-uttarakhand.php. (Last accessed on April 10, 2016).

64. Champion, C., and Liel, A. B. (2012). The effect of near-fault directivity on building seismic collapse risk. *Earthquake Engineering and Structural Dynamics*, 41, 1391-1409.

65. Chandramohan, R., Baker, J. W., and Deierlein, G. G. (2016a). Impact of hazard-consistent ground motion duration in structural collapse risk assessment. *Earthquake Engineering and Structural Dynamics*, 45, 1357–1379.

66. Chandramohan, R., Baker, J. W., and Deierlein, G. G. (2016b). Quantifying the influence of ground motion duration on structural collapse capacity using spectrally equivalent records. *Earthquake Spectra*, 32, 927-950.

67. Charney, F. A. (2008). Unintended consequences of modelling damping in structures. *Journal of Structural Engineering*, ASCE, 134, 581-592.

68. Chaudhuri, S. R., and Hutchinson, T. C. (2011). Effect of nonlinearity of frame buildings on peak horizontal floor accelerations. *Journal of Earthquake Engineering*, 15, 124-142.

69. Chaudhuri, S. R., and Villaverde, R. (2008). Effect of building nonlinearity on seismic response of non-structural components: A parametric study. *Journal of Structural Engineering*, ASCE, 134, 661-670.

70. Chaulagain, H., Rodrigues, H., Silva, V., Spacone, E., and Varum, H. (2015). Seismic risk assessment and hazard mapping in Nepal. *Natural Hazards*, 78, 583-602.

71. Chioccarelli, E., and Iervolino, I. (2010). Near-source seismic demand and pulse-like records: A discussion for L'Aquila earthquake. *Earthquake Engineering and Structural Dynamics*, 39, 1039–1062.

72. Chopra, A. K., and Goel, R. K. (2002). A modal pushover analysis procedure for estimating seismic demands for buildings. *Earthquake Engineering and Structural Dynamics,* 31, 561-582.

73. Chopra, A. K., Goel, R. K., and Chintanapakdee C. (2003). Statistics of single-degree-of-freedom estimate of displacement for pushover analysis of buildings. *Journal of Structural Engineering, ASCE*, 119, 459-469.

74. Chopra, A., and McKenna, F. (2015). Modelling viscous damping in nonlinear response history analysis of buildings for earthquake excitation. *Earthquake Engineering and Structural Dynamics*, DOI: 10.1002/eqe.

75. Computers and Structures Inc. (CSI) (2010). *SAP 2000-Integrated software for structural analysis & design*. Version 14.2.4, Computers and Structures Inc., Berkeley, U.S.A.

76. Computers and Structures Inc. CSI (2016). *ETABS 2016 Integrated building design software*. Version 16.0.1, Computers and Structures Inc., Berkeley, U.S.A.

77. Corodova, P. P., Deierlein, G. G., Mehanny, S. S., and Cornell, C. A. (2000). Development of two parameter seismic intensity measure and probabilistic assessment procedure. *Proceedings of 2nd US-Japan Workshop on Performance Based Earthquake Engineering for Reinforced Concrete Building Structures*, Sapporo, Japan, 11-13 September, 2000.

78. Cosenza, E., Manfredi, G., Polese, M., and Verderame, G. M. (2005). A multi-level approach to the capacity assessment of existing RC buildings. *Journal of Earthquake Engineering*, 9, 1–22.

79. Craig, J. I., Frost, J. D., Goodno, B. J., Towashiraporn, P., Chawla, G., Seo. J., and Duenas-Osorio, L. (2007). *Rapid assessment of fragilities for collection of buildings and geostructures*. Project DS-5 Final Report, Georgia Institute of Technology, United States.

80. Crowley, H., Pinho, R., and Bommer, J. J. (2004). A probabilistic displacement-based vulnerability assessment procedure for earthquake loss estimation. *Bulletin of Earthquake Engineering*, 2, 173-219.

81. D'Ayala, D. (2005). Force and displacement based vulnerability assessment for traditional buildings. *Bulletin of Earthquake Engineering*, 3, 235-265.

82. D'Ayala, D., and Meslem, A. (2013). Derivation of analytical fragility functions considering modelling uncertainties. *11th International Conference on Structural Safety and Reliability - ICOSSAR13*, New York, USA.

83. D'Ayala, D., and Speranza, E. (2002). An integrated procedure for the assessment of seismic vulnerability of historic buildings. *Proceedings of the 12th European Conference on Earthquake Engineering*, London, U.K., Paper no. 561.

84. D'Ayala, D., Kappos, A., Crowley, H., Antoniadis, P., Colombi, M., Kishali, E., and Silva, V. (2012). *Providing building vulnerability data and analytical fragility functions for PAGER*. Final technical report EERI.

85. D'Ayala, D., Meslem, A., Vamvatsikos, D., Porter, K., Rossetto, T., Crowley, H., and Silva, V. (2014a). *Guidelines for analytical vulnerability assessment*. Vulnerability Global Component Project, GEM foundation, Pavia.

86. D'Ayala, D., Meslem, A., Vamvatsikos, D., Porter, K., Rossetto, T., Crowley, H., and Silva, V. (2014b). *Guidelines for analytical vulnerability assessment of low/mid-rise buildings: Methodology*. Vulnerability Global Component Project.

87. D'Ayala, D., Jaiswal, K. S., Wald, D. J., Porter, K., and Greene, M. (2010). Collaborative effort to estimate collapse fragility for buildings worldwide: The WHE-PAGER project. In *9th US National and 10th Canadian Conference on Earthquake Engineering 2010,* Including Papers from the 4th International Tsunami Symposium, 5, 3709-3719.

88. Dadi, S. K. (2015). *Nonlinear modelling of soft storey RC frame based on cyclic testing of components*. Ph.D. Thesis, Department of Earthquake Engineering, Indian Institute of Technology Roorkee, Roorkee, India.

89. Dadi, S. K., and Agarwal, P. (2015). Effect of types of reinforcement on plastic hinge rotation parameters of RC beams under pushover and cyclic Loading. *Earthquake Engineering and Engineering Vibration*, 14, 503-516.

90. Deb, S. K. (2008). Emerging technologies for earthquake risk reduction in construction of buildings. *In Proceedings of the Conference on Managing Earthquake Risk*, New Delhi, 251-259.

91. Deb, S. K., and Geddam, V. K. (2006). Pushover analysis of reinforced concrete buildings with flexible floor diaphragm. *In 1st European Conference on Earthquake Engineering and Seismology*, Geneva, Paper No.75.

92. Deierlein, G. G., Reinhorn, A. M., and Willford, M. R. (2010). *Nonlinear structural analysis for seismic design*. NEHRP Seismic Design Technical Brief No. 4, produced by the NEHRP Consultants joint venture, a partnership of Applied Technology Council and the consortium of Universities for Research in Earthquake Engineering, for the National Institute of Standards and Technology, Gaithersburg, MD, NIST GCR 10-917-5.

93. Dhakal, R. P. (2010). Damage to non-structural components and contents in 2010 Darfield earthquake. *Bulletin of the New Zealand Society for Earthquake Engineering*, 43, 404-411.

94. Dolsek, M., and Fajfar P. (2005). Simplified nonlinear seismic analysis of infilled reinforced concrete frames. *Earthquake Engineering and Structural Dynamics,* 34, 49-66.

95. Dolsek, M., and Fajfar, P. (2007). Simplified probabilistic seismic performance assessment of plan-asymmetric buildings. *Earthquake Engineering and Structural Dynamics*, 36, 2021-2041.

96. Dooley, K. L., and Bracci, J. M. (2001). Seismic evaluation of column to beam strength ratio in reinforced concrete frames. *ACI Structural Journal*, 98, 843-851.

97.   Dymiotis, C., Kappos, A. J., and Chryssanthopoulos, M. K. (1999). Seismic reliability assessment of RC frames with uncertain drift and member capacity. *Journal of Structural Engineering*, ASCE, 125, 1038-1047.

98.   Eads, L., Miranda, E., and Lignos, D. G. (2015). Average spectral acceleration as an intensity measure for collapse risk assessment. *Earthquake Engineering and Structural Dynamics*, 44, 2057-2073.

99.   Eads, L., Miranda, E., and Lignos, D. G. (2016). Spectral shape metrics and structural collapse potential. *Earthquake Engineering and Structural Dynamics*, 45, 1643-1659.

100. Ebrahimian, H., Jalayer, F., Lucchini, A., Mollaioli, F., and Manfredi, G. (2015). Preliminary ranking of alternative scalar and vector intensity measure of ground shaking. *Bulletin of Earthquake Engineering*, DOI 10.1007/s10518-015-9755-9.

101. EERI (Special earthquake report) (2012). *The M_w 6.9 Sikkim-Nepal border earthquake of September 18, 2011*. EERI Report, Earthquake Engineering Research Report, Oakland, United States.

102. Elwood, K. J., and Eberhard, M. O. (2009). Effective stiffness of reinforced concrete columns. *ACI Structural Journal*, 106, 476-484.

103. Elwood, K. J., and Moehle, J. P. (2003). *Shake table tests and analytical studies on gravity load collapse of reinforced concrete frames*. PEER Report 2003/01, Pacific Earthquake Engineering Research Center, University of California, Berkeley, California.

104. Elwood, K. J., Matamoros, A. B., Wallace, J. W., Lehman, D. E., Heintz, J. A., Mitchell, A. D., Moore, M. A., Valley, M. T., Lowes, L. N., Comartin, C. D., and Moehle, J. P. (2007). Update to ASCE/SEI 41 concrete provisions, *Earthquake Spectra*, 23, 493-523.

105. EN 1998-1 (European Committee for Standardization) EC-8 (2004). Design of structures for earthquake resistance- Part 1: General rules, seismic actions and rules for buildings, Brusells.

106. Erduran, E. (2012). Evaluation of Rayleigh damping and its influence on engineering demand parameter estimates. *Earthquake Engineering and Structural Dynamics*, 41, 1905-1919.

107. Erduran, E., and Yakut, A. (2007). Vulnerability assessment of reinforced concrete moment resisting frame buildings. *Journal of Structural Engineering*, ASCE, 133, 576-586.

108. ESRI (2011). *ArcGIS Desktop*, Release 10, Redlands, CA, Environmental Systems Research Institute.

109. Faella, G. (1996). Evaluation of RC structures seismic response by means of nonlinear static pushover analyses. *In Proceedings of the 11th World Conference on Earthquake Engineering*, Acapulco, Mexico, Paper no. 1146.

110. Fajfar, P. (1999). Capacity spectrum method based on inelastic demand spectra. *Earthquake Engineering and Structural Dynamics*, 28, 979-993.

111. Farsangi, E. N., and Tasnimi, A. A. (2016). The influence of horizontal and vertical coupled ground excitations on the collapse margins of modern RC MRF's. *International Journal of Advanced Structural Engineering*, 8, 169-192.

112. FEMA (Federal Emergency Management Agency) (1997). Guidelines for seismic rehabilitation of buildings, FEMA 273, Washington, D.C., United States.

113. FEMA (Federal Emergency Management Agency) (2000). Prestandard and commentary for the seismic rehabilitation of buildings, FEMA 356, Washington, D.C., United States.

114. FEMA (Federal Emergency Management Agency) (2005). Improvement of inelastic analysis procedures. FEMA 440, Washington, D.C., United States.

115. FEMA (Federal Emergency Management Agency) (2009). NEHRP recommended seismic provisions for new buildings and other structures. FEMA P750, Washington, D.C., United States.

116. FEMA (Federal Emergency Management Agency) (2009). Quantification of seismic performance factors. FEMA P695, Washington, D.C., United States.

117. FEMA (Federal Emergency Management Agency) (2012). Seismic performance assessment of buildings -Volume 1 methodology. FEMA P58, Washington, D.C., United States.

118. FEMA (Federal Emergency Management Agency). (2002). Multi-Hazard loss estimation methodology earthquake model. FEMA HAZUS-MH MR 1, Washington, D.C., United States.

119. Filiatrault, A., Lachapelle, E., and Lamontagne, P. (1998). Seismic performance of ductile and nominally ductile reinforced concrete moment resisting frames: Experimental study. *Canadian Journal of Civil Engineering*, 25, 342-358.

120. Flores, F. X., Garcia D. L., and Charney, F. A. (2015). Assessment of floor accelerations in special steel moment frames. *Journal of Constructional Steel Research*, 106, 154-165.

121. Freeman, S. A., Nicoletti, J. P., and Tyrell, J. V. (1975). Evaluations of existing buildings for seismic risk - A case study of Puget Sound Naval Shipyard, Bremerton, Washington. *In the Proceedings of 1st U.S. National Conference on Earthquake Engineering*, Berkeley, U.S.A., 113-122.

122. Galasso, S. M. C., and Rossetto, T. (2015). Assessing spectral shape-based intensity measures for simplified fragility analysis of mid-rise reinforced concrete buildings. *In the Proceedings of the SECED Conference on Earthquake Risk and Engineering Towards A Resilient World*, Cambridge, United Kingdom.

123. Gazetas, G. (2006). Seismic design of foundations and soil-structure interaction. *In the Proceedings of the 1st European Conference on Earthquake Engineering and Seismology*. Paper no. K7.

124. Ghaffarzadeh, H., Talebian, N., and Kohandel, R. (2013). Seismic demand evaluation of medium ductility RC moment frames using nonlinear procedures. *Earthquake Engineering and Engineering Vibration*, 12, 399-409.

125. Ghazizadeh, S. A., Grant, D., and Rossetto, T. (2013). Orientation dependence of ground motion and structural response of reinforced concrete space frames. *In the Proceedings of Vienna Congress on Recent Advances in Earthquake Engineering and Structural Dynamics*, paper no. 71, Vienna, Austria.

126. Goel, R. K., and Chopra, A. K. (1997). *Vibration properties of buildings determined from recorded earthquake motions*. UCB/EERC 97/14, University of California, Berkeley, California.

127. Google Earth, https://earth.google.com (Last accessed on June 07, 2016).

128. Grünthal, G. (1998). European macroseismic scale 1998 (EMS–98). *Cahiers duCentre Européen de Géodynamique et de Séismologie*, Vol. 15, Luxembourg.

129. Gupta, B., and Kunnath, S. K. (1999). Pushover analysis of isolated flexural reinforced concrete walls. *Structural Engineering in the 21st Century, Proc. Structures Congress*, New Orleans.

130. Gupta, B., and Kunnath, S. K. (2000). Adaptive spectra-based pushover procedure for seismic evaluation of structures. *Earthquake Spectra*, 16, 367–391.

131. Haldar, P., and Singh, Y. (2009). Seismic performance and vulnerability of Indian code designed RC frame buildings. *ISET Journal of Earthquake Technology*, 46, 29-45.

132. Haldar, P., Singh, Y., Lang, D. H., and Paul, D. K. (2013). Comparison of seismic risk assessment based on macroseismic intensity and spectrum approaches using 'SeisVARA'. *Soil Dynamics and Earthquake Engineering*, 48, 267-281.

133. Hall, J. F. (2006). Problems encountered from the use (misuse) of Rayleigh damping. *Earthquake Engineering and Structural Dynamics*, 35, 525-545.

134. Hancock, J., Bommer, J. J., and Stafford, P. J. (2008). Number of scaled and matched accelerograms required for inelastic dynamic analyses. *Earthquake Engineering and Structural Dynamics*, 37, 1585-1607.

135. Harder, R. N. (1989). Los Angeles city dynamic analysis. *Professional Paper 89-2*, Los Angeles Tall Buildings Structural Design Council.

136. Hardyniec, A., and Charney, F. (2015). An investigation into the effects of damping and nonlinear geometry models in earthquake engineering analysis. *Earthquake Engineering and Structural Dynamics*, DOI: 10.1002/eqe.2604.

137. Haselton, C. B., and Deierlein, G. G. (2007). *Assessing seismic collapse safety of modern reinforced concrete frame buildings*. PEER Report 2007/08, PEER Center, University of California, Berkeley, CA.

138. Haselton, C. B., Baker, J. W., Liel, A. B., and Deierlein, G. G. (2011a). Accounting for ground-motion spectral shape characteristics in structural collapse assessment through an adjustment for epsilon. *Journal of Structural Engineering*, ASCE, 137, 332-344.

139. Haselton, C. B., Liel, A. B., Deierlein, G. G., Dean, B. S., and Chou, J. H. (2011b). Seismic collapse safety of reinforced concrete buildings. I: Assessment of ductile moment frames. *Journal of Structural Engineering*, ASCE, 137, 481-491.

140. Haselton, C. B., Liel, A. B., Taylor Lange, S., and Deierlein, G. G. (2007). *Beam column element model calibrated for predicting flexural response leading to global collapse of RC frame building*. PEER Report 2007/03, PEER Center, University of California, Berkeley, CA.

141. Hassan, A. F., and Sozen, M. A. (1997). Seismic vulnerability assessment of low-rise buildings in regions with infrequent earthquakes. *ACI Structural Journal*, 94, 31-39.

142. Heo, Y. A., Kunnath, S. K., and Abrahamson, N. (2011). Amplitude-scaled versus spectrum matched ground motions for seismic performance assessment. *Journal of Structural Engineering*, ASCE, 137, 278-288.

143. Housner, G. W., and Jennings, P. C. (1977). *The capacity of extreme earthquake motions to damage structures*. *Structural and Geotechnical Mechanics*, W. J. Hall ed., Prentice Hall, Inc., Englewood Cliffs, N. J., 102-116.

144. Huang, Y. N., Whittaker, A. S., Luco, N., and Hamburger, R. O. (2011). Scaling earthquake ground-motions for performance based assessment of buildings. *Journal of Structural Engineering*, ASCE, 137, 311-321.

145. Ibarra, L. F., and Krawinkler, H. (2005). *Global collapse of frame structures under seismic excitations*. John A. Blume Earthquake Engineering Center, PEER Report 2005/06, September 2005, Department of Civil and Environmental Engineering, Stanford University, United States.

146. Ibarra, L. F., Medina, R. A., and Krawinkler, H. (2015). Hysteretic models that incorporate strength and stiffness deterioration. *Earthquake Engineering and Structural Dynamics*, 34, 1489-1511.

147. IDNDR (1999). RADIUS: Risk assessment tool for diagnosis of urban areas against seismic disasters. *International Decade for Natural Disaster Reduction*, Geneva, Switzerland.

148. Ioannou, I., Douglas, J., and Rossetto, T. (2015). Assessing the impact of ground-motion variability and uncertainty on empirical fragility curves. *Soil Dynamics and Earthquake Engineering*, 69, 83-92.

149. Jaiswal, K., and Wald, D. J. (2008). *Creating a global building inventory for earthquake loss assessment and risk management*. U.S. Geological Survey, Open file report, 2008-1160-106 pp.

150. Jaiswal, K., Wald, D., and D'Ayala, D. (2011). Developing empirical collapse fragility functions for global building types. *Earthquake Spectra*, 27, 775-795.

151. Jangid, R. S. (1996). Seismic response of sliding structures to bidirectional earthquake excitation. *Earthquake Engineering and Structural Dynamics*, 25, 1301-1306.

152. Jangid, R. S. (2001). Response of sliding structures to bi-directional excitation. *Journal of Sound and Vibration*, 243, 929-944.

153. Jangid, R. S., and Datta, T. K. (1999). Evaluation of the methods for response analysis under non-stationary excitation. *Shock and Vibration*, 6, 285-297.

154. Jehel, P., Leger, P., and Ibrahimbegovic, A. (2014). Initial versus tangent stiffness-based Rayleigh damping in inelastic time history seismic analyses. *Earthquake Engineering and Structural Dynamics*, 43, 467-484.

155. Jiang, W., Li, B., Xie, W. C., and Pandey, M. D. (2015). Generate floor response spectra: Part 1 Direct spectra-to-spectra method. *Nuclear Engineering and Design*, 293, 525-546.

156. Kalkan, E., and Kunnath S. K. (2006). Adaptive modal combination procedure for nonlinear static analysis of building structures. *Journal of Structural Engineering, ASCE*, 132, 1721-1731.

157. Kamatchi P., Ramana, G. V., and Nagpal, A. K. (2009). Importance of site – specific studies for medium soil site of Delhi region. *ISET Journal of Earthquake Technology*, Paper No. 510, 47(2-4).

158. Kamatchi, P., Rajasankar, J., Iyer, N. R., Lakshmanan, N., Ramana, G. V., and Nagpal, A. K. (2010). Effect of depth of soil stratum on performance of buildings for site-specific earthquakes. *Soil Dynamics and Earthquake Engineering*, 30, 647-661.

159. Kamatchi, P., Ramana, G. V., Nagpal, A. K., and Lakshmanan, N. (2008). Site-specific analysis of Delhi region for scenario earthquakes. *In the 14th World Conference on Earthquake Engineering*.

160. Kappos, A. J., and Kyriakakis, P. (2000). A re-evaluation of scaling techniques for natural records. *Soil Dynamics and Earthquake Engineering*, 20, 111-123.

161. Kappos, A. J., Panagopoulos, G., Panagiotopoulos, C., and Penelis, G. (2006). A hybrid method for the vulnerability assessment of R/C and URM buildings. *Bulletin of Earthquake Engineering*, 4, 391-413.

162. Kappos, A. J., Pitilakis, K., and Stylianidis, K. C. (1995). Cost-benefit analysis for the seismic rehabilitation of buildings in Thessaloniki, based on a hybrid method of vulnerability assessment. *In Proceedings of the 5th International Conference on Seismic Zonation*, France, 406-413.

163. Kappos, A. J., Stylianidis, K. C., and Pitilakis, K. (1998). Development of seismic risk scenarios based on a hybrid method of vulnerability assessment. *Natural Hazards*, 17, 177-192.

164. Kazaz, I., Gulkan, P., and Yakut, A. (2012). Performance limits for structural walls: An analytical perspective. *Engineering Structures*, 43, 105-119.

165. Kazemi, H., Ghafory Ashtiany, M., and Azarbakht, A. (2013). Effect of epsilon based record selection on fragility curves of typical irregular steel frames with concrete shear walls in Mashhad city. *International Journal of Advanced Structural Engineering*, 5, 1-11.

166. Khose, V. N., Singh, Y., and Lang, D. H. (2012). A comparative study of design base shear for RC buildings in selected seismic design codes. *Earthquake Spectra*, 28, 1047-1070.

167. Khuntia, M., and Ghosh, S. K. (2004). Flexural stiffness of reinforced concrete columns and beams: Analytical approach. *ACI Structural Journal*, 101, 351-363.

168. Kim, S. D., Kim, M. H., and Kim, S. J. (2001). Determination of system ductility capacity using nonlinear dynamic analysis. *The 8th East Asia-Pacific Conference on Structural Engineering and Construction*, Paper No. 1442, 5-7 December, Nanyang Technological University, Singapore.

169. Kircher, C. A., Reitherman, R. K., Whitman, R. V., and Arnold, C. (1997). Estimation of earthquake losses to buildings. *Earthquake Spectra*, 13, 703–720.

170. Kohrangi, M., Bazzurro, P., and Vamvatsikos, D. (2016a). Vector and scalar IMs in structural response estimation, Part I: Hazard analysis. *Earthquake Spectra*, 32, 1507-1524.

171. Kohrangi, M., Bazzurro, P., and Vamvatsikos, D. (2016b). Vector and scalar IMs in structural response estimation, Part II: Building demand assessment. *Earthquake Spectra*, 32, 1525-1543.

172. Kohrangi, M., Bazzurro, P., Vamvatsikos, D., and Spillatura, A. (2017a). Conditional spectrum based ground motion record selection using average spectral acceleration. *Earthquake Engineering and Structural Dynamics,* DOI: 10.1002/eqe.2876.

173. Kohrangi, M., Kotha, S. R., Bazzurro, P. (2017b). Ground-motion models for average spectral acceleration in a period range: Direct and indirect methods. *Bulletin of Earthquake Engineering*, DOI: 10.1007/s10518-017-0216-5.

174. Kohrangi, M., Vamvatsikos, D., and Bazzurro, P. (2017c). Site dependence and record selection schemes for building fragility and regional loss assessment. *Earthquake Engineering and Structural Dynamics,* DOI: 10.1002/eqe.2873.

175. Koopaee, M. E., Dhakal, R. P., and MacRae, G. (2017). Effect of ground motion selection methods on seismic collapse fragility of RC frame buildings. *Earthquake Engineering and Structural Dynamics*, DOI: 10.1002/eqe.2891.

176. Kostinakis, K., Athanatopoulou, A., and Morfiids, K. (2015). Correlation between ground motion intensity measure and seismic damage of 3D RC buildings. *Engineering Structures*, 82,151-167.

177. Krawinkler, H., and Seneviratna, G. D. P. K. (1998). Pros and Cons of a pushover analysis of seismic performance evaluation. *Engineering Structures*, 20, 452-464.

178. Kumari, R., and Gupta, V. K. (2007). A modal combination rule for peak floor accelerations in multi-storied buildings. *ISET Journal of Earthquake Technology*, Paper No. 483, 44, 213-231.

179. Kunnath, S. K., Valles-Mattox, R. E., and Reinhorn, A. M. (1996). Evaluation of seismic damageability of a typical R/C building in Midwest United States. *Proceedings of the 11th World Conference on Earthquake Engineering*, Acapulco, Mexico.

180. Kunnath, S. K., Hoffmann, G., Reinhorn, A. M., and Mander, J. B. (1995). Gravity load designed reinforced concrete buildings – Part I: Seismic evaluation of existing construction. *ACI Structural Journal*, 92, 343-354.

181. Kuntz, G. L., and Browning, J. (2003). Reduction of column yielding during earthquakes for reinforced concrete frames. *ACI Structural Journal*, 100, 573-580.

182. Kurama, Y. C., and Farrow, K. T. (2003). Ground-motion scaling methods for different site conditions and structure characteristics. *Earthquake Engineering and Structural Dynamics*, 32, 2425-2450.

183. Kuwamura, H., and Galambos, T. V. (1989). Earthquake load for structural reliability. *Journal of Structural Engineering*, ASCE, 115, 1446-1462.

184. Lagaros, N. D., and Fragiadakis, M. (2011). Evaluation of ASCE-41, ATC-40 and N2 static pushover methods based on optimally designed buildings. *Soil Dynamics and Earthquake Engineering*, 31, 77-90.

185. Lang, D. H., Singh, Y., and Prasad, J. S. R. (2012). Comparing empirical and analytical estimates of earthquake loss assessment studies for city of Dehradun, India. *Earthquake Spectra*, 28, 595-619.

186. LATBSDC (2014). An alternative procedure for seismic analysis and design of Tall buildings located in The Los Angeles Region. *Los Angeles Tall Building Seismic Design Council*, LA, California, USA.

187. Lawson, R. S., Vance, V., and Krawinkler, H. (1994). Non-linear static pushover analysis-why, when and how?. *In the Proceedings of 5th US National Conference on Earthquake Engineering*, EERI, Oakland, California, 1, 283-292.

188. Leger, P., and Dussault, S. (1992). Seismic energy dissipation in MDOF structures. *Journal of Structural Engineering*, ASCE, 118, 1251-1269.

189. Lew, H. S., and Kunnath, S. K. (2001). Evaluation of nonlinear static procedures for seismic design of buildings. *Presented at the 33rd Joint Meeting of the UJNR Panel on Wind and Seismic Effects*, 1-17.

190. Li, Y., and Hwang, S. (2016). Prediction of lateral load displacement curves for reinforced concrete short columns failed in shear. *Journal of Structural Engineering*, ASCE, DOI: 10.1061/ (ASCE) ST. 1943-541X.0001656.

191. Liel, A. B., and Champion, C. (2012). *The effects of near-fault directivity on building seismic collapse risk. Research Report*. United States Geological Survey, United States.

192. Liel, A. B., Haselton, C. B., and Deierlein, G. G. (2011). Seismic collapse safety of reinforced concrete buildings. II: Comparative assessment of nonductile and ductile moment frames. *Journal of Structural Engineering*, ASCE, 137, 492-502.

193. Liel, A. B., Haselton, C. B., Deierlein, G. G., and Baker, J. W. (2009). Incorporating modelling uncertainties in the assessment of seismic collapse risk of buildings. *Structural Safety*, 31, 197-211.

194. Lin, J., and Mahin, S. A. (1985). Seismic response of light subsystems on inelastic structures. *Journal of Structural Engineering*, ASCE, 111, 400-417.

195. Lin, L., Naumoski, N., Saatcioglu, N., and Foo, S. (2011). Improved intensity measures for probabilistic demand analysis, Part 1: Development of improved intensity measure. *Canadian Journal of Civil Engineering*, 38, 79-88.

196. Lin, T., Haselton, C. B., and Baker, J. W. (2013a). Conditional spectrum-based ground motion selection, Part I: Hazard consistency for risk-based assessments. *Earthquake Engineering and Structural Dynamics*, 42, 1847-1865.

197. Lin, T., Haselton, C. B., and Baker, J. W. (2013b). Conditional spectrum-based ground motion selection, Part II: Intensity-based assessments and evaluation of alternative target spectra. *Earthquake Engineering and Structural Dynamics*, 42, 1867-1884.

198. Lowes, L. N., and Altoontash, A. (2003). Modeling reinforced-concrete beam-column joints subjected to cycling loading. *Journal of Structural Engineering*, ASCE, 129, 1686–1697.

199. Lucchini, A., Franchin, P., and Mollaioli, F. (2016). Probabilistic seismic demand model for nonstructural components. *Earthquake Engineering and Structural Dynamics*, 45, 599-617.

200. Lucchini, A., Franchin, P., and Mollaioli, F. (2017a). Median floor spectra of linear structures with uncertain properties. *Earthquake Engineering and Structural Dynamics*, DOI: http://dx.doi.org/ http://dx.doi.org/ 10.1002/eqe.2899.

201. Lucchini, A., Franchin, P., and Mollaioli, F. (2017b). Uniform hazard floor acceleration spectra for linear structures. *Earthquake Engineering and Structural Dynamics*, 46, 1121-1140.

202. Lucchini, A., Mollaioli, F., and Monti, G. (2011). Intensity measures for response prediction of a torsional building subjected to bi-directional earthquake ground-motion. *Bulletin of Earthquake Engineering*, 9, 1499-1518.

203. Lucchini, A., Mollaioli, F., and Bazzurro, P. (2014). Floor response spectra for bare and infilled reinforced concrete frames. *Journal of Earthquake Engineering*, 18, 1060-1082.

204. Luco, N., and Bazzurro, P. (2007). Does amplitude scaling of ground motion records result in biased nonlinear structural drift response. *Earthquake Engineering and Structural Dynamics*, 36, 1813-1835.

205. Luco, N., and Cornell, C. A. (2007). Structure-specific scalar intensity measure for near-source and ordinary earthquake ground motions. *Earthquake Spectra*, 23, 357-392.

206. Maniyar, M. M., and Khare, R. K. (2011). Selection of ground motions for performing incremental dynamic analysis of existing reinforced concrete buildings in India. *Current Science*, 100, 701-713.

207. Maqsood, T., Edwards, M., Ioannou, I., Kosmidis, I., Rossetto, T., and Corby, N. (2016). Seismic vulnerability functions for Australian buildings by using GEM empirical vulnerability assessment guidelines. *Natural Hazards*, 80, 1625.

208. Martin, J. A., and Harder, R. N. (1989). Seismic design requirements for tall buildings in Los Angeles. *In the Proceedings of Annual Meeting of Los Angeles Tall Buildings Structural Design Council*.

209. Medina, R. A., Sankarnarayanan, R., and Kingston, K. M. (2006). Floor response spectra for light components mounted on regular moment-resisting frame structures. *Engineering Structures*, 28, 1927-1940.

210. Medvedev, S. W., Sponheuer, W., and Karnik, V. (1965). Seismic intensity scale version MSK 1964. *United Nation Educational, Scientific and Cultural Organization*, Paris, 7 pp.

211. Meslem, A., and D'Ayala, D. (2012). Towards worldwide guidelines for the development of analytical vulnerability functions and fragility curves at regional level. *In the Proceedings of the 15th World Conference on Earthquake Engineering, Lisbon, Portugal*.

212. Meslem, A., and D'Ayala, D. (2013). Investigation into analytical vulnerability curves derivation aspects considering modelling uncertainty for infilled RC buildings. *In the Proceeding of the 4th International Conference on Computational Methods in Structural Dynamics and Earthquake Engineering (COMPDYN'13)*.

213. Minas, S., Galasso, C., and Rossetto, T. (2014). Preliminary investigation on selecting optimal intensity measures for simplified fragility analysis of mid-rise RC buildings. *In the Proceedings of the 2nd European Conference on Earthquake Engineering and Seismology (2ECEES),* Istanbul (Turkey).

214. Minas, S., Galasso, C., and Rossetto, T. (2015). Spectral shape proxies and simplified fragility analysis of mid-rise reinforced concrete buildings. *In the Proceedings of the 12th International Conference on Applications of Statistics and Probability in Civil Engineering* (ICASP12).

215. Miranda, E. (1993). Site dependent strength reduction factors. *Journal of Structural Engineering*, ASCE, 119, 3503–3519.

216. Miranda, E. (1999). Approximate seismic lateral deformation demands in multistory buildings. *Journal of Structural Engineering*, 125, 417–425.

217. Miranda, E., Mosqueda, G., Retamales, R., and Peckan, G. (2012). Performance of nonstructural components during 27 February 2010 Chile earthquake. *Earthquake Spectra*, 28(S1), S453-S471.

218. Mirza, S. A. (1990). Flexural stiffness of rectangular RC columns. *ACI Structural Journal*, 87, 425-435.

219. Moehle, J. P., Ghannoum, W., and Bozorgnia, Y. (2006). Collapse of lightly confined reinforced concrete frames during earthquakes. *In the Proceedings of 8th U. S. National Conference on Earthquake Engineering*, San Francisco, California.

220. Moghadam, A. S., and Tso, W. K. (2000). 3-D pushover analysis for damage assessment of buildings. *Journal of Seismology and Earthquake Engineering,* 2, 23-31.

221. Mohammed, H. H., Ghobarah, A., and Aziz, T. S. (2008). Seismic response of secondary systems supported by torsionally yielding structures. *Journal of Earthquake Engineering*, 12, 932-952.

222. Moniri, H. (2017). Evaluation of seismic performance of reinforced concrete buildings under near-field earthquakes. *International Journal of Advanced Structural Engineering*, 9, 13-25.

223. Moshref, A., Moghaddasi, S. M., and Tehranizadeh, M. (2011). Comparison of different non-linear static analysis used for seismic assessment of existing buildings. *In the Proceedings of 3rd ECCOMAS Conference on Computational Methods in Structural Dynamics and Earthquake Engineering*, Corfu, Greece.

224. Mousavi, M., Ghafory-Ashtiany M., and Azarbakht, A. (2011). A new indicator of elastic spectral shape for the reliable selection of ground motion records. *Earthquake Engineering and Structural Dynamics*, 40, 1403-1416.

225. Mukherjee, S., and Gupta, V. K. (2002). Wavelet-based generation of spectrum-compatible time-histories. *Soil Dynamics and Earthquake Engineering*, 22, 799-804.

226. Murthy, C. V. R., Menon, A., Goswami, R., Vijyanarayanan, A. R., Gandhi, S. R., Kalidindi, S. N., Raghukanth, S. T. G., Jaiswal, A., and Seth, A. (2012a). Observations from damages sustained in India during 2011 (India-Nepal) Sikkim Earthquake. *In the Proceedings 15th World Conference on Earthquake Engineering*, Lisbon, Portugal.

227. Murthy, C. V. R., Goswami, R., Vijaynarayanan, A. R., Ramancharla, P. K., and Mehta, V. V. (2012b). *Introduction to earthquake protection in non-structural elements in buildings*. Gujarat State Disaster management Authority, Gandhinagar.

228. Nassirpour, A., Song, B., and D'Ayala, D. (2017). IDA and cloud method for fragility assessment of bare and infilled steel frame structures. *In the Proceeding of the 16th World Conference on Earthquake Engineering*, Santiago, Chile.

229. NEHRP (National Earthquake Hazard Reduction Program) (1997). NEHRP recommended provisions for seismic regulations for new buildings and other structures. FEMA 302, Washington, D.C.

230. NIST (National Institute of Standards and Technology) (2012). Tentative framework for development of advanced seismic design criteria for new buildings. NIST GCR 12-917-20, National Institute of Standards and Technology, United States.

231. NZS 1170.5 (Standards New Zealand) (2004). Structural design actions- Part 5: Earthquake actions- Standards New Zealand. Wellington.

232. NZSEE (2006). Assessment and improvement of the structural performance of buildings in Earthquake. New Zealand Society for Earthquake Engineering.

233. Oliva, M. G. (1980). *Shaking table testing of a reinforced concrete frame with biaxial response*. UCB/EERC 80/28, University of California, Berkeley, California.

236

234. Oropeza, M., Favez, P., and Lestuzzi, P. (2010). Seismic response of non-structural components in case of nonlinear structures based on floor response spectra method. *Bulletin of Earthquake Engineering*, 8, 387-400.

235. Otani, S. (1974). Inelastic analysis of R/C frame structures. *Journal of the Structural Division*, ASCE, 100, 1433-1449.

236. Otani, S. (1980). Nonlinear dynamic analysis of reinforced concrete building structures. *Canadian Journal of Civil Engineering*, 7, 333-344.

237. Pacific Earthquake Engineering Research Center (PEER) (2011). PEER ground motion database. Available at http://peer.berkeley.edu/peer_ground_motion_database/site (last accessed 11 August 2013).

238. Pagni, C. A., and Lowes, L. N. (2004). *Predicting earthquake damage in older reinforced concrete beam-column joints*. Pacific Earthquake Engineering Research Center.

239. Pan, X., Zheng, Z., and Wang, Z. (2017a). A multimode method for estimation of floor response spectra. *Journal of Earthquake Engineering*, DOI:10.1080/13632469.2016.1277440.

240. Pan, X., Zheng, Z., and Wang, Z. (2017b). Estimation of floor response spectra using modified modal pushover analysis. *Soil Dynamics and Earthquake Engineering*, 92, 472-487.

241. Papanikolaou, V. K., and Elnashai, A. S. (2005). Evaluation of conventional and adaptive pushover analysis I: Methodology. *Journal of Earthquake Engineering*, 9, 923-941.

242. Papanikolaou, V. K., Elnashai, A. S., and Pareja, J. F. (2005). Evaluation of conventional and adaptive pushover analysis II: Comparative results. *Journal of Earthquake Engineering*, 10, 127-151.

243. Paret, T. F., Sasaki, K. K., Eilbeck, D. H., and Freeman, S. A. (1996). Approximate inelastic procedures to identify failure mechanisms from higher mode effects. *In the Proceedings of the 11th World Conference on Earthquake Engineering*, No. 966, Acapulco, Mexico.

244. Paul, D. K., Singh, Y., Dubey, R. N., and Sekar, K. (2004). Damage to Andaman & Nicobar Island due to Tsunamigenic earthquake of December 26, 2004. *National Disaster Management Division*, Ministry of Home Affairs, Government of India, Department of Earthquake Engineering, Indian Institute of Technology Roorkee.

245. PEER / ATC-72-1 (Applied Technology Council) (2010). Modelling and acceptance criteria for seismic design and analysis of tall buildings. Applied Technology Council, Redwood City, California, United Sates.

246. Penelis, G. G., Kappos, A. J., and Stylianidis, K. C. (2003). Assessment of seismic vulnerability of unreinforced masonry buildings. *In the Proceedings of 8th International Conference on Structural Studies: Repairs and Maintenance of Heritage Architecture*, Chalkidiki, Greece.

247. Peter, K., and Badoux, M., (2000). Application of the capacity spectrum method to RC buildings with bearing walls. *In the Proceedings of the 12th World Conference on Earthquake Engineering*, Auckland, CD-ROM, Paper 0609.

248. Petrini, L., Maggi, C., Priestley, M. J. N., and Calvi, G. M. (2008). Experimental verification of viscous damping modelling for inelastic time history analyses. *Journal of Earthquake Engineering*, 12, 125-145.

249. Petrone, C., Magliulo, G., and Manfredi, G. (2015a). Seismic demand on light-acceleration-sensitive non-structural components in European reinforced concrete buildings. *Earthquake Engineering and Structural Dynamics,* 44, 1203-1217.

250. Petrone, C., Magliulo, G., and Manfredi, G. (2015b). Floor response spectra in RC frame structures designed according to Eurocode 8. *Bulletin of Earthquake Engineering*, DOI 10.1007/s10518-015-9846-7.

251. Phipps, M. T. (1997). *The impact of non-structural damage on building performance: Reflections on the 1994 Northridge Earthquake*. Report UCB/EERC-97/05, pp-173-178, The EERC-CUREE Symposium in Honor of Vitelmo V. Bertero, Earthquake Engineering Research Centre, University of California, Berkeley, California.

252. Politopoulos, I., and Feau, C. (2007). Some aspects of floor spectra of 1 DOF nonlinear primary structures. *Earthquake Engineering and Structural Dynamics*, 36, 975-993.

253. Prasad, J. S. R. (2009). *Seismic vulnerability and risk assessment of Indian urban housing*. Ph.D. Thesis, Department of Earthquake Engineering, Indian Institute of Technology Roorkee, India.

254. Prasad, J. S. R., Singh, Y., Kaynia, A. M., and Lindholm, C. (2009). Socioeconomic clustering in seismic risk assessment of urban housing stock. *Earthquake Spectra*, 25, 619-641.

255. Qiu, F., Li, W., Pan, P., and Qian, J. (2002). Experimental test on RC columns under biaxial quasi-static loading. *Engineering Structures*, 24, 419-428.

256. Raghunandan, M., and Liel, A. B. (2013). Effect of ground motion duration on earthquake induced structural collapse. *Structural Safety*, 41, 119-133.

257. Rautela, P., Joshi, G. C., Bhaisora, B., Dhyani, C., Ghildiyal, S., and Rawat, A. (2015). Seismic vulnerability of Nainital and Mussoorie, two major lesser Himalayan tourist destinations of India. *International Journal of Disaster Risk Reduction*, 13, 400-408.

258. Reitherman, R., and Sabol, T. A. (1995). Northridge earthquake of January 17, 1994: Reconnaissance report- Non-structural damage. *Earthquake Spectra*, EERI 11 (Supp), 453-514.

259. Reyes, J. C., Riano, A. C., Kalkan, E., and Arango, C. A. (2015). Extending modal pushover based scaling procedure for nonlinear response history analysis of multistory unsymmetric plan buildings. *Engineering Structures*, 88, 125-137.

260. Reyes, J. C., Riano, A. C., Kalkan, E., Quientro, O. A., and Arango, C. A. (2014). Assessment of spectrum matching procedure for nonlinear analysis of symmetric and asymmetric–plan buildings. *Engineering Structures*, 72, 171-181.

261. Rihal, S. S. (1992). Performance and behavior of non-structural building components during the Whittier Narrows, California (1987) and Loma Prieta, California (1989) earthquakes: Selected case studies. *Proceedings Seminar and Workshop on Seismic Design and Performance of Equipment and Non-structural Elements in Buildings and Industrial Structures (ATC-29)*, pp.-119-143, Applied Technology Council, Redwood City, California.

262. Rodrigues, H., Dias Arede, A. J. C., Varum, H., and Costa, A. (2013a). Behaviour of RC building columns under cyclic loading: experimental study. *Journal of Earthquake and Tsunami*, https://doi.org/10.1142/S1793431112500261.

263. Rodrigues, H., Dias Arede, A. J. C., Varum, H., and Costa, A. (2013b). Damage evolution in reinforced concrete columns subjected to biaxial loading. *Bulletin of Earthquake Engineering*, 11, 1517-1540.

264. Rodrigues, H., Dias Arede, A. J. C., Varum, H., and Costa, A. (2013c). Experimental evaluation of rectangular reinforced concrete column behaviour under biaxial cyclic loading. *Earthquake Engineering and Structural Dynamics*, 42, 239-259.

265. Rodrigues, H., Romao, X., Andrade-Campos, A., Varum, H., Dias Arede, A. J. C., and Costa, A. (2012). Simplified hysteretic model for the representation of biaxial bending response of RC columns. *Engineering Structures*, 44, 146-158.

266. Rodrigues, H., Varum, H., Arede, A. J. C., and Costa, A. (2012). A Comparative analysis of energy dissipation and equivalent viscous damping of RC columns subjected to uniaxial and biaxial Loading. *Engineering Structures*, 35, 149-164.

267. Rodrigues, H., Varum, H., Dias Arede, A. J. C., and Costa, A. (2013d). Behaviour of reinforced concrete column under biaxial cyclic loading – State of the art. *International Journal of Advanced Structural Engineering*, 5, 1-12.

268. Rodrigues, H., Varum, H., Dias Arede, A. J. C., and Costa, A. (2013e). Comparative efficiency analysis of different nonlinear modelling strategies to simulate the biaxial response of RC columns. *Earthquake Engineering and Engineering Vibration*, 11, 553-566.

269. Rodriguez, M. E., Restrepo, J. I., and Carr, A. J. (2002). Earthquake-induced floor horizontal accelerations in buildings. *Earthquake Engineering and Structural Dynamics*, 31, 693-718.

270. Rossetto, T., Gehl, P., Minas, S., Galasso, C., Duffour, P., Douglas, J., and Cook, O. (2016). FRACAS: A capacity spectrum approach for seismic fragility assessment including record-to-record variability. *Engineering Structures*, 125, 337–348.

271. Rossetto, T., and Elnashai, A. S. (2003). Derivation of vulnerability functions for European-type RC structures based on observational data. *Engineering Structures*, 25, 1241–1263.

272. Rossetto, T., and Elnashai, A. S. (2005). A new analytical procedure for the derivation of displacement-based vulnerability curves for populations of RC structures. *Engineering Structures*, 27, 397–409.

273. Rossetto, T., D'Ayala, D., Ioannou, I., and Meslem, A. (2014). Evaluation of existing fragility curves. In *SYNER-G: Typology definition and fragility functions for physical elements at seismic risk*, Springer, Netherlands.

274. Rosso, A., Almeida, J. P., and Beyer, K. (2017). Numerical simulation with fibre beam-column models of thin RC column behaviour under cyclic tension-compression. *In the Proceedings of the 16th World Conference on Earthquake Engineering*, Santiago, Chile.

275. Saatcioglu, M., Mitchell, D., Tinawi, R., Gardner, N. J., Gillies, A. G., Ghobarah, A., Anderson, D. L., and Lau, D. (2001). The August 17, 1999, Kocaeli (Turkey) earthquake - damage to structures. *Canadian Journal of Civil Engineering*, 28, 715–737

276. Sankaranarayanan, R., and Medina, R. A. (2007). Acceleration response modification factors for non-structural components attached to inelastic moment-resisting frame structures. *Earthquake Engineering and Structural Dynamics*, 36, 2189-2210.

277. Sarkar, P., Meher Prasad, A., and Menon, D. (2005). Strength distribution in asymmetric buildings: Review of code provisions. *Structural Engineering Convention*, Bangalore.

278. Sarkar, P., Meher Prasad, A., and Menon, D. (2010). Vertical geometric irregularity in stepped building frames. *Engineering Structures*, 32, 2175-2182.

279. Sarkar, P., Meher Prasad, A., and Menon, D. (2016). Seismic evaluation of stepped building frame using improved pushover analysis. *Earthquakes and Structures*, 10, 913-938.

280. Sasaki, K. K., Freeman, S. A., and Paret, T. F. (1998). Multi-mode pushover procedure (MMP) - A method to identify the effects of higher modes in a pushover analysis. *In the Proceedings of 6th US National Conference on Earthquake Engineering*, Seattle, Washington, U.S.A., Paper No. 271.

281. Satake, N., Suda, K., Arakawa, T., Sasaki, A., and Tamura, Y. (2003). Damping evaluation using full-scale data of buildings in Japan. *Journal of Structural Engineering*, ASCE, 129, 470-477.

282. SEAOC Vision 2000 Committee. (1995). Performance-based seismic engineering. *Structural Engineers Association of California*, Sacramento, California.

283. Seo, J., Duenas-Osorio, L., Craig, J. I., and Goodno, B. J. (2012). Metamodel-based regional vulnerability estimates of irregular steel moment-frame structures subjected to earthquake events. *Engineering Structures*, 45, 585-597.

284. Sezen, H., and Moehle, J. P. (2004). Shear strength model for lightly reinforced concrete columns. *Journal of Structural Engineering*, ASCE, 130, 1692-1703.

285. Shahrooz, B. M., and Moehle, J. P. (1990). Seismic response and design of set-back buildings. *Journal of Structural Engineering*, ASCE, 116, 1423-1439.

286. Shakib, H., and Pirizadeh, M. (2014). Probabilistic seismic performance assessment of setback buildings under bidirectional excitation. *Journal of Structural Engineering*, ASCE, 140, 1736-1745.

287. Sharma, M. L., Sinhval, A., Singh, Y., and Maheshwari, B. K. (2011). *A damage survey report on Sikkim earthquake of September 18, 2011*. Department of Earthquake Engineering, Indian Institute of Technology Roorkee, Roorkee, India.

288. Shin, Y., and Moehle, J. P. (2007). *Quarter-Scale reinforced concrete specimen test*. Internal Technical Report, University of California, Berkeley, California.

289. Shome, N., and Cornell, C. A. (1999). *Probabilistic seismic demand analysis of nonlinear structures*. Report No. RMS-35, RMS Program, Stanford University, Stanford, CA.

290. Shome, N., Cornell, C. A., Bazzurro, P., and Carballo, J. E. (1998). Earthquakes, records and nonlinear responses. *Earthquake Spectra*, 14, 469-500.

291. Silva, V., Crowley, H., Pinho, R., and Varum, H. (2013). Extending displacement based earthquake loss assessment (DBELA) for the computation of fragility curves. *Engineering Structures*, 56, 343-356.

292. Silva, V., Crowley, H., Varum, H., Pinho, R., and Sousa, R. (2014). Evaluation of analytical methodologies used to derive vulnerability functions. *Earthquake Engineering and Structural Dynamics*, 43, 181–204.

293. Silva, V., Marques, M., Castro, J. M., and Varum, H. (2015). Development and application of a real-time loss estimation framework for Portugal. *Bulletin of Earthquake Engineering*, 13, 2493-2516.

294. Singh, A., and Ang, A. S. (1974). Stochastic prediction of maximum seismic response of light secondary systems. *Nuclear Engineering Design*, 29, 218-230.

295. Singh, M. P., Moreschi, L. M., Suarez, L. E., and Matheu, E. E. (2006a). Seismic design forces I: Rigid non-structural components. *Journal of Structural Engineering,* ASCE 132, 1524-1532.

296. Singh, M. P., Moreschi, L. M., Suarez, L. E., and Matheu, E. E. (2006b). Seismic design forces I: Flexible non-structural components. *Journal of Structural Engineering,* ASCE 132, 1533-1543.

297. Singh, Y., Gade, P., Lang, D. H., and Erduran, E. (2012). Seismic behaviour of buildings located on slopes - An analytical study and some observations from Sikkim earthquake of 18th September 2011. *In the Proceedings of the 15th World Conference on Earthquake Engineering*, Lisbon, Portugal.

298. Singhal, A., and Kiremidjian, A. S. (1996). Method for probabilistic evaluation of seismic structural damage. *Journal of Structural Engineering*, ASCE, 122, 1459-1467.

299. Sinha, R., Aditya, K. S. P., and Gupta, A. (2008). GIS-based urban seismic risk assessment using Risk.IITB. *ISET Journal of Earthquake Engineering*, 45(3-4).

300. Skokan, M. J., and Hart, G. C. (2000). Reliability of nonlinear static methods for the seismic performance prediction of steel frame buildings. *In the Proceedings of 12th World Conference on Earthquake Engineering*, Paper No. 1972, Auckland, New Zealand.

301. Soong, T. T. (1990). *Seismic performance of non-structural elements during the Loma Prieta earthquake*. Report NIST SP 796, Proc. 22nd Joint Meeting U.S.-Japan Cooperative Program in Natural Resources Panel on Wind and Seismic Effects, pp.-331-336, National Institute of Standards and Technology, Gaithersburg, Maryland.

302. Sousa, L., Marques, M., Silva, V., and Varum, H. (2017). Hazard disaggregation and record selection for fragility analysis and earthquake loss estimation. *Earthquake Spectra*, DOI: 10.1193/062016EQS101M.

303. Spence, R. J. S., Coburn, A. W., and Pomonis, A. (1992). Correlation of ground motion with building damage: The definition of a new damage-based seismic intensity scale. *In 10th World Conference on Earthquake Engineering*, Madrid, Spain.

304. Spence, R. J. S., Coburn, A. W., Sakai, S., and Pomonis, A. (1991). A parameterless scale of seismic intensity for use in seismic risk analysis and vulnerability assessment. *In Earthquake Blast and Impact: Measurement and effects of vibration, (The Society for Earthquake & Civil Engineering Dynamics, eds.),* Elsevier Applied Science, Amsterdam, Netherlands, 19–28.

305. Sponheuer, W., and Karnik, V. (1964). Neue seismische Skala, *Proceedings of the 7th Symposium of the ESC*, 77, 69–76.

306. Standards New Zealand (NZS 1170-5) (2004). Structural design actions- Part 5: Earthquake actions - New Zealand, Wellington.

307. Standards New Zealand (NZS 3101) (2006). Concrete structures standard. Private Bag 2439, Wellington.

308. Sullivan, T. J., Calvi, P. M., and Nascimbene, R. (2013). Towards improved floor spectra estimates for seismic design. *Earthquakes and Structures*, 4, 109-132.

309. Surana, M., Singh, Y., and Lang, D. H. (2016). Seismic performance of concrete-shear-wall buildings in India. *ICE – Structures and Buildings*, 169, 809-824.

310. Suresh, K., Deb, S. K., and Dutta, A. (2008). Parametric system identification of multistoried buildings with non-uniform mass and stiffness distribution. *In the Proceedings of 14th World Conference on Earthquake Engineering*, Beijing, China.

311. Taghavi, A., and Miranda, E. (2005). Approximate floor acceleration demands in multi-storey buildings II: Applications. *Journal of Structural Engineering*, ASCE 131, 212-220.

312. Toro, G. R., McGuire, R. K., Cornell, C. A., and Sewell, R. T. (1989). *Linear and nonlinear response of structures and equipment to California and Eastern United States earthquakes*. Report No. NP-5566, Electric Power Res. Inst. Palo Alto, California.

313. Tothong, P., and Cornell, C. A. (2006). An empirical ground motion attenuation relation for inelastic spectral displacement. *Bulletin of Seismological Society of America*, 96, 2146-2164.

314. Tothong, P., and Cornell, C. A. (2007). *Probabilistic seismic demand analysis using advanced ground motion intensity measures, attenuation relationships and near fault effects*. John A Blume Engineering Center, Department of Civil and Environmental Engineering, Stanford University, Stanford, California, United States.

315. Tothong, P., and Cornell, C. A. (2008). Structural performance assessment under near source pulse-like ground motion using advanced intensity measures. *Earthquake Engineering and Structural Dynamics*, 37, 1013-1037.

316. Tothong, P., and Luco, N. (2007). Probabilistic seismic demand analysis using advanced ground motion intensity measures. *Earthquake Engineering and Structural Dynamics*, 36, 1837-1860.

317. Unnikrishnan, V. U., Meher Prasad, A., and Rao, B. N. (2013). Development of fragility curves using high dimensional model representation. *Earthquake Engineering and Structural Dynamics*, DOI: 10.1002/eqe.2214.

318. Uttarakhand Building Bye Laws and Regulation (2011). *Amendment 2016*. Government of Uttarakhand, India.

319. Vamvatsikos, D., and Cornell, C. A. (2002). Incremental dynamic analysis. *Earthquake Engineering and Structural Dynamics*, 31, 491-514.

320. Vamvatsikos, D., and Cornell, C. A. (2006). Direct estimation of the seismic demand and capacity of oscillators with multi-linear pushovers through IDA. *Earthquake Engineering and Structural Dynamics*, 35, 1097-1117.

321. Vidic, T., Fajfar, P., and Fischinger, M. (1994). Consistent inelastic design spectra: Strength and displacement. *Earthquake Engineering & Structural Dynamics*, 23, 507-521.

322. Vijaynarayanan, A. R., Goswami, R., and Murthy, C. V. R. (2012). Performance of RC buildings along hill slopes of Himalayas during 2011 Sikkim earthquake. *In the Proceedings of 15th World Conference on Earthquake Engineering*, Lisbon, Portugal.

323. Villaverde, R. (1997). Seismic design of secondary structures: State of art. *Journal of Structural Engineering*, ASCE, 123, 1011-1019.

324. Villaverde, R. (2006). Simple method to estimate the seismic nonlinear response of non-structural components in buildings. *Engineering Structures*, 28, 1209-1221.

325. Vukobratovic, V. (2015). *The influence of nonlinear seismic response of structures on the floor acceleration spectra*. Doctoral dissertation. University of Ljubljana, Faculty of Civil and Geodetic Engineering.

326. Vukobratovic, V., and Fajfar, P. (2015). A method for the direct determination of approximate floor response spectra for inelastic structures. *Bulletin of Earthquake Engineering*, 13, 1405-1424.

327. Wang, G. (2011). A ground motion selection and modification method capturing response spectrum characteristics and variability of scenario earthquakes. *Soil Dynamics and Earthquake Engineering*, 31, 611-625.

328. Wang, Q., Shi, Q., and Men, J. (2011). Seismic performance of SRC frames based on incremental dynamic analysis. *Advanced Material Research*, 163, 4331-4335.

329. Weiser, J. D., Pekcan, G., Zaghi, A. E., Itani, A. M., and Maragakis, E. M. (2013). Floor accelerations in yielding special moment resisting frame structures. *Earthquake Spectra,* 29, 987-1002.

330. Whitman, R. V., Hong, S. T., and Reed, J. (1973). *Damage statics for high-rise buildings in the vicinity of the San Fernando earthquake*. Report No. 7, Massachusetts Institute of Technology, 204.

331. Wood, H. O., and Neumann, F. (1931). Modified Mercalli intensity scale of 1931, *Bulletin of the Seismological Society of America*, 21, 277–283.

332. Xu, Z., Lu, X. Z., Guan, H., Han, B., and Ren, A. Z. (2014). Seismic damage simulation in urban areas based on a high fidelity structural model and a physics engine. *Natural Hazards*, 71, 1679-1693.

333. Yakhchalian, M., Nicknam, A., and Amiri, G. G. (2015). Optimal vector-valued intensity measure for seismic collapse assessment of structures. *Earthquake Engineering and Engineering Vibration*, 14, 37-54.

334. Yakut, A. (2004). Preliminary seismic performance assessment procedure for existing RC buildings. *Engineering Structures*, 26, 1447-1461.

335. Yepes-Estrada, C., Silva, V., Rossetto, T., D'Ayala, D., Ioannou, I., Meslem, A., and Crowley, H. (2016). The global earthquake model physical vulnerability database. *Earthquake Spectra*, 32, 2567-2585.

336. Zahrah, T. F., and Hall, W. J. (1984). Earthquake energy absorption in SDOF structures. *Journal of Structural Engineering*, ASCE, 110, 1757-1772.

337. Zareian, F., and Krawinkler, H. (2007). Assessment of probability of collapse and design for collapse safety. *Earthquake Engineering and Structural Dynamics*, 36, 1901-1914.

338. Zareian, F., Krawinkler, H., Ibarra, L., and Lignos, D. (2010). Basic concepts and performance measures in prediction of collapse of buildings under earthquake ground motions. *Structural Design of Tall and Special Buildings*, 19, 167-181.

339. Zeng, X., Lu, X., Yang, T. Y., and Xu, Z. (2016). Application of FEMA P-58 methodology for regional earthquake loss prediction. *Natural Hazards*, 83, 177-192.

PUBLICATIONS FROM THE PH.D. WORK

JOURNAL PUBLICATIONS

1. Surana, M., Singh, Y., and Lang, D. H. (2017). Seismic characterization and vulnerability of building stock in hilly regions. *Natural Hazards Review*, American Society of Civil Engineers, DOI: 10.1061/(ASCE)NH.1527-6996.0000275.

2. Surana, M., Singh, Y., and Lang, D. H. (2017). Floor spectra of inelastic RC buildings considering ground-motion characterisitcs. *Journal of Earthquake Engineering*, DOI: 10.1080/13632469.2016.1244134.

3. Surana, M., Singh, Y., and Lang, D. H. (2017). Comparison of static and dynamic procedures for fragility analysis in context of next generation performance-based seismic design. *Asian Journal of Civil Engineering*, 18 (7), pp. 1167-1181.

4. Surana, M., Singh, Y., and Lang, D. H. (2017). Effect of response reduction factor on peak floor acceleration demand in mid-rise RC frame buildings. *Journal of Institution of Engineers – Series A*, India, 98 (1-2), pp. 53-65.

5. Surana, M., Singh, Y., and Lang, D. H. Effect of structural configuration on floor acceleration demand in hill-side buildings. *Earthquake Engineering and Structural Dynamics* (Under Review).

6. Surana, M., Singh, Y., and Lang, D. H. Effect of strong-column weak-beam design on seismic fragility of RC frame buildings. *International Journal of Advanced Structural Engineering* (Under Review).

7. Surana, M., Singh, Y., and Lang, D. H. Fragility analysis of hill-side buildings designed for modern seismic design codes. *The Structural Design of Tall and Special Buildings* (Under Review).

8. Surana, M., Das, J. Singh, Y., Lang, D. H. and Sharma, M. L. Site-specific seismic fragility analysis of RC frame buildings. *Natural Hazards* (In Preparation).

CONFERENCE PUBLICATIONS

1. Surana, M., Singh, Y., and Lang, D. H. (2016). Seismic fragility analysis of buildings on

steep slopes. ***Proceedings of Structural Engineering Convention-2016***, *Advances in Structural Engineering*, December 2016, Chennai, India, pp. 1490-1495.

2. Surana, M., Singh, Y., and Lang, D. H. (2015). Building typologies prevalent in the Indian Himalayas. ***Proceedings of TIFAC-IDRiM Conference on Disaster Advances***, October 2015, New Delhi, India. (Poster Presentation)

3. Surana, M., Singh, Y., and Lang, D. H. (2015). Seismic fragility analysis of hill-buildings in Indian Himalayas. ***Proceedings of SECED – An International Conference on Earthquake Risk and Engineering Towards a Resilient World***, July 2015, Cambridge, United Kingdom.